N71-33895
NASA CR-121481

TEST AND EVALUATION OF THE SURVEYOR III TELEVISION CAMERA RETURNED FROM THE MOON BY APOLLO XII

VOLUME II APPENDICES

CASE FILE COPY

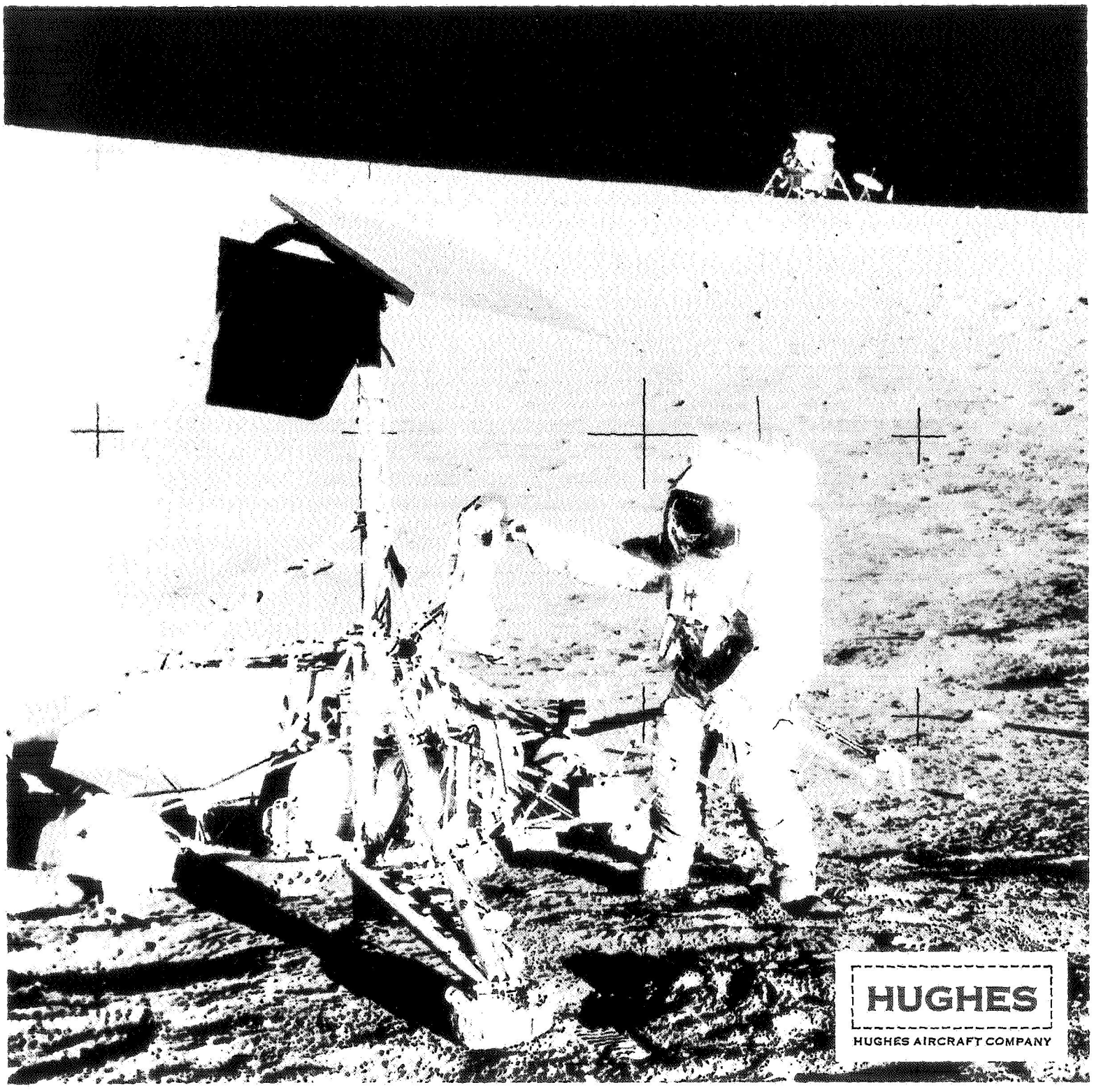

HUGHES
HUGHES AIRCRAFT COMPANY

TEST AND EVALUATION OF THE

SURVEYOR III TELEVISION CAMERA

RETURNED FROM THE

MOON

BY

APOLLO XII

•

SUBMITTED 31 DECEMBER 1970

VOLUME II
APPENDICES

Contract 952792

HUGHES
HUGHES AIRCRAFT COMPANY

COPYRIGHT © HUGHES AIRCRAFT COMPANY 1970

CONTENTS

VOLUME I

		Page
1.	SUMMARY	
	1.1 Introduction and Background Information	1-1
	1.2 Objectives and Scope of Test and Evaluation Program	1-3
	1.3 Assessment of Anomalies	1-9
	1.4 Observed Changes Attributable to Lunar Environment	1-13
	1.5 Absence of Conjectured Effects of Lunar Environment	1-13
	1.6 Concluding Comments and Recommendations	1-13
2.	PROGRAM OBJECTIVES, SCOPE, AND BACKGROUND INFORMATION	
	2.1 Program Objectives	2-1
	2.2 Background Information	2-4
	2.3 Description of TV Camera	2-7
	2.4 TV Camera Test History and Lunar Mission Operations	2-15
	2.5 TV Camera Retrieval and Return to Earth	2-22
	2.6 Scope of the Test and Evaluation Program	2-23
3.	TV CAMERA TESTS IN ASSEMBLED CONFIGURATION	
	3.1 Test Plan	3-1
	3.2 MSC Operations	3-2
	3.3 Shipment to Hughes	3-23
	3.4 Survey Operations	3-23
4.	ELECTRIC CIRCUIT TESTS AND DISMANTLING OF MAJOR SUBASSEMBLIES	
	4.1 Initial Dismantling	4-1
	4.2 Objectives and Scope of Electric Circuit Tests	4-3
	4.3 Selection of Chassis for Functional Performance Tests	4-5
	4.4 Test Equipment Checkout and Preliminary Tests	4-8
	4.5 Functional Performance Tests of Chassis A-4	4-9
	4.6 Functional Performance Tests of Chassis A-5	4-11

4.7 Functional Performance Tests of Chassis A-6 4-15
4.8 Dismantling of Major Subassemblies and Completion of Chassis Tests 4-19

5. OPTICAL SUBASSEMBLY TESTS AND DISMANTLING

5.1 General Discussion 5-1
5.2 Mirror Assembly and Filter Wheel Tests 5-4
5.3 Dismantling of Mirror Assembly and Filter Wheel Assembly 5-6
5.4 Tests and Dismantling of Lens Assembly 5-9
5.5 Tests of Shutter Assembly 5-13

6. VIDICON TESTS

6.1 Vidicon Design Features, Tests, and Operations History 6-1
6.2 Test Program Summary 6-5
6.3 Vidicon Tests on Camera 6-7
6.4 Vidicon Tests off Camera 6-19
6.5 Opening of Vidicon and Diagnostic Tests 6-30

7. ELECTRICAL COMPONENTS TESTS

7.1 Scope and General Test Plan 7-1
7.2 Resistor Tests 7-5
7.3 Capacitor Tests 7-13
7.4 Diode Tests 7-25
7.5 Transistor Tests 7-35

8. MECHANICAL AND ELECTROMECHANICAL COMPONENTS TESTS

8.1 Scope and General Test Plan 8-1
8.2 Potentiometer Tests 8-4
8.3 Stepper Motor Tests 8-7
8.4 Magnetic Components 8-8
8.5 Microdot Connector Tests 8-9
8.6 Thermal Switch Tests 8-13

9. OPTICAL COMPONENTS TESTS

9.1 Introduction 9-1
9.2 Special Photographic and Optical Tests by Science Investigators 9-2
9.3 Tests of TV Azimuth Mirror 9-3
9.4 Tests of Lens Barrel Subassembly 9-13

10. MATERIALS TESTS

10.1 Objectives and Scope of Test Program 10-1
10.2 Electric Circuit Materials 10-3
10.3 Electrical Insulation Materials 10-16
10.4 Organic Materials 10-29

10.5 Adhesive Materials 10-34
10.6 Lubricants: Friction and Wear Evaluation 10-39
10.7 Thermal Control Coatings and Materials 10-54

11. SURFACE DISCOLORATION AND CONTAMINATION STUDIES

11.1 Introduction 11-1
11.2 Data Available From Prelaunch, Landing, and Post-Recovery Examination 11-3
11.3 Evolution of Test Plan 11-7
11.4 Summary of Test Results 11-10
11.5 Damage Model 11-25

12. FAILURE ANALYSIS

12.1 Introduction 12-1
12.2 General Assessment of Anomalies 12-5
12.3 Suspected Cold Weld of Connector J2 Shell to Shroud 12-7
12.4 Analysis of Failed Filter Wheel Potentiometer 12-10
12.5 Open Shutter Anomaly and Related Failures 12-14
12.6 Discoloration and Curling of Teflon Skirt 12-29
12.7 Cracked Glass Envelopes on Diodes and Resistors and Related Component Failures 12-31
12.8 Other Electrical Anomalies 12-38
12.9 Other Mechanical and Electromechanical Analyses 12-47

REFERENCES R-1

VOLUME II

APPENDICES

A Program Management A-1
B Description of Lunar Environment B-1
C Description and Checkout of Electrical Test Equipment C-1
D Functional Description of Chassis A-4 D-1
E Functional Description of Chassis A-5 E-1
F Functional Description of Chassis A-6 F-1
G Supplementary Data on Vidicon and Its Test Program G-1
H Supplementary Data on Components Tests H-1
I Supplementary Data on Materials Tests I-1
J Supporting Data for Surface Effects Study J-1
K Supplementary Data on Failure Analysis K-1

REFERENCES R-1

ILLUSTRATIONS

		Page
2-1	Survey Television Camera	2-8
2-2	Cutaway View of Survey Television Camera	2-9
2-3	Lower Electronic Portion of Survey Television Camera With Mirror Unit Removed	2-10
2-4	Variable Focal Length Lens Assembly	2-12
2-5	Vidicon Tube	2-13
2-6	Electronic Conversion Unit	2-14
2-7	Electronic Circuits for Sweep, Control, and Amplification	2-14
3-1	Test Plan: Surveyor III TV Camera and Its Major Subassemblies	3-4
3-2	Surveyor III TV Camera and Its Plastic Bag at LRL	3-8
3-3	Returned Surveyor III TV Camera	3-9
3-4	Area Under Support Collar Immediately Upon Its Removal in LRL	3-10
3-5	Mirror Elevation Drive Mechanism	3-11
3-6	Removal of External Lower Shroud Connector	3-14
3-7	Removal of External Shroud Connector Retainer Nut	3-14
3-8	Camera Mounting Collar – Left Section With Remnants of Support Struts	3-15
3-9	Camera Support Collar – Right Section	3-15
3-10	External Connectors on Lower Shroud	3-16
3-11	Lower Shroud After Removal of External Connectors	3-17
3-12	Removal of Connector Cable Support Bracket and Biological Assay	3-17
3-13	Biological Assays	3-18
3-14	Biological Assay – Removal of Piece of Foam From TV Electronics	3-20
3-15	Exposed Lower Portion of TV Camera Upon Removal of Lower Shroud	3-21
3-16	Infrared Photograph of TV Camera	3-22
3-17	TV Camera Wrapped for Shipment to Hughes	3-24
3-18	TV Camera Placed in Carrying Case	3-24
3-19	Color Variations on Sunshade and Connector Bracket	3-26
3-20	Evidence of "Mud-Cracking" on Lower Shroud	3-27
3-21	Variations in "Mud-Cracking" on Lower Shroud Area	3-28
3-22	"Sandblasting" and Erosion on Elevation Drive Motor Housing	3-29

3-23	Aluminized Teflon FEP and Nylon on Mirror Housing Connector	3-30
3-24	Glass Fiber Cable Insulation	3-32
3-25	Teflon TFE on Mirror Assembly	3-34
3-26	Teflon TFE Skirt Seal	3-35
3-27	Color Variation and Banding on TV Mirror	3-36
4-1	Azimuth Drive Ring Gear Assembly	4-2
4-2	Bottom View of Upper Shroud of Camera	4-3
4-3	Typical Cordwood Module – TV Camera Electronics	4-6
4-4	Test Setup for Functional Checkout of Chassis A5	4-14
4-5	Test Setup for Functional Checkout of Chassis A6	4-18
4-6	TV Camera After Removal of Mirror Assembly and Shroud	4-22
4-7	Main Deck Structure of TV Camera	4-23
4-8	Front View of Lens Support Structure and Shutter Assembly	4-26
4-9	Star Mode Chassis A10 After Disassembly	4-26
4-10	Top View of Shutter Assembly	4-27
4-11	Bottom View of Lens Assembly	4-27
4-12	Chassis A5	4-28
4-13	Cordwood Module Sides of Various Chassis	4-30
4-14	Etched Braided Circuit Board Side of Chassis A6	4-33
4-15	Electronic Conversion Unit	4-34
4-16	Rear View of Vidicon Housing Assembly	4-35
4-17	Vidicon Boron Nitride Collar	4-36
4-18	Vidicon Deflection Coil	4-36
5-1	Mirror Assembly With Filter Wheel Subassembly	5-2
5-2	Lens and Shutter Assembly	5-3
5-3	Removal of Filter Wheel Potentiometer	5-4
5-4	Filter Wheel Subassembly	5-8
5-5	Lens Frame With Focus Mechanism in Vacuum Chamber	5-12
6-1	Vidicon Tube of Surveyor III Camera	6-2
6-2	Cross-Sectional View of Front Portion of Vidicon	6-3
6-3	Functional Diagram of Vidicon Transducing Process	6-4
6-4	Vidicon Test Program Flow Diagram	6-6
6-5	Front View of Vidicon Faceplate	6-8
6-6	Diagrammatical Representation of Vidicon for Functional Tests	6-12
6-7	Beam Transmission Characteristics	6-16
6-8	Surveyor III Vidicon Transfer Characteristics: Cathode and Beam Currents	6-17
6-9	Vidicon Prior to Removal From Camera	6-18
6-10	Front View of Transparent Faceplate of Surveyor III Vidicon, Showing Cathode in Rear	6-20
6-11	Measurement of Nesa Conductivity on Surveyor III and Spare Vidicon	6-22
6-12	Appearance of Faceplate Photoconductor of a Spare Vidicon After 118 Hours Exposure in Thermal Simulation Test	6-26
6-13	Torn Piece of Grid 5 Mesh During Thermal Simulation Test	6-26

6-14	Block Diagram of Test Setup for Measurement of Vidicon Gas Content	6-26
6-15	Results of Microscopic Examination of Pieces of Grid 5 Mesh	6-32
6-16	Optical Transmission Measurements of Nesa Coatings: Surveyor III Vidicon and Two Spare Vidicons	6-35
7-1	Resistance Versus Temperature of 1.5 Megohm Carbon Composition Resistor	7-6
7-2	Impedance Versus Frequency of Three Carbon Composition Resistors	7-6
7-3	Metallographic Section of 1.5 Megohm Carbon Composition Resistors	7-8
7-4	Resistance Versus Temperature of Six Carbon Film Resistors	7-9
7-5	Impedance Versus Frequency of Five Carbon Film Resistors	7-10
7-6	Resistance Versus Temperature of Precision Wire-Wound Resistor	7-12
7-7	Dissipation Factor Versus Susceptance of Solid Tantalum Capacitors	7-17
7-8	Leakage Current Versus Temperature of Tantalum Capacitors	7-18
7-9	Capacitance Versus Temperature of Dipped Mica Capacitors	7-22
7-10	Capacitance and Q Versus Temperature of Glass Dielectric Capacitors	7-24
7-11	Insulation Resistance Versus Temperature of Dipped Mica Capacitors	7-24
7-12	Insulation Resistance Versus Temperature of Glass Dielectric Capacitors	7-24
7-13	Voltage Versus Temperature of Zener Diodes	7-32
7-14	SEM Photographs of Intermetallic Growth Bonds on Low Noise Transistor	7-46
7-15	SEM Photograph of Base Lead of Transistors	7-48
8-1	Apparent Cracks in Abrams Motor	8-6
8-2	Bent Connector Pin	8-12
8-3	TV Camera Connector Peeling of Gold Plating From Base Metal of Contact	8-12
9-1	Experiment Setup for Specular Reflectance Measurements of TV Mirror	9-7
9-2	TV Mirror Regions Measured for Reflectance	9-7
9-3	Results of Specular Reflectance Measurements	9-8
9-4	Test Setup for Original Measurement of Flatness of TV Mirror on Mirror Assembly	9-10
9-5	Illustration of Double-Pass Interference of Flatness Measurement	9-10
9-6	Interference Patterns During Flatness Measurements of TV Mirror	9-12
9-7	Lens Barrel Subassembly	9-13
9-8	Results of Lens Transmission Measurements	9-17

10-1	Etched Circuit Board Sandwich Construction	10-4
10-2	Solder Flux on Cordwood Module of Chassis A1	10-6
10-3	Wrinkled Solder Joint on Mother Board of Chassis A1	10-7
10-4	Void in Solder Joint of Cordwood Module	10-8
10-5	Cross Sections of Solder Joints	10-9
10-6	Conductor Peel Strength Test Setup	10-11
10-7	Flaking of ML Coating From Surveyor III Internal Wire Harness	10-14
10-8	Infrared Spectra of Polyurethane Foam	10-18
10-9	Cracking of Conformal Coating on ECU of Surveyor III Camera	10-21
10-10	Infrared Spectra of Samples of Conformal Coating	10-24
10-11	Infrared Spectrogram of Filled Encapsulant of Magnetic Reactor	10-26
10-12	SEM Photographs of Polyimide-Coated ML Wire	10-30
10-13	Modified Probe for Shore A Tester for Hardness of Adhesives	10-36
10-14	Photomicrograph of Spur Gear From Mirror Elevation Drive (13X Magnification)	10-41
10-15	Photomicrograph of Ball Surface From TV Mirror Support Bearing (250X Magnification)	10-41
10-16	Elevation Drive Outer Bearing (20X Magnification)	10-42
10-17	Film of Transferred Lubricant on Outer Bearing of Elevation Drive (50X Magnification)	10-42
10-18	Interference Rings on Outer Bearing of Elevation Drive (200X Magnification)	10-42
10-19	Galled Teeth Surfaces on Focal Length Potentiometer Spur Gear (17X Magnification)	10-44
10-20	DAP Carriage Lip of Focal Length Potentiometer (30X Magnification)	10-44
10-21	Pitting of Bearing Balls of Focal Length Potentiometer (200X Magnification)	10-45
10-22	Wear of Focal Length Potentiometer Slip Rings (45X Magnification)	10-46
10-23	Helical Winding of Focal Length Potentiometer	10-48
10-24	Wear Track on Wires of Surveyor III Focal Length Potentiometer Winding (65X Magnification)	10-49
10-25	Surface Wear of Wiper Contact of Surveyor III Focal Length Potentiometer (100X Magnification)	10-49
10-26	Surface Wear of Test Wiper Contact After Friction Test (40X Magnification)	10-51
10-27	Appearance of Surveyor III Focal Length Potentiometer Wire After Friction Test (40X Magnification)	10-51
11-1	Lower Shroud of Surveyor III Camera, Showing TRW Measurement Positions	11-13
11-2	White Painted Tube Section Returned From Moon in SESC in Quartz Vacuum Chamber	11-14
11-3	Separated Radiation and Dust Effects on Spectral Reflectance	11-22
11-4	Effect of Radiation on Spectral Reflectance of White Inorganic Painted Surfaces of Surveyor III Camera	11-29

12-1	J2 Connector Showing Area of Suspected Cold Weld	12-8
12-2	Segment of Shroud in Contact With Connector J2 (3X Magnification)	12-9
12-3	Surveyor III TV Potentiometer	12-11
12-4	Wiper Block and Shaft Assembly of Potentiometer	12-11
12-5	Cracked and Broken Off Guide Block of Filter Wheel Potentiometer (30X Magnification)	12-12
12-6	Simplified Schematic of Shutter Coils and Drive Circuits	12-15
12-7	Logic Block Diagram Showing Relationship and Sequence of Failures of Shutter Drive Transistor, Shutter Coil, and Vidicon Photoconductor and Grid	12-17
12-8	Failed Shutter Solenoid Drive Transistor (Q5), Showing Open Emitter Lead (10X Magnification)	12-20
12-9	Damaged Shutter Solenoid Coil	12-22
12-10	Possible Causes of Line Voltage Across Shutter Coil Circuit	12-26
12-11	Cracked Diode Glass Envelope	12-32
12-12	Construction of Solid Tantalum Electrolytic Capacitor	12-42
12-13	Tantalum Capacitor Anode Slug, Showing Suspected Areas of Breakdown	12-44
12-14	Deformed and Galled Teeth of Azimuth Drive Gear Train	12-49
12-15	Scratch Marks on Filter Wheel Gear Caused by Broken Safety Wire	12-52
A-1	Surveyor Parts Test Program Organization	A-1
A-2	Surveyor Parts Test Program Master Schedule	A-5
A-3	Sketch of Surveyor Parts Test Facility	A-8
C-1	Test Fixture for Supporting Camera During Dismantling	C-3
D-1	Schematic of Chassis A4	D-3
D-2	Normal Mode Sweep Generating and Sync/Blanking Function	D-5
D-3	Vertical Sweep Generator Waveforms – Normal Mode	D-6
D-4	Vertical Blanking Timing Sequence – Normal Mode	D-7
D-5	Horizontal Sweep Generator Waveforms – Normal Mode	D-8
D-6	Horizontal Sync/Blank Timing Sequence – Normal Mode	D-12
D-7	Composite Sync/Blank Timing Sequence – Normal Mode	D-13
E-1	Schematic of Chassis A5	E-3
E-2	Normal Mode Logic Timing Sequence	E-8
E-3	Vidicon Thermal Control Timing Sequence – Normal Mode	E-16
F-1	Schematic of Chassis A6	F-2
F-2	Block Diagram of Shutter Control Circuits – 150 ms and Time Exposure Modes	F-6
F-3	Block Diagram of Mirror Drive Circuits for Mirror Stepping	F-7
F-4	150 ms Exposure Mode – Pulse Timing Sequence	F-8
F-5	Time Exposure Mode – Pulse Timing Sequence	F-11
G-1	Mounting of Grid 5 Mesh	G-2
G-2	Pressure Versus Heater Voltage Calibration of Non-Flight Vidicon	G-6
G-3	Heater Voltage Versus Current Calibration of Flight Vidicon	G-6

H-1	Example of Preliminary Test Plan Format – Solid Tantalum Capacitor	H-4
H-2	Resistance Versus Temperature Measurements of Ten Carbon Composition Resistors	H-6
H-3	Resistance Versus Temperature Measurements of 510 Ohm Carbon Composition Resistor	H-7
H-4	Resistance Versus Temperature Measurements of 10 Megohm Carbon Composition Resistor	H-7
H-5	Platinum Resistance Thermometer After Removal of Lead, Showing Deformation of Coils	H-10
I-1	Photomicrograph of Surveyor III ML-FEP Internal Harness Wire (50X Magnification)	I-9
I-2	Photomicrograph of Surveyor III Internal Harness Wire Strands (1000X Magnification)	I-9
I-3	Photomicrograph of TAT Camera Internal Harness Wife Strands (1000X Magnification)	I-10
I-4	Photomicrograph of Surveyor III Internal Coaxial Cable (25X Magnification)	I-10
I-5	Photomicrograph of Shield Conductors of Surveyor III Coaxial Cable (1000X Magnification)	I-11
I-6	Photomicrograph of Shield Conductors of TAT Camera Coaxial Cable (1000X Magnification)	I-11
I-7	Infrared Transmission Spectra of Teflon TFE From Camera Mirror Assembly Collars	I-14
I-8	Infrared Transmission Spectrum of Surveyor III Camera Mirror Hood	I-15
I-9	Ultraviolet Transmission Spectrum of Teflon TFE From Surveyor III Camera	I-17
I-10	DTA Thermograms	I-21
I-11	Schematic of Friction and Wear Test Assembly	I-24
I-12	Detailed Schematic of Location and Relative Motion of Wire Specimen and Wipers in Friction Test	I-25
J-1	Surveyor III on Crater Wall	J-2
J-2	Orientation of Surveyor III in Crater	J-4
J-3	Shadow Photograph of Surveyor III Model, Simulating Position of Sun at 10 Degrees Before Sunset, Viewed From Lunar Module Position	J-5
J-4	Approach and Landing Configurations of Lunar Module Relative to Surveyor III	J-6
J-5	View of Relative Locations on Lunar Surface of Surveyor III and Lunar Module	J-7
J-6	Illustration of Shadow Through Hole in Camera Clamp	J-9
J-7	Shadow Patterns on Elevation Drive Motor Housing	J-10
J-8	Spectral Reflectance of White Inorganic Paint Before and After Laboratory Ultraviolet Exposure	J-11
J-9	Lower Shroud of Surveyor III Camera, Showing TRW Measurement Positions	J-12
J-10	Reflectance Versus Wavelength of Surveyor III Camera Lower Shroud at Various TRW Locations Shown in Figure J-9	J-15

J-11	Quartz Chamber With Light-Tight Shield for Vacuum Tests of White Painted Tube	J-17
J-12	Sketch of White Painted Section of Tube Returned in SESC, Showing Measurement Positions	J-18
J-13	Spectral Reflectance Versus Wavelength of Four Samples of White Painted Tube – High Vacuum Prior to Light Exposure	J-19
J-14	Spectral Reflectance Versus Wavelength of Four Samples of White Painted Tube – Medium Vacuum Prior to Light Exposure	J-20
J-15	Spectral Reflectance Versus Wavelength of Four Samples of White Painted Tube – 1 AU Prior Prior to Light Exposure	J-21
J-16	Spectral Reflectance Versus Wavelength of One Sample of White Painted Tube (Sample 778-70) After 6 Days at 1 AU Prior to Light Exposure	J-22
J-17	Spectral Reflectance Versus Wavelength of Different Sample of White Painted Tube (Sample 800-70 in Figure J-12) After 48 Hours Exposure to Light at 1 AU	J-22
J-18	Spectral Reflectance Versus Wavelength of Four Samples of White Painted Tube After 48 Hours	J-23
J-19	Lower Shroud of Surveyor III Camera With Attached Cable Bracket Upon Return From Moon	J-24
J-20	Cable Bracket Superimposed on Lower Shroud of Surveyor III Television Camera: Shroud Exposed to Light for About 5 Months, Cable Bracket Unexposed	J-25
J-21	Location of Samples Cut From Cable Bracket	J-25
J-22	Spectral Reflectance Versus Wavelength of Sample of Camera Cable Bracket (Sample 518 of Figure J-21): Measurements Taken in May 1970 Prior to Light Exposure	J-26
J-23	Support Collar of Surveyor III Television Camera	J-28
J-24	Photograph of Surveyor III on the Moon, Showing TV Support Tubing	J-29
J-25	Reflectance of Bipod Bracket Tube	J-31
J-26	Experimental Configuration for Thermal-Vacuum Exposure of Surveyor III Sample 909	J-39
J-27	Ratio of Reflectance of Painted Surfaces Covered With Lunar Dust to Reflectance of "Clean" Surfaces (White Inorganic Paint)	J-43
K-1	J2 Connector Thread Area, Showing Metal Blob (13X Magnification)	K-2
K-2	SEM Photograph of Metal Blob of Figure K-1 (230X Magnification)	K-2
K-3	Transverse Cross Section of Metal Blob Shown in Figure K-2 (100X Magnification)	K-2
K-4	Microprobe Scan of Area Adjacent to Metal Blob of Figure K-2 (200X Magnification)	K-4
K-5	Edge of Shroud in Contact With J2 Connector Shell (22X Magnification)	K-6
K-6	SEM Photographs of Edge Surface of Hole in Shroud	K-7

K-7	Typical Cold Welded Area of 2014 Aluminum Specimen After Separation (1400X Magnification)	K-7
K-8	Surfaces of Potentiometer Blocks Under Broken Off Guides	K-9
K-9	SEM Comparison of DAP Materials	K-11
K-10	Chip of Shutter Coil Drive Transistor Q5, Showing Melted Metallization Under Emitter Bond (44X Magnification)	K-12
K-11	"Punch Through" Region of Shutter Drive Transistor Q5	K-14
K-12	Solenoid Coil Showing Effects of Excessive Heat	K-15
K-13	Shorted Wires of Figure K-12 (50X Magnification)	K-16
K-14	Drive Circuit of Shutter Solenoid A2	K-17
K-15	Command and Power Control Circuit of ECU	K-19
K-16	Internal View of Open Diode Showing Intermittent Contact (12X Magnification)	K-21
K-17	Die of High Leakage Diode, Showing Fracture of Chip (110X Magnification)	K-23

TABLES

		Page
1-1	Summary of Mission Performance of Surveyors	1-1
1-2	Program Tasks and Referenced Report Sections	1-5
1-3	Results of Investigation of Specific Anomalies	1-8
1-4	Observed Possible Effects of Lunar Environment	1-14
1-5	Significant Observations Relative to Absence of Effects of Lunar Environment	1-16
2-1	Primary Program Objectives - Acquisition of Engineering Design Data	2-2
2-2	Secondary Program Objectives - Support of Scientific Investigation	2-3
3-1	Removal Torques of Lower Shroud Mounting Hardware	3-19
4-1	Results of Functional Performance Tests of Electrical Parameters of Chassis A-4	4-10
4-2	Power Sources and Terminations for Functional Tests of Chassis A-4	4-11
4-3	Results of Functional Performance Tests of Electrical Parameters of Chassis A-5	4-12
4-4	Results of Functional Performance Tests of Electrical Parameters of Chassis A-6	4-16
4-5	Terminations for Functional Tests of Chassis A-6	4-19
4-6	Mounting Hardware Removal Torques	4-24
4-7	Mounting Hardware Installation Torques	4-24
5-1	Measured Torques During Removal of Components of Iris and Focal Length Mechanism	5-12
5-2	Measured Torques During Removal of Components of Focus Mechanism	5-13
5-3	Resistances of Shutter Assembly Coils	5-14
6-1	Results of Emission Measurements of Flight Vidicon and Two Spare Vidicons	6-12
6-2	Results of Gas Ratio Measurements	6-14
6-3	Results of Gas Content Measurements on Samples From Spare and Surveyor III Vidicons	6-28
6-4	Results of Microprobe Tests of Samples of Grid 5 Mesh	6-33
7-1	Types and Quantities of Electrical Components	7-2
7-2	Resistor Test Plan Summary	7-4
7-3	Resistance Versus Temperature Characteristics of Platinum Resistance Thermometer	7-12

7-4	Capacitor Test Plan Summary	7-14
7-5	Summary of Leakage Tests on Seven Tantalum Capacitors	7-16
7-6	Diagnostic Tests of Metallized Paper-Mylar Capacitors	7-21
7-7	Results of Measurements of Capacitance of Glass and Mica Capacitors	7-22
7-8	Diode Test Plan Summary	7-26
7-9	Functional Tests of High Speed Switching Diodes 1N3070	7-28
7-10	Functional Tests of Switching Diodes 1N3730	7-30
7-11	Functional Tests of Zener Voltage Reference Diodes	7-30
7-12	Functional Tests of Zener Voltage Regulator Diodes 1N754A	7-32
7-13	Functional Tests of High Voltage Diode Stack FA3075	7-34
7-14	Functional Tests of Silicon Controlled Rectifiers 2N1930	7-34
7-15	Transistor Test Plan Summary	7-35
7-16	Number of Transistors Tested on Chassis Versus Total on Camera	7-38
7-17	Functional Tests of General-Purpose Amplifier Transistors NPN 2N718A	7-40
7-18	Functional Tests of General-Purpose Amplifier Transistors PNP 2N722	7-40
7-19	Functional Tests of High Frequency Transistor 2N2192A	7-42
7-20	Functional Tests of High Voltage Transistors 2N871	7-42
7-21	Comparison of $V_{CE(sat)}$ Measurements of High Voltage Transistor	7-44
7-22	Functional Tests of Power Transistor 2N1936	7-46
7-23	Functional Tests of Low Noise Transistors 2N2586	7-46
8-1	Mechanical Components Test Plan Summary	8-2
8-2	Summary of Potentiometer Tests	8-5
8-3	Measurements of Tests of Toroidal Inductors	8-10
8-4	Results of Temperature Cycling of Thermal Switches	8-14
9-1	TV Azimuth Mirror Tests	9-4
10-1	TV Camera Materials Selected for Test and Evaluation	10-2
10-2	Circuit Board Materials	10-5
10-3	Solder Joint Pull Strength Test Results	10-10
10-4	Circuit Peel Strength Test Results	10-11
10-5	Hardness of Circuit Board Samples	10-13
10-6	Results of Visual Inspection of Conformal Coatings	10-20
10-7	Results of Electrical and Physical Measurements of Conformal Coatings	10-22

10-8 Electrical Measurements of Potting Compounds
10-9 Results of Hardness Measurements of Potting Compounds
10-10 Measurements of Tensile Strength and Elongation of Organic Materials
10-11 Surveyor III Camera Adhesives Tested
10-12 Measurements of Hardness of Adhesives
10-13 Measurement of Shear Strength of Adhesives
10-14 Surveyor III Camera Gears and Bearings Examined for Wear
10-15 Results of Friction Test of Worn Area of Surveyor III Focal Length Potentiometer Wire
10-16 Results of Friction Test of Unworn Area of Surveyor III Focal Length Potentiometer Wire
10-17 Relative Values of Friction Coefficients for Lubricated and Unlubricated Surfaces
11-1 Reflectance Measurements of Samples From Lower Shroud of Surveyor III Camera
11-2 Variation of Reflectance With Times as Result of Photo Bleaching
11-3 Effect of Thermal Bleaching (Vacuum Versus Air) on Spectral Reflectance of Irradiated Samples of Inorganic White Paint Used for Surveyors
11-4 Comparison of Several Techniques for Assessment of Fractional Area Covered by Lunar Dust
11-5 Possible Sources of Dust Contribution to Discoloration
12-1 List of Anomalies
12-2 Failure Analysis Summary Matrix
12-3 Summary of Components of Surveyor III Camera With Cracked Glass Envelopes
12-4 Electrical Component Anomalies Induced by Lunar Environment
A-1 Program Tasks
A-2 Surveyor III TV Camera Test Log Books
B-1 Solar Energy Distribution
B-2 Ultraviolet Radiation Spectrum at 1 AU
B-3 Some Twentieth Cycle Solar Proton Events
B-4 Nineteenth Cycle Solar Proton Events
G-1 Mass Spectrometer Measurements of Gas Samples From Spare and Surveyor III Vidicons
H-1 Electrical Components in Surveyor III TV Camera
H-2 Location of Components Selected for Tests on TV Chassis
H-3 Potentiometer Noise Measurements - Ambient and Vacuum Tests
I-1 Measurements of Capacitance of Internal Harness
I-2 Measurement of Conductor Resistance of Internal Harness

I-3	Measurements of Resistance of Contact to Wire Junction of J2 Connectors	I-6
I-4	Results of Microhardness Tests of Internal Wire and Cable	I-6
I-5	Measurement of Tensile Strength and Elongation of Internal Wires and Cable	I-8
I-6	Results of Measurement of Insulator Cut-through Ratings	I-12
I-7	Measurement of Tensile Strength of Connector Solder Joints in Internal Cable Connector	I-13
I-8	Results of Elemental Analysis of Organic Materials	I-18
I-9	Electron Paramagnetic Resonance Measurements of Organic Materials	I-20
J-1	Normal Emittance Measured on Lower Shroud Surface	J-13
J-2	Percent of Spectral Reflectance Versus Wave Length of Samples From Surveyor III Camera Connector Bracket After Exposure to White Light Photo Bleaching	J-27
J-3	Samples of Surveyor III Camera Shroud Cut in July 1970 for Science Studies	J-33
J-4	Percent Reflectance of Samples From Surveyor III Camera Shroud Cut for Science Studies in July 1970	J-34
J-5	Percent Reflectance of Samples From Surveyor III Camera Shroud Cut for Science Studies in October 1970	J-36
J-6	Effect of Thermal Annealing in Air on Spectral Reflectance of Samples Cut From Lower Shroud of Surveyor III Camera in October 1970	J-37
J-7	Effect of Thermal Annealing on Spectral Reflectance of Surveyor III Camera and Laboratory Samples of White Inorganic Painted Surfaces	J-38
K-1	Relative Contents of Copper, Manganese, and Chromium in Connector and Shroud	K-4
K-2	Results of Detent Breakaway Voltage and Current Measurements of Shutter Assembly	K-15
K-3	Measured Electrical Characteristics of Open Diode With Contact Restored by Lead Manipulation	K-21
K-4	Voltage Characteristics of High Leakage Diode	K-22

APPENDIX A. PROGRAM MANAGEMENT

Management of the Surveyor III TV Camera Test Program posed some challenges because of several unusual requirements. A special facility and associated security and parts control measures were required. Close coordination with the customer was essential on a day-to-day basis for decisions regarding continuation of planned tests or changes in test procedures. Integration of the technical effort with the companion NASA Surveyor Parts Test Program and with the parallel science program had to be accomplished. A variety of technical disciplines and, consequently, a relatively large number of Hughes organizations and outside sources were involved. The management program outlined here was structured and implemented to fulfill these requirements.

A. 1 ADMINISTRATION

The program organization is shown in Figure A-1. The program was directed by the Hughes Space Systems Division, which was responsible for the original Surveyor project. As evident from Figure A-1, many other Hughes organizations were involved. Key personnel were appointed, many of whom had considerable experience with the design and testing of the original Surveyor camera.

Figure A-1 also shows the organization of the companion NASA program, both under the single management of Dr. Edward I. Hawthorne to provide for close coordination of related tasks.

Strict administrative, technical, and financial controls were established early in the program as formal Administrative Bulletins and less formal administrative memoranda, as well as by close personal supervision. This personal contact was provided by the regularly observed weekly coordination meetings of the Program Manager with all task leaders, attended by the JPL Technical Manager.

HUGHES AIRCRAFT COMPANY
AEROSPACE GROUP
SPACE SYSTEMS DIVISION
SURVEYOR III TEST PROGRAM

E I HAWTHORNE
PROGRAM MANAGER

R K RONEY
MANAGER

4-1-70 PRIME DIVISION APPROVAL

PROGRAM ORGANIZATION CHART

SUPPORTING DIVISION APPROVAL:

E H MEIER
VICE PRESIDENT
AND MANAGER
RESEARCH AND DEVELOPMENT
DIVISION

J T MENDEL
MANAGER
ELECTRON DYNAMICS DIVISION

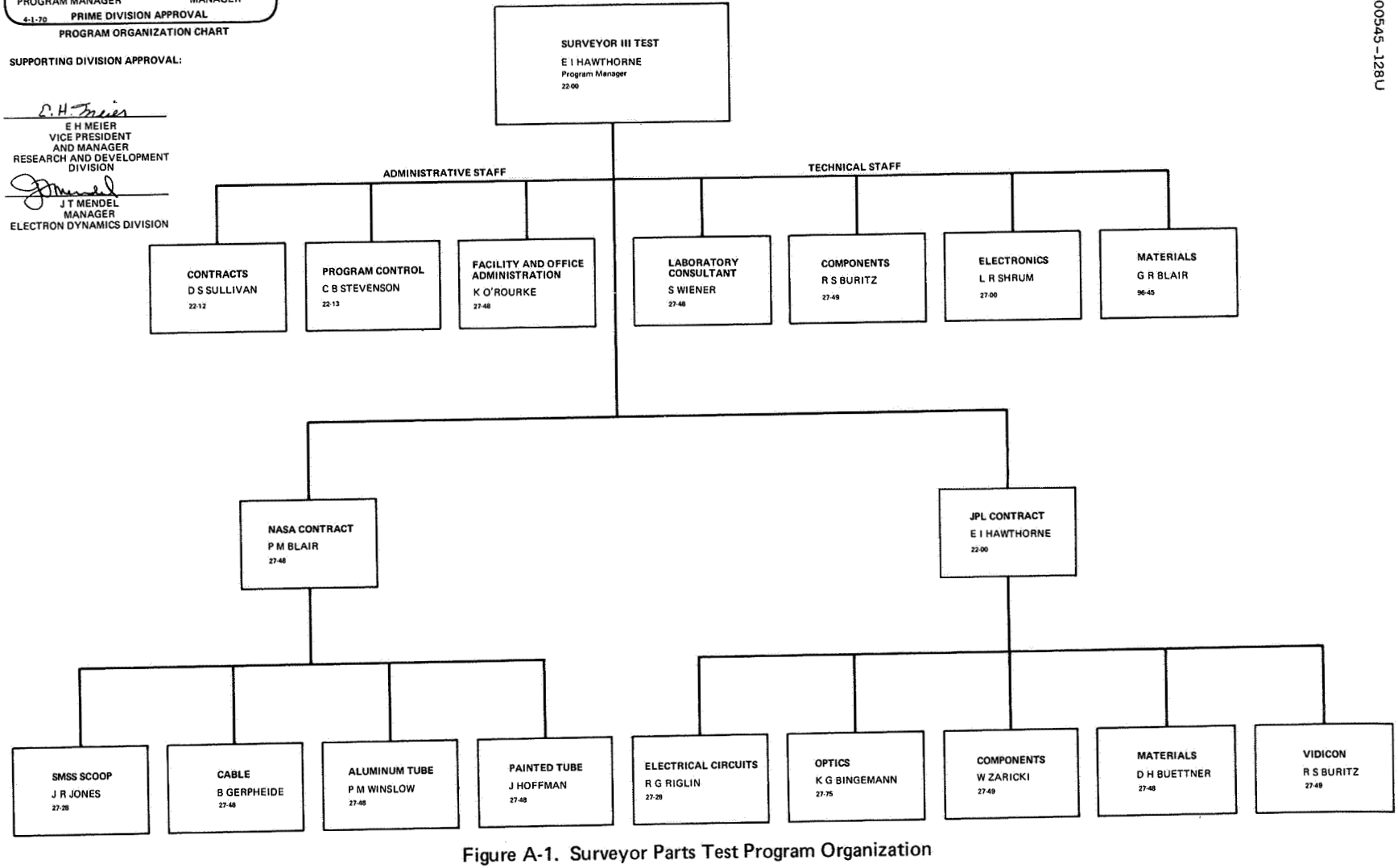

Figure A-1. Surveyor Parts Test Program Organization

The following Administrative Bulletins were issued:

1) Security Plan – This bulletin defined the security measures adopted for the Surveyor facility and established controls for program personnel and visitor access, and for removal of parts.

2) Project Coordination – This bulletin was addressed to the task of managing and coordinating the participation of the many Hughes organizations involved.

3) Responsibilities of Facility Supervisor – This bulletin defined the functions associated with the management of the Surveyor facility, including maintenance of cleanliness, observation of security measures, documentation, and all administrative functions.

4) Cost Control – This bulleting defined the system adopted for authorizing, controlling, and reporting all expenditures on the program.

5) Test Procedures – This bulletin defined the requirements for and the scope of all test procedures and assigned responsibilities for the preparation and approval of test procedures.

6) Task Structure – This bulletin defined the program tasks and assigned responsibilities for their execution.

7) Log Books – This bulletin established the system for recording all test data in controlled Surveyor Test Program Log Books.

8) Trouble and Failure Report (TFR) System – This bulletin established the program TFR system, similar to that used on the Surveyor program. It defined requirements for employing the system; outlined the responsibilities and decision processes involved; and set forth the method of implementation, entailing reporting, documentation, and disposition.

Strict financial controls were instituted in the form of Contractor Work Orders (CWOs) to ensure optimum allotment, expenditure, and monitoring of funds without overruns. Separate CWOs were issued for each program task and were revised in the course of the program, as required, within total funding allotment. In all cases, CWO forms employed included a brief description of the scope of the effort authorized.

At the weekly coordination meetings, technical progress of all tasks was systematically reviewed, and expenditures incurred were reported and analyzed in accordance with the system established in Administrative Bulletin 4 (defined above). All other administrative, contractual, and technical aspects of the program were also considered and resolved, including coordination with the companion NASA contract and relationship to the related science investigations. Customer technical and contractual representation ensured continuous and complete coordination throughout the program.

A. 2 TECHNICAL MANAGEMENT AND PLANNING

The TV Camera Test and Evaluation Program was pursued in accordance with the task structure defined in Administrative Bulletin 6 and discussed in more detail in Section 2. 6. 2. Table A-1 lists these tasks in order of their activation; the CWOs used for cost control were numbered correspondingly.

Considerable attention was given to the planning of all tests prior to their institution and throughout their execution. Test procedures were prepared and approved prior to testing in compliance with Administrative Bulletin 5. The technical effort was further directed and modified, as appropriate, by Technical Direction Memoranda (TDMs) issued by JPL and approved by the Program Manager; in all, 12 TDMs were issued.

Technical planning included periodic publication of detailed schedules. Major official revisions were published at approximately 10 week intervals. Program schedules included a master schedule and supplementary schedules. Supplementary schedules entailing detailed breakdown of test and evaluation operations were issued for mirror assembly tests, lens and shutter assembly tests, vidicon tests, materials tests, components tests, and surface contamination studies. Figure A-2 presents the fourth and final issue of the master schedule, which constitutes in retrospect the final documentation of the chronological execution of the major test and evaluation phases of the program.

An important feature of the technical management was the close coordination with the customer observed throughout the course of the program. This coordination entailed integration of the technical effort with the companion NASA contract and with the science investigators. Various selected TV camera samples were provided to scientists to support these studies. Consultation, as well as active participation in some cases, was provided, both outside of Hughes and in the Surveyor facility where science investigators conducted certain measurements. This technical

FINAL ISSUE
NOV 15, 1970

E I HAWTHORNE, PROGRAM MGR.

00545-129(U)

TASK NO.	TASK	W/E	JAN 9	16	23	30	FEB 6	13	20	27	MAR 6	13	20	27	APR 3	10	17	24	MAY 1	8	15	22	29	JUN 5	12	19	26	JUL 3	10	17	24	31	AUG 7	14	21	28	SEP 4	11	18	25	OCT 2	9	16	23	30	NOV 6	13	20	27	DEC 4	11	18	25
	START PROGRAM - 1/7/70		▲																																																	
1	MANAGEMENT OPERATIONS		━	━	━	━	━	━	━	━	━	━	━	━	━	━	━	━	━	━	━	━	━	━	━	━	━	━	━	━	━	━	━	━	━	━	━	━	━	━	━	━	━	━	━	━	━	━	━	━	━	━	━	━
2	MSC OPERATIONS		━	━	━																																															
N/A	SHIPMENT TO HUGHES - 1/16/70			▲																																															
N/A	FACILITY PLANNING AND SETUP		≈	━	━	━	━																																													
3	SURVEY OPERATIONS					━	━	━	━	━	━																																										
4	ELECTRICAL TEST PROCEDURE AND EQUIPMENT CHECKOUT			━	━	━	━	━	━	━	━	━	━																																							
13	DISMANTLING OPERATIONS										━	━	━	━	━	━	━	━	━	━	━	━	━																															
15	ELECTRICAL CHASSIS TESTS											━	━	━	━	━	━	━																																			
6	MIRROR ASSEMBLY TESTS AND DISASSEMBLY														━	━	━	━	━																																		
6	LENS AND SHUTTER ASSEMBLY TESTS															━	━	━	━	━	━	━																														
9	OPTICAL COMPONENTS TESTS						━	━	━	━	━	━					━																																				
9	LENS ASSEMBLY OPTICAL TESTS																				━	━	━	━	━	━	━																										
7	VIDICON TEST PROGRAM											━	━	━	━	━	━	━	━	━	━	━	━	━	━	━	━	━	━	━	━	━	━	━	━	━	━	━	━	━	━	━	━	━	━	━	━	━	━	━	━	━	━	━	━	━	━
8	MECHANICAL COMPONENTS TESTS											━	━	━	━	━	━	━	━	━	━	━	━	━	━	━	━	━	━	━	━	━	━	━	━	━	━	━	━	━	━	━	━	━	━	━	━	━	━	━	━	━	━	━	━
14	ELECTRICAL COMPONENTS TESTS											━	━	━	━	━	━	━	━	━	━	━	━	━	━	━	━	━	━	━	━	━	━	━	━	━	━	━	━	━	━	━	━	━	━	━	━	━	━	━	━	━	━	━	━
10	MATERIALS TESTS																		━	━	━	━	━	━	━	━	━	━	━	━	━	━	━	━	━	━	━	━	━	━	━	━	━	━	━	━	━	━	━	━	━	━	━	━
17	SURFACE CONTAMINATION STUDIES (DOR)														━	━	━	━	━	━	━	━	━											━	━	━	━	━	━	━	━	━	━	━	━	━	━	━	━	━	━	━	━	━	━	━	━
11	FAILURE ANALYSIS															━	━	━	━	━	━	━	━	━	━	━	━	━	━	━	━	━	━	━	━	━	━	━	━	━	━	━	━	━	━	━	━	━	━	━	━	━	━	━	━
16	SCIENCE SUPPORT		≈	≈	≈	≈	≈	≈	≈	≈	≈	≈	≈	≈	≈	≈	≈	≈	≈	≈	≈	≈	≈	≈	≈	≈	≈	≈	≈	≈	≈	≈	≈	≈	≈	≈	≈	≈	≈	≈	≈	≈	≈	≈	≈	≈	≈	≈	≈	≈	≈	≈	≈	≈	≈	≈
12	EVALUATION																━	━	━	━	━	━	━	━	━	━	━	━	━	━	━	━	━	━	━	━	━	━	━	━	━	━	━	━	━	━	━	━	━	━	━	━	━	━	━	━
12	MONTHLY REPORTS							▲				▲			▲			▲			▲			▲			▲			▲			▲			▲			▲			▲			▲			▲			▲			▲	
1	ORAL PRESENTATIONS														(1) ▲												(2) ▲																											SCHEDULED 1/26/71 (3) →
12	FINAL REPORT PREPARATION																																																			
18	FINAL REPORT PUBLICATION																																																			

Figure A-2. Surveyor Parts Test Program Master Schedule

TABLE A-1. PROGRAM TASKS

(Numbered in Sequence of Activation)

Task Number	Title
1	Program Management
2	MSC Operations
3	Survey Operations
4	Checkout of Electrical Test Equipment
5	System Tests*
6	Optical Subassembly Tests
7	Vidicon Tests
8	Mechanical and Electromechanical Components Tests
9	Optical Components Tests
10	Materials Test
11	Failure Analysis
12	Evaluation and Reporting
13	Camera Dismantling
14	Electrical Components Tests
15	Electric Circuit Tests
16	Support of Science Investigations
17	Surface Contamination Studies
18	Publication of Final Report

*Deleted from the program.

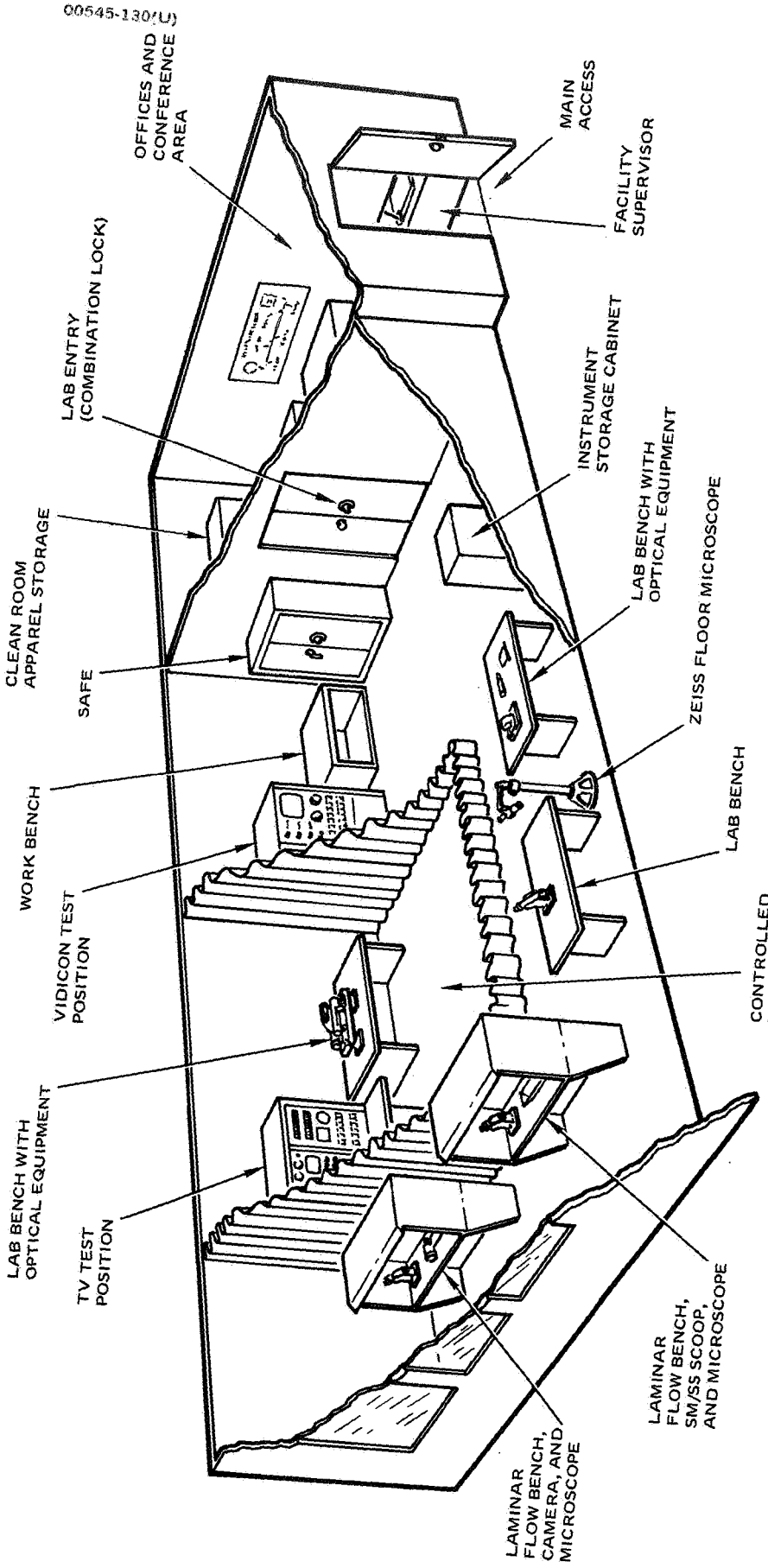

Figure A-3. Sketch of Surveyor Parts Test Facility

coordination was instrumental in arriving at quick decisions relative to continuation or changes in the test program. It also provided for effective implementation of the TFR system to ensure that anomalies were pursued to the desired degree of depth, when appropriate, and to ensure that relatively unimportant failures such as those not attributable to the lunar environment did not consume an unwarranted effort.

A. 3 FACILITY AND PARTS CONTROL

A special facility was established for the Surveyor Parts Test Program, including the TV camera program reported here and the companion NASA contract. This facility was located on the east side of Building 5 in the Hughes Aircraft Company Culver City plant, and included a laboratory area of approximately 35 by 20 feet and an adjacent office area of approximately 15 by 20 feet. A view of the facility is shown in Figure A-3. The facility was completed 10 January 1970, prior to the arrival of the Surveyor parts.

The Surveyor facility was maintained and operated as a self-enclosed laboratory to provide for the required degree of cleanliness and security. Controlled access was provided through a single entry point. Limited access to the laboratory itself was provided through a locked door between the office and the laboratory area and was closely monitored. The security system, described in detail in Administrative Bulletin 1, also featured an alarm system and periodically revised passwords.

The required degree of cleanliness was maintained by ensuring that the facility met the general requirements of a Class 100,000 clean area, as defined by Hughes HP 10-220. The airborne particle count was monitored according to the methods established by ASTM F-25. Two Agnew-Higgins laminar flow benches were provided for work on critical parts. These benches meet all requirements for Class 100 clean work stations.

A facility supervisor was appointed to administer the Surveyor facility and to monitor compliance with all required regulations. The duties of the facility supervisor, described in Administrative Bulletin 3, included the management of the parts control system described in Administrative Bulletin 1 and the preparation and maintenance of a comprehensive inventory system. All parts of the TV camera upon their removal from the camera, down to the smallest identifiable item (screw, piece of teflon, etc.), were carefully identified and inventoried. Periodic checks were

TABLE A-2. SURVEYOR III TV CAMERA TEST LOG BOOKS

Journal Number	Task Numbers*	Title
F1995	3 and 9	Survey Analysis and Optical Components Tests
F2450	4,13, and 15	Dismantling and Circuit Tests
F2452	6	Mirror Assembly and Optical Subsystems Tests
F2448	7	Vidicon Tests
F2451	14	Passive Components Tests
F2446	14	Diodes and Transistor Tests
F2447	8	Electrical and Mechanical Components Tests
F2637	8 and 14	Calculations and Notes on Components Tests
F1761	10	Conformal Coatings Tests
F1762	10	Physical Properties of Organic Materials
F2284	10	Adhesives Tests
F2286	10	Circuit Materials Tests
F2287	10	Chemical Properties Tests
F2289	10	Lubrication, Friction, and Wear Tests
F2640	10	Chemical Tests
F2638	10	Metallurgy Tests
F2291	10	Wire and Cable Tests
F2290	17	Surface Contamination Studies
F2449	11	Failure Analysis

*See Table A-1.

conducted to ensure total accountability. An important feature of this control system was the institution of special provisions for monitoring and documentation of the movement of all parts out of the Surveyor facility, including written statements of purpose of removal and signatures whenever an occasion arose to perform special tests on fixed test facilities at other Hughes or outside laboratories.

The latest issue of the complete inventory of all parts is available in Hughes files. This inventory includes some 920 items into which the TV camera has now been disassembled and also some 100 items relating to the NASA contract. All parts are accountable – none has been misplaced.

A.4 DOCUMENTATION AND REPORTING

It was recognized that a most vital aspect of this program was a careful documentation and reporting of all test results because of the uniqueness of parts returned from the moon and the potential value of some of the data obtained. Accordingly, a carefully planned system was instituted for recording of all test data. This system, described in the Administrative Bulletin 7, featured maintenance of accountable log books, recording of all data in these log books, and accountability of all photographs. Separate log books were assigned to the principal investigators. The requirement to record all data in the log books was not restricted to Hughes investigators inside the Surveyor facility. All data taken by Hughes personnel on the TV camera parts outside of the Surveyor facility had to be transferred to and recorded in these log books. All data taken by outside investigators in the Survey facility was recorded in appropriate log books. Furthermore, data taken by outside investigators relative to the TV camera test program were, in many instances, transmitted to Hughes and subsequently recorded in these log books. The 19 log books used, listed in Table A-2, constitute a comprehensive history of all the tests conducted. A complete log of all photos taken is also available in the Surveyor files.

Documentation of anomalies and failures uncovered was recognized as a separate requirement; and appropriate provisions for documenting these problem areas and their disposition were instituted in the form of the TFR system described in Administrative Bulletin 8. Complete files on work conducted on each of these identified TFRs are also available.

An effort was initiated early in the program prior to receipt of the TV camera at Hughes to obtain past data on relevant design features and test histories of the various subsystems, components, and materials of the TV camera. This task continued throughout the program. A library of such data was established, maintained, and updated, and was extensively utilized by all investigators.

The reporting system on the program included weekly coordination meetings, monthly reports, oral presentations, and the final report. Eleven monthly reports were issued. Three oral presentations were scheduled, and two have been held to date: the first on 22 April 1970 and the second on 6 August 1970. Copies of Vu-graphs used in these presentations were provided to the customer and to the audience. The final presentation has been scheduled to take place 26 and 27 January 1971.

APPENDIX B. DESCRIPTION OF LUNAR ENVIRONMENT

This appendix contains a brief description of the lunar environment. The information was compiled from data available at Hughes in support of the analysis and evaluation of the tests of the retrieved Surveyor III camera.

B. 1 THERMAL ENVIRONMENT (References 20 through 22)

Measurements of the lunar surface temperature as a function of phase angle indicate that the temperatures on the lunar equator vary from approximately 240° to 260°F at lunar noon (noneclipse) to approximately -250°F at lunar midnight. Actual temperatures vary slightly with surface characteristics, such as the thickness and composition of the dust layer; but these temperatures are considered good approximations. Reference 22 indicates that the temperatures seen by Surveyor III may have dropped to approximately -280°F just before lunar sunrise.

The expected lunar surface brightness at touchdown of Surveyor III was about 0°F. This was confirmed by camera temperatures. The peak lunar temperature rose to over 200°F within 6 earth days after touchdown, when camera operations were discontinued. Within this period, a total eclipse of the sun occurred, during which the surface temperatures dropped from over 200°F to less than -100°, and then rose back again to over 200° in about 6 hours.

B. 2 VACUUM

The lunar surface is a hard vacuum environment. Pressure is considered less than 10^{-11} Torr.

B. 3 ELECTROMAGNETIC RADIATION (Reference 23)

The sunlight environment is mentioned in passing. It is estimated that a photoelectric current of about 10^{-8} amp/cm^2 is produced by sunlight at 1 AU from most metallic surfaces. The solar wind current, for comparison, is 10^{-11} amp/cm^2. The solar electromagnetic radiation environment is described in Table B-1.

The ultraviolet spectrum base on the solar constant at 1 AU of 0. 14 watt/cm^2 is summarized in Table B-2.

TABLE B-1. SOLAR ENERGY DISTRIBUTION

Type	Wave Length, Å	Percent of Total Energy
Far ultraviolet	1 to 2,000	0. 02
Near ultraviolet	2,000 to 3,800	7. 28
Visible	3,800 to 7,000	41. 51
Near infrared	7,000 to 10,000	22. 1
Infrared	10,000 to 20,000	22. 97
Far infrared	20,000 to 100,000	6. 0

TABLE B-2. ULTRAVIOLET RADIATION SPECTRUM AT 1 AU

Wavelength, Å	Fraction of Total Energy Below hc/λ	Energy, ergs/cm^2/yr
1.0	10^{-11}	$10^2 - 10^3$
10	10^{-8}	$10^5 - 10^6$
100	10^{-6}	$10^7 - 10^8$
500	10^{-6}	10^8
1000	10^{-5}	10^8
1500	10^{-5}	10^9
2000	10^{-4}	4.0×10^9
2500	1.3×10^{-3}	6.0×10^{10}
3000	1.2×10^{-2}	5.0×10^{11}
4000	9.0×10^{-2}	4.0×10^{12}
5000	2.4×10^{-1}	1.1×10^{13}

TABLE B-3. SOME TWENTIETH CYCLE SOLAR PROTON EVENTS

Date of Event	Energy, protons/cm^2				
	>5 Mev	>10 Mev	>25 Mev	>30 Mev	>60 Mev
23 May 67	2×10^8		7×10^6		
9 June 68		3×10^8		1×10^7	3×10^6
6 July 68		7×10^7		3×10^6	1×10^6
26 Sept 68		7×10^7		1×10^7	4×10^6
28 Oct 68		2×10^8		1×10^7	9×10^5
17 Nov 68		1×10^9		2×10^8	3×10^7
3 Dec 68		2×10^8		4×10^7	5×10^6

B. 4 SOLAR FLARES (References 23 through 24)

Solar flare proton events occurring during the upper half (1956-1962) of the nineteenth solar cycle have been analyzed by several investigators. From Webber's data (References 24 and 26), the total proton fluence of the nineteenth cycle has been presented by

$$\phi sp\ (>E) = 1.5 \times 10^{12}\ E^{-1.53}\ p/cm^2,\ E \text{ in Mev}$$

Analysis of flare particulate radiation indicates that the alpha particle-proton ratio is approximately 0. 1. An estimate of the total alpha particle spectrum for the nineteenth cycle is given by

$$\phi\alpha(>E) = 7.5 \times 10^{10}\ E^{-1.53}\ \alpha/cm^2,\ E \text{ in Mev}$$

The presence of heavier nuclei has been reported by several investigators. Such contributions are probably quite small, however. Electrons in solar flares have also been observed, but little information is available on energy and fluences of the solar flare electrons. An equal number of electrons is believed to be emitted with the positively charged components as a sort of plasma cloud. Electron energies are probably considerably less than the proton energies.

Hughes has obtained some data on twentieth cycle solar flare events from ESSA. During the time period between the Surveyor III mission and the Apollo XII mission, there were a number of solar flares. Hughes has obtained preliminary flux data for some of the larger flares. These data are presented in Table B-3 where the proton flux numbers represent the total integrated flux of protons with energy greater than the energies shown.

Again, the data in Table B-3 are preliminary and not all-inclusive. For comparison, data for 30 solar proton events in the nineteenth solar cycle are presented in Table B-4. These data are also not all-inclusive, including only the larger events from early in the nineteenth cycle when data acquisition was not as sophisticated.

B. 5 GALACTIC RADIATION (Reference 23)

This is a minor contributor to the lunar environment. Galactic radiation intensity is estimated at approximately 4 particles/cm^2-sec.

TABLE B-4. NINETEENTH CYCLE SOLAR PROTON EVENTS

Date of Event	Energy, protons/cm^2			
	>1 Mev	>10 Mev	>30 Mev	>100 Mev
23 Feb 56		1.8×10^9	1.0×10^9	3.5×10^8
3 Aug 56			2.5×10^7	6.0×10^6
20 Jan 57			2.0×10^8	7.0×10^6
29 Aug 57			1.2×10^8	3.0×10^6
20 Oct 57			5.0×10^7	1.0×10^7
23 Mar 58		2.0×10^9	2.5×10^8	1.0×10^7
7 July 58		1.8×10^9	2.5×10^8	9.0×10^6
16 Aug 58		4.0×10^8	4.0×10^7	1.6×10^6
22 Aug 58		8.0×10^8	7.0×10^7	1.8×10^6
26 Aug 58		1.5×10^9	1.1×10^8	2.0×10^6
22 Sept 58		9.0×10^7	6.0×10^6	1.0×10^5
10 May 59	2.0×10^{11}	5.5×10^9	9.6×10^8	8.5×10^7
10 July 59	3.0×10^{11}	4.5×10^9	1.0×10^9	1.4×10^8
14 July 59	5.0×10^{11}	7.5×10^9	1.3×10^9	1.0×10^8
16 July 59	3.0×10^{11}	3.3×10^9	9.1×10^8	1.3×10^8

Table B-4 (continued)

Date of Event	Energy, protons/cm^2			
	>1 Mev	>10 Mev	>30 Mev	>100 Mev
1 Apr 60		1.5×10^7	5.0×10^6	8.5×10^5
28 Apr 60		1.3×10^7	5.0×10^6	7.0×10^5
4 May 60		1.2×10^7	6.0×10^6	1.2×10^6
13 May 60		1.5×10^7	4.0×10^6	4.5×10^5
3 Sept 60		9.0×10^7	3.5×10^7	7.0×10^6
26 Sept 60		2.0×10^7	2.0×10^6	1.2×10^5
12 Nov 60	1.0×10^{11}	4.0×10^9	1.3×10^9	2.5×10^8
15 Nov 60	8.0×10^{10}	2.5×10^9	7.2×10^8	1.2×10^8
20 Nov 60		1.4×10^8	4.5×10^7	8.0×10^6
11 July 61	7.0×10^{10}	1.7×10^7	3.0×10^6	2.4×10^5
12 July 61		5.0×10^8	4.0×10^7	1.0×10^6
18 July 61	6.0×10^9	1.0×10^9	3.0×10^8	4.0×10^7
20 July 61		1.5×10^7	5.0×10^6	9.0×10^5
28 Sept 61		5.0×10^7	6.0×10^6	1.1×10^6
23 Oct 62		6.0×10^5	1.2×10^5	1.0×10^4

Galactic radiation consists primarily of protons and alpha particles with some heavier positive nuclei, electrons, and protons. The galactic particles have energies estimated at approximately 10^8 to 10^{19} ev. The particles of lower energies are affected by solar activity.

B.6 SOLAR WIND (Reference 23)

The solar wind is a plasma emitted more or less continuously by the sun. The only particles definitely identified are protons, although a small (<1 percent) alpha particle component may also be present. Electrons have been harder to detect, but theories on the nature and origin of the plasma indicate the cloud should be approximately electrically neutral. The proton density is probably about 1 to 10/cc at 1 AU. The directed velocity of the plasma cloud is rather high, varying from about 300 km/sec (quiet sun) to about 1000 im/sec (active sun) at 1 AU. The protons in the solar wind have thermal energies of about 1 to 10 kev, corresponding to thermal velocities of about 100 km/sec at 1 AU.

There is considerable variation in the solar wind in both particle energies and fluences. Short-term (on the order of minutes) fluctuations of 50 percent have frequently been observed. Greater variations are observed between quiet sun and active sun periods.

B.7 METEORITES (References 20, 27, and 28)

NASA defines the maximum cometary meteoroid flux as one impact/m^2/sec, corresponding to particle weights of 10^{-10} to 10^{-11} grams of 1.94×10^{-5} cm diameter. Based on this information, meteoroic erosion for magnesium and aluminum in the lunar atmosphere is calculated at 1.5×10^{-13} cm/sec. The rates for corpuscular sputtering and sublimation are 1 to 2×10^{-13} gm/cm^2-sec.

This is not the whole story, however. It is estimated that 99 percent of the meteoric mass which impacts on the moon consists of dust balls with masses less than 10^{-6} gram. Except for the case where the lunar surface material is such that particles penetrate the mean surface to a depth of many particle diameters before coming in contact with lunar material, the mass of material excavated is three to five orders of magnitude greater than that of the primary impacting meteoroids. Adding the effects of secondary material will, at most, double the mass of the lunar material estimated.

The velocities of most secondary particle population is much less than the velocity of the primary meteoroid particles. However, secondary particles with velocities of 50 to 100 m/sec are sufficiently energetic to cause production of tertiary particles.

Hence, damage from secondary and tertiary dust particles must be considered along with the effects of primary meteoric impacts to obtain the total picture.

APPENDIX C. DESCRIPTION AND CHECKOUT OF ELECTRICAL TEST EQUIPMENT

In order to conduct the electrical performance tests of the selected flight camera chassis, it was required to establish and check out a suitable test facility. Fortunately, major components of this facility were available from the Surveyor program at JPL. This appendix briefly describes the major components of this test facility and summarizes the calibration and checkout tests conducted.

The test facility included, in addition to the special TV camera Surveyor test position, certain commercial equipment and special tooling. The complete list is given below.

C. 1 TV CAMERA EQUIPMENT

TV Camera Test Position, consisting of:

Monitor, Command Generator, HAC E242926

Panel, Test Paint, HAC E242930

Panel, Sync Separator, HAC 242998

Monitor, Conrac TV Model C55-6

Panel, Bridge, Temperature Sensing, HAC E242976

Panel, TV Monitor Input

Voltmeter, Digital, NLS Model 484A

VTVM, HP Model 412AR

Supply, Power, Power Designs Model 3650

Supply, Power, Power Designs Model 5015A

Light Box, Variable Intensity, HAC 264821-100

Test Patterns

Vertical resolution	4 each
Horizontal resolution	4 each
Iris setting	1 each

Photometer, Spectra

Brightness Source, Spectra

Transformer, Variac Model W-20-M

C.2 COMMERCIAL EQUIPMENT

Oscilloscope, Tektronix Model 535A

Plug-in, Tektronix Type Z

Plug-in, Tektronix Type CA

Frequency Counter, HP Model 5233L

Supply, Power, Power Designs Model 5015A (4 each)

VTVM, HP Model 412AR

Voltmeter, Digital, NLS Model 484

Camera, Scope, Tektronix, Model C12

Oscillator, HP 200 CDR

C.3 SPECIAL EQUIPMENT AND TOOLING

Torque, Screw Driver

Torque, Wrench

Tripod

Mount, Universal

Adapter, Pull Gauge

Fixture, Camera Test

Bracket, ECU Support

Collar, Camera Mount

Fixture, ECU

Wrench, Yoke

Wrench, Spanner

The procurement of the equipment and tooling involved locating much of the camera test equipment and tooling utilized during the original Surveyor program. In some cases, some of the essential items had been salvaged and required the purchase or fabrication of that particular item to support the operation. For example, a TV camera test fixture for supporting the camera during test and dismantling had to be fabricated. This test fixture is shown in Figure C-1.

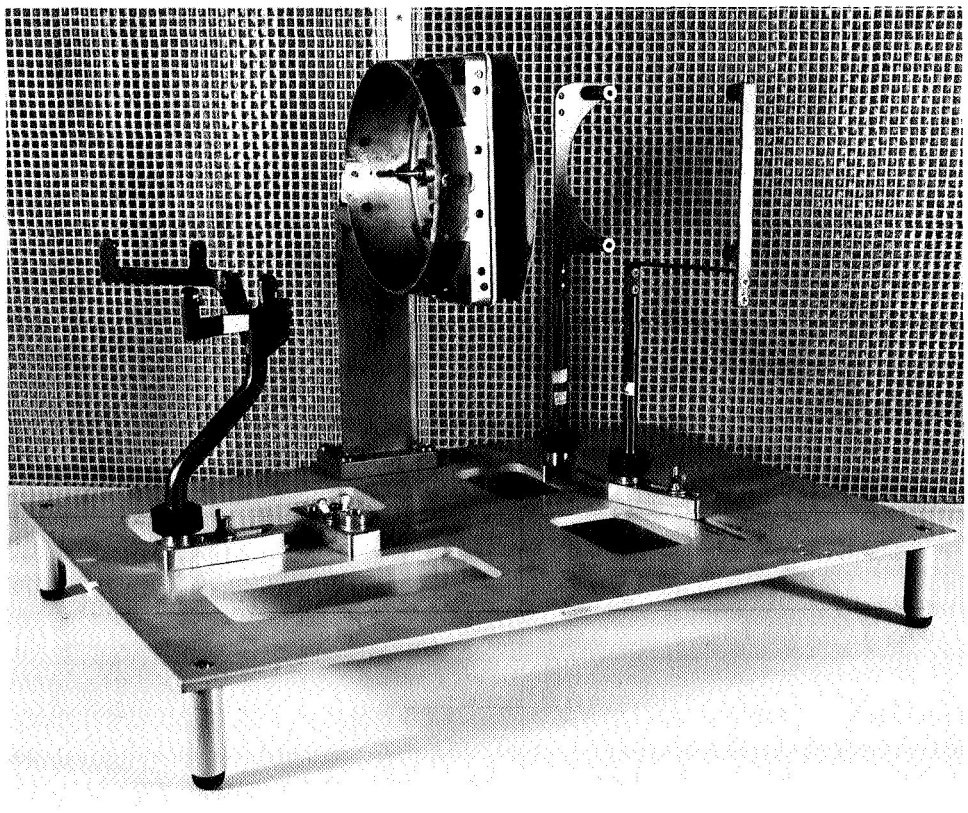

Figure C-1. Test Fixture for Supporting Camera During Dismantling (Photo 4R15897)

All the equipment used in measuring precise torques, parameters, etc., were processed through the Hughes Primary Standards and Instrument Calibration Laboratory for checkout and calibration.

The TV test equipment and its support equipment also were checked out for proper operation, and the necessary repairs were made.

As a final checkout of the equipment, an operational check of the spare TV camera was performed to the original test specification to verify the complete test setup.

All the calibration and checkout operations were successfully completed, validating proper functioning of the test facility.

APPENDIX D. FUNCTIONAL DESCRIPTION OF CHASSIS A-4

The functional description of electronic chassis A-4, which was tested for its electrical performance (as summarized in Section 4.5), is presented here. The chassis schematic diagram, Hughes Document 284346, is presented in Figure D-1.

Chassis A-4 contained the sweep, blanking, and synchronization circuits required for operation of the vidicon in its primary 600-line mode of operation. Figure D-2 is a block diagram of these functions.

D.1 VERTICAL SWEEP/BLANK CIRCUIT

D.1.1 General Description

The vertical sweep and blanking pulses are generated by a free running sawtooth generator. The sawtooth output is used to provide the required sawtooth current for the deflection yoke. Three vertical blanking pulses are provided by the circuit:

1) One output blanks the vidicon during vertical retrace time.

2) The second output is combined with the horizontal blanking and sync pulse for subsequent summing with the video in the video amplifier.

3) The third output provides retrace time reference for the video logic circuit.

D.1.2 Vertical Sweep Generator and Constant Current Source

Transistors Q16 and Q17 form a free-running multivibrator which produces, in conjunction with A18, the normal mode sawtooth waveform necessary for vertical deflection of the vidicon beam. The period of the vertical sawtooth, including retrace, appearing across charge capacitor C14 is 1.2 seconds +15 to -8 percent. The charge capacitor is located on the ECU assembly and identified as 652C14. The capacitor is electrically connected to chassis 4 at pins 340-10 and 340-16.

Reference to the waveforms in Figure D-3 will aid in the explanation of the circuit. Time t_0 is the time immediately following Q17 cutoff and Q16 turnon. Figure D-3e illustrates the voltage waveform at the junction of 652C13 and CR8. This voltage is the sum of the collector voltage of Q16 and the negative charge of C13. Since C13 is tied to +25 volts through R57 and R58, it begins to charge exponentially from its initial negative potential to some positive potential (25 volts - Q16 collector voltage). A t_0 negative voltage from the junction of R59 and R60 keeps Q17 cut off. While Q17 is cut off, charge capacitor C14 charges linearly through constant current source Q18. At time t_1 (Figure D-3e), the voltage at the junction of CR8 and C13 has risen sufficiently to overcome the back bias on CR8.

Conduction through the diode raises the potential on the base of Q17 above cutoff. Conduction through Q17 raises the potential at the junction of R56 and CR7, thereby decreasing the collector current of Q16. Regenerative action rapidly reverses the state of the multivibrator, and the multivibrator remains in this condition during the period t_1 to t_2. Q17 will conduct for 0.2 second, discharging sweep capacitor C14 and forming the retrace portion of the sweep waveform. The retrace time is determined primarily by the RC time constant of R56 and C14. During this 0.2 second period, C13 accumulates a negative charge on the side tied to CR8. 652C13 is mounted on the ECU and is electrically connected to chassis 4 at pins 340-12 and 340-22. At t_2, the decrease in base and collector voltages of Q17 results in transistor turnoff and reversal of the multivibrator back to its original state.

The purpose of CR7 is to prevent the voltage applied to the emitter of Q16 from exceeding the V_{BE} rating of the transistor. CR8 removes R59 from the discharge path of C13, and it prevents the V_{BE} rating of Q17 from being exceeded. The sawtooth voltage appearing across C14 is coupled to the base of Q19 as the normal mode vertical sweep. The positive pulse from the junction of R54 and R55 is coupled to the base of Q15 as the normal mode vertical blanking signal.

D.1.3 Emitter Follower

The vertical sawtooth sweep signal is applied to emitter follower Q19. Q19 prevents loading of the sweep generator circuit. The output signal from the emitter of Q19 is directly coupled to the base of Q20 by zener diode CR9. Direct coupling is required because of the low frequency of the vertical sweep. Use of the zener diode allows unattenuated direct coupling of the sweep signal. It also provides proper biasing for Q20. C15 reduces any noise produced by CR9.

D.1.4 Vertical Driver

The vertical driver Q20 provides a sawtooth current waveform to the vertical deflection yoke during normal mode operation. The amplitude of the current waveform is determined by the selection of normal mode vertical

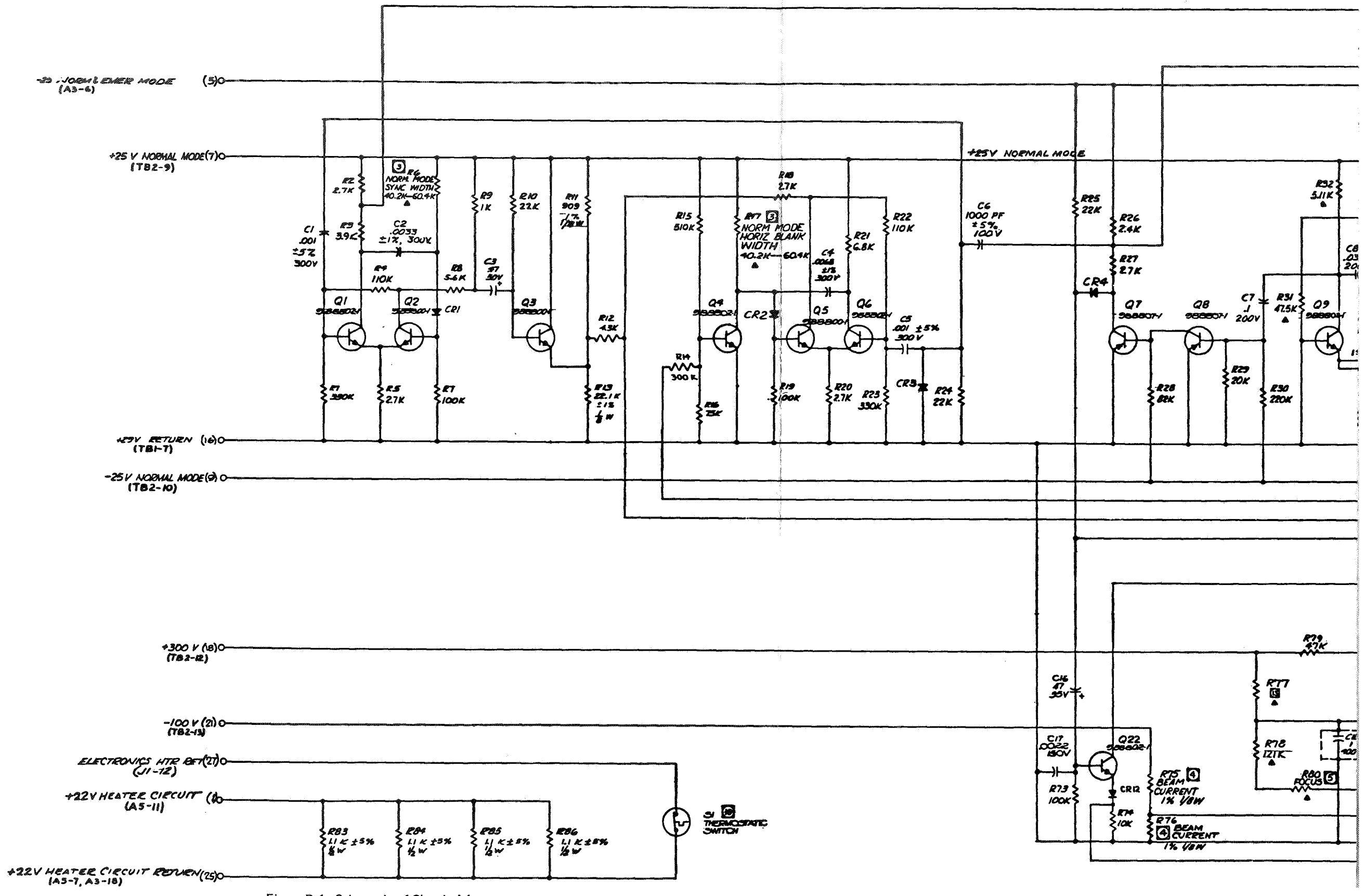

Figure D-1. Schematic of Chassis A4

(22) VERTICAL FREQ CAPACITOR (TB1-C13A)

(2) NORMAL MODE KEYED CLAMP DRIVE (A3-1)

(3) NORMAL MODE HORIZONTAL SWEEP OUTPUT (A3-1)

(26) TEST HORIZONTAL BLANKING PULSE (J1-28)

(24) NORMAL MODE VERTICAL BLANKING PULSE (J3-14, A3-9)

(23) NORMAL MODE VERTICAL SWEEP OUTPUT (L1-4, A3-7)

(10) VERT SWEEP CAPACITOR (TB1-C14A)

(11) NORM. MODE SYNC/BLANKING (A3-3)

(A) EMER MODE VIDICON BLANKING (A3-13)

(12) VERTICAL FREQ CAPACITOR (TB1-C13B)

(8)

(13) +25V NORM & EMER MODES (TB2-5)

R38 221K

R36 383K

R37 22.6K

R34 ③ H. FREQ 5.1K–16.9K

R39 1K

R43 ③ NORM MODE HORIZ CENT 24.9 – 1.33K ±1%, ¼W

R44 ③ 12K OR 14K

Q11 2N3807-1

Q12 2N3808-3

Q13 2N3838-1

Q10 2N3568-1

CR1 5.1V

C10 15 20V

CR10

R45 182 ±1% ⅛W

R46 ③ NORM MODE HORIZ AMPLI. RANGE 10 THRU 243Ω 1%, ½W

R35 10K

R38 48.7K

C9 .068 ±5% 200V.

R40 22K

R41 5.11K ±1% ½W

R42 10K ±1% ½W

R47 1.2K

+C11 100 20V

+23V RETURN

-25V NOM.

R48 2K

R51 10K

CR6

R49 3K

CR5

Q14 2N3807-1

Q15 2N3807-1

C12 47 35V

Q16 2N3802-1

R50 82K

R52 20K

R53 220K

R54 6.2K

R55 332K

C13 ② ⑥

CR7

R56 48.7K

R57 681K

R58 ③ VERT FREQ 301K–549K

CR8

R59 82K

R60 1 MEG

R61 68.1K

R62 10.2K

CR11

Q17 2N3800-1

Q18 2N3807-1

R63 274K

C14 ⑥ ⑥

Q19 2N3808-3

R64 1K

R65 68K

R66 68K

R81 330

CR9 1N3754

C15 47 35V

Q20 2N3802-1

Q21 2N3802-1

R67 1.3K ±1% ½W

R68 ③ 715 – 2.21K ±1%, ½W

NORM. MODE VERT AMPL

R69 ③ NORM MODE VERT. CENT. 1.10K–5.36K ±1%, ½W

R70 2.32K ±1% ½W

R71 47K

R72 1 MEG

TARGET VOLTAGE

(17) VIDICON TARGET VOLTAGE (A5-4)

③ RB2 - 1.96K-69.8K

(20) GRID NO. 5 VOLTAGE (TB4-3, A3-11)

⑦ C19 .1 400V

(15) GRID NO.2 & NO.4 VOLTAGE (TB1-C18-A)

⑥

(4) GRID NO. 3 VOLTAGE (XV1-3)

RB1 FOCUS ⑥

(9) GRID NO. 1 VOLTAGE (XV1-2)

(13) CATHODE VOLTAGE (XV1-7)

TO V1 (VIDICON TUBE)

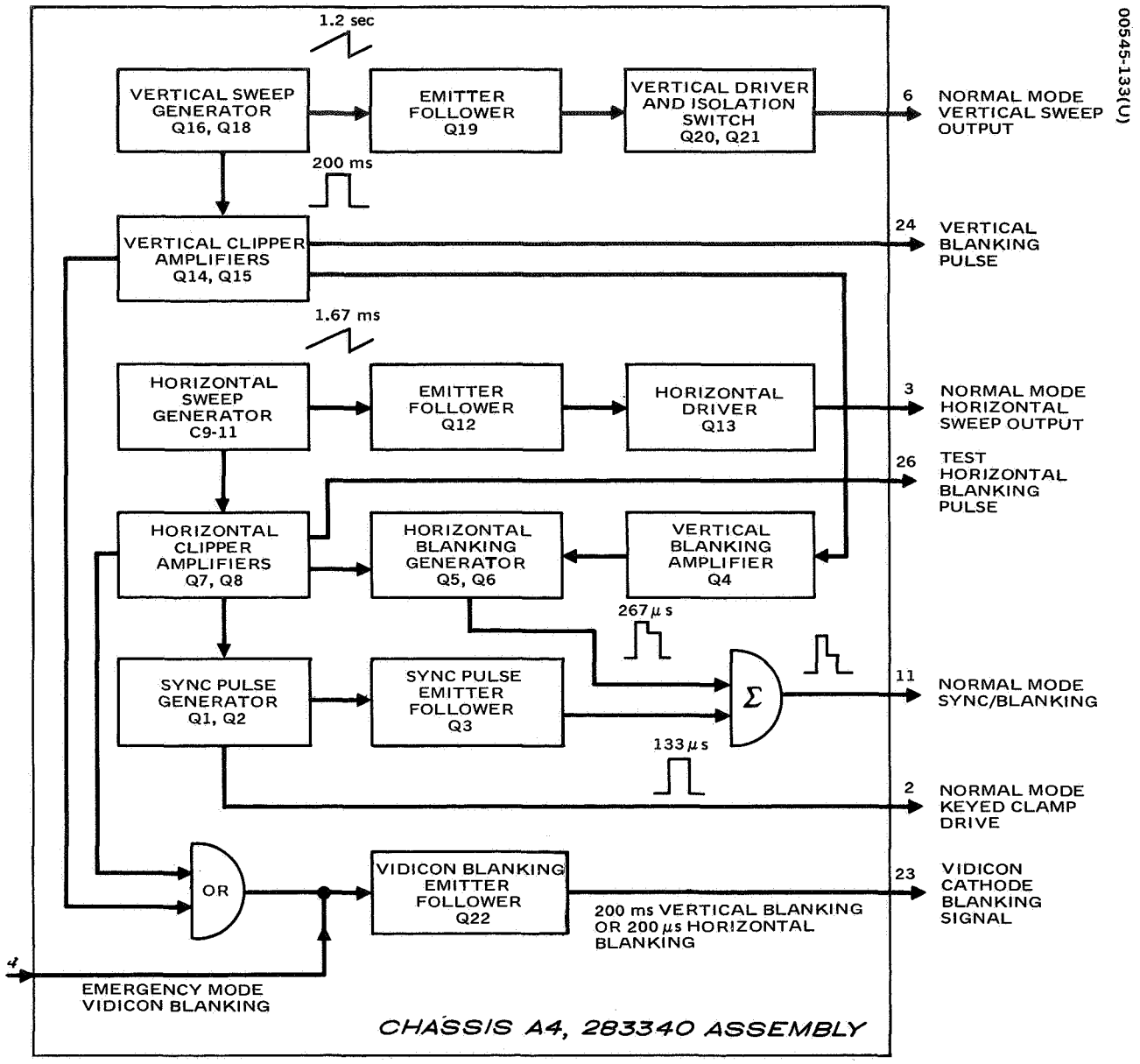

Figure D-2. Normal Mode Sweep Generating and Sync/Blanking Function

amplitude resistor R68. The dc level of the current through the deflection yoke is determined by the value of normal mode vertical centering selected resistor R69. The vertical sweep signal is sent out of chassis 4 to the yoke at pin 340-6.

D. 1. 5 Isolation Switch

During normal mode operation, the voltage on the base of Q21 is sufficiently positive to allow current flow through the transistor. A portion of this current flows through Q20 and the rest flows through the deflection coil to ground. During 200 line mode operation, Q21 is cut off by the negative voltage applied to the base. Thus, 200 line mode vertical deflection current cannot be coupled through the deenergized resistor networks in the collector circuits of Q21 and Q13 to the horizontal deflection yoke.

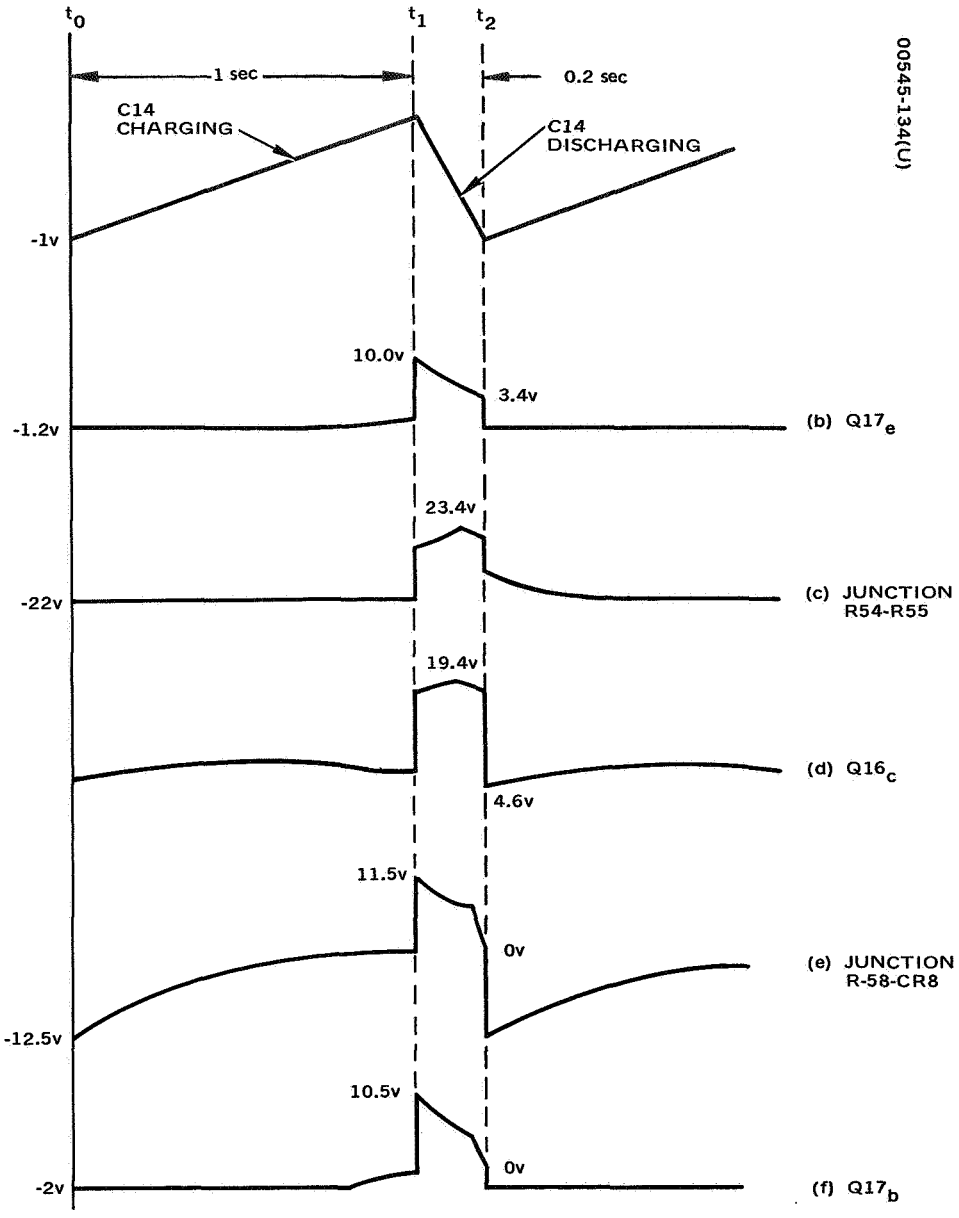

Figure D-3. Vertical Sweep Generator Waveforms – Normal Mode

D. 1. 6 Clipper Amplifiers

The positive pulse appearing at the junction of R54 and R55 during the vertical sweep retrace period is coupled through Q12 to the base of first clipper amplifier Q15. The pulse is amplified and shaped by Q15 and also by second clipper amplifier Q14. Three positive pulse outputs are provided in the collector circuit of Q14 as shown in Figure D-4. The first output is taken from the junction of R48 and R49, coupled through diode CR6, sent out of chassis 4 at pin 340-24, applied to chassis 5 at pin 650-9, and finally applied to the video logic circuits. CR6 of chassis 4 is part of an OR gate; the other half of the OR gate is CR9 of chassis 3. The output of the OR gate

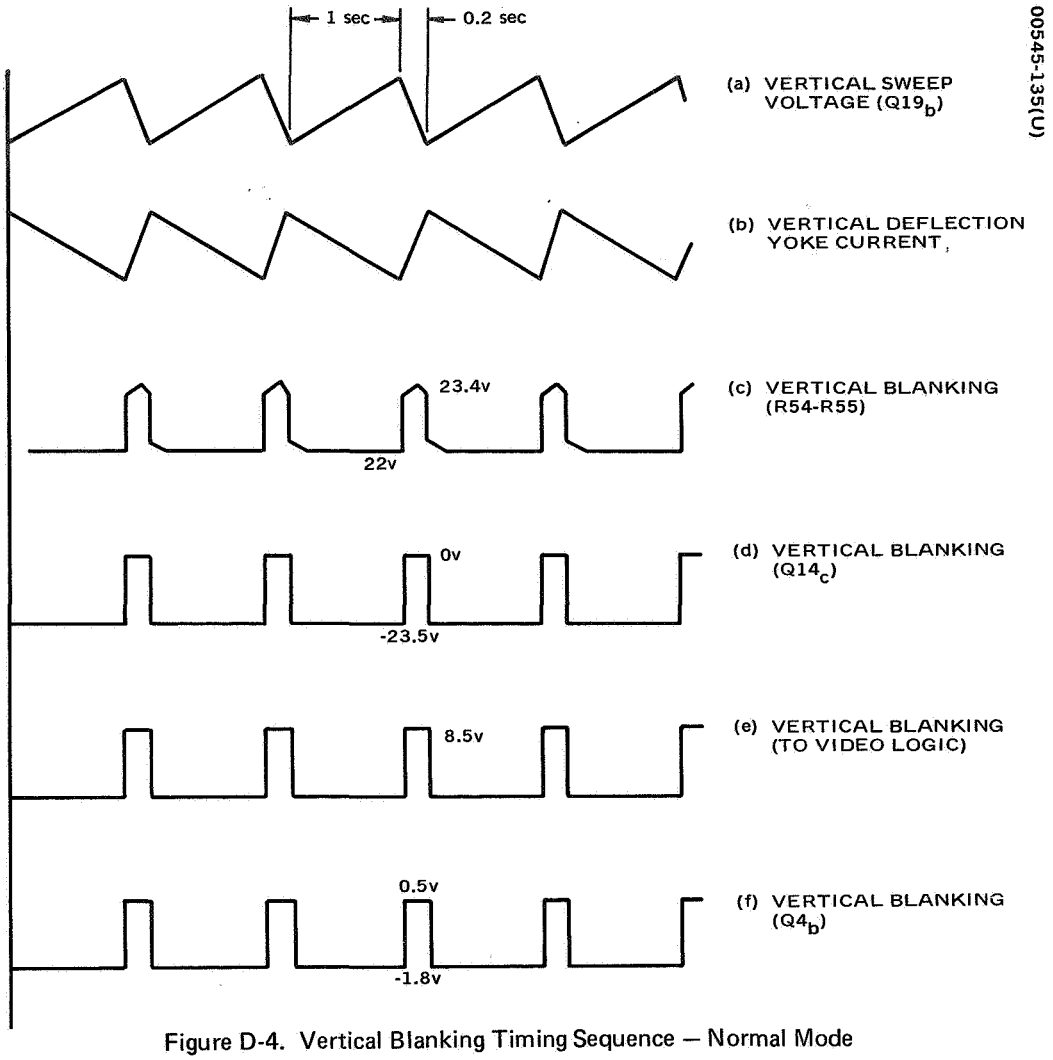

Figure D-4. Vertical Blanking Timing Sequence – Normal Mode

is either the normal mode vertical blanking reference signal – which is the signal under discussion – or the 200 line mode vertical blanking reference and is utilized in video logic A and B circuits.

The OR gate output is also made available for external use at J1-14. A second output of Q14, taken directly off the collector, is applied through R14 to the base of vertical blanking amplifier Q4. The summation of this signal with the horizontal blanking pulse is covered in Section D.3. The third output from Q14 is applied to CR5 which is part of a four input OR gate (CR4 and CR5 in chassis 4 and CR4 and CR8 in chassis 3). The OR gate output is applied to the base of vidicon blanking emitter follower Q22. The signal provides horizontal and vertical blanking of the vidicon during either normal or 200 line mode operation.

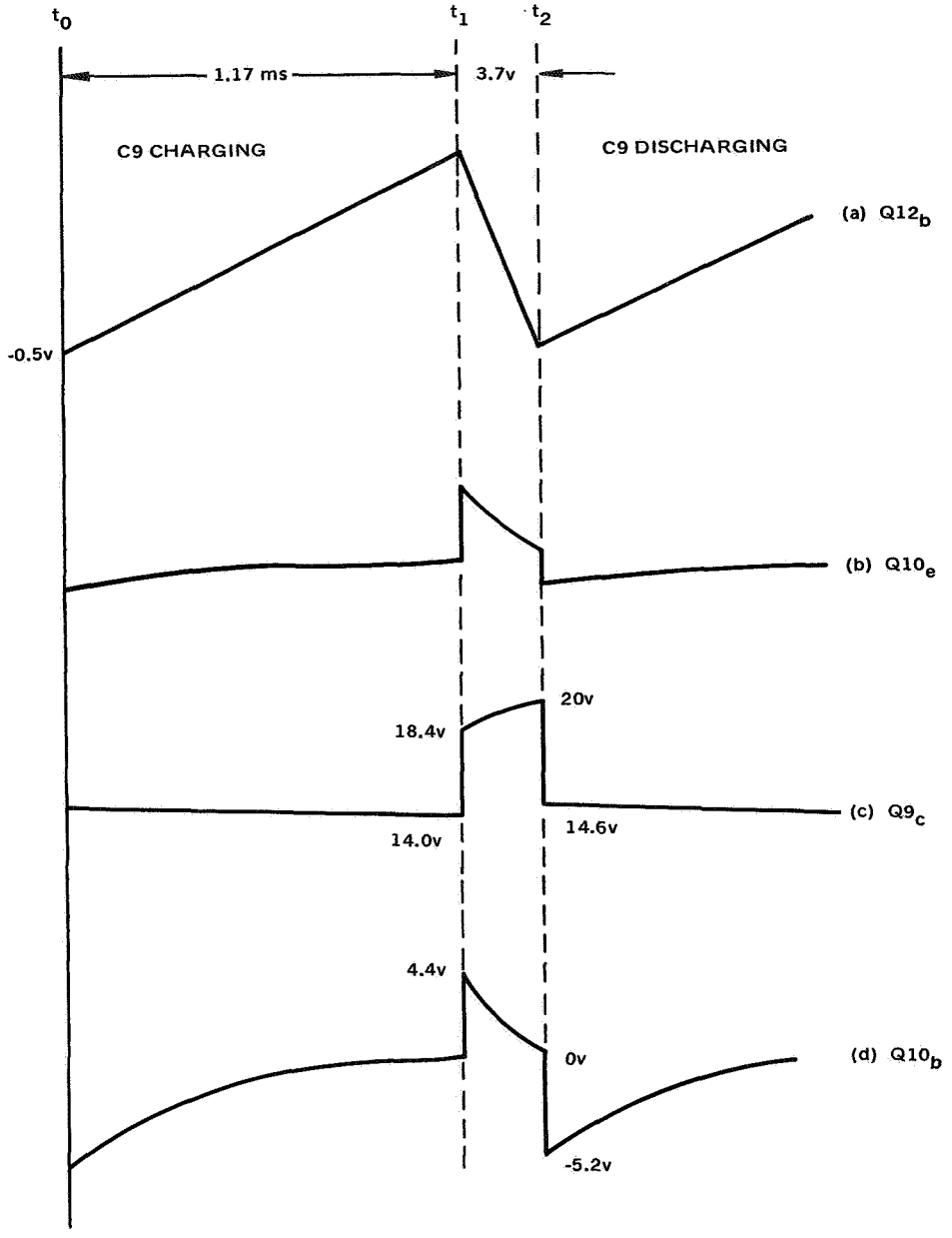

Figure D-5. Horizontal Sweep Generator Waveforms – Normal Mode

D. 2 HORIZONTAL SWEEP/BLANK CIRCUIT

D. 2. 1 General Description

The horizontal sweep and blanking pulses for the normal mode are generated by a free-running multivibrator in conjunction with a charging transistor which acts as a constant current source. The sawtooth output is

utilized to provide the required sawtooth current for the deflection yoke. The horizontal blanking pulses are utilized to perform the following functions:

1) Triggering horizontal sync generator

2) Triggering horizontal blanking generator

3) Blanking vidicon during horizontal retrace time

4) Synchronizing external monitor display

D. 2. 2 Horizontal Sweep Generator and Constant Current Source

The horizontal sweep generator, Q9 and Q10, in conjunction with the constant current source transistor, Q11, generates a 600 cps sawtooth waveform across sweep capacitor C9 (Figure D-5a). Q9 and Q10 form a free-running multivibrator, and the sweep waveform is generated during the time that Q10 is cut off. C9 charges linearly through Q11 while Q10 is cut off. Reference to the waveforms in Figure D-5 will aid in the explanation of the circuit. Time t_0 is the time immediately following Q10 cutoff and Q9 turnon. The charge on the side of a capacitor C8 that is tied to the base of Q10 will be negative at this time. The capacitor charges positively from this initial negative potential toward some positive value (determined primarily by the values of R31 and R33). When the exponential rise is sufficient on the base of Q10, the transistor will conduct discharging sweep capacitor C9. When Q10 conducts, the increase in its emitter voltage appears on the emitter of Q9. Current flow through Q9 falls off, resulting in a rise in the collector voltage. This voltage rise is coupled to the base of Q10, and the regenerative action rapidly reverses the state of the multivibrator. The multivibrator will remain in the reversed state, i. e., with Q10 on and Q9 off, for 0. 2 ms. The retrace time of 1. 2 ms is determined primarily by the RC time constant of R35 and C9. During this 0. 2 ms period, capacitor C8 acquires a negative charge and the base voltage of Q10 decreases. The decrease in base voltage in conjunction with the decrease in collector voltage of Q10 results in transistor turnoff. The drop in emitter voltage of Q10 is directly coupled to the emitter of Q9, causing it to conduct and returning the multivibrator back to its original state. The cycle is then to be repeated, resulting in the generation of another horizontal sawtooth waveform. Normal mode horizontal frequency resistor R43 is selected during test to produce the desired 600 cps sawtooth.

D. 2. 3 Emitter Follower

The horizontal sawtooth sweep signal developed across C9 is applied to the base of emitter follower Q12. Q12 prevents loading of the sweep generator circuit. The output signal is coupled through C10 to the base of horizontal driver Q13. The corresponding circuit in the vertical sweep circuit utilized direct coupling since the frequency was much lower.

D. 2. 4 Horizontal Driver

The horizontal driver Q13 provides a sawtooth current waveform to the horizontal deflection yoke during the normal mode of operation. The amplitude of the current waveform is determined by the selection of the normal mode horizontal amplitude resistor R46. The dc level of the current through the deflection yoke is determined by the value of the selected normal mode horizontal centering resistor R43.

D. 2. 5 Clipper Amplifiers

The positive pulse appearing at the collector of Q9 during the retrace period of the sweep is coupled through C7 to the base of the first clipper amplifier Q8. The pulse is amplified and shaped by Q8, and the negative pulse appearing at the collector is directly coupled to the base of second clipper amplifier Q7. The pulse is again amplified and shaped by amplifier Q7. Three outputs are provided from the collector circuit of Q7: One output is fed through CR4 (part of a four input OR gate consisting of CR4 and CR8 in chassis 3 and CR4 and CR5 in chassis 4) and C16 to the base of Q22, the vidicon blanking emitter follower. The second output is taken from the junction of R26 and R27 and is fed through C6 and utilized as a trigger for the sync generator (Q1 and Q2) and the horizontal blanking generator (Q5 and Q6). The third output, which is also taken from the junction of R26 and R27, is sent out of chassis 4 at pin 340-26 to J1-28. It is utilized for blanking of a viewing monitor external to the camera.

D. 3 COMPOSITE BLANKING CIRCUIT

D. 3. 1 General Description

The composite blanking circuit generates horizontal sync pulses and horizontal blanking pulses and sums these two signals with the vertical blanking pulse to form a single composite normal mode sync/blank output. The output is then summed with the video signal in chassis 5 to complete the composite video signal required by the ground monitor for picture reproduction.

D. 3. 2 Horizontal Blanking Generator

The 200 microsecond blanking pulse from the collector circuit of Q7 is differentiated by C6 and R24. The positive differentiated pulse, which is coincident with the leading edge of the blanking pulse, is coupled through C9 to the base of Q6 and through C1 to the base of Q1 to serve as a trigger for both stages. Q1 is the sync pulse generator, and its operation is discussed in Section D. 4. CR3 clips the negative spike generated by differentiating of the trailing edge of the blanking pulse.

C5 and Q6 form a monostable multivibrator with Q5 normally conducting and Q6 normally cut off. The positive voltage applied to the base of Q5 from the voltage divider consisting of R19, CR2, and R17 is sufficient to allow conduction. Conduction of Q5 results in a positive voltage being applied to the emitter of Q6, preventing conduction of Q6. When the positive trigger pulse is applied to the base of Q6, collector current flows and collector voltage drops. The decrease in Q6 collector voltage is coupled through C4 to the anode of CR2, back-biasing the diode. The positive bias is removed from the base of Q5, resulting in turnoff of Q5. Hence, the trigger pulse reverses the state of the multivibrator. Since C4 is connected to 25 volts through R17, the voltage at the junction of C4 and CR2 rises toward that value at an exponential rate. When the voltage rises sufficiently, the back bias is removed from CR2, resulting in a positive voltage being applied to the base of Q5. When this voltage is positive enough to overcome the bias on the emitter Q5 due to the conduction of Q6, the multivibrator reverts back to its original state. The horizontal blanking pulse appearing at the collector of Q5 is a positive pulse of 267 microsecond duration (Figure D-6h).

D.3.3 Vertical Blanking Amplifier

The base of vertical blanking amplifier Q4 is tied to a voltage divider consisting of R14, R15, and R16. Under normal circumstances, the positive voltage applied to R15 and the negative voltage applied to R14 results in a negative voltage on the base of Q4 which keeps the transistor cut off. During vertical blanking time, a positive going pulse from the collector of Q14 raises the voltage applied to R14 to approximately ground potential. This voltage, in conjunction with the positive voltage applied to R15, results in a positive pulse appearing on the base of Q4 that will allow the transistor to conduct. When Q4 conducts, the collector voltage falls to a value very close to ground potential. This decrease in collector voltage is sufficient to cut Q5 off. When Q5 cuts off, the voltage applied to the emitter of Q6 decreases, allowing conduction through Q6. The multivibrator remains in the reversed condition until the vertical blanking pulse is removed. Removal of the blanking pulse returns the multivibrator to its stable condition. The sync trigger pulses are still applied to the base of Q6 during vertical blanking time but have no effect since the transistor is already conducting. The signal at the collector of Q5 is a positive 0.2 second pulse of the same amplitude as the horizontal blanking pulse as illustrated in Figure D-7a.

The vertical/horizontal blanking pulses appearing at the junction of R12 and R18 are combined with the sync pulse from Q3 to form the normal mode sync/blanking signal. The signal leaves chassis 4 at pin 340-11 and enters chassis 5 at pin 650-5, where it is applied to an OR gate in the video circuits.

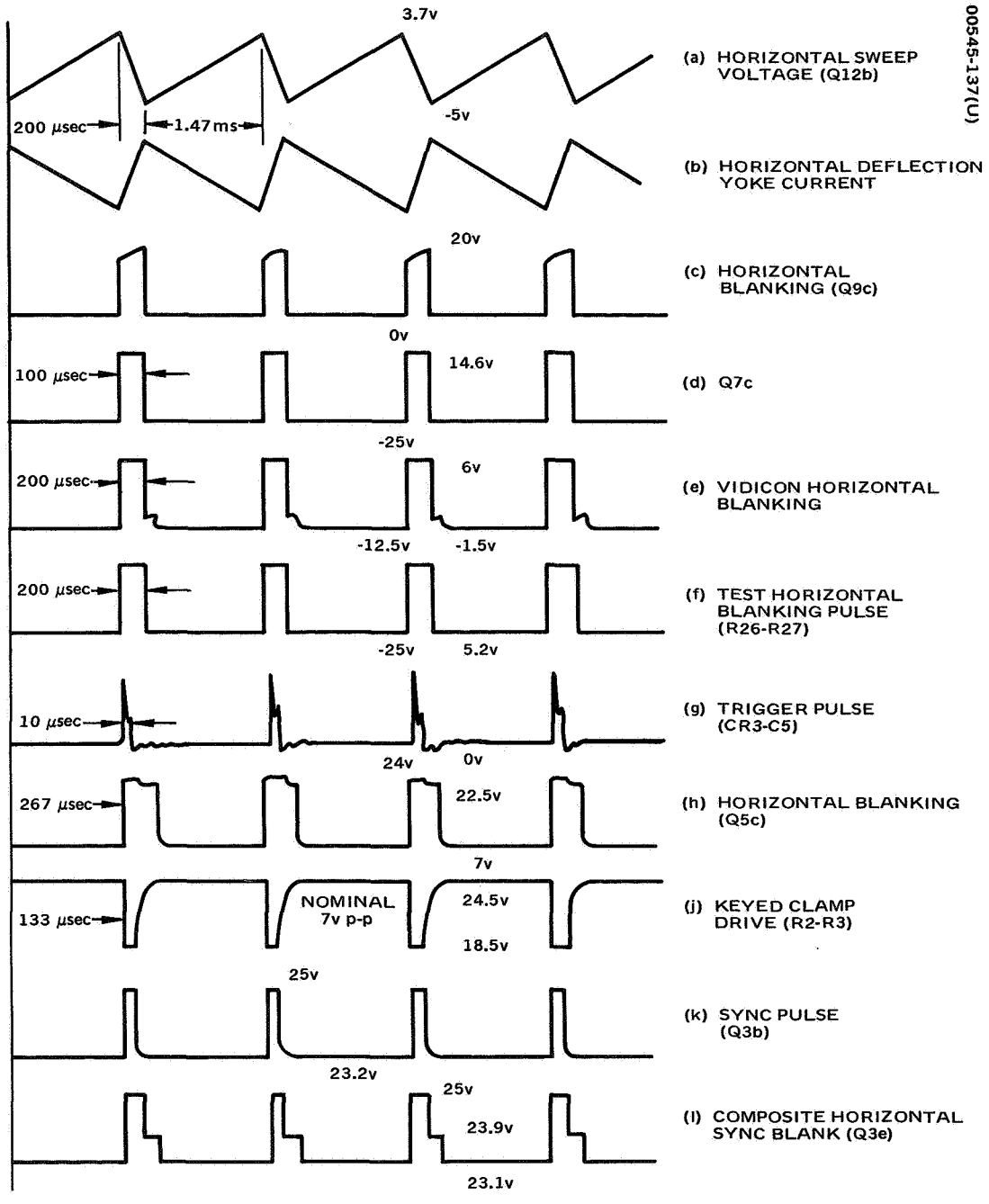

Figure D-6. Horizontal Sync/Blank Timing Sequence — Normal Mode

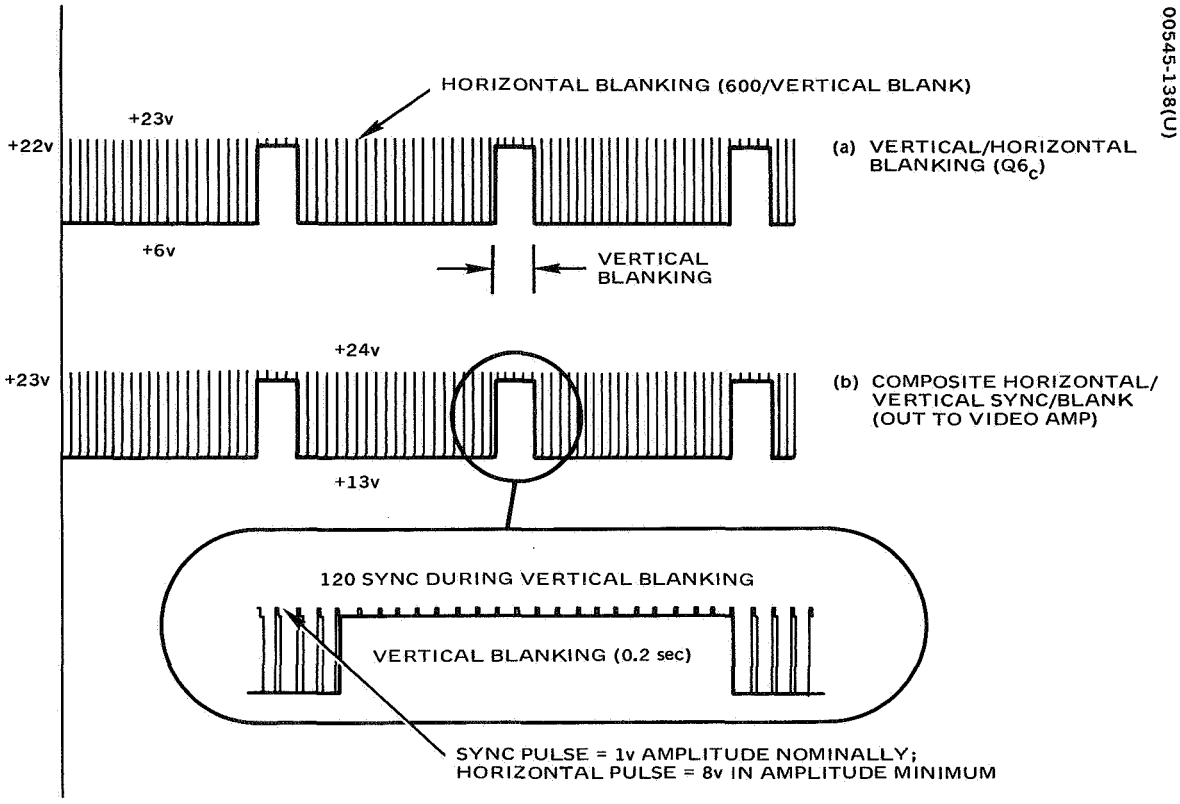

Figure D-7. Composite Sync/Blank Timing Sequence – Normal Mode

D.4 SYNC PULSE CIRCUIT

D.4.1 General Description

The sync pulse circuit generates positive 133 microsecond pulses, the leading edges of which are coincident with the leading edges of the horizontal blanking pulses. The sync pulses are summed with the vertical/horizontal blanking pulses from the horizontal blanking generator Q5-Q6.

D.4.2 Sync Pulse Generator

The positive sync trigger pulse from the differentiating network composed of C6 and R24 is coupled through C1 to the base of Q1. Q1 and Q2 form a monostable multivibrator with Q1 normally off and Q2 normally on. The trigger causes Q1 to conduct, and the decreasing collector voltage of Q1 is coupled through C2 to the anode side of CR1. Prior to receipt of the trigger pulse, conduction through CR1 placed a positive voltage on the base of Q2, allowing it to conduct. With CR1 back biased Q2 is cut off, and the multivibrator state is reversed. Since C2, which is initially charged negative, is tied to 25 volts through R6, the voltage at the junction of C2 and CR1 will rise at an exponential rate. When the voltage at this point goes positive, the back bias on CR1 is overcome, allowing current flow through R7. When the voltage across R7 is of sufficient magnitude, Q2 conducts, and the transistor reverts back to its original state. The time that the multivibrator is in the reversed state is determined primarily by the RC time constant of C2, R6, and R5. The normal mode sync width resistor R6 is selected during camera test to provide sync pulses of 133 ms duration. A negative going sync pulse taken from the junction of R2 and R3 is the normal mode keyed clamp drive (Figure D-6j), which is utilized by the clamping circuits in the video amplifier. The signal leaves chassis 4 at pin 340-2 and enters chassis 5 at pin 650-1. A positive going sync pulse is taken from the junction of R8 and R9. The pulse is coupled through C3 to the base of Q3, the sync pulse emitter follower.

D.4.3 Sync Pulse Emitter Follower

The sync pulse emitter follower isolates the sync pulse generator, Q1 and Q2, from the horizontal blanking generator, Q6 and Q5. The positive sync pulse on the base of Q3 causes a similar voltage rise on the emitter of Q3. This voltage rise occurs during the first 133 microseconds of the horizontal blanking pulse. The positive going 267 used horizontal blanking pulse appears at the collector of Q5 and also at the junction of R12 and R18. Hence, the voltage rise of the emitter of Q3 will cause a positive sync pulse to appear on top of the horizontal blanking pulse at the junction of R12 and R16. The sync pulse will also be added to the vertical blanking pulse during vertical blanking time. The resulting signal at the junction of R12 and R18 is shown in Figure D-7b. The output normal mode sync/blanking signal is delivered to the video amplifier in chassis 5 for summing with the video information.

The signal leaves chassis 4 at pin 340-11 and enters chassis 5 at pin 650-5. The combined signal in chassis 5 is the composite video signal that contains all the information necessary to reproduce the scene viewed by the TV camera on a ground monitor.

D. 5 VIDICON BLANKING AND BIAS

D. 5. 1 General Description

Operation of the vidicon requires various dc voltages for the grids and the signal electrode and a blanking signal for the cathode. The desired dc voltages +300 volts, -100 volts, and +25 volts normal and emergency mode – are obtained from the ECU. The required cathode blanking signal is obtained from the blanking emitter follower, Q22.

D. 5. 2 Vidicon dc Voltages

Negative 100 volts from TB2-13 of the ECU is supplied to chassis 4 at pin 340-21. The voltage is applied to a voltage divider network consisting of two selected resistors R75 and R76. The negative voltage from the junction of R75 and R76 is sent out of the chassis at pin 340-19 to grid 1 of the vidicon. R75 and R76 are selected during test to provide the proper value of vidicon beam current.

Positive 300 volts from TB2-12 of the ECU is supplied to chassis 4 at pin 340-18. The voltage is applied to a voltage divider consisting of R77, R78, R80, and R81, and voltages from this divider are utilized by grids 2, 3, and 4 of the vidicon. Focus resistors R80 and R81 resistance ratio (determines grid 3 voltage) determines the proper focusing of the vidicon beam. The total resistance of R80 and R81 determines the voltage on grids 2 and 4. Adjustment of the voltage on grids 2 and 4 will affect the deflection linearity of the vidicon beam. Adjustment of this voltage will also affect focus somewhat; so after making this adjustment, one should readjust grid 3 voltage.

The +25 volts normal and emergency mode is supplied to chassis 4 at pin 340-8 and TB2-5 on the ECU assembly. The 25 volts is applied to a voltage divider network consisting of R82 in chassis 4 and R53 in chassis 5. Connection between the two resistors is made from chassis 4 pin 340-17 to chassis 5 pin 650-4. The output of the junction of R82 and R53 is the vidicon target voltage and can vary between 10. 2 and 24. 1 volts, depending on the selected value of R82. The target voltage to be used is determined prior to the vidicon tube's installation in the camera. The determining factors are the sensitivity and erasure characteristics of the vidicon.

The vidicon also requires 6. 3 volts dc for the filaments, but the voltage is not obtained from chassis 4. Instead, it is routed directly to the vidicon tube socket from TB2-3 of the ECU assembly.

D. 5. 3 Vidicon Blanking Emitter Follower

The input to the vidicon blanking emitter follower Q22 is obtained from an OR gate consisting of CR4 and CR5 in chassis 4 and CR4 and CR8 in chassis 3. The 200 line mode blanking signal from this OR gate leaves chassis 3 at pin 730-13 and enters chassis 4 at pin 340-4. The output from the chassis 4 portion of the OR gate is either the normal mode horizontal blanking signal or the normal mode vertical blanking signal. Q22 is normally cut off, but conducts upon receipt of a blanking signal on the base. When Q22 conducts, the voltage drop across its emitter resistor R74, which also acts as the vidicon cathode resistor, goes positive. This voltage rise, which is coincident with sweep reference time, is sufficient to cut off the vidicon.

D. 6 THERMOSTATIC CONTROL

The thermostatic control circuit is composed of four heater resistors — R83, R84, R85, and R86 — and thermostatic switch S1. When the temperature on the chassis falls below a preselected value, switch S1 closes. If a 22 volt return is present at chassis 4, pin 340-27, when S1 closes, power is applied to the heater resistors.

APPENDIX E. FUNCTIONAL DESCRIPTION OF CHASSIS A-5

The functional description of electronic chassis A-5, which was tested for its electrical performance (as summarized in Section 4.6), is presented here. The discussion is presented with reference to the chassis schematic diagram, Hughes Document 283656, shown in Figure E-1.

The chassis comprised the video amplifier and sum circuits, video logic circuits, and vidicon thermal control circuits. Accordingly, the description of these circuits is presented in three parts.

E.1 VIDEO AMPLIFIER AND SUM CIRCUITS

The purpose of the video amplifier and sum circuits was to amplify the output of the vidicon and combine the horizontal sync/blanking and vertical blanking pulses in order to provide a composite video output signal.

E.1.1 Vidicon Operation

The vidicon is a small electron tube that converts an optical image to video information by means of an electron beam which scans a light-irradiated photoconductive element. The tube consists of a highly evacuated envelope of glass containing an electron gun at one end and a transparent flat at the other end. An extremely thin electrically conductive film, which is also light transparent, is deposited on the inner surface of this optical flat and acts as the video output or signal plate. A photoconductive film is deposited upon this thin layer, and the image to be televised is focused upon this film by means of an external lens. When the light from the subject is focused upon the photoconductive material, the film becomes conductive to a degree related to the relative brightness of each corresponding portion of the image. The individual photoconductive areas behave similarly to a charged capacitor with leaky insulation with one plate at a fixed potential and the other plate floating. This action causes the photoconductive surface potential to rise toward the signal plate potential to a degree related to the individual illumination of each picture element. While scanning, the electron beam deposits electrons on the photoconductive layer in sufficient quantities to return each surface element cathode potential. This process creates

a current flow in the signal output voltage across a load resistor. Electrostatic or magnetic focusing and deflection methods can be utilized, depending upon the vidicon utilized. The vidicon utilized in the Surveyor TV camera employs electrostatic focusing and magnetic deflection.

The vidicon cell assembly 283644 contains the vidicon tube, the deflection yoke, the vidicon shield, and the vidicon faceplate heater. The majority of the vidicon control circuitry is contained in chassis 4 and is discussed in the document applicable to that chassis. The vidicon target voltage will be between 10.2 and 24.1 volts, depending on the value of target resistor selected. The target voltage is taken from the junction of 650R53 and 340R82 and sent to the vidicon signal plate through 555R54 and pin 1 of the 233555 video preamplifier.

E.1.2 Video Amplifier Circuits

The excitation voltage (+25 volts) for the video and summing amplifiers is provided through an OR gate consisting of 555CR16 and 555CR17. The 200 line mode 25 volts is obtained from TB2-8 on the ECU and enters chassis 5 at pin 650-13. The normal mode 25 volts is obtained from TB2-9 on the ECU and enters chassis 5 at pin 650-3.

The preamplifier consists of one emitter follower and two voltage amplifiers. The signal is routed to the preamplifier from the vidicon by means of a shielded target lead. The length of this lead is kept very short to reduce any losses between the vidicon and the preamplifier.

The video output of the vidicon is applied to the base of emitter follower 555Q1, and the in-phase output at the emitter is applied to the base of 555Q2. The in-phase signal at the emitter of Q1 is also applied to the shield of the video input lead to reduce the effective input lead capacity by reducing the voltage differential between the lead and its shield. 555Q2 provides voltage amplification for the video signal, and the output at the collector is applied to the base of 555Q3. Q3 provides voltage amplification for the video signal which is greater in the 200 line mode than in the normal mode. The 200 line mode requires greater amplification since the sweep rate of the vidicon beam is slower than in the normal mode. The output of Q3 is taken from the junction of R9 and R10 during normal mode operation and from the junction of R10 and R11 during 200 line mode operation. The values of R9 and R10 are selected during test to provide the proper gain in the video amplifier during normal mode operation. The sum of the resistance of R9 and R10 is kept constant at 5000, so the gain in 200 line mode is not affected. CR2 is back-biased during normal mode operation, and CR1 is back-biased during 200 line mode operation. Preamplifier components 555R12, 555R13, and 555C5 form a lead network, and selection of C5 during test provides an adjustable amount of aperture correction. Aperture correction is compensation for a reduction in amplitude response at high frequencies due to the finite size of the scanning spot in the vidicon.

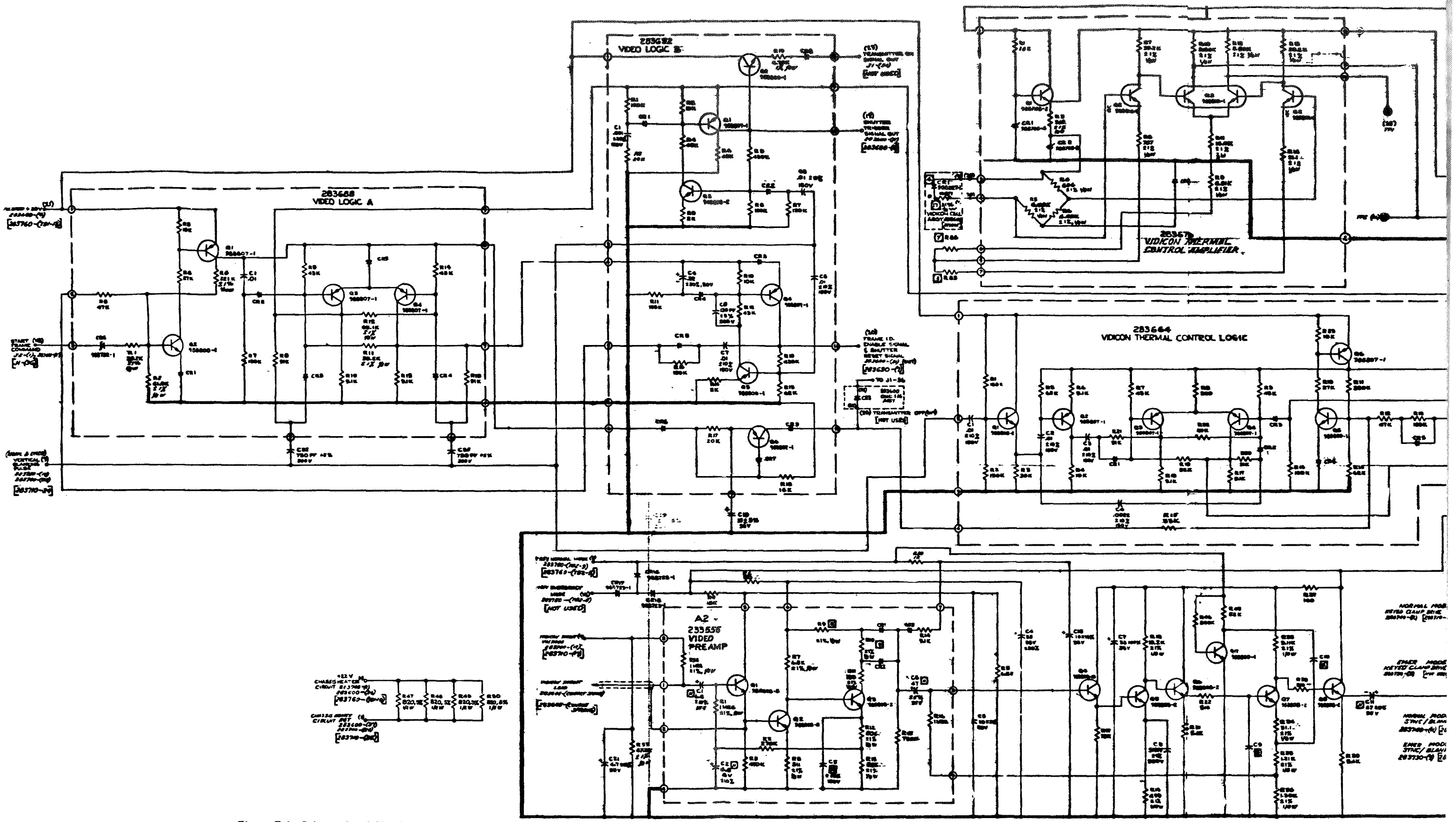

Figure E-1. Schematic of Chassis A5

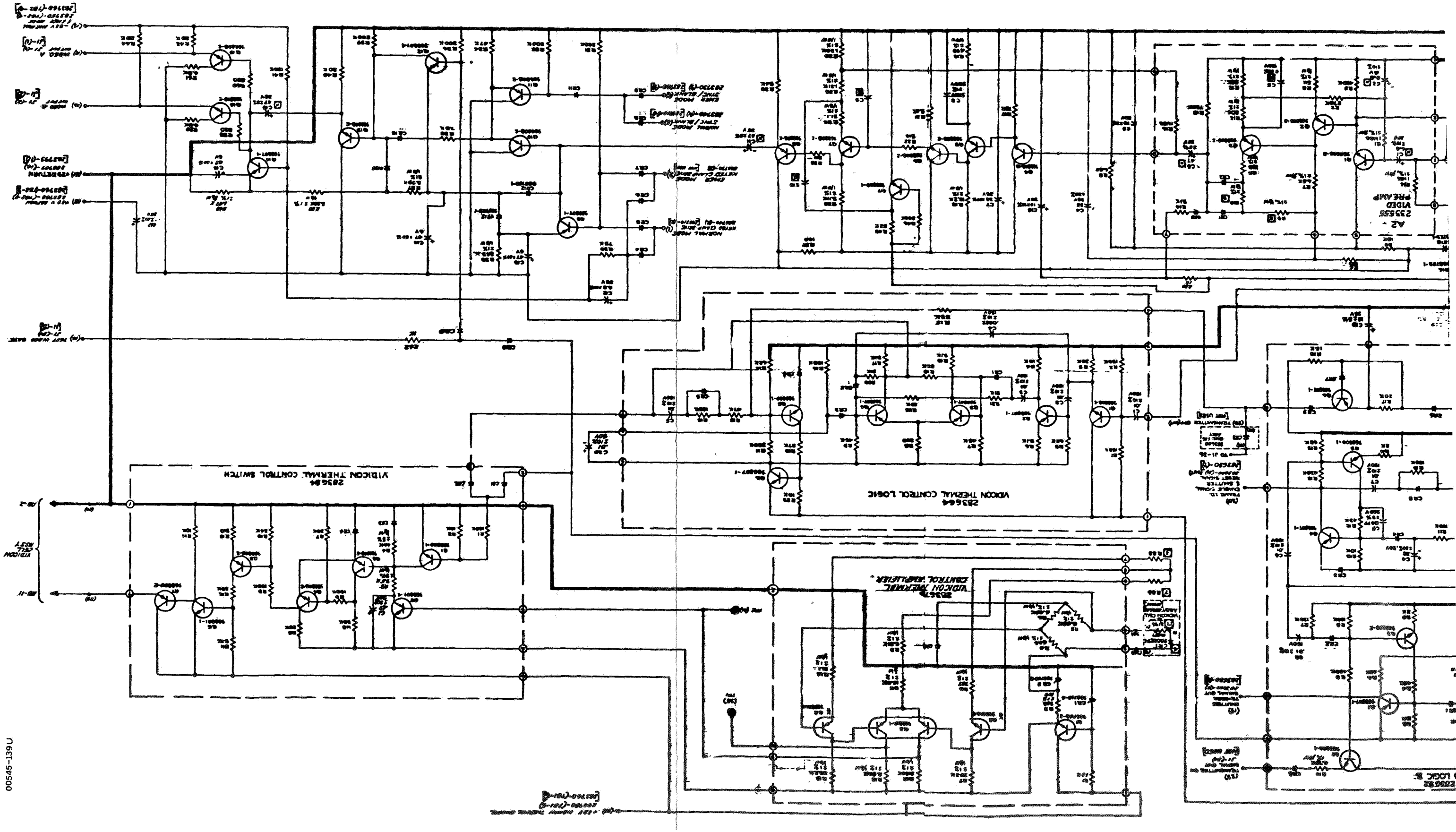
A2
235658
VIDEO
PREAMP
VIDICON THERMAL CONTROL AMPLIFIER
235670
VIDICON THERMAL CONTROL LOGIC
235664
VIDICON THERMAL CONTROL SWITCH
235694

00545-139U

Amplifier Q3 provides an increasing gain with increasing frequency. The output of the collector circuit of Q3 is coupled through 555C6 to the base of video emitter follower 650Q4.

The video amplifier in conjunction with the preamplifier provides the desired amplification of the video signal. The desired voltage gain characteristic of the combination should be flat from 0.1 Hz to 20 kHz, should rise at a rate of 6 dB per octave from 20 to 55 kHz and at a rate of 12 dB per octave from 20 to 55 kHz, and should fall sharply to zero beyond 220 kHz.

Video amplifier Q5 amplifies and inverts the video signal and dc couples the output signal on its collector to the base of second video emitter follower 650Q6. Capacitor C8 in the emitter circuit produces negative feedback resulting in reduced gain of the stage at the lower frequencies.

The output of the preamplifier is applied to the base of emitter follower 650Q4, and the output at the emitter is dc coupled to the base of first video dc amplifier 650Q5.

The output of the emitter of second video emitter follower Q6 is applied to a lag network consisting of 650R22 and 650C9. The function of the network is to attenuate the very high frequencies that are above the usual range of the video signal. The output of the lag network is directly coupled to the base of second video amplifier 650Q7.

The second video amplifier amplifies the video signal and provides negative feedback through 650R16 to the input of 650Q4. Capacitor C10 and resistors R24, R25, and R26 form a lead network during the normal mode of operation. 650Q17 provides the ground return for C10 during normal mode operation. During 200 line mode operation, Q17 is disabled, opening the ground path for C10. The lead network provides negative feedback, but the magnitude of the feedback decreases as the frequency increases. Hence, the gain of the stage increases as the frequency of the input increases. The network compensates for the frequency rolloff caused by the capacity of the input stage and the vidicon capacity from the target to all other electrodes. Since the required bandwidth in emergency mode is only 1 kHz, leaving the lead network in the circuit would only provide greater amplification for the higher frequency noises. Hence, it is eliminated in 200 line mode.

The amplified video signal from the collector of Q7 is dc coupled to the base of the third emitter follower 650Q8. The emitter output is coupled through 650C11 to the video summing amplifier 650Q10. The value of C11 and other coupling capacitors utilized in the video circuits is rather large. This ensures good low frequency response of the amplifiers.

E. 1. 3 Summing Circuits and Keyed Clamp Circuits

Transistors 650Q10 and 650Q11 comprise a summing circuit which combines the clamped video signal and the sync-blank pulses to form the composite video signal. Transistor 650Q9 serves as a keyed clamp switch which restores the dc level of the video signal so that the video can be combined with the sync-blank pulses.

The emitter of Q9 is held at approximately 22 volts through the action of voltage divider 650R43, 650R38, 650R37, 650CR13, 650R33, 650CR18, and 650CR16 or 650CR17. The potential on the base of Q9 is normally slightly above 24 volts as a result of the input from OR gate 650CR5 and 650CR7. This voltage is sufficiently positive to hold Q9 cutoff. During a portion of the time that the vidicon is blanked, the input to CR5 or CR7 decreases and the voltage on the base of Q9 falls to 19 volts. This allows Q9 to conduct charging capacitor 650C11 and places a potential of approximately 21. 8 volts on the base of 650Q10. Thus, when the video is at the known black level (vidicon blanked), the base of Q10 will be at the 21. 8 volt reference. During vidicon unblanking time, the voltage on the base of Q20 will decrease to lower values for various degrees of picture brightness. 650CR12 functions as a noise level clamp. If the voltage on the anode of CR12 tends to increase above 22 volts due to noise in the video signal, the noise level clamp will conduct and clip off that portion of the signal above 22 volts. This prevents noise spikes from interfering with the horizontal sync.

The sync/blank pulses from chassis 3 during 200 line mode operation or from chassis 4 during normal mode operation are coupled through the OR gate, 650CR8 and 650CR9, to the sync/blank summing amplifier 650Q11. The normal mode input during vertical retrace time is a positive 200 ms pulse. Transistor Q11 conducts during horizontal and vertical blanking times, and the voltage across 650R24 due to the conduction of Q11 is sufficient to keep 650Q10 cut off. During the time between horizontal blanking pulses, the voltage on the base of Q11 is much lower than the voltage on the base of Q10. Under such circumstances, Q10 is conducting and Q11 is cut off. The dc restored video from Q10 and the sync/blank pulses from Q11 are summed across their common emitter resistor R34, and the resultant composite video signal is coupled to emitter follower 650Q13.

E. 1. 4 Emitter Follower and Video Inhibit Gate

The composite video signal from Q10 and Q11 is coupled through R35 and CR15 to the base of emitter follower 650Q13, providing that CR15 is not back-biased. If the video inhibit gate Q12 is conducting, the voltage on its collector is approximately 21. 2 volts. This voltage is applied to the cathode of CR15, and it is sufficiently positive to prevent conduction of the diode. The composite video signal is inhibited under such circumstances. If the video inhibit gate is not conducting, CR15 can conduct and the video is not inhibited.

White level clamp 650CR14 conducts should the composite video signal at the base of Q13 attempt to drop below +16 volts. Thus, the white level is clamped at +16 volts. The composite output of Q13 is developed across emitter resistor 650R40 and coupled through 650C13 to the A and B output emitter followers.

E.1.5 Output Emitter Followers and Output Level Clamp

The composite video signal is applied to the base of the output emitter followers 650Q15 and 650Q16. The dc level of the compositive video signal is set by output level clamp Q14. During horizontal sweep time, capacitor 650C16 in the emitter circuit of Q14 charges to a voltage determined by the voltage divider 650R43, 650R38, 650R37, 650CR13, 650R33, 650CR18, and 650CR17 or 650CR16. When the negative going keyed clamp drive signal from the keyed clamp drive OR gate, 650CR4 and 650CR6, is applied to the base of Q14, the transistor saturates charging 650CR15 to a value determined by the voltage divider network. When Q14 conducts, the voltage at the junction of C15 and the base of Q16 rises to +3.1 volts. Since the composite video sync pulse is in time coincidence with the keyed clamp drive pulse, the composite video signal is referenced to this value at the input of Q15 and Q16.

The A and B output emitter followers, Q15 and Q16, develop identical composite video signals across their respective emitter resistors 650R42 and 650R44. The voltage differential between the base and the emitter of the output stages is 0.6 volt. Hence, the sync pulse portion of the composite video outputs of both Q15 and Q16 is referenced to +2.5 volts. Video output A is sent out of chassis 5 at pin 650-17 to J1-1 of the TV camera. Video output B is sent out of chassis 5 at pin 650-16 and leaves the camera at J1-2.

E.2 VIDEO LOGIC

The video logic circuit provided activation signals for the following functions: shutter operation, video gating, vidicon thermal control, and video or frame identification signals to the transmitter. A detailed description of how the circuit operated is presented in the following paragraphs.

E.2.1 29 Volt Logic Power Switch

The video logic power switch controls the application of power to the video logic circuitry upon receipt of a START FRAME command. The START FRAME command is a 20 ms positive pulse that is applied to the base of 668Q2 through the zener diode 668CR6. The command pulse, which exceeds the zener breakdown voltage of the diode, triggers Q2 into conduction, resulting in a voltage drop at the junction of 668R3 and 668R4. This voltage drop creates a forward emitter bias on 668Q1, driving it into conduction. When Q1 conducts, current flow through 668R2 serves as positive feedback for Q2, driving it further into conduction. The regenerative action

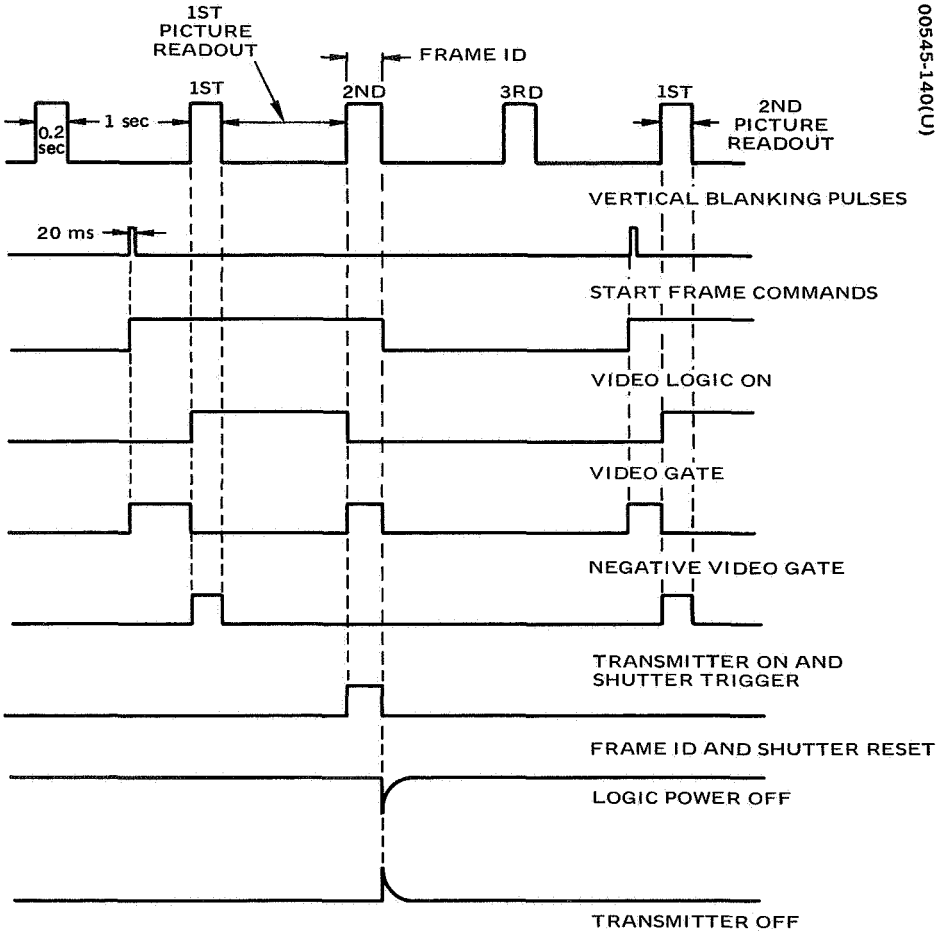

Figure E-2. Normal Mode Logic Timing Sequence

continues until Q1 and Q2 are in the saturation state. Thus, Q2 provides lockup of Q1 after the removal of the START FRAME command. The circuit will remain in this condition until an external trigger is received. Typical voltages on the bases of Q1 and Q2, respectively, are 21.5 and 4.5 volts when the power switch is on. The 28.5 volts at the collector of switch Q1 is applied to the video logic multivibrator (688Q3 and 688Q4) as a video logic-on voltage, as seen in Figure E-2 which shows the logic timing sequence.

E.2.2 Video Logic Multivibrator

The bistable video logic multivibrator, 668Q3 and 668Q4, acts as a 28 volt power switch for various circuits on chassis 5. The multivibrator is activated by the 28.5 volt power from Q1. This voltage is applied to the emitters of Q3 and Q4 through 668CR5 and also to the RC network composed of 668C1 and 668R7. When power is first applied to the RC combination, charging current through R7 causes a positive voltage to be coupled through diode 668CR2 to the base of Q3. Q3 will be cut off by this action, and Q4 will be allowed to conduct. Conduction of Q4 couples a positive voltage to the base of Q3 through 668R11, keeping the transistor cut off. The bistable multivibrator will remain in this state until triggered. The collector voltage outputs of Q3 and Q4 at this time are +1.9 and +28 volts, respectively.

Positive vertical pulses are applied through capacitor 650C22 to diode 668CR3 and through capacitor 650C23 to diode 668CR4. When the leading edge of the first vertical blanking pulse following the activation of video logic multivibrator is applied, CR3 is back-biased and CR4 forward-biased. The pulse applied to C23 is differentiated and routed to the base of Q4. The positive pulse on the base of Q4 cuts the transistor off, resulting in a reversal of the state of the multivibrator. The multivibrator remains in this state until arrival of the next vertical blanking pulse. The leading edge of the next blanking pulse cuts off Q3, reverting the multivibrator back to its original condition. See Figure E-2 for the appropriate waveforms. The video gate pulse appearing at the collector of Q3 reaches the 28 volt level on its positive excursion and it is applied to the following circuits: 1) the shutter trigger circuit to initiate shutter action, 2) the vidicon thermal control circuits to inhibit the vidicon heater during picture readout, and 3) the video amplifier to prevent inhibiting of the video signal. The +1.9 volt negative video gate pulse appearing at the collector of Q4 is applied to the frame identification and shutter reset circuit to prevent frame identification until the second vertical blanking pulse following the start frame command.

E.2.3 Shutter Trigger and Transmitter on Circuit

A shutter trigger signal is generated when the video gate and the vertical blanking pulse are applied simultaneously to the circuit. The shutter trigger signal in turn triggers the transmitter on circuit. The +28 volt video gate pulse from the video logic multivibrator is applied

directly to the emitter of the shutter trigger amplifier 692Q1. When this voltage is first applied, there is a voltage drop across 692R2 due to the charging of capacitor 692C1. This voltage drop is sufficient to allow conduction through Q1. When Q1 conducts, its collector voltage rises from 0 to 27.5 volts and is utilized as a trigger signal for three separate circuits.

The 27.5 volts from the collector of Q1 applied to voltage divider 692R5 and 692R8 raises the base voltage of 692Q3 to +6 volts. The positive voltage on the base of Q3 results in current flow through R2, R4, Q3, and R9. The voltage drop across R2 is sufficient to allow continued conduction of Q1, which in turn allows continued conduction of Q3. The collector output of Q1 is also sent out pin 650-19 to chassis 6 as the shutter trigger signal and to 692Q2 as a trigger for the transmitter on circuit. The collector of Q2 is connected directly to 29 volts, so this emitter follower will produce an output as long as the 27.5 volts due to the conduction of Q1 is present on the base. The transmitter on signal is sent out of pin 650-23 to J1-34 where it is then routed to the transmitter. The transmitter on signal and the shutter trigger signal have the same time duration and are illustrated in Figure E-2.

The leading edge of the video gate pulse that turns Q1 on is in time coincidence with the leading edge of the first vertical blanking pulse following the START FRAME command. The vertical blanking pulses are applied to a differentiating network consisting of 692C3 and 692R7. Diode 692CR2 blocks the positive spikes generated by the differentiating network. However, the negative spikes that are generated by the trailing edge of the vertical blanking pulse are coupled through the diode to the base of Q3. Q3 is cut off by the first negative spike received following circuit activation by the video logic multivibrator. When Q3 cuts off, the voltage at the junction of R2 and R4 rises to 27.5 volts, causing Q1 to turn off. The collector voltage of Q1 then returns to 0 volt, and the shutter signal which is taken from this point is terminated. The base of Q2 is tied directly to this point, and the base of Q3 ties to it through R5. Hence, Q2 cuts off, terminating the transmitter on signal, and Q3 remains cut off.

The shutter trigger signal will be a +27.5 volt pulse that is in coincidence with and of the same time duration as the first vertical blanking pulse following the start frame command. The transmitter on signal will be in time coincidence with the blanking and shutter signals, and its amplitude will be +4.7 volts when the output is connected to the transmitter.

E.2.4 Frame ID and Shutter Reset Circuit

The frame ID and shutter reset circuit produces a positive pulse that initiates shutter reset action. The pulse occurs coincident with the second vertical blanking pulse following the START FRAME command. The pulse is also utilized to turn off the 29 volt logic power switch (688Q1 and 688Q2) to remove the power from the video logic multivibrator (688Q3 and 688Q4).

The voltage appearing at the collector of the video logic multivibrator 688Q4 is coupled through diode 692CR3 to the emitter of frame ID and shutter reset transistor 692Q4. This voltage is +28 volts immediately following the application of the START FRAME command, decreases to +1.9 volts upon receipt of the leading edge of the first vertical blanking pulse following the START FRAME command, and returns to +28 volts upon receipt of the second vertical blanking pulse, as seen in Figure E-2. When +28 volts is first applied to the RC combination composed of 692C4 and 692R11, the charging action of C4 causes a positive pulse to be coupled through 692CR4 to the base of Q4. This ensures that Q4 does not conduct at this time. Upon receipt of the first vertical blanking pulse, the video logic multivibrator reverses its state. The collector output of 688Q4, which serves as the supply voltage for Q4 and Q5, falls to +1.9 volts so both transistors remain nonconducting. Upon receipt of the leading edge of the second vertical blanking pulse, the video logic multivibrator again changes its state, and the output of 688Q4's collector rises to +28 volts. The vertical blanking pulse is also fed to a differentiating network consisting of 692C6 and 692R15. The output of this network is delivered to the base of Q5, and the differentiated leading edge of the pulse causes Q5 to conduct. Conduction of Q5 causes a voltage drop across 692R10 which, in turn, allows Q4 to conduct. Conduction of Q4 places +3.5 volts on the base of Q5. Hence, both transistors remain conducting after the positive differentiated pulse disappears. A negative spike appears on the base of Q5 when the trailing edge of the vertical blanking pulse is differentiated. This results in cutoff of Q5 and Q4. The frame ID enable and shutter reset signal at the collector of Q4 is a +27.5 volt pulse of the same width and in coincidence with the second vertical blanking pulse. The pulse is routed to chassis 6 through pins 650-20 and 600-51.

692C7, 692CR5, 692R16, 688R6, and 688R2 form a differentiating network that couples a negative logic power off spike to the input of the video logic power switch. The negative spike on the base of 688Q2 cuts off the transistor. Cutoff of 688Q2 turns off 688Q1 which, in turn, removes the positive holding voltage from the base of 688Q2. This action takes place during the trailing edge of the vertical blanking pulse, as illustrated in Figure E-2. Turnoff of the video logic power switch removes power from the video logic multivibrator. The circuit remains in this condition until receipt of another START FRAME command.

E.2.5 Transmitter Off Pulse Generator

During the time that video logic power is applied to capacitor 650C19, it charges toward the applied +28.5 volt potential. At this time, the voltage applied to 692CR7 in the base circuit of 692Q6 is +28 volts, and the transistor does not conduct. When the video logic power is removed (trailing edge of the second vertical blanking pulse following a START FRAME command), C19 discharges through 692R17 and 692R18. During the discharge time of C19, the emitter of Q6 is positive with respect to its base, allowing conduction

through the transistor. Q6 conducts until the decreasing charge on C19 is no longer sufficient to support conduction. The transmitter off pulse is illustrated in Figure E-2.

The transmitter off pulse is taken from the collector circuit of Q6 and is delivered to chassis 6 through pins 650-22 and 600-52. Another output of Q6 is delivered to the vidicon thermal control logic circuit to inhibit vidicon heating during the period that the vidicon face is being primed for a second picture.

E.3 VIDICON THERMAL CONTROL

The vidicon thermal control circuits automatically provided power to the vidicon faceplate heater to maintain the faceplate within a specified temperature range. This function was performed upon receipt of the VIDICON TEMPERATURE CONTROL ON command. The temperature of the vidicon collar was sensed and power applied to the faceplate heater when the temperature dropped below the desired value. The vidicon thermal control circuits included the thermal control amplifier, the vidicon thermal control switch, and control logic circuits. The logic circuits allowed the application of power to the faceplate heater only during the second erase frame. This prevented distortion of the video information during the picture readout and priming frames.

A detailed description of the various elements of vidicon thermal control is presented in the following paragraphs.

E.3.1 Vidicon Thermal Control Amplifier

The major portion of the vidicon thermal control amplifier is contained in module assembly 283676. This assembly, in conjunction with a temperature sensing diode that is mounted on the vidicon collar, senses the temperature of the vidicon faceplate and produces an output signal that activates or deactivates the vidicon thermal control switch. When the thermal control switch is activated, 29 volt power is applied to four heating resistors in the vidicon cell assembly. The vidicon thermal control amplifier contains a voltage regulator circuit, a bridge circuit, and a differential amplifier.

Voltage Regulator

Two voltage regulator circuits, one in the base circuit of 676Q1 and the other in Q1's emitter circuit, provide voltage regulation for the power applied to a temperature sensing bridge network. Upon receipt of a VIDICON TEMPERATURE CONTROL ON command, the ECU provides 29 volt power to the thermal control circuits at pin 650-27. This voltage is applied to a voltage divider consisting of 676R1 and zener diode 676CR1.

The output taken from the junction of the diode and the resistor is 15.75 volts ±5 percent, and it is applied to the base of 676Q1. Q1 serves as an emitter follower, and its output voltage is approximately 15 volts. Q1's emitter voltage serves as a power source for the remaining transistors in the video thermal control amplifier and for Q1 through Q4 in the vidicon thermal control switch. The emitter voltage is also applied to a voltage divider consisting of 676R3 and zener diode 676CR2. The output taken from the junction of the diode and the resistor in this network is 6.2 volts ±5 percent. This regulated voltage is applied to a bridge circuit consisting of 676R4, 646R5, 676R6, and temperature sensing diode 644CR1. The gound return for the bridge circuit is made through 676CR3. The variation in the applied bridge voltage due to temperature change will be ±0.001 percent/°C.

Temperature Sensing Bridge

The temperature sensing bridge is composed of resistors 676R4, 676R5, and 676R6, and temperature sensing diode 644CR1. The excitation voltage for the bridge network and series diode 676CR3 is a regulated 6.2 volts. The forward voltage drop of the diode is 0.60 ±0.03 volt at 77°F and 1.0 ma. The forward voltage drop changes -1.0 mv/°F. The desired vidicon heater turnon temperature is 77°F; so the bridge network should be nearly balanced at this temperature. The output of the bridge network is fed to a differential amplifier. Resistors in the differential amplifier are selected at 77°F to compensate for unbalance in the bridge network or other circuit unbalance. The bridge network has two outputs. A reference voltage is taken from the junction of R4 and R6 to be applied to the base of 676Q2B. The signal voltage, which decreases with a decrease in temperature, is taken from the junction of R5 and 644CR1 and applied to the base of 676Q2A.

Differential Amplifier

The differential amplifier amplifies the dc voltage from the bridge in two stages of amplification by a factor in excess of 200. A small differential voltage in the bridge is amplified sufficiently to trigger the vidicon thermal control switch on or off.

When the temperature falls below the nominal value of 77°F at the faceplate of the vidicon, the action of the temperature sensing diode results in increased voltage being applied to the base of Q2A. The input to the base of the other half of the differential amplifier Q2B remains constant. Decreased current flow through Q2A results in increased collector voltage, and increased current flow through Q2B (due to the effect of common emitter resistors) results in decreased collector voltage. The outputs of Q2A and Q2B, respectively, are applied to the bases of 676Q3A and 676Q3B (the two transistors utilized in the differential amplifier are not identified as A or B). The output of Q3 is negative going at TP-2 and positive going at TP-1 under decreasing temperature conditions, resulting in turnon of the vidicon thermal control switch.

Resistors 676R55 and 676R56 are selected during test to provide proper control of vidicon heating. R55 is selected so that the voltage between TP-2 and TP-1 is from 0 to +0.2 volt, and R56 is selected so that the vidicon heaters turn on at the proper temperature. Tests are conducted over a wide range of temperatures to determine the proper value for these two resistors.

Diode 676CR3 provides temperature compensation for the differential amplifier. If the circuit ambient temperature increases, resulting in increased conduction of the first differential amplifier, there is a corresponding decrease in the forward voltage across CR3. This voltage decrease is reflected at the bases of Q2A and Q2B, which tends to restore conduction to the original value.

E.3.2 Vidicon Thermal Control Switch

The vidicon thermal control switch assembly consists of a level detector, a power switch, and a thermal control inhibit circuit. The level detector circuit monitors the output of the differential amplifier in the vidicon thermal control amplifier to determine when switching action to activate the vidicon heaters is necessary. The thermal control switch is tied to the +29 volt line and provides heater power to four resistors in the vidicon cell assembly when triggered by the level detector circuit. The vidicon thermal control inhibit circuit inhibits the thermal control on signal during the first and third frames of a picture taking sequence. This prevents distortion of the video information during the picture readout and priming frames.

Level Detector Circuit

The level detector circuit operates from a power source of approximately 15 volts from the emitter of 676Q1. When the vidicon faceplate temperature decreases below the nominal value, the input voltage to the base of 684Q2 decreases, thereby increasing current flow through the transistor. Q2 is an emitter follower and reduces the loading of the level detector stage on the differential amplifier 676Q3. The increased voltage on the emitter of Q2 results in increased conduction of 684Q3. The voltage drop in the collector circuit of Q3 is reflected on the base of 684Q4, resulting in decreased current flow through Q4. Decreased current through Q4 results in an increase in the collector voltage which is coupled to the base of 684Q5. Q5 is part of the power switch that controls vidicon heating, and when the voltage on its base is sufficiently positive, the switch will be activated.

Power Switch

The power switch consists of transistors 684Q5, 684Q6, and 684Q7 which control application of power to the vidicon heater resistors. Q5 is normally cut off by conduction of Q4. When the vidicon faceplate temperature falls below the nominal value, a positive going voltage on the base of Q5 turns the transistor on. Conduction of Q5 decreases the voltage on the

base on Q6, allowing Q6 to conduct. When Q6 conducts, the positive voltage appearing on its emitter turns Q7 on. When Q7 is turned on, +29 volt power is applied to four heater resistors in the vidicon cell assembly.

Thermal Control Inhibit Circuit

The thermal control inhibit circuit inhibits the thermal power on signal upon receipt of a signal from either the video logic or the vidicon thermal logic circuit. These inputs are applied to an OR gate, consisting of 684CR1 and 684CR2, and occur during the first and third frames of a picture taking sequence. When either of the positive inputs is applied to the base of Q1, conduction of Q1 places a potential that is very close to ground on the base of Q3. With the base of Q3 at such a low positive potential, conduction of Q3 and activation of the power switch is not possible.

E.3.3 Vidicon Thermal Control Logic

The thermal control logic circuit utilizes the transmitter off signal from the video logic circuit and the vertical blanking pulses from the vertical sweep circuit to generate a thermal control inhibit signal. This signal is generated during the period between the third and fourth vertical blanking pulses following a START FRAME command. The purpose of the inhibit signal is to prevent distortion of the video generated during the next picture taking sequence. The logic circuit consists of a power switch, a bistable multivibrator, an inverter amplifier, and an emitter follower.

Power Switch

When the camera is on, 29 volts is applied to the emitter of 664Q6 and the collector of 664Q5. When the positive transmitter off pulse which occurs immediately after the second blanking pulse following a START FRAME command is applied to the base of Q5, the transistor will conduct. Conduction of Q5 decreases the voltage on the base of Q6, allowing it to conduct. Conduction of Q6 applies +25 volt power to bistable multivibrator 664Q3 and 664Q4, and to inverter amplifier 664Q2. Turnon of Q6 also applies a holding voltage to the base of Q5, keeping the transistor turned on. The circuit remains in the conducting state until a pulse is received from the bistable multivibrator coincident with the trailing edge of the next vertical blanking pulse. When the negative trigger pulse is applied to the base of Q5, the transistor is cut off. Turnoff of Q5 results in turnoff of Q6. Turnoff of Q6 removes the switched 29 volt power from the thermal control logic circuits and also removes the holding voltage from the base of Q5. 664CR4 ensures that Q5 is not inadvertently triggered.

Emitter Follower

When the camera is turned on, +29 volt power is applied to emitter follower 664Q1. A positive dc voltage is applied to the base of Q1 through voltage dividers 664R1 and 664R2, which allows conduction through the

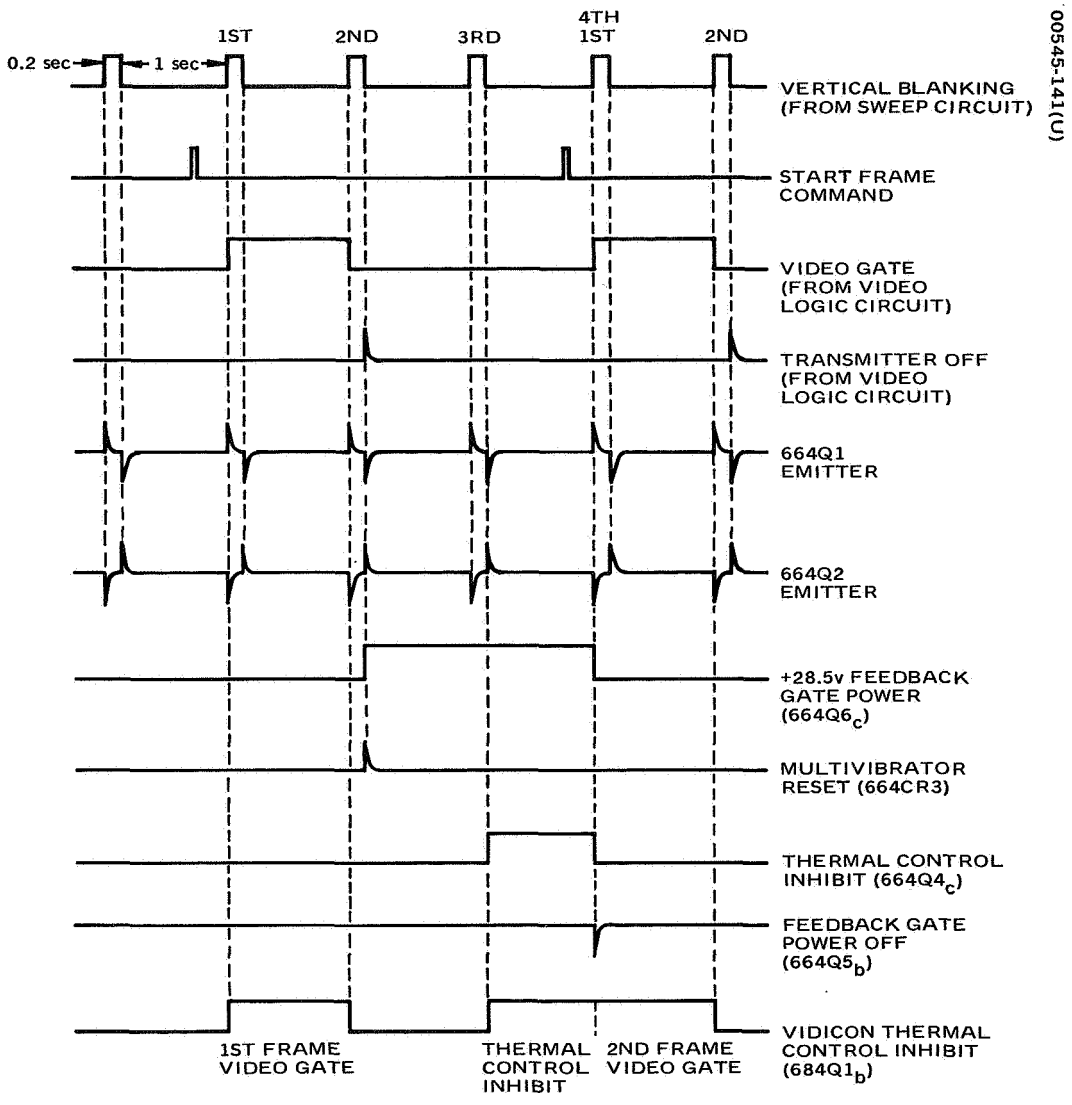

Figure E-3. Vidicon Thermal Control Timing Sequence – Normal Mode

transistor. The vertical blanking pulses from the vertical sweep circuit are applied to a differentiating network composed of 664C1 and 664R2. The positive and negative spikes that appear on the base as the result of the differentiation also appear on the emitter. The emitter output is applied to inverter amplifier 664Q2 and to one-half of the bistable multivibrator. Neither of these stages has power applied to them until receipt of the transmitter off pulse. Hence, only the third and fourth blanking pulse following the START FRAME command have any effect on the circuits.

Inverter Amplifier and Bistable Multivibrator

Power of +29 volts is applied to amplifier Q2 and multivibrator Q3 and Q4 upon turnon of power switch 664Q6. Q6 is activated by the transmitter off pulse which occurs immediately following the second vertical blanking pulse following the application of a START FRAME command to the camera. The switch power is applied to RC combination 650C20 and 664R16, resulting in a positive pulse being applied through 664CR3 to the base of 664Q4. The base of Q3 is tied to a voltage divider network which places a voltage on the base that is less positive than the emitter voltage. Hence, at initial turnon, Q3 is conducting and Q4 is turned off. The leading edge of the third vertical blanking pulse appears as a negative spike at the collector of Q2. The negative spike is blocked by CR1 so that it has no effect on the multivibrator. However, the trailing edge of the vertical blanking pulse, which appears as a positive spike on the collector of Q2, is coupled to the base of Q3, causing the transistor to cut off. The decreasing voltage at the collector of Q3 is coupled through 664R22 to the base of Q4, causing Q4 to begin conduction. The multivibrator remains in this state until receipt of the next vertical blanking pulse. The voltage on the collector of Q4 at this time is approximately 28 volts, and this positive pulse is coupled through 684CR2 to the base of 684Q1 to serve as the thermal control inhibit pulse. This is shown in Figure E-3, which gives the vidicon thermal control timing sequence.

The leading edge of the fourth vertical blanking pulse appears as a positive spike on the emitter of Q1, and the spike is coupled through 664C4 and 664CR2 to the base of Q4. The pulse turns Q4 off, and the decreasing voltage at the collector of Q4 is coupled to the base of Q3 through 664R19. The multivibrator is thus returned to its original state, and the thermal control inhibit pulse from the collector of Q4 is terminated. The trailing edge of the inhibit pulse is applied to a differentiating network consisting of 664C5, 664CR5, 664R12, and 664R14. The negative spike that appears on the base of Q5 will cut off the transistor. Turnoff of Q5 causes Q6 to cut off, which removes the 29 volt power from the bistable multivibrator and the inverter amplifier.

APPENDIX F. FUNCTIONAL DESCRIPTION OF CHASSIS A-6

The functional description of electronic chassis A-6, which was tested for its electrical performance (as summarized in Section 4.7), is presented here. The discussion below is presented with reference to the chassis schematic diagram, Hughes Document 283621, shown in Figure F-1.

Chassis A-6 contained shutter control circuits, mirror drive circuits, temperature readout circuits for the two TV camera temperature sensors, and pulse generators for the filter wheel, focus, and focal length control functions. The functional characteristics of these circuits are presented in sequence. Figure F-2 is a block diagram of the shutter control circuits, and Figure F-3 is a block diagram of the mirror drive circuits.

F.1 SHUTTER CONTROL CIRCUITS

The shutter control electronic circuits provided the drive signals to the shutter solenoids. The solenoids actuated the shutter blades, causing them to move back and forth across an aperture hole, exposing the vidicon faceplate in the process. The two modes of shutter operation were the time exposure mode and the 150 ms exposure mode. During the time exposure mode, the shutter opened on command and remained open until commanded to close. An inhibit circuit prevented shutter operation when a signal from the iris servo indicated that the light intensity was too high. This inhibit circuit functioned only during the 150 ms exposure mode. If the light intensity was still too high to allow shutter operation when the iris was stepped down to f/22, shutter operation was achieved by means of an external START FRAME SHUTTER INHIBIT OVERRIDE command. Functional descriptions of the two modes of shutter operation are presented in Sections F.1.1 and F.1.2.

F.1.1 Functional Description of 150 ms Mode

Shutter Open Driver

The shutter trigger signal is a +27 volt 200 ms pulse from the video logic circuits in chassis 5, which is in coincidence with and of the same time duration as the first vertical blanking pulse following the START FRAME command. The pulse enters chassis 6 at pin 600-17 and is applied to the

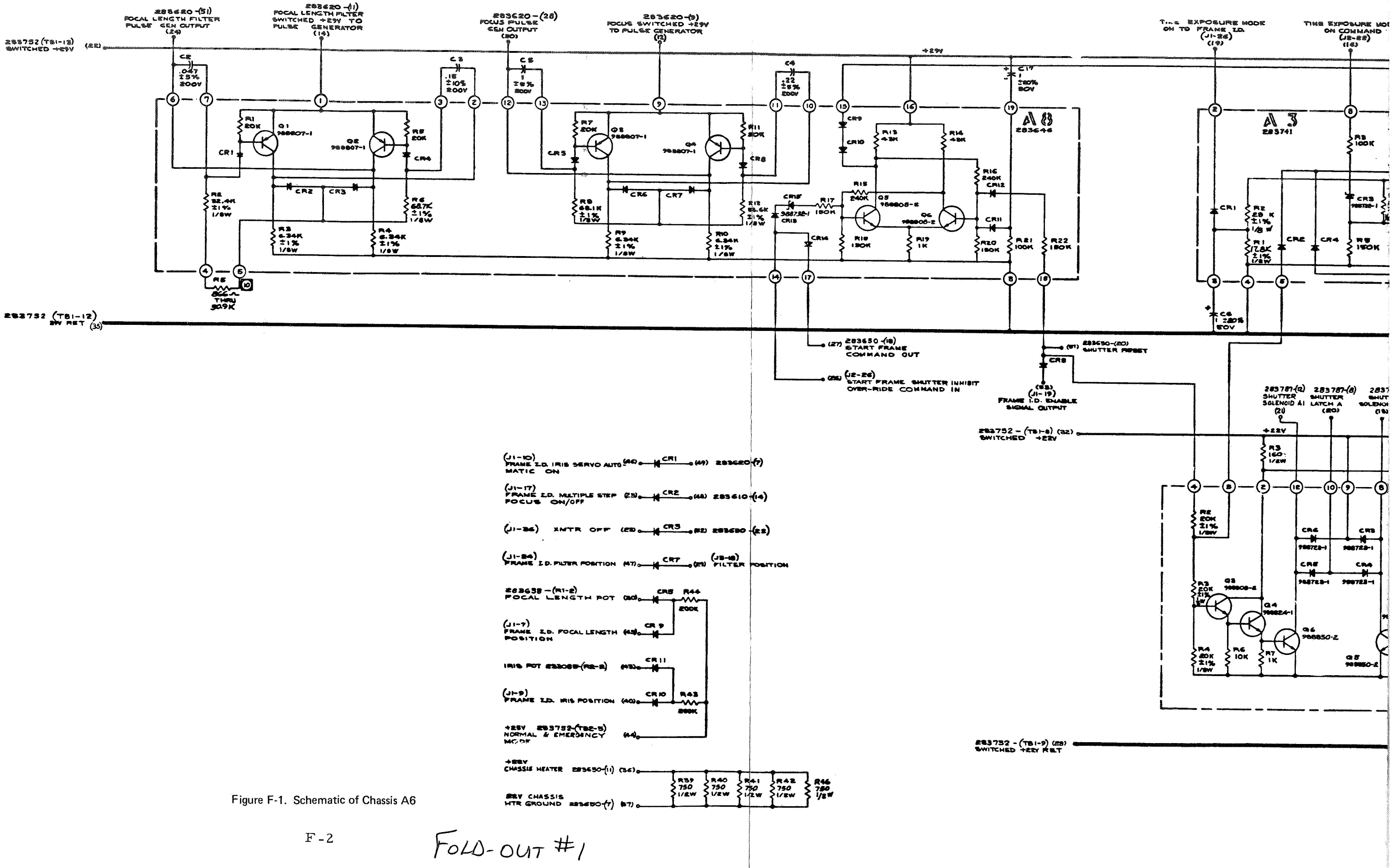

Figure F-1. Schematic of Chassis A6

FOLD-OUT #1

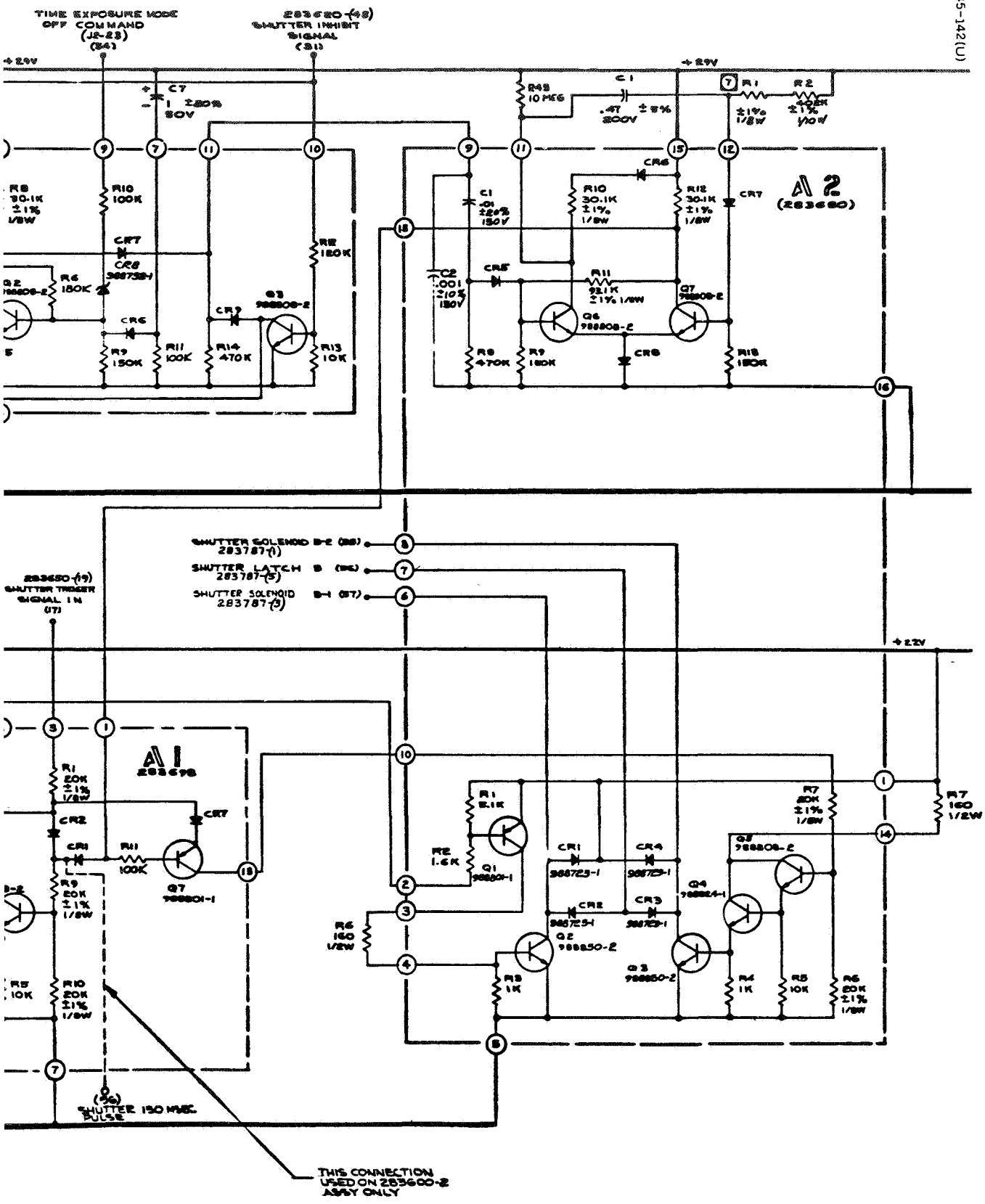
TIME EXPOSURE MODE OFF COMMAND (J2-23) (S4)
283620-(48) SHUTTER INHIBIT SIGNAL (S11)
+29V
+22V
A2 (283680)
A1 283678
283650-(19) SHUTTER TRIGGER SIGNAL IN (J7)
SHUTTER SOLENOID B-2 (J8) 283787-(1)
SHUTTER LATCH B (J8) 283787-(5)
SHUTTER SOLENOID B-1 (J7) 283787-(3)
(J6) SHUTTER 150 MSEC PULSE
THIS CONNECTION USED ON 283600-2 ASSY ONLY

FOLD-OUT #2

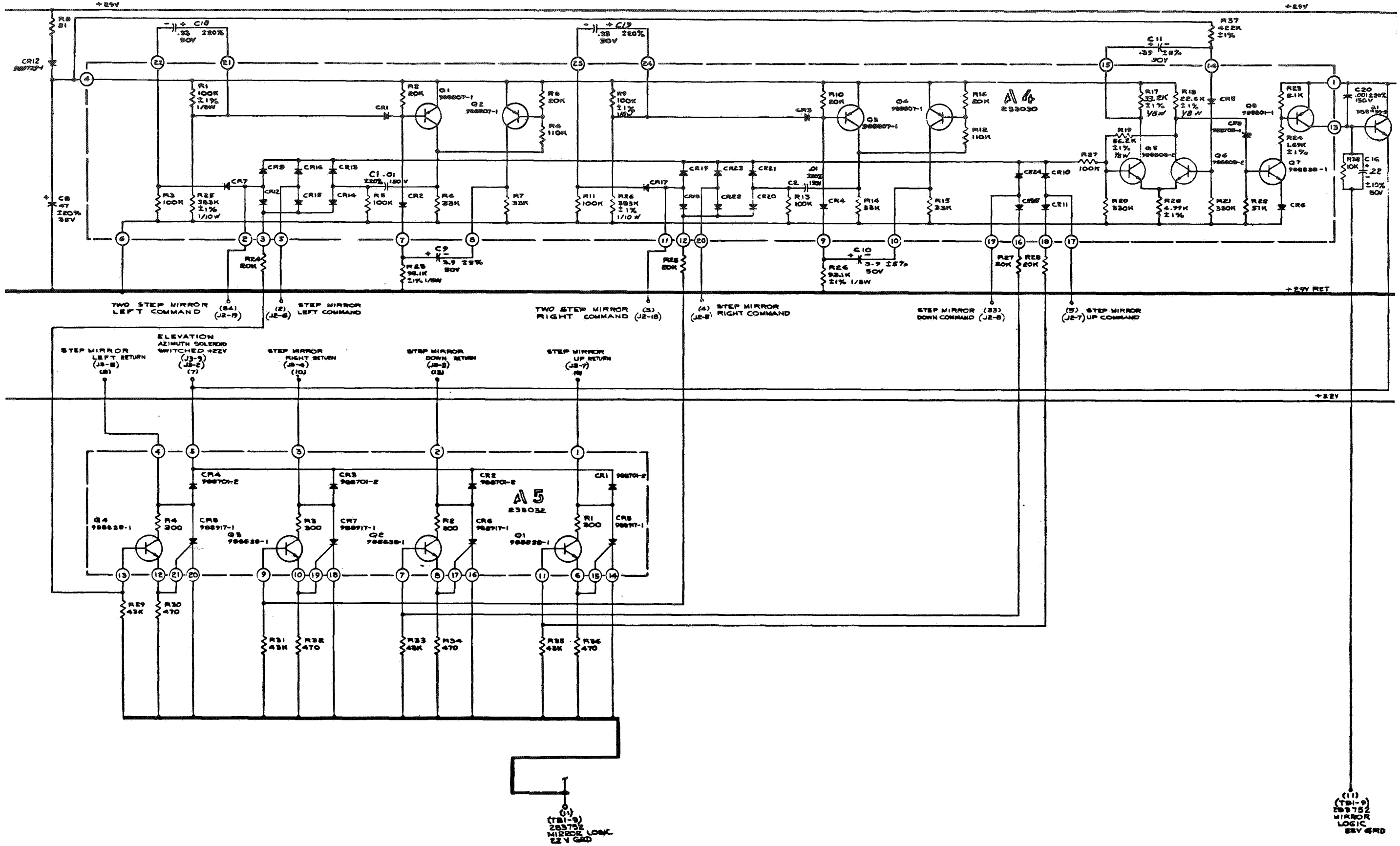

Figure F-1 (continued). Schematic of Chassis A6

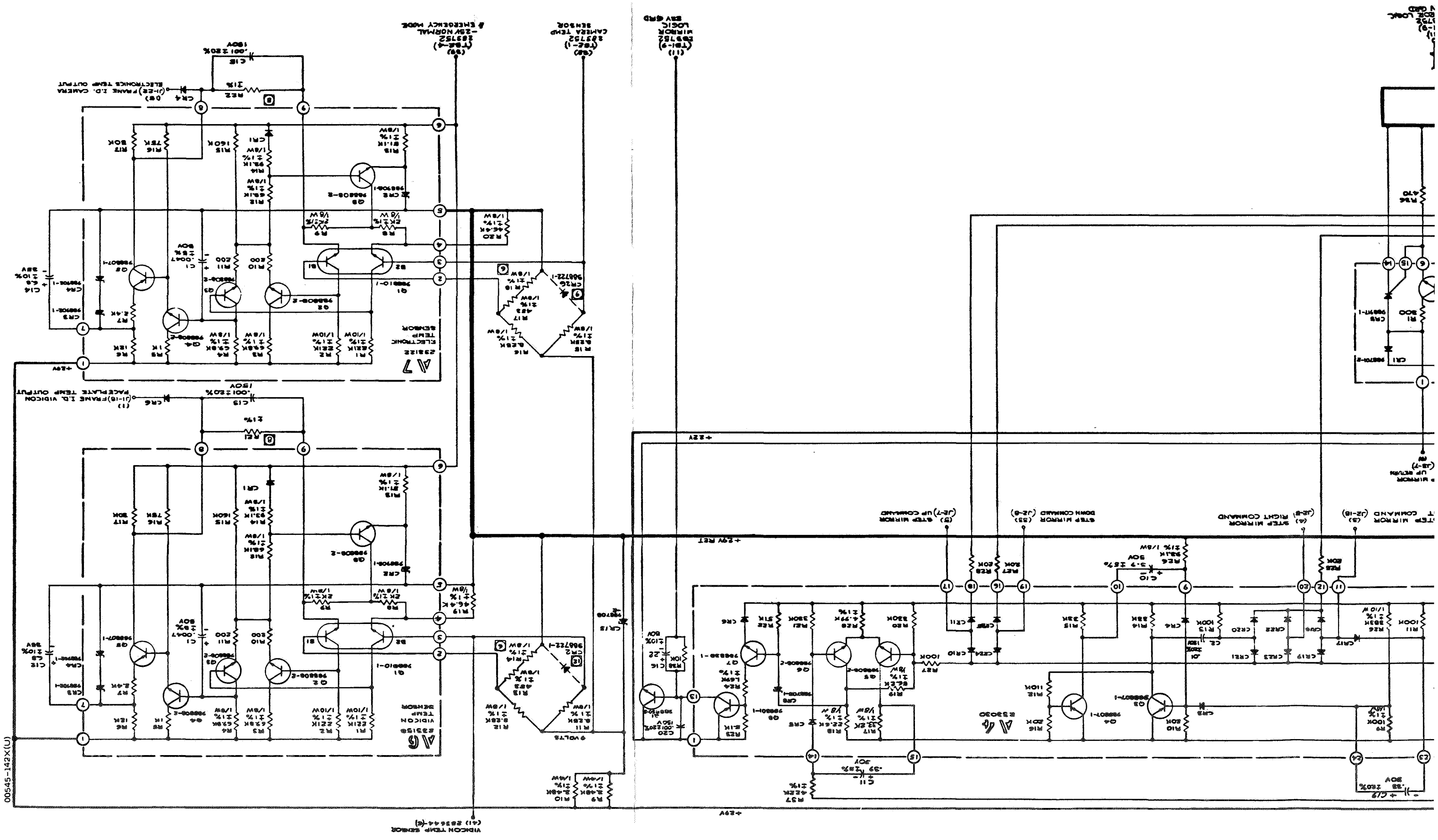
A7
2312122
ELECTRONIC TEMP SENSOR
A6
2312159
VIDICON TEMP SENSOR
A4
2312030
VIDICON TEMP SENSOR (4) 2831644-(6)
9 VOLTS
+25V
+22V
+29V RET
-25V NORMAL
& ENDEDECKY MODE
CAMERA TEMP SENSOR
5V GND
LOGIC
ELECTRONICS TEMP OUTPUT
FACEPLATE TEMP OUTPUT
FRAME I.D. CAMERA
FRAME I.D. VIDICON
STEP MIRROR UP RETURN
STEP MIRROR RIGHT COMMAND
STEP MIRROR DOWN COMMAND
STEP MIRROR UP COMMAND
00545-142X(U)

base of 698Q1 through 698R1, CR2, and R9. Q1 is an emitter follower, and the positive output pulse developed across 698R5 is applied to the base of another emitter follower, 698Q2. The positive pulse developed in the emitter circuit of Q2 is applied to the base of 698Q5. The emitter of Q5 is at ground potential, and the collector is tied to +22 volts through the 2 shutter solenoid. Q5 conducts upon application of the 200 ms pulse, thereby providing a ground return for the A2 solenoid; energizing of the A2 shutter solenoid pushes the A blade away until the B blade follows the A blade and closes the shutter 150 ms later. The shutter solenoids are located on the 284389 shutter assembly. The timing sequence is shown in Figure F-4.

Shutter Timing Multivibrator

The shutter timing multivibrator is a 150 ms monostable multivibrator consisting of 680Q6 and 680Q7 and associated circuitry. The positive shutter trigger signal appearing at pin 600-17 is applied to the base of Q6 through 698R1, 696CR9, 680C1, and 680CR5. C1, CR5, and 680R9 form a differentiating network; and the leading edge of the shutter trigger signal appears as a positive spike across R9. The normal state of the multivibrator is Q6 off and Q7 on. The positive trigger reverses the state of the multivibrator. When Q6 turns on, the drop in collector voltage is coupled through 600C1 to the anode of 680CR7, back-biasing the diode and causing the potential on the base of Q7 to drop to zero. C1 discharges through resistors 600R1 and 600R2 and transistor Q6, causing the voltage at the anode of CR7 to rise exponentially. When the voltage on the anode of CR7 goes positive, conduction through 680R13 places a positive potential on the base of Q7. When this voltage is sufficiently positive, Q7 conducts. The drop in Q7's collector voltage is sufficient to cut off Q6, and the multivibrator reverts to its original stable condition. Resistor 600R1 is chosen during test to produce a 150 ms multivibrator output. The positive output from the multivibrator is taken off the collector of Q7 and applied to the base of delayed pulse generator 698Q7.

Delayed Pulse Generator

The collector of 698Q7 is returned to ground through 698R7 and 698R6. The positive 200 ms shutter trigger signal is applied to the emitter of Q7 at the same time that the 150 ms positive pulse from the timing multivibrator is applied to its base. Q7 conducts during the last 50 ms period of the shutter trigger signal, developing a positive pulse across 680R6. This positive pulse is utilized as a trigger for 680Q5, part of the shutter close driver.

Shutter Close Driver

Operation of the shutter close driver (680Q5, Q4, and Q3) is similar to that of the shutter open driver. The trigger applied to this circuit is delayed 150 ms from the leading edge of the shutter trigger signal. Triggering of Q5 results in turnon of Q4 and Q3. A ground return path is provided for shutter solenoid B2 at pin 600-55 through transmitter switch Q3. Energizing the shutter B2 solenoid results in the B blade being pulled toward the A blade. When the B blade makes contact with the A blade, the shutter is completely closed, ending the 150 ms exposure time. The blades remain in this condition until a reset signal returns them to their original condition.

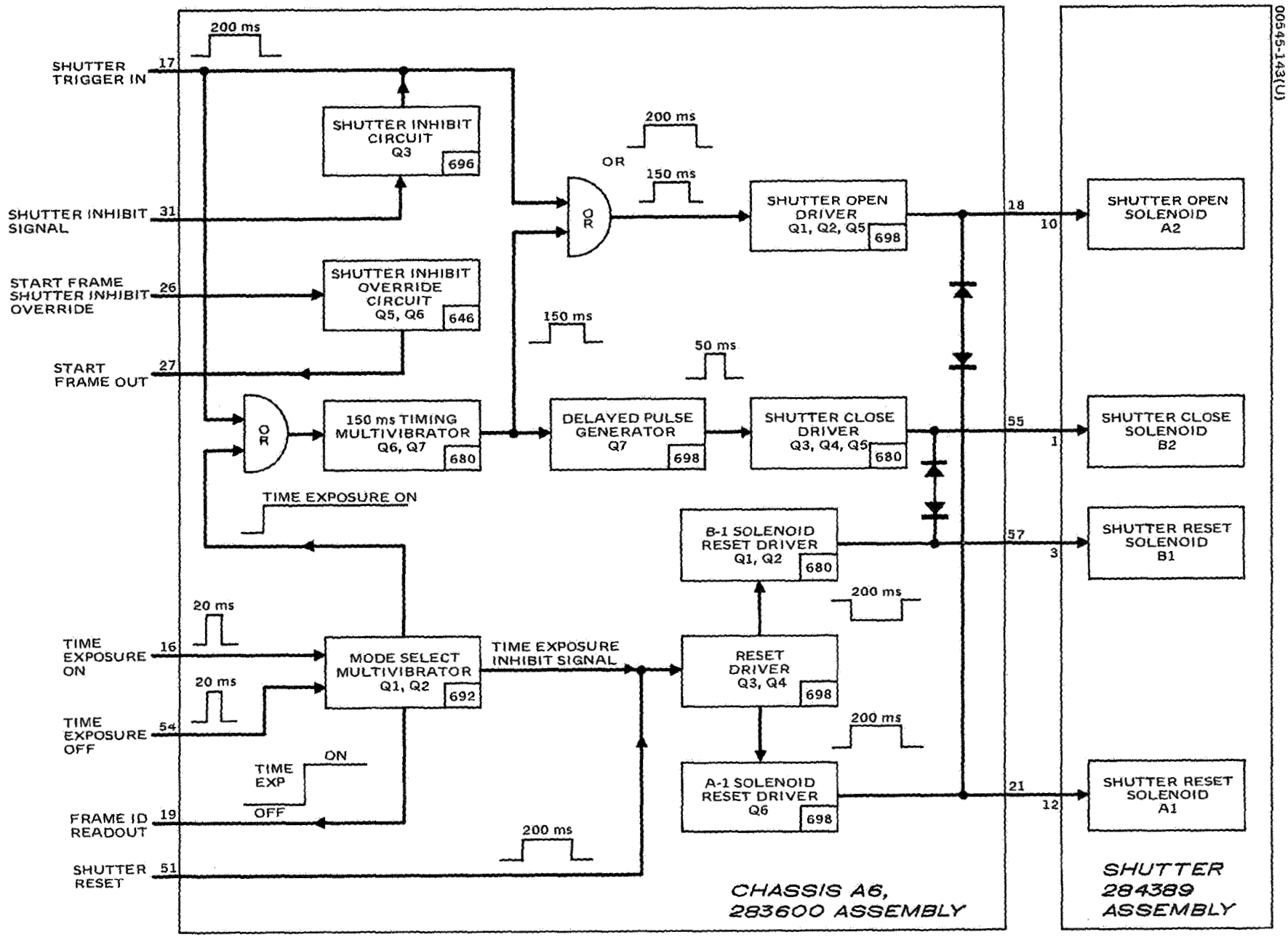

Figure F-2. Block Diagram of Shutter Control Circuits — 150 ms and Time Exposure Modes

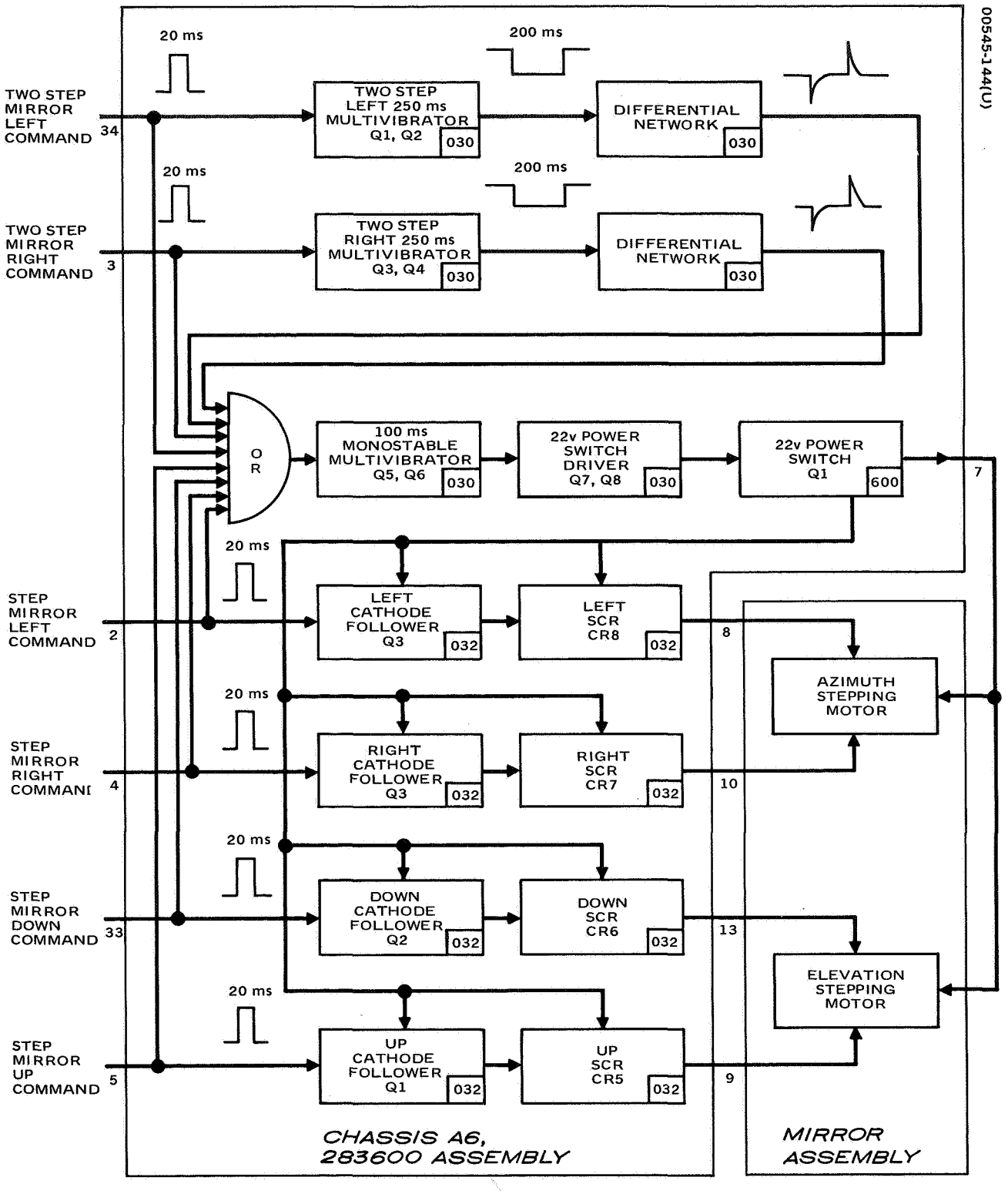

Figure F-3. Block Diagram of Mirror Drive Circuits for Mirror Stepping

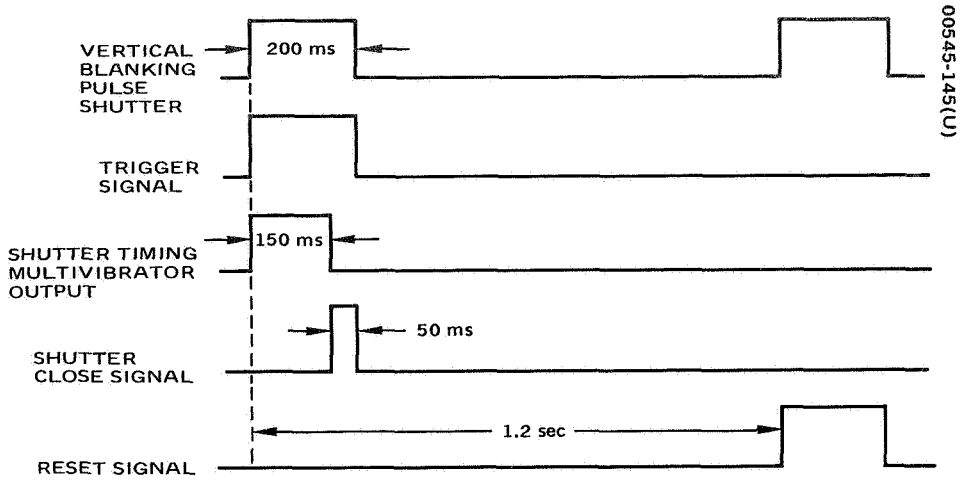

Figure F-4. 150 ms Exposure Mode — Pulse Timing Sequence

Shutter Reset Driver

The purpose of the shutter reset circuitry is to drive the A and B blades simultaneously back to their original positions. Transistors Q3, Q4, and Q6 control movement of the A blade, while transistors Q1 and Q2 control movement of the B blade.

The shutter reset signal from the video logic circuits on chassis 5 enters chassis 6 at pin 600-51 and is applied to the base of 698Q3. The shutter reset signal is a positive 200 ms pulse which is in time coincidence with the second vertical blanking pulse following the application of a START FRAME command. The positive output from the emitter of Q3 is applied to the base of 698Q4. The positive output pulse from the emitter of Q4 is applied to the base of 698Q6, while the negative output pulse from the collector of Q4 is applied to the base of 680Q1.

The positive pulse on the base of Q6 turns the transistor switch on. While turned on, the transistor switch supplies a ground return to the shutter solenoid A1. Since 22 volts is applied to the other ends of the solenoid, it becomes energized. Energizing the A1 solenoid causes the A blade to move in such a direction as to push against the B blade. Q1, which receives the negative output pulse from Q4, turns on at the same time as Q6 and applies a positive pulse to the base of transistor switch, 680Q2. Q2 turns on and completes the ground return path for the shutter solenoid B1. Since the solenoid is tied to 22 volts, completion of the ground return at 600-57 causes it to energize. Energizing the shutter B1 solenoid causes the B blade to move back to its original position. The A blade, which is moved at the same time as the B blade, exerts a slight pressure against the B blade in the direction that both blades are moving. Hence, there is no separation of the blades, which would expose the vidicon faceplate, during shutter reset operation.

Shutter Inhibit Circuit

When the light intensity is too high during the manual iris mode or too low during the automatic iris mode, a shutter inhibit signal generated in chassis 2 is applied to pin 600-31 on chassis 6. From there, it is applied

to the base of 698Q3. The positive dc voltage on the base of Q3 turns the transistor on, and Q3's collector voltage drops to nearly ground potential. The shutter trigger signal is applied to the collector of Q3 through 698R1. Hence, the shutter trigger signal is shorted to ground upon the receipt of a shutter inhibit signal from chassis 2.

Start Frame Shutter Inhibit Override Circuit

Provision is made to override the shutter inhibit signal by means of an external START FRAME SHUTTER INHIBIT OVERRIDE command input at pin 600-26 of chassis 6. This positive command pulse is applied to the base of 646Q5 through diode 646CR13, zener diode 646CR15, and resistor 646R17. 646Q5 and 646Q6 and their associated circuitry form a bistable multivibrator. When voltage is first applied to this circuit, capacitor 600C17 will charge through resistor 646R21. The charging current develops a positive pulse across R21, which is applied to the base of Q6 through 646CR11. Hence, Q6 is initially conducting, and the decrease in Q6's collector voltage is applied to the base of Q5. The multivibrator remains in this state unless triggered by an external pulse. When the command pulse is applied to the base of Q5, the multivibrator reverses its state. It remains in this condition until another external trigger is received. When Q5 is on, it provides a low impedance series circuit consisting of Q5, R19, CR10, and CR9. This low impedance combination is in parallel with resistors 696R12 and 696R13. The shutter inhibit voltage is obtained from a high impedance source; so turnon of Q5 causes the voltage appearing at pin 600-31 to drop considerably. Since only 7.7 percent of the voltage appearing at pin 600-31 is applied to the base of 696Q3, Q3 turns off. When Q3 turns off, the shutter trigger signal is no longer inhibited.

The START FRAME SHUTTER INHIBIT OVERRIDE command also performs the functions of the START FRAME command. The signal enters chassis 6 at pin 600-26 and is coupled through diode 646CR14 to pin 600-27. From pin 600-27, it is applied to the same circuit in the video logic circuits as the START FRAME command would normally be applied. Hence, the override command replaces the START FRAME command, and all the logic waveforms will be referenced to the new command.

F.1.2 Functional Description of Time Exposure Mode

The shutter opens and remains open upon receipt of a TIME EXPOSURE MODE ON command. The shutter closes upon receipt of a TIME EXPOSURE MODE OFF command followed by a START FRAME command.

Shutter Mode Bistable Multivibrator

Transistors 696Q1 and 696Q2 and associated circuitry form the shutter mode bistable multivibrator. When power is first applied to this multivibrator, current flows through 696R9 and 696CR6 and also through 696R11, charging 600C7. The charging current through R9 results in a positive voltage being applied to the base of Q2. The positive voltage is more than sufficient to allow conduction of Q2, and the resulting current

flow causes a drop in the collector voltage of the transistor. The base of Q1 utilizes Q2's collector voltage as a bias source, and Q1 will be cut off when Q2 is conducting. Upon receipt of a TIME EXPOSURE MODE ON positive pulse at pin 600-16, which is coupled to the base of Q1 through 696R3 and zener diode 696CR3, the multivibrator will reverse its state. The multivibrator will remain in the reversed state until a TIME EXPOSURE MODE OFF command is received. This command enters the chassis at pin 600-54 and is applied to the base of Q2 through 696R10 and 696DR8. The multivibrator returns to its normal state and awaits the next TIME EXPOSURE MODE ON command.

Two outputs are provided by the shutter multivibrator from the collector of C2. One output is coupled through 696CR7, 680C1, and 680CR5 to the base of 680Q6 which is part of the 150 ms multivibrator. The other output is applied to a voltage divider consisting of 696R2 and 696R1. The voltage at the junction of R1 and R2 is coupled through 696CR1 to pin 600-19. When this voltage is 4.5 volts, it represents the time exposure mode of operation. When this voltage is less than 0.5 volt, it indicates that the camera is not in the time exposure mode.

Shutter Timing Multivibrator and OR Gate

Diodes 696CR7 and 696CR9 form an OR gate which applies either a 200 ms positive shutter trigger signal or a positive dc voltage from the shutter mode multivibrator to the shutter timing multivibrator. The shutter trigger signal is utilized during the 150 ms exposure mode. When the shutter mode multivibrator is commanded into the time exposure mode, the collector voltage of 696Q2 rises. This voltage rise is applied through the OR gate to a differentiating network composed of 680C1 and 680R8. The positive pulse from the differentiating network is coupled to the base of 680Q6 through diode 680CR5, causing the multivibrator to reverse its state for 150 ms. The output from the multivibrator, a 150 ms positive pulse, is taken from the collector of 680Q7 and applied to an OR gate in the shutter open driver circuit. The appropriate waveforms are illustrated in Figure F-5.

Shutter Open Driver and OR Gate

During the 150 ms exposure mode, the input to the OR gate consisting of 698CR1 and 698CR2 is a 200 ms positive shutter trigger signal. During the time exposure mode, the input is a positive 150 ms pulse from the shutter timing multivibrator. Either of these pulses is applied to the base of 698Q1, the first stage of the shutter open driver circuit. Except for the time duration of the input signal, operation of the shutter open driver is the same in either mode. This circuit energizes the shutter solenoid A2 for 150 ms during the time exposure mode, causing the A blade to move away from the B blade. Movement of the A blade away from the B blade opens the shutter, and the shutter remains open until receipt of a TIME EXPOSURE MODE OFF command and a START FRAME command.

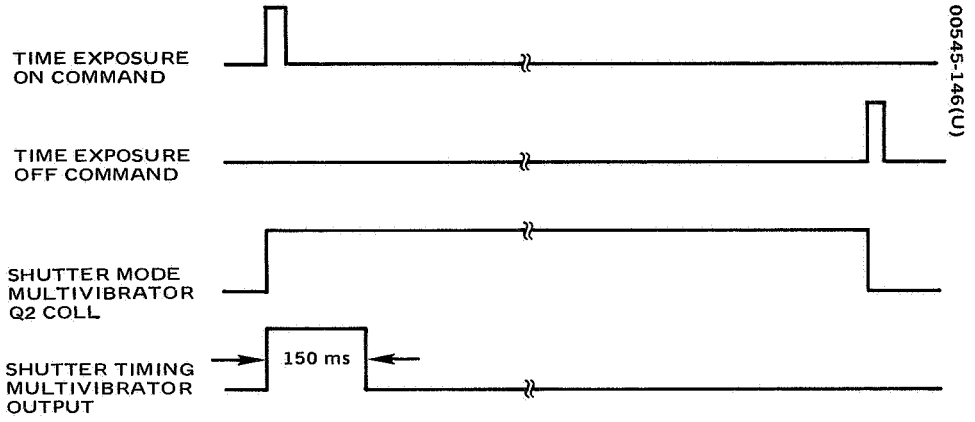

Figure F-5. Time Exposure Mode – Pulse Timing Sequence

Shutter Close and Reset Operation

The TIME EXPOSURE MODE OFF command is applied through pin 600-54, resistor 696R10, and zener diode 696CR8 to the base of 696Q2, part of the shutter mode bistable multivibrator. The multivibrator reverses its state; and the frame ID voltage at pin 600-19 drops to almost 0 volt, indicating that the shutter circuits are no longer in the time exposure mode of operation. With one exception, the circuits operate in the same manner as previously explained upon application of a START FRAME command to the camera. Since the A blade is already positioned away from the B blade, receipt of a shutter trigger signal (this signal occurs in time coincidence with the first vertical blanking pulse following a START FRAME command) results only in movement of the B blade. The B blade is moved into contact with the A blade and remains there until receipt of a shutter reset signal.

The shutter reset signal is in time coincidence with the second vertical blanking pulse following a START FRAME command and enters chassis 6 at pin 600-51. This pulse triggers the shutter reset driver. The final result is to move the A and B blades simultaneously back to the reset position. Since the blades move simultaneously, the vidicon is not exposed to light during the reset operation. The shutter remains closed until receipt of either a START FRAME command or a TIME EXPOSURE MODE ON command.

F.2 MIRROR DRIVE CIRCUITS

The Surveyor TV camera, which was fixed-mounted to the spacecraft, had the capability of scanning through use of a mirror assembly. The camera lens and vidicon directly viewed the mirror, which was incrementally adjustable in both azimuth and elevation. The mirror drive motors were dc rotary solenoids and capable of single-step or double-step operation as determined by the mirror drive circuits. Each azimuth step moved the field of view by approximately 3 degrees with a minimum stepping capability of 360 degrees (±180 degrees from the dead-ahead position). The mechanical movement of the mirror assembly in azimuth was equivalent to the optical movement in azimuth. For instance, if the mirror was rotated to the right 15 degrees, the scene observed was located 15 degrees to the right of the scene originally observed (as viewed by the camera). Each elevation mirror step moved the mirror 2-1/2 degrees, but the optical movement due to one step was 5 degrees. The number of mechanical steps from the fully closed to the fully opened position was in excess of 50, but no scene could be viewed during more than half of the elevation steps. The minimum optical viewing requirement for the camera was that it be capable of viewing scenes from 20 degrees above to 45 degrees below the dead-ahead position of the camera.

Functional descriptions of single and double-step operations are presented in Sections F.2.1 and F.2.2.

F. 2. 1 Functional Description of Single-Step Operation

The mirror stepping commands are 23 volt pulses with a time duration of 20 ±5 ms. The pulses enter chassis 6 (283600) and pass into module 233030. In module 233030, the commands are combined in an eight-section OR gate consisting of CR 9, 10, 13, 16, 19, 21, 23, and 24. The elevation command inputs are STEP MIRROR UP and STEP MIRROR DOWN. The azimuth command inputs are STEP MIRROR LEFT, STEP MIRROR RIGHT, TWO STEP MIRROR LEFT, and TWO STEP MIRROR RIGHT. The remaining two inputs are from the two-step left multivibrator and the two-step right multivibrator. The positive output pulse from the OR gate is applied to the base of 030Q5, which is part of a 100 ms multivibrator.

100 ms Monostable Multivibrator

The base of 030Q6 is connected to the junction of 030R21 and 030CR5, part of a voltage divider network. The positive voltage on the base of Q6 is sufficient to sustain conduction. The collector voltage of Q6 is applied to the base of Q5 through a voltage divider. The positive voltage on the base of Q5 is not sufficient to allow conduction, and the normal state of the multivibrator is Q5 off and Q6 on. When the positive 20 ms command pulse from the eight section OR gate appears on the base of Q5, the transistor conducts, resulting in decreased collector voltage. This decrease is coupled through 600C11 to the anode of 030CR5. The effect is to back-bias the diode and discharge C11 (the CR5 side of C11 is initially charged negatively, and back-biasing CR5 causes the diode side of the capacitor to "see" a positive 29 volt source). After a time, determined primarily by the RC time constant of 600C11 and 600R37, the voltage applied to the anode of CR5 will be positive, allowing conduction through the diode. This results in a positive voltage being applied to the base of Q6, causing it to conduct. When Q6 conducts, the decrease in its collector voltage results in cutoff of Q5 and the multivibrator reverts to its original condition. The output, a 100 ±10 ms positive pulse, from the collector of Q6 is applied to the base of 030Q7 through zener diode CR8.

22 Volt Power Switch

The positive 100 ms pulse applied to the base of 030Q7 allows conduction, resulting in a voltage drop at the junction of 030R23 and 030R24. This voltage drop is applied to the base of 030Q8, allowing the transistor to conduct. 030CR6 ensures that 030Q7 will not conduct until receipt of the 100 ms trigger pulse. Conduction of Q8 places a positive voltage on the base of 600Q1. Q1 then conducts, sending 22 volts out of the chassis at pin 600-7 to the azimuth and elevation rotary solenoids in the mirror assembly. The 22 volt power switch remains on for the duration of the 100 ms multivibrator pulse. A 0.001 microfarad capacitor is tied between the base and collector of Q1 to prevent oscillation during the mirror stepping operation.

Solenoid Return Switching Circuit

The 233032 module assembly contains transistors Q1 through Q4, silicon-controlled rectifiers CR5 through CR8, and other components which, together with some external resistors, form the solenoid ground switching circuit. The purpose of this circuit is to provide the ground return to the appropriate mirror stepping solenoid upon receipt of a STEP MIRROR command. When the +23 volt STEP MIRROR LEFT command enters the chassis at pin 600-7, it is applied to the base of emitter follower 032Q4 through 030CR15 and 600R24. The positive output pulse on the emitter of Q4 will have the same 20 ms time duration as the command pulse and will have an amplitude of approximately 15 volts. This pulse is applied to the gate of SCR 032CR8. At the same instant, a positive 100 ms pulse from the 22 volt power switch is applied to the anode of CR8 through 032CR4. Since the cathode of CR8 is tied directly to ground, the SCR fires upon the application of these pulses. The SCR acts almost as a short circuit while it is conducting and provides the ground return to the appropriate azimuth stepping coil via pin 600-8. The left stepping mirror coil of the stepping motor has a positive pulse applied to it from the 22 volt switch at this time, and simultaneous application of a ground return to its other side energizes the solenoid, causing the motor to move the mirror one step.

Operation of the stepper motor is similar to the operation of the stepper motors contained in the lens assembly. The STEP MIRROR RIGHT command enters the chassis at pin 600-4 and is applied to the base of 032Q3 through 030CR22 and 600R25. Operation of Q3 and its associated SCR 032CR7 is identical to that of Q4 and CR8. A ground return path during SCR switching is provided for the step mirror right coil of the stepping motor at pin 600-10. The STEP MIRROR DOWN command enters the chassis at pin 600-33 and is applied to the base of 032Q2 through 030CR25 and 600R28. Operation of Q2 and its associated SCR, 032CR6, is identical to that of Q4 and CR8. A ground return path during SCR switching is provided for the step mirror down coil of the stepping motor at pin 600-13. The STEP MIRROR UP command enters the chassis at pin 600-5 and is coupled to the base of 032Q1 through 030CR11 and 600R28. Operation of Q1 and its associated SCR, 032CR5, is identical to that of Q4 and CR8. The ground return path during SCR switching is provided for the step motor up coil of the stepping motor at pin 600-9.

F. 2. 2 Functional Description of Azimuth Two-Step Operation

Two-Step Left 250 ms Multivibrator

The TWO STEP MIRROR LEFT command enters the chassis at pin 600-34 and is applied to 030Q5 through 030CR9 and 030R27 and to 032Q4 through 030CR12 and 600R24. Operation of these circuits is the same as in single-step operation, and the motor is caused to step as described above.

The input command pulse is also applied to the base of 030Q1 through 030CR7, 600C18, and 030CR1. 030Q1 and 030Q2 form a 250 ms monostable multivibrator with Q1 normally conducting and Q2 cut off. The positive command pulse on the base of Q1 cuts off Q1 and reverses the state of the multivibrator. After receipt of the common pulse, 030CR2 is back-biased and 030C9 starts discharging. At the end of 250 ms, the capacitor has discharged sufficiently to allow conduction through diode CR2. Conduction through CR2 and R2 decreases the base voltages of Q1, and the multivibrator reverts to its stable state. The output at the collector of Q1, a negative 250 ms pulse, is applied to a differentiating network consisting of 030C1 and 030R5. The trailing edge of the 250 ms pulse appears as a positive spike at the output of the differentiating network. The positive spike is applied to the base of 030Q5 through 030CR13 and 030R27 and to the base of 032Q4 through 030CR14 and 600R24. This pulse, which occurs 250 ms after the leading edge of the TWO STEP MIRROR LEFT command, triggers these circuits in the same manner as does the STEP MIRROR LEFT command. Hence, the mirror azimuth drive motor steps twice upon receipt of a TWO STEP MIRROR LEFT command.

Two-Step Right 250 ms Multivibrator

Operation of the two-step right 250 ms multivibrator (030Q3 and 030Q4) is similar to that of the two-step left multivibrator. The TWO STEP MIRROR RIGHT command enters the chassis at pin 600-3 and is applied to the 100 ms multivibrator, the 250 ms multivibrator, and the SCR circuit. The motor steps once upon receipt of the common pulse and steps again when the 250 ms multivibrator returns to its original stable state.

F.3 TEMPERATURE READOUT CIRCUITS

The temperature readout circuits were utilized in the TV camera to measure the temperature of the vidicon faceplate and that of the electronic circuitry in the ECU. The temperature sensing elements were passivated planar microdiodes. Each of the two diodes was part of a bridge network, and the bridge circuit output voltage was applied to a highly stable dc differential amplifier. The differential amplifier circuit delivered a voltage representation of the sensed temperature. Functional descriptions of the vidicon and the electronic temperature sensor circuits are presented in Sections F.3.1 and F.3.2.

F.3.1 Vidicon Temperature Sensor Circuit

Bridge Network

The temperature sensing bridge consists of resistors 600R11, 12, 13, and 14 and microdiode 644CR2. Zener diode 600CR13 provides a constant 9 volts of excitation for the bridge network. The microdiode temperature

sensor is physically located within a collar which mounts on the circumference of the vidicon at its faceplate. The thermal conductivity of the metallic collar is such that the vidicon faceplate and the diode are at the same temperature. Diode CR2 has a nominal forward voltage of 0.60 ±0.03 volt dc at 77°F, and the voltage change due to temperature is -1.0 mv/°F. The output of the bridge is balanced at approximately 77°F, and equal voltages are applied to the bases of the first differential amplifier under such circumstances. Resistor 600R14 is selected during camera test so as to produce 0 volt at the output stage at the lowest temperature to be monitored.

Differential Amplifiers

At approximately 77°F, the bridge is balanced and equal voltages are applied to the bases of the first differential amplifier 158Q1. The collector outputs of the first differential are applied to the bases of the second differential amplifier, 158Q2 and 158Q3. The output of the second differential amplifier is taken from the collector of Q3 and applied to the base of emitter follower 158Q4. The output voltage of Q3 increases with a decrease in temperature. A feedback voltage developed across 158CR1 and 158CR14 is applied to the base of constant current generator 158Q8.

Emitter Follower and Output Amplifier

Emitter follower 158Q4 prevents loading of the differential amplifier by the output amplifier. The output of Q4 is applied directly to the base of output amplifier 158Q5. Zener diodes 158CR3 and 158CR4 in conjunction with capacitor 600C12 provides a constant voltage of 13.8 volts at the junction of R6 and R7 in the emitter circuit of Q5. The readout voltage is taken directly off the collector and sent through CR6 to pin 600-1. A feedback voltage is sent back to the emitter (E1) of the first differential amplifier. The overall gain of the amplifier is approximately equal to the ratio of 600R21 and 158R9. R21 is selected during test to provide a 5 volt dc output at pin 600-1 at the maximum temperature to be measured (160°F).

Constant Current Generator

Constant current generator 158Q8 provides for stable operation of the first differential amplifier 158Q1. If the conduction of Q1 increases because of an increase in temperature, there is a decrease in emitter voltages. This decrease is coupled to the bases of Q2 and Q3, resulting in less current flow through CR1 and R14 in the emitter circuits of the transistors. The decreased current flow through CR1 and R14 decreases the voltage applied to the base of Q8. The emitter voltage of Q8 is kept constant at -6.9 volts by the zener diode 158CR2. The result of a decrease in the base voltage of Q6 is less current flow through Q8 and hence less current flow through Q1. The overall effect of the feedback circuit is to maintain an essentially constant current flow through the first differential amplifier with large variations in the chassis temperature.

F.3.2 Electronic Temperature Sensor Circuit

The electronic temperature sensor circuit measures the temperature of the electronic circuitry within the ECU assembly. The temperature sensing element is diode 750CR26 which is mounted inside the ECU. Diode CR26 and resistors 600R15, 16, 17, and 18 form a bridge network which receives its excitation from the 9 volt source previously described. Resistor 600R18 is selected during camera test to produce 0 volt at the output stage (122Q5 and 600CR4) at the lowest temperature to be monitored. The output of the bridge network is applied to electronic temperature sensor module A7 (assembly 233122). Operation of the 233122 module is identical to that of the 233158 vidicon temperature sensor module. Resistor 600R22 determines the overall gain of the amplifier and is selected to produce 5 volts output at the highest temperature to be monitored (160°F). The temperature readout voltage, which varies between 0 and 5 volts depending on the temperature, is taken off the cathode of 600CR4 and sent out of the chassis at pin 600-15.

F.4 OPTICS CONTROL PULSE GENERATORS

The filter/focal length pulse generator and the focus pulse generator, part of the optics control function, were located on chassis 6. The filter/focal length pulse generator generated 100 pps which were applied to the sequence logic portion of the optics control function. During filter wheel operation, pulses were generated for 900 ms and the end result was 90 degrees of filter wheel rotation. During focal length operation, pulses were generated for 3.5 seconds. The focal length ring gear was driven from one end to the other during this 3.5 second period. During focus operation, the focus pulse generator generated 16 pps for a period of 250 ms or for an indefinite period. During STEP FOCUS operation, the 250 ms period was in effect, and each command stepped the focus ring gear 4 degrees. Upon receipt of a MULTIPLE STEP FOCUS command, the focus pulse generator continued to operate until receipt of another MULTIPLE STEP FOCUS command. The output of the focus pulse generator was applied to the sequence logic portion of the optics control function. Functional descriptions on the filter/focal length and focus pulse generators follow.

F.4.1 Filter/Focal Length Pulse Generator

Transistors Q1 and Q2, along with associated circuitry, form a free-running multivibrator which produces 100 pps when activated. Switched 29 volt power enters the chassis at pin 600-14 and is applied to the emitters of Q1 and Q2. The power is received via pin 620-11 from an OR gate (620CR1 and 620CR2) in chassis 2. The 29 volt filter power switch or the 29 volt focal length power switch located in module 283678 on chassis 1 supplies the input to the OR gate. The 29 volt filter power switch is turned on

for 0.9 second whenever a STEP FILTER command is received. The focal length 29 volt power switch is turned on for 3.5 seconds whenever a SET 100 MM FOCAL LENGTH or SET 25 MM FOCAL LENGTH command is received. Hence, the 29 volt input power to Q1 and Q2 is a pulse of either 0.9 or 3.5 seconds duration. The value of 600R5 is selected during test to produce a pulse repetition rate of 100 ±5 pps. The output is taken from the collector of Q2 and sent out of the chassis at pin 600-24. The pulses, which are 28 ±1 volt in amplitude, are routed to an OR gate on chassis 2 (263620) and then to the filter/focal length/focus ring counter.

F.4.2 Focus Pulse Generator

Transistors Q3 and Q4 and associated circuitry form a free-running multivibrator which produces 16 pps. This 29 volt power, which enters the chassis at pin 600-12, is applied to the emitters of Q3 and Q4. The 29 volt power is received from the focus 29 volt power switch located in module 283666 on chassis 1 (283610). The 29 volt focus power switch is turned on for 0.25 second whenever a STEP FOCUS command is received and for an indefinite period when a MULTIPLE STEP FOCUS command is received. In multiple step focus operation, the switch remains on until a second MULTIPLE STEP FOCUS command is received. The pulse output, which is 16 ±2 pps, is taken from the collector of Q4 and sent out of the chassis at pin 600-50. The pulses, which are 28 ±1 volts in amplitude, are sent to chassis 2 pin 620-28. In chassis 2, the pulses are applied to an OR gate and then to the filter/focal length/focus ring counter.

APPENDIX G. SUPPLEMENTARY DATA ON VIDICON AND ITS TEST PROGRAM

G. 1 CONSTRUCTION AND OPERATION OF VIDICON

Supplementary details on the construction and operation of the vidicon are presented here with reference to Figures 6-1, 6-2, and 6-3 in Section 6.

G. 1. 1 Vidicon Construction

The vidicon is composed of two major subassemblies: the tube element subassembly and the faceplate. The tube element subassembly was manufactured in accordance with standard vacuum tube assembly practice, and consists of the cathode assembly, support rods and clamps, five grids, lower and upper bulb retainer wire meshes, and target ring. These elements can be seen in Figure 6-1. The base assembly was pushed into the envelope and the glass base sealed to it. The second subassembly consists of the faceplate which is attached to the envelope by means of an indium seal. The tube was evacuated as the final step of the manufacturing process.

The vidicon construction shown in Figure 6-1 is a ruggedized version of an earlier design. A still more ruggedized redesign called a "super-ruggedized" vidicon was employed on later spacecraft. In the latter version, the upper bulb retainer wire mesh was strengthened and widened.

The principal mechanical support members between the base and the tube elements are two pieces of mesh welded to the base and to the grid 1 cup. Some support is furnished by two straps, in cross section 0.005 by 0.080 inch, which connect the stem wires with the heater support legs. At the other end of the electrode assembly, the grid 5 retainer cap is push-fit into a necked-down portion of the envelope. The upper and lower bulb retainer mesh support the tube elements and provide vibration isolation. The several parts of the electrode assembly are held in the desired spatial relationship by means of ceramic rods fastened by metal clamps.

The electrode assembly in the envelope behaves as a non-uniform clamped supported bar. During transverse vibration, the electrode assembly is relatively rigid. The stem leads bend, and the mesh pieces joining the electrode assembly to the base leads flex. The upper end of the assemblies slides and pivots on the grid 5 retainer in the necked-down portion of

the envelope. The flexing of the mesh at the bottom of the electrode assembly and the sliding of the retainer ring in the envelope both consume appreciable energy and tend to lower the magnification factor in vibration. The resonance is broad, and peaks between 200 and 400 cps.

Details of the front end assembly are seen in Figure 6-2 (Section 6), which shows a section of the grid 5 and grid 6 signal electrode assembly. Grid 5 is a 700 line by 700 line copper mesh. The spacing between the grid 5 mesh and the photoconductor is shown as 0.146 inch. If the spacing is too large, resolution is lost; if too small, the mesh pattern appears in the signal. To maintain these critical dimensions, the grid 5 mesh is spot welded between the support and retainer rings, and the assembly is heated to shrink the mesh taut. The construction is illustrated in Figure G-1. The grid 5 assembly is then welded to a ring of Kovar whose thermal expansion is lower than that of the copper mesh. This is done to minimize possible wrinkling of the grid 5 at low temperatures. This wrinkling occurred in earlier designs at the welds or between the welds because of the differential expansion between the ring and the mesh.

The electron gun part of the vidicon, known as the triode portion, is composed of the cathode, grid 1, and grid 2. Grid orifices, the spacing between the cathode and grid 1, and between grid 1 and grid 2, are critical because their alignment controls the vidicon cutoff voltage.

The faceplate of the vidicon is made of Vycor glass, ground and polished flat, and parallel. As shown in Figures 6-2 and 6-3, the faceplate is coated with a transparent conductive coating of tin oxide (Nesa) upon which is deposited the photoconductive layer. The photoconductor is a semi-transparent, proprietary, selenium derivative material. Deposited layers are less than 1 mil thick. A matrix of nichrome dots, comprising a reseau, is deposited on the surfaces of the faceplate. This matrix is utilized in correcting image information for nonlinearities and distortions. Additional reference marks are included in each corner of the scan format to provide an electronic level in the video signal, representing optical black for a photometric reference.

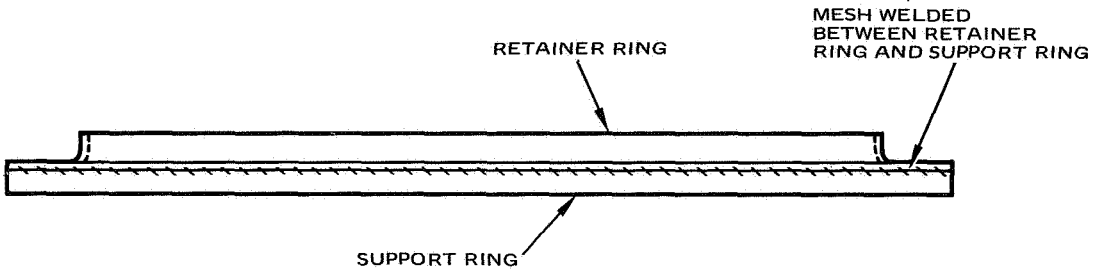

Figure G-1. Mounting of Grid 5 Mesh

G. 1. 2 Vidicon Operation

The process of obtaining television pictures starts with the receipt of the patterns of input light signals by the photoconductive faceplate. As mentioned in Section 6. 1, the output signals are obtained as voltage varies from the backplate circuit across the output resistor. By means of the combined target, photoconductivity, and secondary emission action of the scanning beam, writing and reading are accomplished simultaneously.

Writing is carried out by focusing a pattern of light on the target, whose conductivity increases at the areas which are illuminated. The target conductivity varies with the intensity of the incident light; the elements shift their potentials positive by varying amounts because of leakage currents to the backplate, which is slightly biased. In this manner, a pattern of potential variations is established on the target surface corresponding to the input light signal.

Reading is accomplished simultaneously with writing by scanning the target with the primary beam. Those elements that were not shifted positive in writing cause complete reflection of the primary beam. Those elements shifted positive in writing allow primary electrons to land. Each target element is shifted to substantially the cathode potential when scanned during reading. In this process, an amount of negative charge is deposited on each target element proportional to the amount of potential shift which occurred in writing. As a result, capacity-current variations flow to the backplate and voltage variations corresponding to the input light signal are produced across the output resistor.

In this device, separate erasing action is not required before the application of input signals since the action of the scanning beam in reading is to automatically shift the potentials of the target elements to the cathode potential, as required before writing a new pattern.

This device is capable of half-tone operation. The photoconductive process permits a relatively linear charge pattern to be established in writing at the lower light levels. Since each target element is charged to essentially the cathode potential in reading, this process also produces a linear output.

The low velocity primary electrons are focused and deflected magnetically to maintain good focusing and to cause them to arrive perpendicularly at all points of the target. To provide a uniform decelerating electric field for the primary electrons approahcing the target, a fine mesh screen at anode potential is placed at the end of the anode near the target.

Further details on construction and operation of the vidicon are given in References 8 and 29 through 31.

G. 2 EXAMINATION OF VIDICON FACEPLATE FILM

As described in Section 6.3, the slightly discolored residue found in the center portion of the vidicon faceplate was analyzed to determine the nature of the materials which may have condensed or deposited. This examination is summarized below.

The cotton Q-tips used for swabbing the front surface of the vidicon faceplate were carefully cleaned to remove any organic contaminants. This was done by repeatedly boiling the Q-tips in spectral-quality carbon tetrachloride.

Using one of the clean Q-tips and a separate reservoir of spectral-quality carbon tetrachloride, the film was then removed from the vidicon faceplate as follows: the Q-tip was dipped in the reservoir and saturated with the carbon tetrachloride, and the film on the faceplate was gently removed with it. The Q-tip was then dipped in the reservoir to remove the residue. This procedure was repeated seven times. The carbon tetrachloride reservoir containing the traces of the extracted film was then sealed off for subsequent tests.

The carbon tetrachloride reservoir with the film residue was then heated slowly, allowing the carbon tetrachloride to evaporate. The concentrated residue, which weighed about 2 mg, was placed on a small sodium chloride crystal. The remaining carbon tetrachloride was allowed to evaporate, and the crystal was put in a beam condenser set into the infrared spectrophotometer.

An infrared spectrum of the sodium chloride crystal with the film residue was then taken. Two other spectra were taken for comparison: one of a pre-extracted Q-tip which had been cleaned but had not been in contact with the vidicon, and the second of a clean sodium chloride blank crystal.

Results of the infrared spectral photometry showed that there were no detectable infrared absorption peaks from the crystal with the vidicon residue that were not characteristic of the background. The spectra for all samples were virtually identical. It was concluded that the film contaminant did not contain any appreciable organic compound such as oil, plastic, plasticizer, etc. The technique was capable of identifying as little as 0.1 mg of organic matter.

The above technique was not presumed to determine the presence of small amounts of inorganic compounds. These would not have been extracted by carbon tetrachloride, and other extraction techniques would have been required. Large pieces of inorganic matter, if present on the vidicon faceplate, would have been removed by the Q-tip. Therefore, this test also indicated the absence of such large pieces of inorganics.

Attempts were made to photograph the film prior to its removal. However, these attempts were unsuccessful because of the very small thickness of the film.

G. 3 PIRANI GAUGE MEASUREMENTS OF VIDICON PRESSURE

This section of the appendix contains a brief description of the Pirani gauge technique for measuring pressure inside the vidicon and a discussion of the tests performed and results obtained. The calibration was conducted on a spare vidicon (S/N 2957 877).

As stated in Section 6. 3. 2, the Pirani gauge technique is based on the unique relationship between the vidicon pressure and the resistance of its filament at a constant filament current. With the filament current maintained constant at some convenient value, if the pressure in the vidicon were to be changed, the applied voltage across the filament would have to be adjusted correspondingly to maintain the current constant.

The above can be explained as follows: An increase in pressure increases thermal conductivity. Assuming that the principal mechanism of heat loss from the filament is by conduction and that the heat loss by radiation is small and reasonably constant, a lower equilibrium temperature would be reached at the increased pressure.* The resistance of the tungsten filament at this lower temperature would be lower, so that a corresponding decrease in the applied voltage would have to be made to maintain the current level. Conversely, a reduction in pressure would necessitate an increase in the applied voltage.

The above calibration of pressure versus filament voltage was conducted on the spare vidicon at the constant filament current of 87 ma, corresponding to about 50 percent of the rated vidicon filament current. As explained in Section 6. 3. 2, this was done to prevent damage to the flight vidicon when corresponding measurements at this current were made on its filament in case its internal pressure was excessive.

A spare vidicon was opened and placed in an evacuated chamber to obtain the calibration data. With the constant filament current of 87 ma, the pressure in the chamber was varied from about 7×10^{-4} Torr to about 2×10^{2} Torr and filament voltage adjusted accordingly. The results are plotted in Figure G-2.

The shape of Figure G-2 illustrates the underlying physics of this experiment. The saturation effect at high pressure occurs because a high level of gas conductivity is reached whereby no further appreciable decrease in the equilibrium temperature occurs with increase in pressure; accordingly, incremental reduction in tungsten resistance (and therefore in the applied voltage) is successively smaller. The saturation effect at low pressure is due to the fact that the conductivity of the gas no longer decreases sub-

---

*Strictly speaking, this presumes constant power input. At a constant filament current, the voltage (hence, power input) is decreased at the higher pressure lower temperature final equilibrium point, but the net effect is still a decrease in temperature.

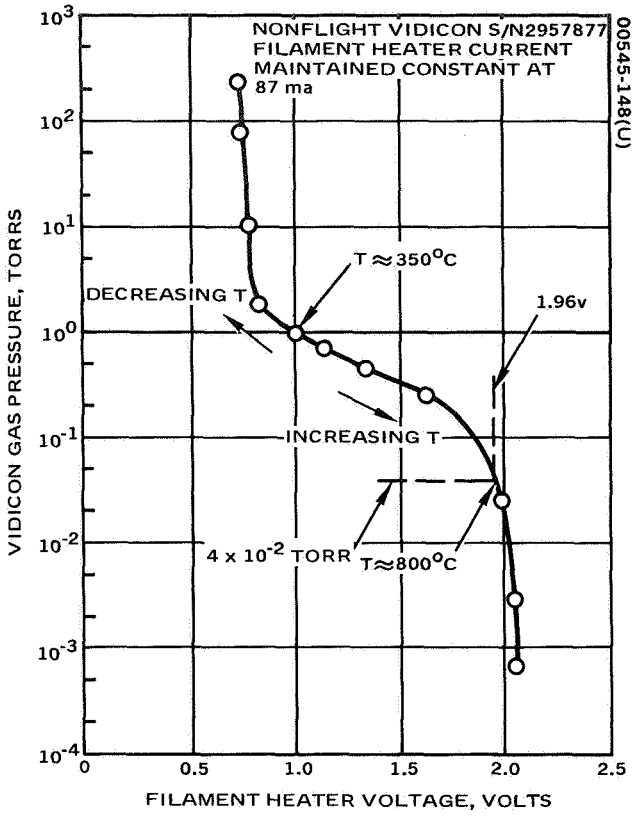

Figure G-2. Pressure Versus Heater Voltage Calibration of Non-Flight Vidicon

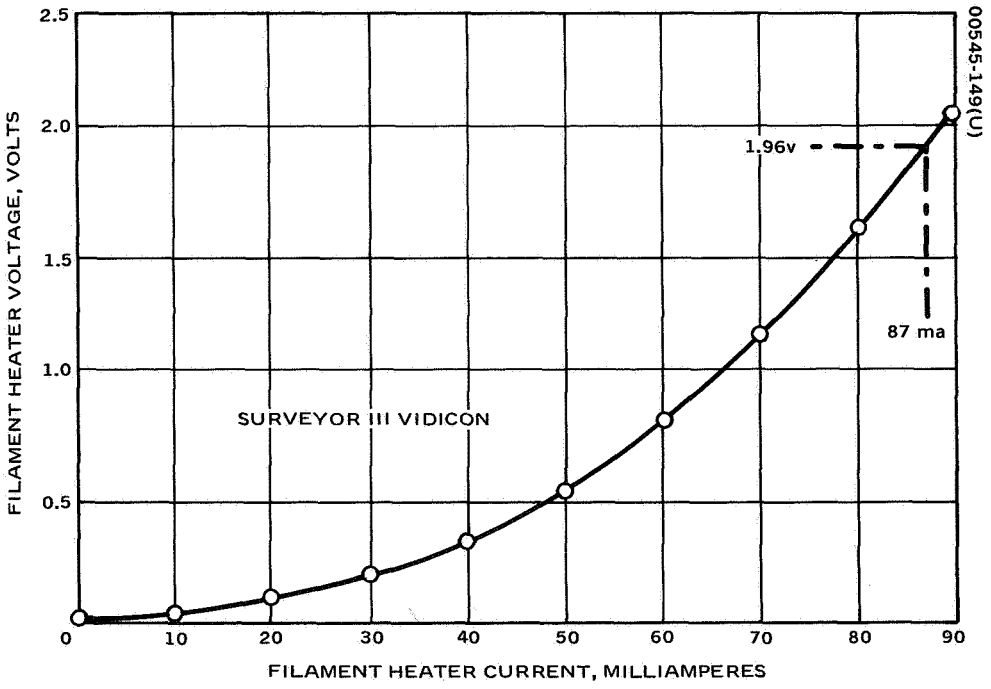

Figure G-3. Heater Voltage Versus Current Calibration of Flight Vidicon

stantially as the pressure is reduced. The primary loss of heat is now by radiation. Consequently, the incremental temperature increase is small; as the pressure is reduced, the increase in tungsten resistance is small and so is the required incremental increase in applied voltage (to maintain a constant filament current).

The approximate equilibrium temperatures are also noted at several points in Figure G-2. The low-pressure saturation region at this filament current of 87 milliamperes coresponds to a filament temperature of 800 °C. It should be noted that the emissivity of tungsten varies from about 0.03 at 0 °C to about 0.1 at 500 °. These numbers illustrate the validity of the previously noted underlying assumption that in the linear range in Figure G-2, corresponding to the critical range of pressures distinguishing bad vidicons from good vidicons, the heat loss by conduction dominates that caused by radiation. The Pirani gauge technique is most accurate in this region.

Pressure in any vidicon similar to the one used in obtaining Figure G-2 could now be readily inferred if the resistance of its filament were known at the filament current of 87 ma, i.e., if the voltage drop across its filament were measured at that current level. The pressure could be inferred simply by reading the ordinate in Figure G-2 corresponding to that voltage level. To this end, a filament voltage versus filament current plot was made on the flight vidicon in the range of currents from 0 to 90 ma, i.e., below 60 percent of rated value. Results of this measurement are plotted in Figure G-3. The voltage corresponding to the current of 87 ma was determined to be 1.96 volts. The corresponding pressure inside the flight vidicon was accordingly found to be approximately 4×10^{-2} Torr, as indicated in Figure G-2.

The fundamental limitation of the degree of accuracy obtained by the Pirani gauge technique is the degree of similarity between the two vidicons. It is estimated that the difference in the two resistances, in the temperature range corresponding to the resulting pressure level, is not greater than about 5 to 10 percent. As seen from Figure G-2, this range of uncertainty of resistance would correspond to an uncertainty of pressure less than one order of magnitude in the linear range. At the 4×10^{-2} Torr point in Figure G-2, this uncertainty is perhaps as high as a factor of two on the high pressure side. Thus, it can be concluded that the flight vidicon pressure was definitely lower than 10^{-1} Torr. On the other hand, on the low pressure side, an uncertainty in resistance of as little as 5 percent would result in an uncertainty of pressure of three orders of magnitude. Results of this test, therefore, do not preclude the possibility that the flight vidicon pressure was, indeed, as low as 10^{-5} Torr.

The conclusion of the Pirani gauge test was that the vidicon was definitely operable and that its vacuum was adequately high: at least 10^{-1} Torr and perhaps as high as 10^{-5} Torr. The test confirmed that no major leaks had occurred and that no appreciable outgassing took place inside the vidicon. A pressure level of 10^{-2} Torr could easily be expected to be reached on high-quality undamaged vidicons, which had remained in shelf storage for this 2-1/2 year length of time. It should be noted that at the time of these tests the flight vidicon had been re-exposed to the atmosphere for about 6 months since its return from the moon. A much lower pressure could actually have

existed on the lunar surface, and a minute leak in the seal could also account for the results obtained.

G.4 CALCULATION OF VIDICON PRESSURE FROM GAS RATIO MEASUREMENTS

The theory underlying the calculation of pressure inside a vacuum tube from the measurement of the gas ratio is summarized here. The gas ratio measurement and the nomenclature used were discussed in Section 6.3.4. The present discussion summarizes the underlying theory given in References 15 through 17.

The gas ratio, G_r, can be shown to be proportional to the ratio of the electron beam path length, L, and the electron mean free path, λ. The mean free path is inversely proportional to the gas pressure, P. Thus, the gas ratio is a measure of the gas pressure.

The above relationship can be written in the form

$$G_r = L/\lambda = L\, p_i\, P$$

where p_i is the probability of an ionizing collision by electrons in the gas per centimeter of electron path at 1 Torr of pressure, and P is the pressure in Torr. This relation is valid for constant velocity electrons; p_i is a function of electron velocity.

Using the relationship for the Surveyor III vidicon, with the second anode voltage of 300 volts, which corresponds to $p_i = 7.5$ for nitrogen, and taking the beam path length, L, as 9.2 cm, yields approximately

$$P = 1.5 \times 10^{-2}\, G_r \text{ Torr}$$

Substituting for G_r the value of 1.1×10^{-3}, measured in Section 6.3.4, the pressure is calculated to be approximately 1.6×10^{-5} Torr.

G.5 DISCUSSION OF GAS CONTENT MEASUREMENTS

Measurement of the gas content of both the spare and the Surveyor III vidicons was briefly described in Section 6.4.5 and depicted in Figure 6-14. The GE monopole 300 mass spectrometer used for this measurement is a very accurate instrument capable of measuring gases up to a mass number of 300.

The theory of operation is as follows. Gas molecules in the monopole are ionized by electron bombardment and accelerated to the analyzer region by a combined dc and RF electric field. The resultant ion oscillations depend in amplitude (and frequency) on the electric field and on the mass-to-charge ratio of the ions. For any given set of conditions, only one particular

group of molecules of a fixed mass-to-charge ratio follows a stable trajectory. The amplitudes of other ions are such that their isolation is not confined to the analyzer region. The stable ions are then directed from the analyzer to the electron multiplier, whose inherent amplification factor is 10^6. The output of the electrometer for each measurement of the gases of a preset mass-to-charge ratio thus is proportional to the relative content of these molecules. As the field conditions are varied to successively analyze each mass-to-charge constituent of the gas, a set of peaks is obtained, the amplitude of each corresponding to the relative concentration of the respective mass-to-charge component.

A measure of the quality of the mass spectrometer is the degree to which its sensitivity is constant over a wide range of mass numbers. The sensitivity of the spectrometer used for the tests of the vidicons was virtually constant up to mass numbers in excess of 50 and useful up to a mass number 0 in the order of 300.

The sensitivity of the mass spectrometer was 50 amp/Torr for atomic nitrogen. This permits detection of partial pressures as low as 2×10^{-11} Torr. As indicated in Figure 6-18, a Kintel microvolt-ammeter preamplifier, available with a mass spectrometer, was utilized to further amplify by some five orders of magnitude the output of the electron multiplier. With this added capability, partial pressures as low as 10^{-13} Torr or lower could be measured. The output of the system was plotted on an XY recorder. Without the electrometer amplifier rapid scanning was possible. For lower partial pressures the electrometer response limited this capability.

The dynamic range of the system, i.e., the range of pressure over which measurements can be made, depend on the noise. The limiting factor is the noise of the ion beam scattering at the highest pressure measured. In practice, the dynamic range is approximately 10^6. Thus, for a vidicon at a total pressure of 10^{-5} Torr, the minimum detectable pressure was in the 10^{-11} Torr range.

The vacuum pump used was a Varian vac-ion pump, capable of a speed of 8 l/sec. The vacuum gauge and the valves were high quality components, as indicated in Figure 6-14. To minimize the risk of breaking the manifold during the opening of the vidicon, the tubing and the manifold were constructed of pyrex glass, which is much stronger than the 7052 glass of the vidicon envelope. The manifold was constructed with a side arm and bellows to which a pointed rod was connected, as shown in Figure 6-14.

Opening of the vidicon was accomplished by gently tapping the rod until its pointed end cracked the envelope of the vidicon. Practice on several samples ensured the success of this technique, which was chosen in preference to various heating techniques considered to minimize the danger of inadvertent contamination of the gas in the vidicon by products of evaporation from the indium seal or other components.

The vacuum system was roughed down with a mechanical pump until the pressure was sufficiently low to start the vac-ion pump. The roughing pump was then sealed off as indicated in Figure 6-14 and the ion pump turned on. When the pressure was brought down to about 10^{-6} Torr, the system was baked out by wrapping a heating tape around the manifold and glass tubing.

A number of background measurements were made before the vidicon was opened. The measurement taken at the end of the initial pumpdown with the ion pump on and the vacuum gauge connected and reading 10^{-7} Torr indicated major peaks at mass numbers 2, 18, 28, 40, and 44. Minor peaks were also recorded at mass numbers from 12 to 17 (typical methane cracking pattern) and at 19, 20, 29, and 30.

With maximum gain, some traces were observed at the higher mass numbers: 57, 78, 92, 101, and 102. Mass number 102 was attributed to mercury, and the double peak at mass numbers 101 and 102 was attributed to doubly ionized mercury. The other readings were characteristic of hydrogen-carbon cracking patterns. The readings for masses greater than 44 corresponded to partial pressures lower than 1/1000 of those for lower masses. Since these background measurements of higher mass numbers were made at a sensitivity several orders of magnitude greater than that planned for the vidicon gas tests, they were considered insignificant and were disregarded for the subsequent comparison with vidicon gas measurements.

Background measurement was next performed with the ion pump and vacuum gauge off at a pressure estimated to be 10^{-6} Torr. Essentially the same type of background was measured. Additional background measurements were made up to the time the vidicon was opened under various conditions of the vacuum configuration: with valves V1 and V2 closed, with valves V1 and V2 opened, with the ion gauge on and off, with the ion pump working or shut off, and with various combinations thereof. The pressures during these background measurements varied from 10^{-6} Torr with pump and gauge shut off to as low as 10^{-8} Torr. The background readings in all these tests were quite similar.

The spare vidicon was then opened with valves V1 and V2 closed and a system pressure of about 3×10^{-8} Torr. As noted above, the opening was made by tapping the rod with a hammer. The vidicon envelope cracked circumferentially near the lower mesh retainer ring in the vicinity of the cathode where the rod struck the vidicon envelope. This region was selected intentionally to minimize potential damage to the photoconductor-grid 5 region.

The technique for sampling and examining the content of the gas utilized sequential operation of the two valves, V1 and V2, which were incorporated for this purpose. The sequence was as follows: Valve V1 was

opened to allow a sample of the gas to enter the volume between valves V1 and V2, remembering that the vidicon pressure was significantly higher than the system pressure. Valve V1 was then closed, and valve V2 opened slowly, until the system pressure as measured by the vacuum gauge rose to about 9×10^{-8} Torr. At this point, valve V2 was closed. The measurement of the gas content in the system beyond valve V2 was then made with the spectrometer. Subtracting the previously measured background content from these readings yielded the measured gas content of the released vidicon gas sample.

After a suitable time interval to allow the ion pump to remove the vidicon gas from the system and to lower the system pressure back to the original level of 3×10^{-8} Torr, the procedure was repeated. This measurement was conducted a number of times on successive samples: in each case, measurements of the background case preceded the measurements of the vidicon sample.

The spare vidicon was removed from the manifold, and the entire procedure was repeated from the start for the Surveyor III vidicon. Breaking of the Surveyor III vidicon resulted in a small hole, approximately 0.060 inch in diameter, in the glass envelope near the cathode.*

Table G-1 gives the results obtained for one of the samples of the spare vidicon and one of the samples of the Surveyor III vidicon. The corresponding background measurements are also indicated. The vidicon relative amplitude readings in Table G-1 were obtained by subtracting the corresponding background readings from the readings of the spectrometer taken after the sample of gas from the vidicon entered the system.

The values shown in Table G-1 were selected from a number of similar results obtained for the various samples as most accurate and representative although differences among the various tests were not large. The differences in the background readings for the two vidicons evident from the table were real and merely reflect the different conditions of the pumping system; they are not significant in themselves. The values recorded for the vidicons and obtained by subtracting the readings of the background taken immediately before the readings of the samples were consistent for the various samples and are believed to be reasonably accurate.

Results in Table G-1 were then used to calculate the approximate gas contents of the vidicons, as discussed in Section 6 and presented in Table 6-3.

---

*Compared to the circumferential crack produced on the spare vidicon.

TABLE G-1. MASS SPECTROMETER MEASUREMENTS OF GAS SAMPLES FROM SPARE AND SURVEYOR III VIDICONS

Mass Number	Spare Vidicon		Surveyor III Vidicon	
	Background (Relative Amplitude)	Vidicon (Relative Amplitude)	Background (Relative Amplitude)	Vidicon (Relative Amplitude)
1	0.03	2.9	0.45	1.11
2	0.33	54.0	20.0	15.5
3	0	0.65	0.015	0.100
4	0	0.5	0.01	1.55
12	0.013	0.5	0.42	0.12
13	0.001	0.13	0.04	0.28
14	0.011	5.1	2.9	0.3
15	0.001	0.95	0.35	0.45
16	0.031	1.5	0.95	0.45
17	0.034	0.07	0.25	0.035
18	0.083	0.12	0.045	0.05
19	0.01	0.01	0	0
20	0.005	0.8	0.025	0.155
28	0.144	37.3	49.0	1.0
32	0.01	0.02	0.01	0.005
40	0.07	14.5	0.85	2.95
44	0.058	3.5	1.75	0.33

APPENDIX H. SUPPLEMENTARY DATA ON COMPONENTS TESTS

This appendix contains additional data in support of the summary of components tests presented in Sections 7, 8, and 9.

H. 1 ELECTRICAL COMPONENTS SELECTION AND TEST PLAN

Table H-1 is a breakdown of all electrical components in the TV camera, grouped by types and quantity. Each type is identified by class designation, manufacturer, and Hughes Aircraft Company part number for reference. Also shown are the priority designations arrived at in consultation with the customer for the purpose of making an initial selection. The last column of Table H-1 indicates the types which were ultimately selected for testing.

The priority designation was made on the basis of the following definitions:

- Priority 1 — Parts which are currently being used in circuit design or which relate to current technology
- Priority 2 — Parts which are no longer employed but where the basic technology or a significant portion thereof is still utilized in design and fabrication
- Priority 3 — Parts no longer employed, for which construction and fabrication technology have been supplanted by new techniques

The last column of Table H-1 represents a further selection from Priority 1 types on the basis of construction or fabrication similarity, as discussed in Section 7. 1.

Additional data on the types and quantities selected for test showing their location on the various chassis in the TV camera are provided in Table H-2.

TABLE H-1. ELECTRICAL COMPONENTS IN SURVEYOR III TV CAMERA

Part Designation				Total Quantity in Camera	Selection for Testing	
Type	Generic Class	Manufacturer	Hughes Reference Part No.		Initial Priority Assignment*	Quantity Selected for Test
Resistors	GB-1/4	A/B	988601	424	1	53
	EB	A/B	988602	44	2	--
	GB	A/B	988603	2	3	--
	HB	A/B	988604	1	3	--
	CG-1/8	TI	988610	240	1	58
	CG-1/4	TI	988611	15	2	--
	NF85	MEPCO	988612	16	2	--
	CAH	A/B	988620	33	2	--
	1120S	Sage	988637	2	1	2
	60001 (or R9900)	Daven (or Ultrnx)	988640	2	1	1
	3XXX (or 118)	RDF (or RSMT)	988653	2	1	2
Capacitors	KG	Kemet	988500	76	1	38
	118P	Sprague	988501	26	1	13
	HRDM	Eimot	988502	5	1	2
	CYFR	Corning	988503	7	1	5
	VK	VIT	988504	25	2	--
Diodes	1N3070	FA	988703-1	261	1	25
	1N969B	HU-HO-PS	988704-22	4	1	--
	1N1313	HU-PS	988705-1	1	2	--
	1N1316	HU-PS	988705-4	1	2	--
	1N1317	HU-PS	988705-5	4	1	--
	1N827	MO-TR	988706-3	1	1	1
	1N938B	MO-DI	988708-2	1	1	1
	FA3075 Select	FA (FD200 series)	988719-2	2	1	2
	1N3206	MicroSem	988722-1	1	2	--
	1N3730 Select	RA	988723-1	37	1	14
	1N754A Select	CD	988732-1	17	1	10
	1N1317	PS/TRU	988735-6	1	3	--
	2N2323	GR-TR	988900-1	1	3	--
	FSP358-1	FAS	988902-1	14	2	--
	2N1930 Select	TI	988917-1	4	1	2
Transistors	2N718A	FA-PSI	908800-1	20	1	15
	2N722	FA-HU	988801-1	31	1	11
	2N871	FA	988802-1	36	1	16
	2N859	SPR	988807-2	49	3	--
	2N930	TI	988808-2	45	2	--
	2N2586	TI	988808-3	5	1	3
	2N871	FA	988810-1	10	2	--
	2N2691	FA	988814-1	2	3	--
	2N2150	TI	988817-1	2	1	--
	2N2151	TI	988817-2	1	2	--
	2N1132 Matched	FA	988823-1	3	2	--
	2N2192A	FA-GE	988824-1	5	1	1
	2N2193A	FA-GE	988824-2	2	3	--
	2N1936	TI	988830-2	1	1	1
	2N2193 Select	FA-GE	988833-1	1	3	--
	2N871 Select	FA	988838-1	6	1	--
	2N3891	FA-MH	988850-2	18	1	--
	2N2880	MH	988850-5	5	1	--

*Defined in text.

TABLE H-2. LOCATION OF COMPONENTS SELECTED FOR TESTS ON TV CAMERA

Part Designation		Quantities in Various TV Chassis									
Type	Hughes Reference Part No.	A-1	A-2	A-3	A-4	A-5	A-6	ECU	Others and A-10	Total	Quantities Selected for Testing
Composition resistor	988601	63	57	45	46	100	75	32	6	424	53
Carbon film resistor	988610	39	36	2	6	29	45	82	1	240	58
Power WW resistor	988637				1			1		2	2
Precision WW resistor	988640			1					1	2	1
Platinum thermometer	988653							2		2	2
Tantalum capacitor	988500	6	2	7	6	20	12	22	1	76	38
Metallized capacitor	988501	3		4	3		5	11		26	13
Mica capacitor	988502			1	3	1				5	2
Glass capacitor	988503			2	2	3				7	6
Diode	988703-1	62	58	12	11	38	65	6	9	261	25
Diode	988706-2					1				1	1
Diode	988708-2						1			1	1
Diode	988719-2							2		2	2
Diode	988723-1		12			5	13	7		37	14
Diode	988732-1	4				1	4	5	3	17	10
SCR	988917-1						4			4	2
NPN transistor	988800-1	4		5	5	6				20	15
PNP transistor	988801-1	5	12			2	3	9		31	11
NPN transistor	988802-1			8	8	16		3	1	36	16
NPN transistor	988808-3				2	3				5	3
NPN transistor	988824-1						3	2		5	1
NPN transistor	988830-3							1		1	1

SURVEYOR PARTS TEST PLAN — SURVEYOR CAMERA

CLASS / CAPACITOR	1/6	2/2	3/7	4/6	5/20	6/12	A/10/1	ECU	OTHER		PRIORITY
								22			1

00545-150U

HUGHES P/N	VENDOR AND VENDOR'S P/N	EIA OR MIL EQUIV.
988500	Kemet KG	CSR

		QTY
BASIC PART DESCRIPTION	Solid Tantalum Capacitor	
PART CONSTRUCTION DETAILS AND APPLICABILITY	Solid electrolyte solid tantalum capacitor. Hermetically sealed. Same basic part is used today on all high reliability and space programs.	
PARTS SELECTION TECHNIQUE	Visually examine for fractured end seals or defection terminations. Measure capacitance and D.F. and leakage current at 20% of rated voltage.	76
CHARACTERISTICS OF INTEREST	Relationship of parameters to original characteristics, effects of temperature cycling on seal and parametric performance.	
PROBABLE FAILURE MODES AND MECHANISMS	Change to contact structure due to hand vacuum effects on silver/epoxy material. This could cause a change in D.F. fractures in oxide structure due to temperature extremes causing increases in leakage current.	
PROPOSED NONDESTRUCTIVE TESTING AND JUSTIFICATION	Visual microscopic and x-ray examination to establish condition of part and configuration of internal structure. Measure parameters over temperature and voltage especially leakage current. Establish scintillation activity and voltage level and compare with new parts. This will help establish the degradation effect of the lunar environment on the oxide structure. Measure ESR with frequency to see if contact structure has changed.	6
PROPOSED DESTRUCTIVE TESTING AND OBJECTIVE	Internal microscopic examination to determine if visual changes in material appear to have occurred. X-ray diffraction and SEM analysis of oxide structure on exposed portion of lead.	2
REQUIRED SYSTEM TESTS AND JUSTIFICATIONS		

Figure H-1. Example of Preliminary Test Plan Format – Solid Tantalum Capacitor

Electrical components tests were generally conducted within the framework of established components test procedures, modified as appropriate. Early in the program, a format was developed to serve as a guide for preparing test plans for each class of components. Preliminary plans for each component were then generated. An example of such a preliminary test plan for a solid tantalum capacitor is shown in Figure H-1. Engineering judgment was used in expanding, reducing, or otherwise modifying standard test procedures, as deemed appropriate. The final detailed test procedures for each of the parts tested were prepared. These test procedures are available in program files.

H-2 DISCUSSION OF RESISTOR TESTS

H. 2. 1 Carbon Composition Resistors

Dc resistance mesurements of the 53 carbon composition resistors on the chassis indicated resistance changes ranging from a maximum of ±1. 3 percent to a minimum of -4 percent. Forty-three resistors showed a decrease and ten an increase. This is consistent with the direction of change expected for this type of construction after exposure to prolonged vacuum. Measurements of the ten resistors off the chassis showed an even narrower spread. Measurements were compared with original data available on all but three of the parts tested. It is likely that while in the lunar environment the parts shifted in resistance more than their present readings indicate because of the evaporation of moisture from the resistance element. This process would have been reversed to a great extent upon return to the earth.

Current noise measurements on the ten carbon composition resistors off the chassis correlated extremely well with the original readings, with a maximum difference of 3. 5 dB. The current noise readings reflect the total noise measured on the Quantec Model 315 noise test set used; no adjustments were made for applied voltage and system noise. This measurement technique is identical to the one originally employed in the Surveyor program in obtaining data used for comparison.

Resistance temperature characteristics measured on the ten carbon composition resistors are shown in Figure H-2. Figures H-3 and H-4 compare results obtained for two of these resistors, a 510 ohm and a 10 megohm resistor, with specification limits. A similar curve for a 1. 5 megohm resistor is shown in Figure 7-2. Curve shapes and magnitudes are what is expected for this component. No abnormalities are indicated.

The two carbon composition resistors selected for microsectioning, 1. 5 megohm and 510 ohm components, exemplify the range of these components on the TV camera. Each of the resistors was potted along with

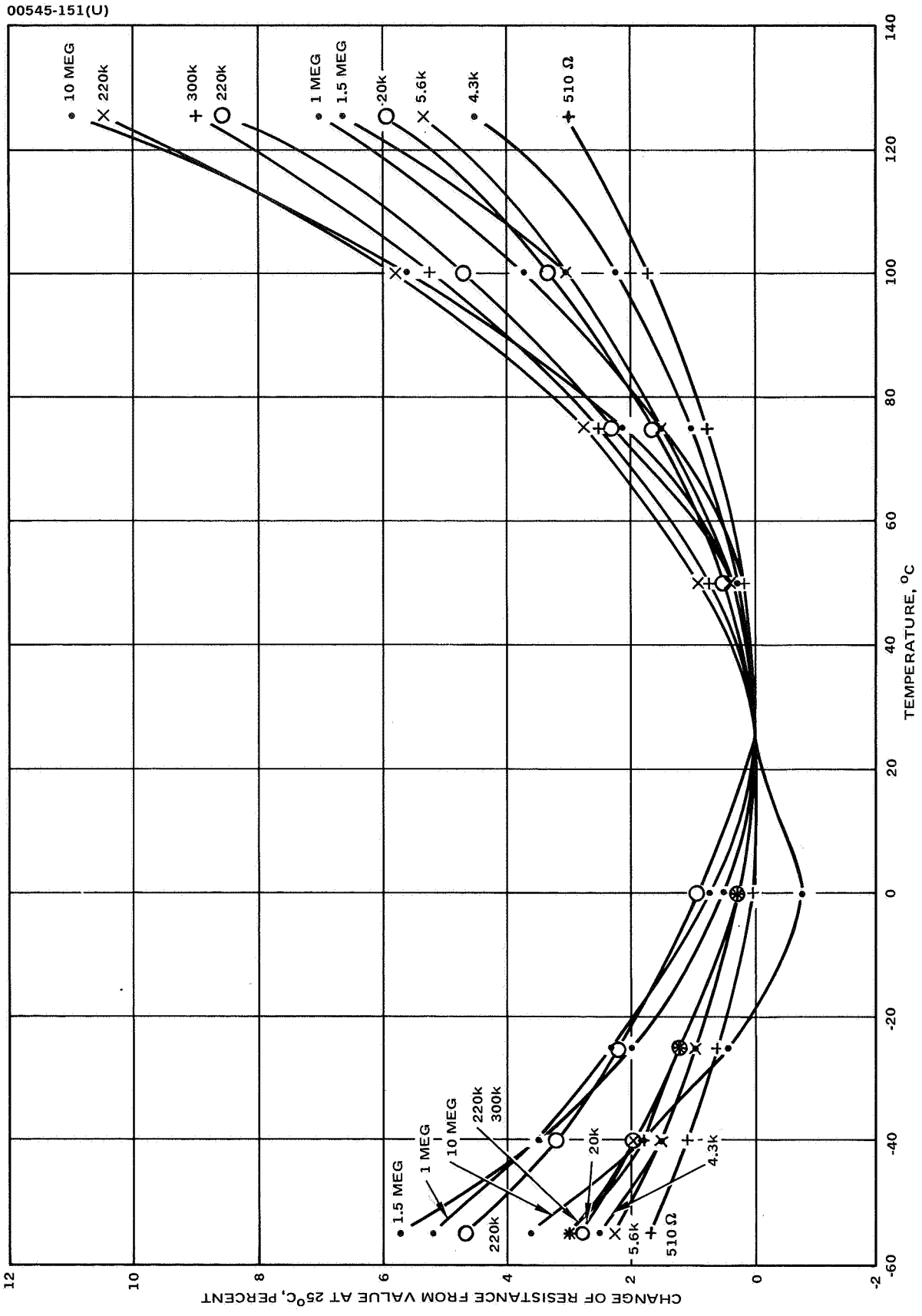

Figure H-2. Resistance Versus Temperature Measurements of Ten Carbon Composition Resistors

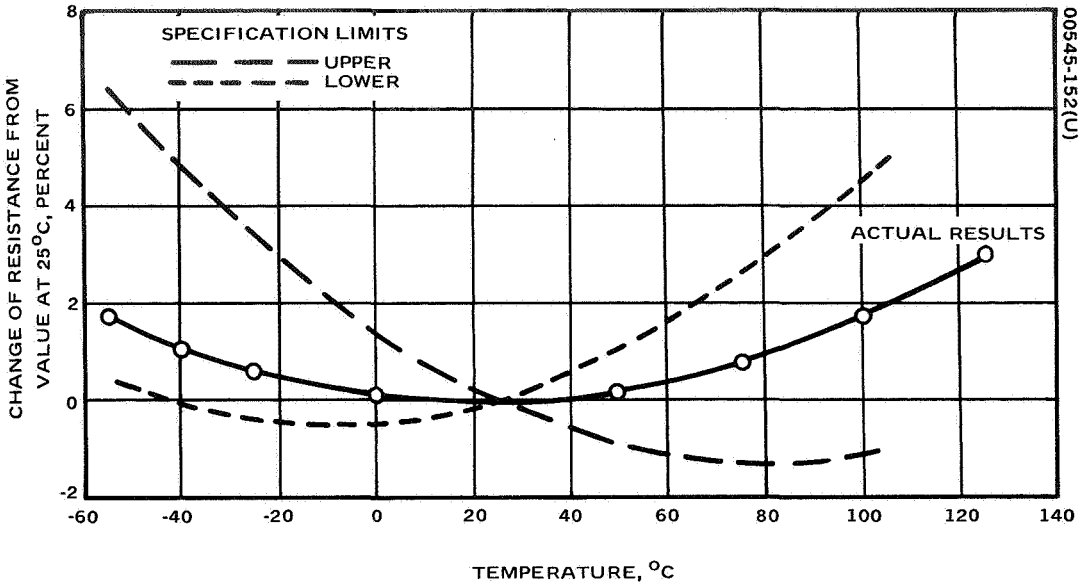

Figure H-3. Resistance Versus Temperature Measurements of a 510 Ohm Carbon Composition Resistor

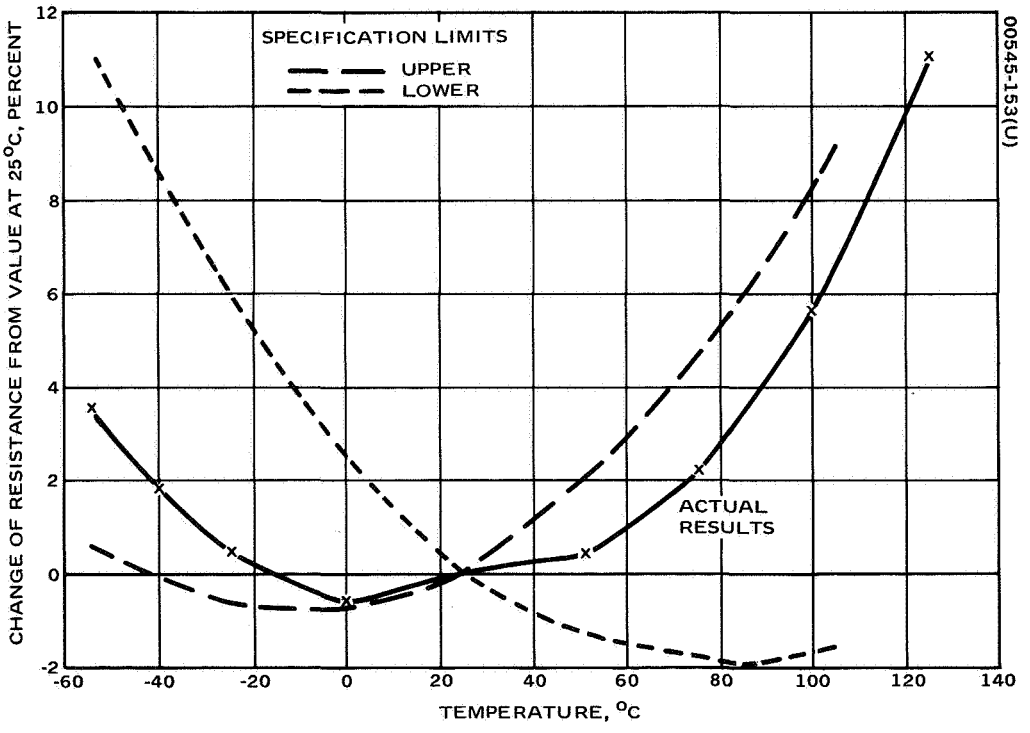

Figure H-4. Resistance Versus Temperature Measurements of a 10 Megohm Carbon Composition Resistor

two new parts produced by Allen-Bradley of the same nominal value. The new parts provided a comparison sample. Each set of three resistors was ground to approximately midpoint, polished, and examined under 200X magnification. The structure of the phenolic jacket was compared between the Surveyor part and the controls and the same was done for the bulk resistor material. Evidence of voids, cavities, or unusual changes in the grain structure or differences in structures were checked. The most likely changes believed to be brought about by the lunar environment were cracking or fracturing of the phenolic pocket in the resistance element and the formation of voids in the resistor element through the evaporation of the more volative materials in its composition. Electrically, such changes could be observed by a significant increase in the current noise figure, improvement in the impedance versus frequency performance, significant changes in resistance, and marked change in the resistance temperature characteristic. Structurally, such cracks and voids should be detectable through the metallographic sectioning and comparison with new resistance samples. As indicated in Figure 7-3, no discrepancies were noted.

H. 2. 2 Carbon Film Resistors

Ohmic resistance measurements of the carbon film resistors indicated that 19 decreased in resistance, 18 increased in resistance, and 6 showed essentially no change with respect to original data. Original data on the remaining resistors were not available.

As noted in Section 7. 2. 2, the spread on the minus side was as high as -0. 44 percent for all but one 51 ohm resistor which changed -1. 4 percent. Although the overall range of resistance change was less than that observed on the composition resistors, it was somewhat larger than expected considering the comparatively small changes found on the composition parts. In relationship to the composition resistors, it was expected that the carbon film parts would not change more than 0. 2 percent in either direction. The noted maximum and minimum changes are still well within the design tolerances for these parts. The allowable long-term drift for this part type is between 0. 5 and 1 percent.

A 93 kilohm resistor was examined under a microscope at 30X by breaking away the glass and examining the surface of the film and the edge of the spiral cut. Based upon the measured electrical characteristics, little if any change was expected. The film appeared uniform though thin, as was expected for this high resistance value; and the edge of the spiral was smooth and sharp, typical of this Texas Instrument component.

It is conjectured that lunar stress, caused by extreme temperature cycling and prolonged low temperature exposure, would most likely affect these resistors by causing fracturing or microcracks in the ceramic substrate and producing localized defects in the carbon film or increased contact resistance where the end caps join the substrate. Such changes

would have been reflected in increased current noise, erratic temperature characteristics, and large increases in resistance. None of these was detected.

H. 2. 3 Platinum Resistance Thermometer

The apparent change in the resistance and temperature coefficient of the platinum resistance thermometer appears to be worse at higher temperatures. While the basic reason for the change has not been uncovered, the fact that the temperature coefficient has changed partially accounts for this variation of the change with temperature. The resistance versus temperature characteristic is defined by a fourth-order equation in which the temperature coefficient term dominates at higher temperatures.

The decrease in both the temperature coefficient and the resistance at higher temperatures could not be explained by the postulated strains developed at low temperatures and during lunar temperature cycling. The stress caused by these environments would tend to increase the resistance and the temperature coefficient of platinum. This decrease could, however, be a result of an annealing effect.

Diagnostic investigation consisted of initial X-ray, followed by detailed examination of the resistance thermometer after the removal of the lid. No unusual construction features were found upon visual inspection. The strain loops formed during manufacture at both of the output terminals appeared normal. The platinum coils were well imbedded in the cement, and the tops of the coils were free of cement as required. The only anomaly noted in X-ray examination, and confirmed in the diagnostic inspection, was that several turns were uniformly deformed at one end of most of the coils. This is clearly visible in Figure H-5. It appeared as if something has rubbed over the coils. This deformation could have been produced during the original manufacture and assembly process.

The deformation might have resulted in a partial short of the coils during or after launch by vibration or thermal cycling, and such an effect could indeed account for an apparent change in resistance. However, such an effect could not explain the change in the temperature coefficient.

One other possible explanation for the observed change in resistance is the altering by the lunar environment of the characteristics of the cement used to anchor the platinum coils. This change might, in turn, produce sufficient change in the shunting/leakage current values to account for both the small observed coil resistance changes and the temperature coefficient change. However, this conjecture is speculative at best. Further tests of the platinum thermometer or of the second thermometer left intact might be considered, but such additional effort does not appear promising in view of the difficulty in devising and performing conclusive tests.

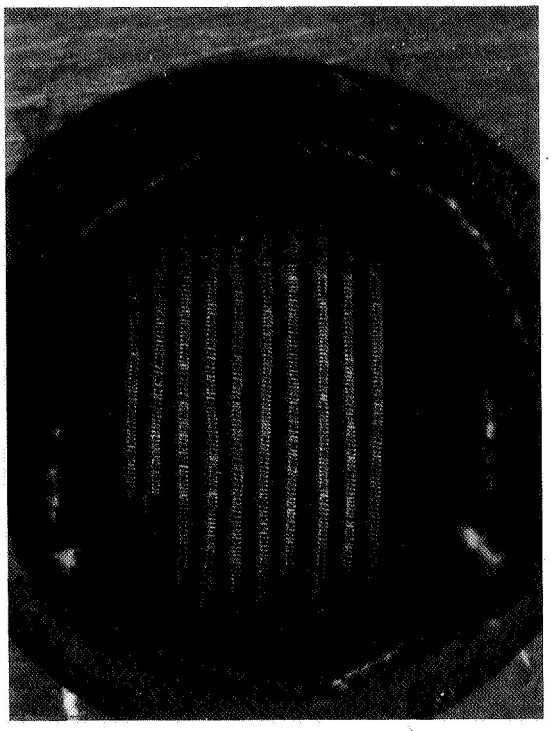

Figure H-5. Platinum Resistance Thermometer After Removal of Lead, Showing Deformation of Coils (Photo 00545-154)

H. 3 DIAGNOSTIC TESTS OF SOLID TANTALUM CAPACITORS

The significant anomaly noted in Section 7. 3. 1 was an apparent change in the dielectric of some of the tantalum capacitors, notably two of the three 47 microfarad 35 volt capacitors (samples C and D). The evidence was high leakage and high slope of leakage current versus temperature curves of these two samples. The third 47 microfarad 35 volt capacitor was nominal (sample E). Accordingly, samples D and E were selected for diagnostic examination.

The anodes were removed from their cases by melting the solder with a heat gun and then pulling on the external lead. The coatings were then removed from the anodes using a solution of 30 percent hydrogen peroxide and 10 percent potassium iodide. The two components were then examined internally. There was no evidence of scintillation of the anode surfaces. However, it was observed by comparison with the color charts of tantalum oxide that sample E had been formed at 140 volts and sample D at 130 volts.

The specification requirements for the leakage current of sample E were found to have been 0. 5 microampere, whereas the specifications for the anomalous sample D were 1. 5 microampers. Apparently, the manufacturer had increased the forming voltage requirement for sample E by 10 volts for increased insurance of meeting specifications and presumably compensated for the resulting reduction in capacitance by employing higher purity, higher yield powder. It is conjectured that this difference in the original manufacture accounted for the fact that sample E was more immune to the effects of the lunar environment.

It was concluded from the analysis of the test results and diagnostic inspection that the apparent change in the characteristics of the dielectrics of some tantalum capacitors is a definite consequence of their exposure to the lunar environment, notably low temperature and thermal cycling.

The nominal slopes of the leakage current versus temperature curve of the four capacitors, which also do not have excessively high leakage currents, are consistent with the normal characteristics of amorphous tantalum pentoxide. The higher slopes of the other units cannot be accounted for by simple resistance versus temperature dependence since the slopes are too steep: This pronounced dependence of leakage current on temperature is more typical of a dielectric phenomenon. For these samples it is conjectured that the dominant factor is crystallization of the amorphous tantalum pentoxide at defect sites. Temperature cycling presumably has increased the number of these oxide defect sites.

Another contributing mechanism of degradation may have been aggravation of the dielectric by a combination of lunar environment and application of voltage. The dielectric with greater oxide defect sites would have a lower breakdown voltage and would be more prone to scintillation upon the application of nominal voltages. These scintillations would further degrade the dielectric. This hypothesis is consistent with the scintillation at less than rated voltage, observed in tests on several of the units. This mechanism of degradation may be cumulative. It would not only lead to a high leakage current as a result of lunar exposure, but it may have also been further aggravated during the testing. Thus, the high leakage current of the two samples may have, in part, been caused by the breakdown tests conducted earlier on the dielectric degraded by lunar environment.

The evidence that the capacitor with a higher forming voltage retains its nominal characteristics tends to support the above conclusions. The mechanisms of degradation postulated above are also consistent with the mechanism of failure of the tantalum capacitor discussed in Section 12.

H.4 VACUUM TEST OF IRIS POTENTIOMETER

Noise and torque measurements under vacuum conditions were performed on the elevation and iris potentiometers in order to shed additional light on the excessive noise observed under ambient conditions, as discussed in Section 8.2. A pressure of 8×10^{-9} Torr was achieved by the ion pump system after 24 hours, using the technique of heating and subsequent cooling. As soon as this pressure was reached, noise tests were conducted using a magnetically coupled feedthrough for the drive. The noise readings for these two potentiometers under vacuum as well as in ambient tests and the results of the repeated ambient tests after the vacuum tests are summarized in Table H-3.

The apparent reduction in noise under vacuum conditions appeared initially to comply with expectations until it was discovered that the potentiometers had not been lubricated. Further analysis then indicated that the apparent reduction in noise was caused by the characteristics of the test

TABLE H-3. POTENTIOMETER NOISE MEASUREMENTS – AMBIENT AND VACUUM TESTS

Potentiometer	Noise – Equivalent Resistance, ohms		
	Original Ambient Tests	Test at 8×10^{-9} Torr	Ambient Tests After Vacuum Exposure
Elevation (1 turn)	440	28	70 (clockwise) 450 (counterclockwise)
Focus (3 turn)	70	Not tested	---
Iris (3 turn)	900	16	250 (clockwise) 700 (counterclockwise)

setup, rendering the results shown in Table H-2 anomalous. This anomaly was explained, as follows.

While the chamber pressure was down to the 8×10^{-9} Torr level at the end of the 24 hour pumping period, the inside of the potentiometer was calculated to be at a much higher pressure. The potentiometer is partially sealed. Making a reasonable estimate as to the open area around the bearing and of the outgassing rates for plastics used in construction, the pressure differential between the inside of the potentiometer and the vacuum chamber was calculated. The assumptions made were: 1) an effective orifice diameter of 0.1 mm^2 and 2) outgassing rates for the plastic materials of 0.35 Torr-l/sec/cm^2. The molecular mass for the gas was taken as 29. It was estimated that 50 hours after achieving an initial

chamber pressure in the 10^{-9} Torr range, the pressure inside the potentiometer would still be in the 10^{-6} Torr range. A valid test would therefore have required that the 10^{-9} Torr pressure level in the chamber be maintained for a considerable length of time before performing the potentiometer noise measurements. The available pumping rate of 125 l/sec would have been adequate to maintain this chamber pressure level while the potentiometer was outgassing.

Had proper vacuum conditions been attained, the noise level of these unlubricated potentiometers would be expected to have increased. However, such an increase is not expected at pressures higher than 10^{-9} Torr. Available test data indicate that there is very little increase in friction, galling, or abrasion of the contacting surfaces until a level of 10^{-9} Torr or lower is reached. The improvement in the noise observed during this test is not necessarily surprising. Under the pressure conditions inside the potentiometers during this test, the wire surfaces could actually have improved. Contaminants such as water vapor would evaporate, but at least a monolayer of water would remain on the surfaces. This moisture, plus any other low vapor pressure material, could result in noise reduction. Furthermore, removal of certain contaminants that are essentially resistive could also improve the conditions of contacts.

The starting torque was also measured during the above vacuum test with no significant changes relative to the ambient test. This test result is also consistent with the explanation postulated above.

In view of the fact that the potentiometers were found not to have been lubricated, it was decided not to conduct a second vacuum test under conditions which would ensure the maintenance of an adequately low pressure inside the potentiometers. The expected increase in the noise characteristics of these unlubricated potentiometers under hard vacuum conditions would not materially add to the understanding of their observed wear.

H.5 DISASSEMBLY OF MICRODOT CONNECTOR

To ensure the validity of the measurements of the contact separation forces, described in Section 8.5, a careful procedure for the required disassembly of the connector was developed. This disassembly, which was first performed on a non-flight connector, is briefly described here.

The connector was placed in a jig using regular harness assembly swivel clamps for support. This was done to avoid inadvertent transmission of extraneous forces.

The wrapping was removed from the cable. The wires were then cut to uniform lengths, the wire bundle combed out, and each wire stripped

0.25 inch from the end. Individual wires were numbered and identified at both ends of the connector with an ohmeter. Contact voltage drops were then measured in the mated condition.

The connector plug half was then disassembled without unmating the connector, as follows: The rear insert clamp and shell were sawed through, thus exposing the insert. The nut follower which holds the insert was removed, as well as the sawed clamp and bracket. The plastic insert was then removed.

Individual pins were then removed and their separation forces measured in the process. When all the pins had been separated in this manner, the connector shell was separated and its separation force measured.

H.6 VISUAL EXAMINATION OF LENS BARREL SUBASSEMBLY

Results obtained during the visual examination of the lens barrel subassembly, conducted by Bell and Howell, are presented here in support of the discussion in Section 9.4.3*.

The results are presented with reference to the following orientation of the lens barrel and Figure 9-7 of Section 9. The lens barrel was viewed from the front with the side plates vertical, the reflex condenser at 9 o'clock, and the focus seal rotated clockwise to the infinity end stop.

H.6.1 Fog on Beam Splitter Plate

A thin, colorless, fog-like film was noted on the beam splitter plate. The film was densest in the area farthest from both the reflex condensing lens and the shutter, at the 3 o'clock location. The film thinned out gradually from this dense area and was apparent on most of the beam splitter glass surface.

The coating could best be seen by looking through the lens from the front with bright oblique backlighting. It could also be observed by reflected light. It is expected that this coating would have a measurable effect on the lens transmission characteristic and that it might cause a certain amount of veiling glare as a result of its scattering effect on the incident light.

---

*This discussion is based on the report prepared by R. J. Nelson, Senior Optical Test Engineer, Bell and Howell Company, Optical Development Laboratories.

The material appeared to be easily removable with a wood stick although only a very small corner area was so examined in observance of the test ground rules. It is conjectured that the source of this film was outgassing from the burned-out shutter solenoid coil located in the vicinity of the lens barrel. Similar deposits were noted on other surfaces in the vicinity of the coil. A sizable dull area was also noted on the surface of the prime lens cell structure adjacent to the beamsplitter. This discoloration was in the 12 o'clock region and also appeared to be readily removable with a wood stick.

H. 6. 2 Fog on Front Lens Surface

A very thin film producing a highly specular reflection was noted on a chord-shaped area of the front lens surface. The area affected was from 6 to 10 o'clock, extending to a maximum distance of about 0. 25 inch from the visible edge of the glass. The remainder of this surface may also have had a trace of this coating, but this was not obvious.

The film was thinnest and reflected predominantly blue light in the central region of the lens element. The reflected light was colorless at the extreme lens edge. Light transmission in the area principally affected was obviously reduced, but only a moderate effect on the total lens transmission characteristic would be expected since this area is relatively small.

The film appeared to be readily removable. A minute edge area was touched with a small wood stick to demonstrate this.

While the area affected was reported to have been exposed to direct solar radiation, it is believed that the source of this contamination was outgassing from nearby materials or from original vacuum testing.

Films of similar appearance were noted after high vacuum tests of prototype lens. Similar films were also noted on the fixed focal length lens of the approach TV camera incorporated and tested on early Surveyor models, but not flown on the Surveyor spacecraft. The suspected source was oil backstreaming from the diffusion pumps of the solar-thermal-vacuum chamber and other vacuum chambers used in tests. The process involved was believed to be directional, affecting only one side of the lens. Other lens areas were protected by the filter wheel or other intervening parts. Several instances of minute droplets of oil, deposited on these intervening parts, provided additional confirmation of these effects.

H. 6. 3 Fractures in the Focal Length (Zoom) Cell

Two small internal fractures were noted in the glass element of the zoom cell: one at 12 o'clock, at the extreme edge of the cell, and

another one at 3 o'clock (more difficult to observe). The former fracture can best be seen by looking obliquely through the lens from a 12 o'clock direction, with a white background.

Similar edge fractures had been noted in the past in a few cases. Investigation indicated that these fractures were in the lens element 6 in the vicinity of one of its four holes. These fractures occurred after the modification of the original design. This entailed inseration of a small amount of epoxy through each of these holes outside of the lens aperture for the purpose of retaining the lens element. In no case, did such fractures extend far enough into the lens aperture to affect the optical characteristics. Analysis of these fractures revealed the cause to be the difference in thermal expansion coefficients between the glass and the epoxy.

H. 6. 4 Spots on Reflex Condenser Lens

Numerous circular spots were noted on the surface of the reflex condenser lens. These spots varied in size from a few thousandths of an inch to about 1/8 inch in diameter, with most of them smaller than 1/32 inch.

The spots appeared to be identical to those observed frequently on other lenses following humidity tests or thermal cycling in air. They are believed to have been caused by the deposit of water vapor droplets.

The spots appeared to rub off very easily, as confirmed by touching some of them with a fine wood stick. Based on past experience, the effect of these spots on the performance of the lens is entirely negligible.

H. 6. 5 Minor Effects on Front Lens Element

A small amount of material of brown color was noted at the extreme edge of the front lens element. The affected area extended about 0. 04 inch into the exposed glass area at the 8 o'clock location. This discoloration could only be seen with a hand magnifier under reflected light.

A similar discoloration was noted nearby on the white felt ring under the retaining ring of the front lens element. This white felt ring serves as a shield from stray light. This discoloration was on the inner half of the exposed ring width, directly adjacent to the masking retainer ring. Its orientation was principally between 6 and 11 o'clock. Lesser discoloration was noted in several other areas of the felt ring.

Comparison with previous experience suggested that this discoloration was probably due to outgassing from the adhesive used to seal the nearby retaining screws. Similar effects were noted in the past after low temperature tests. Exposure to the lunar environment may have

aggravated this condition. It is also possible that exposure to solar radiation may have contributed to it. In any event, effects on lens performance are negligible.

A small dig about 0.01 inch in diameter also was noted in the front lens element at 2 o'clock. This dig undoubtedly occurred in handling and has no bearing on lens performance.

H.6.6 Particles and Dust on Optical Elements

Several areas of apparent concentration of particles and dust were noted, as discussed below. In all cases, these concentrations were minute and are believed to have had a negligible effect on the performance of the lens.

Two small patches of opaque particles were noted inside the focal cell. These were symmetrically located at 3 and 9 o'clock about 0.25 inch from the edge. Similar patches were noted in the symmetrical location in other lenses after vibration testing. Analysis indicated that they consisted of Microseal lubricant dust.

A centered patch of low concentration and similar appearance was noted just behind the iris blades. This observation is typical of results noted on nearly all microsealed lenses after iris cycling. Previous explanation, also applicable here, attributed this to the falling of the Microseal dust from the iris blades upon the front surface of the prime lens subassembly as a result of the cycling of the blades.

The prime lens subassembly is a positively seated and piloted cell which could be easily removed for external cleaning and replaced without affecting the performance of the lens. Similar patches on other flight cameras were cleaned prior to flight.

The patch noted here was much less noticeable than the many seen previously and is expected to have had a negligible effect on the performance of the lens system.

Numerous tiny particles were also noted through the optical assembly. All of these were very small, and most are believed to have been present prior to launch. They are also believed to be Microseal dust particles and are not functionally significant.

H.6.7 Deposits on Support Structure Surfaces

Several small, irregularly shaped dull patches were noted on the front outer diameter of the lens barrel. They were located in the region between 7 and 8 o'clock outside the focus cell. When touched with a wood stick, they felt rough and did not wipe off.

Several dull spots were noted on the Microsealed ring gears. These spots resembled those described in Section H. 6. 4 on the reflex condenser lens and are believed to be also attributable to evaporated vapor droplets. These spots were partially removable with a wood stick.

The above discolorations are very minor and have no effect on the performance of the lens.

APPENDIX I. SUPPLEMENTARY DATA ON MATERIALS TESTS

This appendix contains additional data in support of the discussion of results of the materials tests presented in Section 10.

I.1 TESTS OF INTERNAL WIRE AND CABLE

I.1.1 Visual Examination

Insulation

As indicated in Section 10.2.4, some flaking was noted on the ML-FEP wire harness. These flaws occurred on wires which were wrapped beneath the teflon tape MIL-D-22241 as well as those which were held in place with nylon tie wraps with no teflon tape over the wire bundles. The flaws were usually a separation of, or flaking off, of the ML external coating from the FEP teflon inner insulation (used directly over the conductor). In some cases, this condition was aggravated by the tie wraps and particularly by the epoxy used to secure the knots of the tie wraps. In many cases, the epoxy material stuck to the ML coating or ran down the coating to fuse two adjacent wires.

When wires were separated or the tie wraps removed, a portion of the ML coating adhered to the adjacent surface of the tie wrap. This condition was more pronounced in those cases where the nylon tie wraps were not covered with the teflon wrap, but it also occurred in cases under the teflon wrap. Flaking of the ML coating was not limited to those areas under the tie wrap but seemed to occur with equal regularity between tie wraps, especially where the wire was bent. This was the case where the bundle entered connector J2. It also occurred at cable branches, where in some cases the wire was bent back upon itself almost 180 degrees, with about 1/8 inch bend radius. In one case a bare conductor was exposed, and in another the adjacent conductors in a straight wire bundle broke down at 1000 volts at 60 Hz in less than 1 minute at a spot where the ML coating was obviously damaged.

It has been speculated that this condition may have been present prior to exposure to the lunar environment since considerable flaking of the outer ML polyimide coating from the inner FEP teflon was experienced during the assembly of the spacecraft harnesses. However, an examination of the type approval test (TAT) harness did not confirm this speculation. Two cracks were observed in the ML coating of the TAT wire servicing board A6, but there was no evidence of the ML coating flaking off, even under the tie wraps. In those cases where epoxy was used to secure the tie wraps, some remained on the surface of the ML coating, but none of the ML coating had flaked off.

Solder

Some minor corrosion or greenish discoloration of the conductor occurred near the stripped end of the wire in both the Surveyor III and the TAT harness. This discoloration is typical of that caused by the wicking of the solder flux up the conductor, often found in electronic wiring. The discoloration seemed to be superficial or cosmetic in nature. No evidence has been uncovered in this investigation to indicate that this condition affected either the physical or electrical properties of the harness wires.

Solder joints appeared to be generally unaffected by lunar exposure. Some dulling of the solder surface was noted, particularly in the solder joints between the pin and wire of the J2 connector contacts on the Surveyor III harness; the solder joints of the J2 connector contacts of the TAT harness did not display quite as dull a finish. Both harnesses showed evidence of excess flux around the solder junctures. In general, the wires from both harnesses indicated non-uniform stripping of insulation and varying lengths of bare wire exposed from the solder fillet of the contact to the wire insulation.

Other

The silver plating on the conductor was bright and free of visual corrosion on both the Surveyor III and the TAT harnesses. Except for the minor corrosion already mentioned, conductor surfaces seemed unaffected by the lunar exposure.

The lacing cord tie wraps on the Surveyor III harness under the TFE teflon tape were clean and white, and the epoxy used to secure the knots was not discolored. In those cases where the lacing cord was over the TFE teflon wrap or exposed over the wire bundle, the epoxy was discolored, as were the nylon cords. The comparable tie wraps in the TAT harness did not indicate this slight discoloration. Damage to the ML coating seemed to be prevalent under most of the tie wraps examined on the Surveyor III cable. In the case of the chassis A5 wire branch, some "blocking" of the wire insulation was noted after the outer teflon tape and tie wrap were removed. The wire tended to take the shape of the open

space available in the bundle because of the flow of the plastic insulation. This condition tended to make the insulation wall non-uniform in thickness.

The two coaxial cable leads were protected by a wrap of teflon tape. After the tape was removed, the cables were visually examined and found to be unaffected by lunar exposure. The silver braid was bright, and the teflon sleeving was clear and free from cracks or other visual evidence of material damage.

Leads insulated with teflon TFE were examined visually for evidence of change. These leads were composed of six solder color TFE leads (red, yellow, purple, blue, black, and green), which were partially exposed to the lunar environment through the mirror opening. The insulation was soft and resilient with no evidence of cracking or crazing. The nylon ties were clear and in place. The colors were bright and easily distinguishable.

The six wire lead assembly from the filter wheel potentiometer, partially exposed to lunar environment, was also examined. Three of the wires were ML-FEP, and three were TFE-insulated, painted black, white, and green, respectively. All six were partially covered with clear TFE sleeving, about 3 inches of the wire were inside the tubing, and about 1-1/4 inches were outside. The wires appeared unaffected by exposure. The leads were neither cracked nor crazed. The insulation was soft and flexible and the colors clearly identifiable. The teflon tubing over the six wires was similarly unaffected.

I.1.2 Electrical Measurements

Capacitance measurements were made on a Tektronix 130 L-C meter which reads directly in picofarads. Lead lengths from the meter to the specimen were as short as possible (about 2 inches) in order to reduce the lead capacitance to a minimum. For simplicity, capacitance measurements were made between conductors of a twisted pair, triplet, or quadruplet, except in the case of the coaxial table. The instrument was nulled to compensate for lead capacitance. Results of the capacitance tests on the various typical twisted pairs, triplets, and quadruplets are given in Table I-1.

Results indicated that the capacitance values of the Surveyor III camera were very similar to those obtained on the TAT camera. However, calculations indicated that the values obtained were somewhat lower than theoretical. For example, the theoretical value of the twisted quadruplet in Table I-1 is 15 pf/ft, compared with the measured value of 11.2 pf/ft. This difference was attributed to some untwisting of the TV harness over the time of exposure and to some loosening of the wrapping during disassembly of the harness. To confirm this, two TV camera wires from Surveyor III were removed from a twisted group of six and retwisted at about two twists per inch. The capacitance of this sample was then measured to be about 14 pf/ft.

TABLE I-1. MEASUREMENTS OF CAPACITANCE OF INTERNAL HARNESS

Sample Description	Length of Sample, inches		Capacitance of Samples, picofarads		Capacitance per Foot, pf/ft	
	Surveyor III Camera	TAT Camera	Surveyor III Camera	TAT Camera	Surveyor III Camera	TAT Camera
Twisted pair, ML-FEP (from internal harness)	7.5	10.0	7.0	7.75	11.9	9.3
Twisted triplet, ML-FEP (from internal harness)	10.5	8.5	9.08 average (3 pairs)	7.6 average (3 pairs)	10.4	10.7
Twisted quadruplet, ML-FEP (from internal harness)	6.0	14	5.6 average (4 pairs)	13.2 average (4 pairs)	11.2	11.3
Twisted triplet, ML-FEP (from filter wheel potentiometer harness)	2.5		2.75 average (2 pairs)		10.9	
Twisted pair, TFE (from filter wheel potentiometer harness)	2.5		2.0		9.6	
Coaxial cable (from internal harness)	7.5	11.25	6.5 (between conductor and shield)	9.5 (between conductor and shield)	10.4	10.0

TABLE I-2. MEASUREMENT OF CONDUCTOR RESISTANCE OF INTERNAL HARNESS

Sample Description	Resistance per 1000 feet, ohms/ft		
	Surveyor III Camera	TAT Camera	Theoretical Maximum
Single conductor, ML-FEP wire AWG 26 (from internal harness)	24.0	25.8	25.8
Single conductor, ML-FEP wire AWG 22 (from internal harness)	14.0		14.6
Single conductor, TFE wire (from filter wheel potentiometer harness)	25.3		25.8
Single conductor, coaxial cable (from internal harness)	85.6	87.6	

Conductor resistance measurements were made with a Leeds and Northrup Kelvin bridge, Model 4286. Although the accuracy of some of the measurements conducted on samples less than 3 inches long was somewhat poor, the values obtained were considered sufficiently accurate for comparison purposes. Results of these measurements, summarized in Table I-2, indicate close correlation between the Surveyor III and TAT cameras and with theoretical values.

Dielectric strength of the insulation of ML-FEP wires was measured with an Associated Research high potentiometer test set. Tests were made on twisted pairs at twice the rated voltage for each wire. The tests entailed the application of 1500 volts at 60 Hz for 1 minute, followed by the application of 3000 volts ac for 1 minute. The criterion for satisfactory performance was that the leakage current measured be under 200 microamperes. All Surveyor III samples tested, including a twisted pair from the 22 volt chassis heater circuit as well as corresponding samples from the TAT camera, passed this test with one exception. In one case, where the ML coating had flaked off the surface of the FEP in a group of wires from the Surveyor III camera, a breakdown occurred at 1000 volts. In this case, the breakdown also occurred between wires near the same spot in the wire bundle.

Insulation resistance measurements were made between the ML-FEP insulated wires of a twisted pair of 500 volts dc on an Industrial Instruments Corporation Model L-7 megohm meter. Insulation resistance of typical twisted pairs of ML-FEP 24 AWG wires taken from the Surveyor III internal harness and of samples of the TAT camera internal harness exceeded 10^6 megohms in all cases. In a few instances, the values were as high as 5×10^6 megohms. These values were considered extremely good.

The pins of the Surveyor III internal harness connector J2 and of the J2 TAT internal harness connector were removed from the respective connectors, and the voltage drop across the soldered junction (between the wire and the pin socket) was measured. The joints were examined under 45X magnification prior to the voltage drop test to determine if there was any correlation between the voltage drop and the appearance of the soldered joint.

The voltage drop measurements were made on a Leeds and Northrup 4287 Kelvin bridge. Voltage drop values on the TAT J2 connector contacts and the Surveyor III J2 connector contacts are shown in Table I-3. Results indicate that no apparent changes in voltage drops were induced by the lunar exposure. Physical appearance of the solder joints was nominal, and no correlation was observable between the physical appearance of the various solder joints and their slightly different values of voltage drops.

I.1.3 Metallographic Examination and Physical Measurements

A microscopie examination was conducted on samples of the internal hookup wire and of the internal harness coaxial cable of both the Surveyor III and the TAT camera. Cross-sectional specimens were prepared by the

TABLE I-3. MEASUREMENTS OF RESISTANCE OF CONTACT TO WIRE JUNCTION OF J2 CONNECTORS

Contact Designation	Contact Resistance, milliohms	
	TAT Camera	Surveyor III Camera
1	0.1003	0.1250
2	0.1032	0.1338
3	0.1296	0.1086
4	0.1378	0.1316
5	0.1035	0.1304
6	0.1442	0.1077
7	0.1185	0.1331
8	0.1398	0.1165
Average	0.1221	0.1233

TABLE I-4. RESULTS OF MICROHARDNESS TESTS OF INTERNAL WIRE AND CABLE

Sample Description	Hardness, Rockwell F Scale Number	
	Surveyor Camera	TAT Camera
Copper alloy wire (ML-FEP) harness – ten samples tested		
Minimum reading	82.5	91.0
Maximum reading	90.5	91.5
Average reading	87.0	91.4
Soft copper shield wire (coaxial cable) – ten samples tested		
Minimum reading	57.0	57.0
Maximum reading	63.5	67.0
Average reading	60.0	62.0

structural preparation techniques and a number of photomicrographs taken. No significant metallographic changes were noted. Figures L-1 through I-6 are examples of these photomicrographs.

A cross section of the internal harness wire taken at a magnification of 50X is shown in Figure I-1. Each of the 19 strands is a copper alloy wire, AWG 36 (0.005 inch in diameter). The rating of the 19-strand conductor is AWG 24 (0.025 inch in diameter); the diameter of the wire including the insulation is 0.0389 inch.

Photomicrographs of adjacent strands, taken at a magnification of 1000X are shown in Figures I-1 and I-2 for the Surveyor III camera and for the TAT camera wires, respectively. The appearance of the two samples is similar.

A cross section of the Surveyor III coaxial cable taken at a magnification of 25X is shown in Figure I-4. The internal strands are steel conductors, copper-covered and silver-coated, AWG 34. The shield conductors are silver-plated braided copper wires, AWG 38. Photomicrographs of the shield conductors, taken at a magnification of 1000X, are shown in Figures I-5 and I-6 for the Surveyor III camera and for the TAT camera cables, respectively. Again, the metallographic appearances are similar.

Microhardness tests were conducted on this metallographic specimen using a Lietz hardness tester with a 25 gram load. Results are summarized in Table I-4. Ten different samples of the ML-FEP copper alloy wire were measured along with ten samples of the soft copper shield wire of the coaxial cable of both cameras. Results indicated that no significant changes in hardness of either of the two materials occurred as a result of the lunar exposure.

Tensile strength and elongation measurements were conducted on the various samples listed in Table I-5. These properties were measured both on the conductor and on the insulation. Although insulation measurements conducted as part of tests of the assembled wires were inherently inaccurate, they were conducted as a contingency in the event that subsequent tests of the insulation alone (discussed in Section 10.4.3) proved unsuccessful. The values recorded here are therefore superseded by the data presented in Section 10.4.3. Measurements on the internal ML-FEP wire and on the internal cable were also recorded for comparison on the TAT camera. The other samples included both the ML-FEP and the TFE type wires from the filter wheel potentiometers; the latter included protected samples, as well as those partially exposed.

The tensile strength and elongation tests were performed on an Instron tester, per Federal specification QQ-W-343 for wires and ASTM specification D-882 for the insulation. Results are summarized in Table I-5. The results of tensile strength measurements of the Surveyor III samples are all within the requirements of the original Hughes specifications and compare favorably with values obtained for the TAT camera. For example, the specified minimum breaking strength of the ML-FEP wire conductors is 18 pounds. Results of elongation measurements indicate a general

TABLE I-5. MEASUREMENT OF TENSILE STRENGTH AND ELONGATION OF INTERNAL WIRES AND CABLE

Sample Designation	Tensile Strength, pounds		Elongation, percent	
	Surveyor III Camera	TAT Camera	Surveyor III Camera	TAT Camera
FEP-ML insulator wires (from internal harness)	Conductor 24.8 Insulator 2.6	Conductor 21.8 Insulator 3.1	9 (in 2 inches) 10 for ML coating; 170 for FEP	 30 for ML coating; 80 for FEP
Coaxial cable (from internal harness)	Conductor 15.9 Primary Insulation 12.3 Shield 16.9 Jacket 9.5	Conductor 16.1 Primary Insulation 12.7 Shield 12.7 Jacket 8.0	4 70 18 80	24 318 247
FEP-ML wire (filter wheel potentiometer, under TFE tubing)	Wire 18.3 Insulator 2.62		11 (in 2 inches) 75	
TFE insulation (filter wheel potentiometer, under TFE tubing)	Wire 10.0 Insulator 3.83		21 120	
TFE insulation (filter wheel potentiometer, outside TFE tubing)	Wire 12.3 Insulator 5.5		18 248	

compliance with specifications. The minimum specified elongation of the ML-FEP wire, for example, is 6 percent. On the other hand, a reduction in elongation of the Surveyor III wires relative to that measured for the TAT camera wires is inferred. This difference reflects the apparent increase in wire brittleness caused by the lunar exposure.

A test to determine the cut-through rating of insulation was conducted at room temperature on the various samples are shown in Figure I-6, using a standard cut-through fixture. The cut-through rating of the insulation was defined as the force in grams sustained by the insulation for a minimum of 24 hours at the point of wedge contact. A sensing relay indicated the "cut-through" when the load wedge made an electrical contact with the central conductor of the wire.

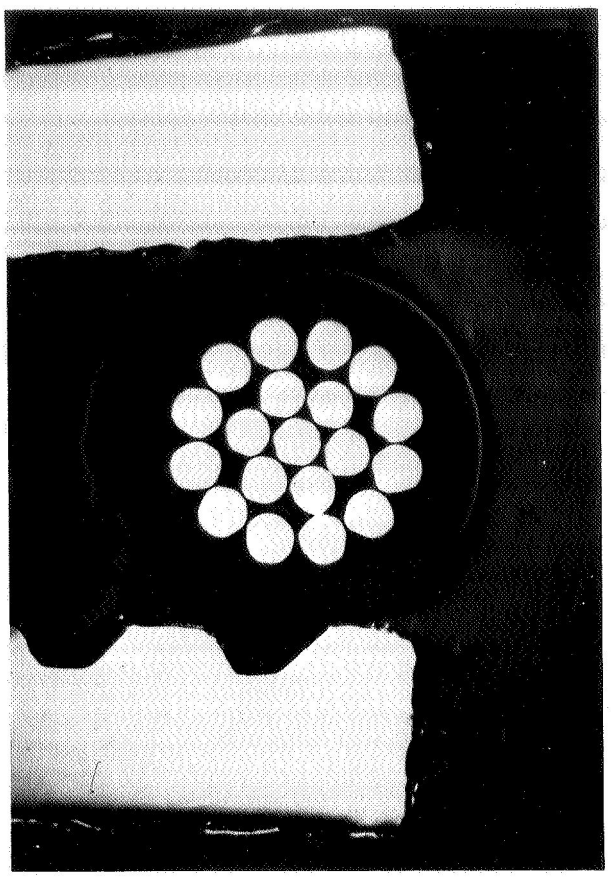

Figure I-1. Photomicrograph of Surveyor III ML-FEP Internal Harness Wire (50X Magnification) (Photo 00545-155)

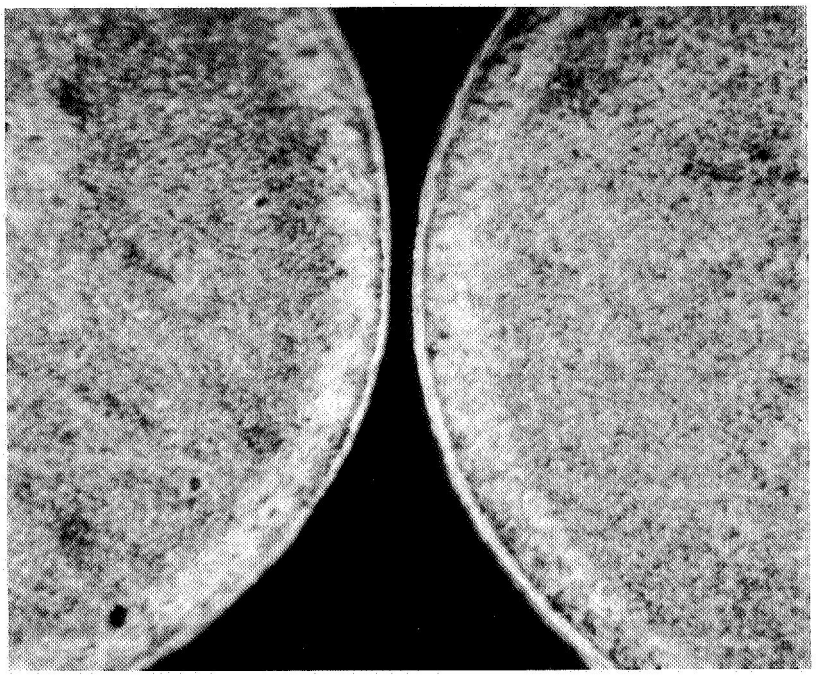

Figure I-2. Photomicrograph of Surveyor III Internal Harness Wire Strands (1000X Magnification) (Photo 00545-156)

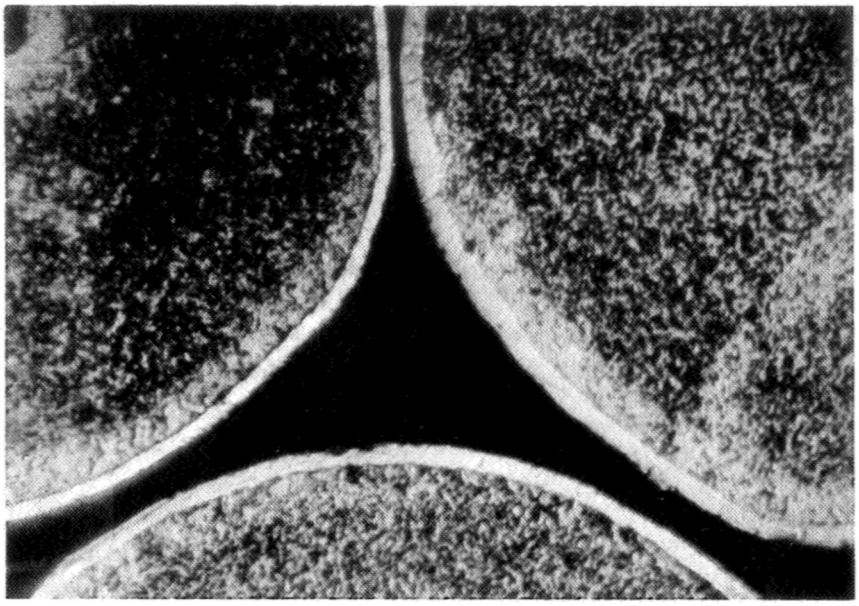

Figure I-3. Photomicrograph of TAT Camera Internal Harness Wire Strands (1000X Magnification) (Photo 00545-157)

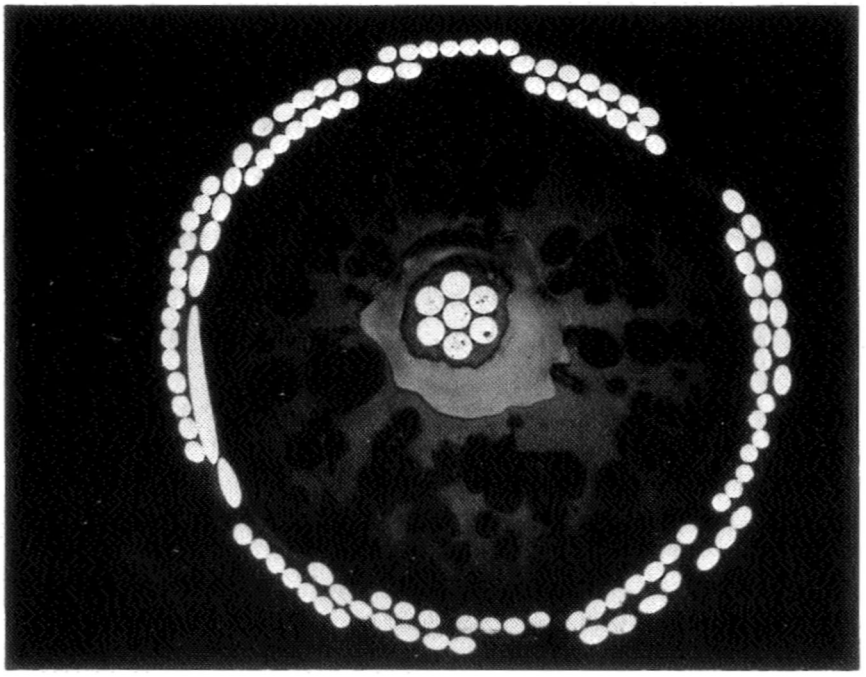

Figure I-4. Photomicrograph of Surveyor III Internal Coaxial Cable (25X Magnification) (Photo 00545-158)

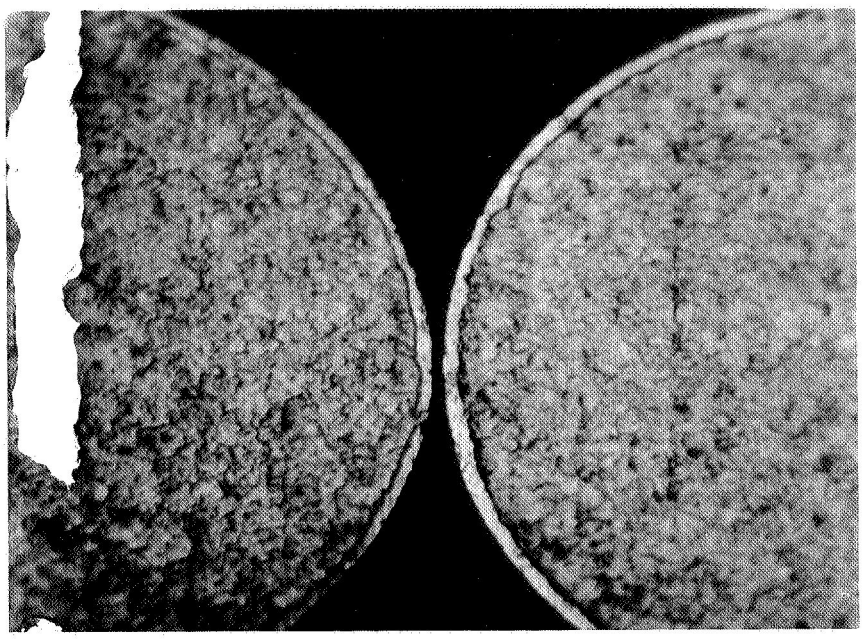

Figure I-5. Photomicrograph of Shield Conductors of Surveyor III Coaxial Cable (1000X Magnification) (Photo 00545-159)

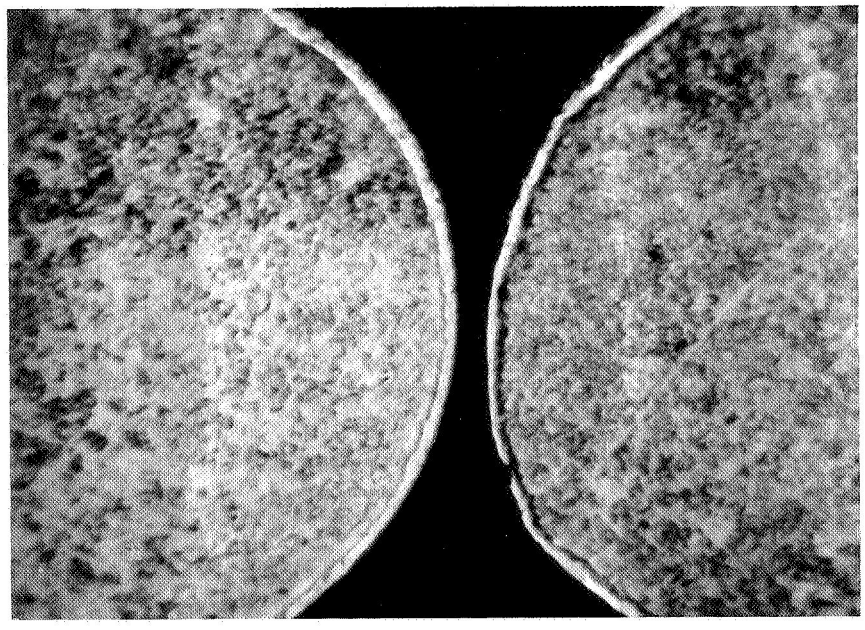

Figure I-6. Photomicrograph of Shield Conductors of TAT Camera Coaxial Cable (1000X Magnification) (Photo 00545-160)

TABLE I-6. RESULTS OF MEASUREMENT OF INSULATOR CUT-THROUGH RATINGS

Sample Designation	Insulator Cut-Through Rating, grams	
	Surveyor III Camera	TAT Camera
ML-FEP wire (internal harness)	280	280
ML-FEP wire (filter wheel potentiometer, under TFE tubing)	230	
ML-FEP wire (filter wheel potentiometer, outside TFE tubing)	140	
TFE wire (filter wheel potentiometer, under TFE wire)	200	
TFE wire (filter wheel potentiometer, outside TFE tubing)	140	

Test results shown in Table I-6 indicate that the internal ML-FEP wire of the Surveyor III camera had a cut-through rating of 280 grams, identical with that of the wire from the TAT camera. However, a similar wire used as a component lead for the filter wheel potentiometer, partially exposed to the solar radiation through the mirror assembly opening, had a lower cut-through rating. The decrease depended on the degree of exposure. The partially exposed ML-FEP exhibited a reduction in the cut-through rating of about 25 percent; the same wire outside the TFE tubing, which was more directly exposed to the radiation, exhibited a decrease of 50 percent. Similar changes were also observed for the TFE wire, as indicated in Table I-6.

Measurements of the tensile strength of solder joints between the wire and pins of the J2 connector of the internal coaxial cable were conducted, using the Instrom tester. The same measurements were also conducted on the connector of the TAT camera for comparison. Ten contact solder joints were tested to failure, and the results are summarized in Table I-7. No apparent degradation by the lunar environment could be derived from these readings although the average of the ten samples indicated an apparent reduction of about 2 pounds.

TABLE I-7. MEASUREMENT OF TENSILE STRENGTH OF CONNECTOR SOLDER JOINTS ON INTERNAL CABLE CONNECTOR

Designation	Tensile Strength of Surveyor III Camera J2 Connector, pounds	Tensile Strength of TAT Camera J2 Connector, pounds
1	24.5	23.0
2	29.0	28.5
3	23.5	27.3
4	24.0	27.2
5	24.5	27.3
6	24.5	26.0
7	24.9	28.5
8	25.0	27.5
Average	24.9	26.9

I.2 CHEMICAL ANALYSIS OF ORGANIC MATERIALS

I.2.1 Infrared Spectrochemical Analysis

Teflon TFE

Infrared transmission measurements as a function of wavelength were conducted on three samples of the teflon TFE film: one from the mirror assembly base collar of the Surveyor III camera, one from the collar of the TAT camera, and one from the horseshoe-shaped base of the mirror housing of the Surveyor III camera. In addition, spectra of the samples were obtained by measurement of the attenuated total reflectance.

The infrared spectra of the two samples of teflon TFE film from the collar of the Surveyor III camera and from the TAT camera are shown in Figure I-7. The two spectra are quite similar. The characteristic absorption peaks noted at 8.3 and 8.7 microns are as expected for this type of materials. No evidence of any contamination or of any chemical changes was uncovered.

The spectrum obtained of the teflon TFE film from the horseshoe-shaped seal of the mirror housing is shown in Figure I-8. The resulting plot reflects the presence of the adhesive used to bond the seal to the mirror assembly hood. Again, no effects of chemical changes by lunar exposure can be seen.

No data of additional significance were obtained from the attenuated total reflectance measurement.

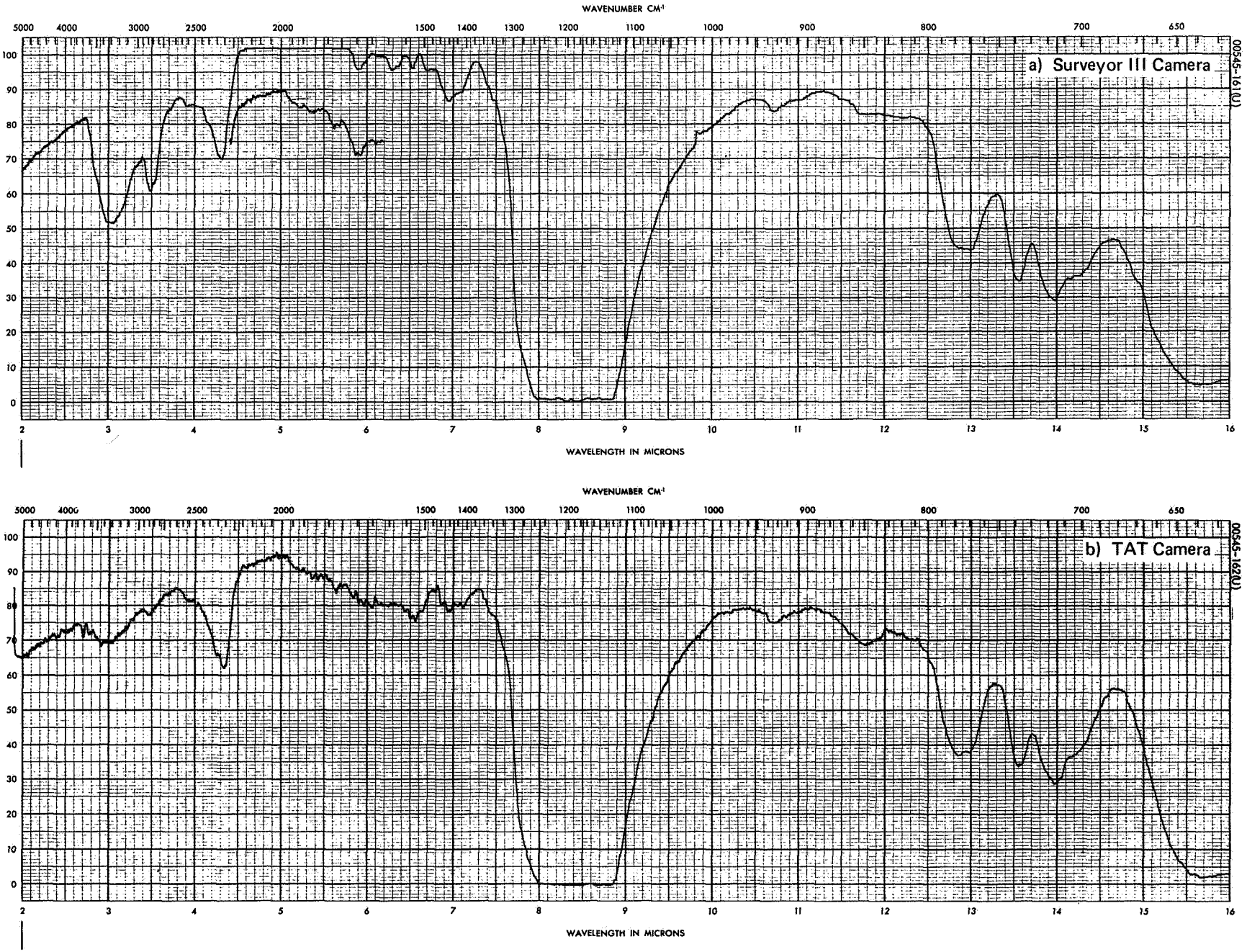

Figure I-7. Infrared Transmission Spectra of Teflon TFE From Camera Mirror Assembly Collars

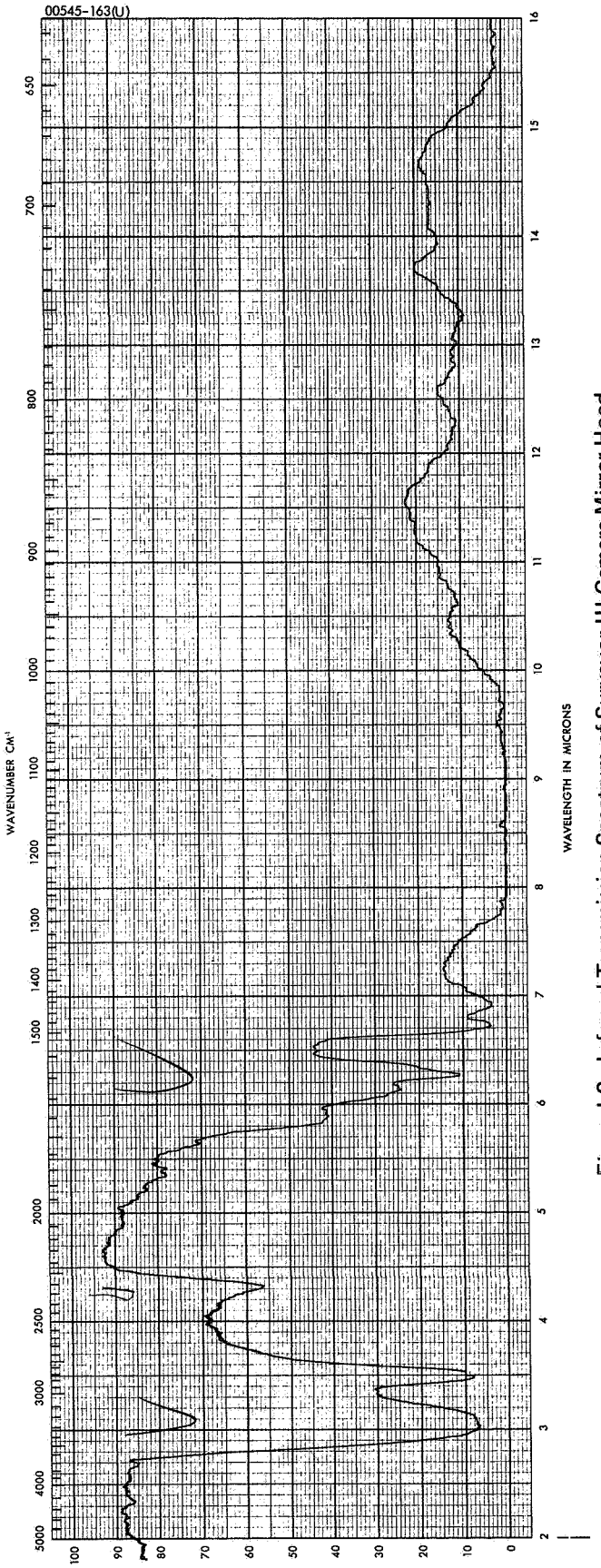

Figure I-8. Infrared Transmission Spectrum of Surveyor III Camera Mirror Hood

Nylon

Infrared transmission measurements were made of the nylon material from the cable ties of both the Surveyor III camera and the TAT camera. The technique used was to disperse the nylon from the cable ties in potassium bromide, and to perform the test on pellets made from the dispersion. Samples tested included those taken from the light and dark areas of the Surveyor III nylon ties. Tests included samples of both the 6 nylon and the 6, 6 nylon materials. Additional spectra were then taken of samples which were dissolved and precipitated.

Results of these measurements were all nominal. No differences were noted between the Surveyor III samples and samples which had not received lunar exposure.

Attempts to conduct attenuated total reflectance measurements were not successful due to the insufficient area of contact with the braided nylon. This effort was abandoned in view of the nominal results obtained from the transmission tests.

Polyimide

Infrared transmission tests were conducted on the polyimide wire insulation film after its removal from the teflon. Samples were tested from both the Surveyor III camera and the TAT camera. The infrared spectra were all identical, indicating no apparent effect of the lunar environment. However, the spectra differed considerably from those of a sample of pure polyimide.

Further analysis indicated that this difference is entirely attributable to the high content of teflon on the removed polyimide films. The difficulty of separating polyimide from teflon resulted in a very significant teflon content in the tested film samples from both camera. The infrared spectra of these samples both indicated a teflon content on the order of 75 to 80 percent. This was in complete agreement with similar findings reported below in the course of the conduct of elemental analysis.

I.2.2 Ultraviolet Measurements

The above teflon TFE nylon and polyimide samples were then subjected to transmission measurements in the ultraviolet and visible regions from 0.2 to 0.75 micron. Results were compared with runs on a pure solvent used as reference. The tests were conducted using a Perkin-Elmer 202 ultraviolet visible spectrometer.

Results of tests conducted on the teflon TFE film are shown in Figure I-9. It is seen that the film exhibited high absorption in the ultraviolet range and had a diffuse edge at 0.45 micron. No evidence of structure was noted, and results were nominal. Therefore, it was concluded that no significant chemical changes took place.

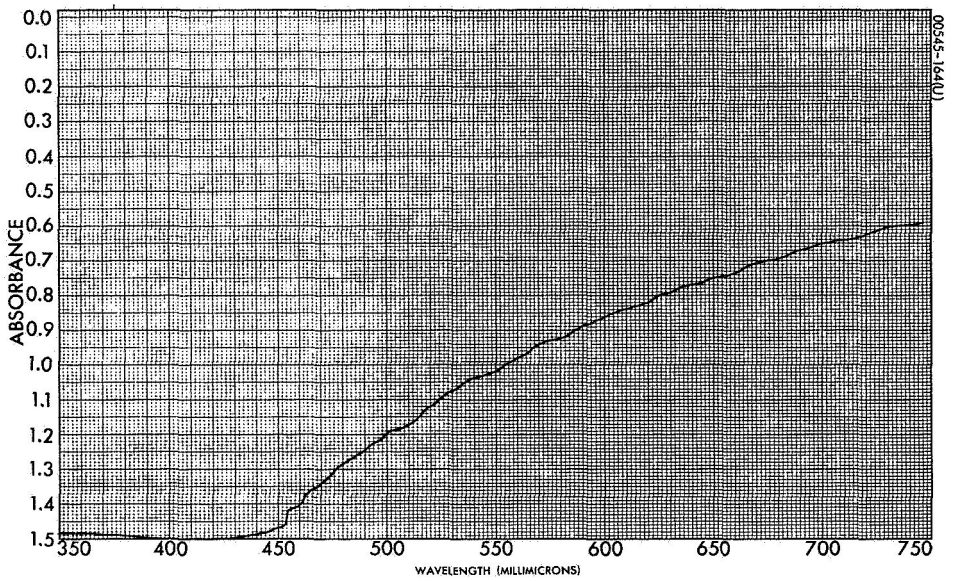

Figure I-9. Ultraviolet Transmission Spectrum of Teflon TFE From Surveyor III Camera

Ultraviolet transmission tests of nylon were performed by testing solutions of exposed nylon in formic acid from which unsoluble material was filtered. There was no evidence of chemical changes induced by the lunar environment.

Ultraviolet transmission tests were then conducted on the polyimide films removed from the wires of the Surveyor III and TAT cameras. As noted above, the removal process was difficult, so the films retained a high teflon content. Resultant spectra confirmed the presence of teflon and showed no evidence of any effects of the lunar environment. The absorption edge was observed to occur at 0.44 micron for the polyimide film from the Surveyor III camera, as opposed to 0.455 micron for the film from the TAT camera. This difference may be compared with results obtained in the elemental analysis (Section I.2.3), which indicate a relatively lower content of teflon retained by the polyimide film taken from the TAT camera during its removal from the wires.

I.2.3 Elemental Analysis

Results of the elemental analysis conducted on teflon TFE, nylon, and polyimide samples from the Surveyor III and TAT cameras are summarized in Table I-8. The location from which the samples were taken is also indicated, as well as the elemental content theoretically expected for teflon TFE and nylon. The percentage weights found do not add to 100 because the analysis was limited to the measurements of carbon, hydrogen, nitrogen, and fluorine.

Results obtained for teflon indicate that the content of all samples closely corresponded to that expected for their carbon fluoride structure. No significant difference was noted between the TAT and Surveyor III

TABLE I-8. RESULTS OF ELEMENTAL ANALYSIS OF ORGANIC MATERIALS

Material	Percentage by Weight*			
	Carbon	Hydrogen	Nitrogen	Fluorine
Teflon TFE, Surveyor III camera	23.42	0.08		70.68
Teflon TFE, TAT camera	23.96	0.14		70.72
Theoretical values	24.00	0	0	76.00
Nylon tie, Surveyor III mirror housing connector	61.69	9.40	11.35	
Nylon tie, Surveyor III filter wheel motor	62.00	9.43	11.43	
Nylon tie, TAT camera	67.35	10.48	9.15	
Theoretical values	63.69	9.80	12.38	
Polyimide, Surveyor III filter wheel potentiometer wire	25.83	0.33		68.36
Polyimide TAT camera wire	27.83	0.45		65.76

*Only C, H, N, and F content measured.

samples. The darkening noted on the Surveyor III sample in visual examination is believed to be a very small trace of free carbon, too small to identify by the elemental analysis technique.

Results of the elemental analysis of nylon were not conclusive because an undetermined amount of epoxy adhesive may have contaminated the sample. However, had a significant breakdown or evaporation occurred in the nylon during the lunar exposure, the resulting change would have been expected to become evident during this test.

Elemental analysis of the polyimide insulation samples confirmed the presence of the teflon, as previously noted. Analysis of the numbers given in Figure I-7b indicated that the teflon content was on the order of 75 to 80 percent. The important observation here is that no apparent significant difference was found between the Surveyor III and the TAT samples, indicating that no major changes could be attributed to the effect of lunar exposure.

I.2.4 Molecular Weight Measurements

The molecular weight was determined only for the nylon samples. This determination was made by measuring the relative viscosity of similar

solutions, one containing dissolved nylon from the TV camera, and the other one used as reference. The nylon samples were dissolved in formic acid. The insolubles noted (probably epoxy adhesive) were filtered off, washed, and dried. The viscosities of the nylon solution and of the pure solvent were determined by measuring the flow rate on a 100 Ostwald viscometer. The elution periods on each solution measured were reproduced at flow times of 85 to 100 seconds, with a maximum spread of 0.1 second.

Results indicated that the molecular weight of nylon from the Surveyor III camera was 26,000, compared to 20,000 for the sample from the TAT camera. Two possible explanations were suggested: A minor degree of polymer crosslinking resulting from the radiation environment could explain this difference. On the other hand, the two samples had originally come from different lots and could readily differ by the amount measured. Consequently, no definite conclusions can be drawn on the effect of the lunar environment; it can be stated, however, that any effect of radiation, if it did occur, could not have been a major one.

I.2.5 Electron Paramagnetic Resonance Measurements

The electron paramagnetic resonance tests were conducted to study possible radiation damage to the teflon TFE, nylon, and polyimide materials. Samples from both the Surveyor III camera and the TAT camera were measured on the EPR spectrometer at room temperature and approximately -140°C.

Results of these measurements are summarized in Table I-9. The maximum spin density, the significant parameter derived from the EPR measurements, is dependent on the sample size and on the sensitivity of the instrument multiplied by the observed line width of the measured spectra. For the materials tested, the line width is on the order of 60 gauss. The sensitivity of the EPR spectrometer used was 6×10^{14} spins. Results shown in Table I-9 do not indicate any major surprises.

However, a closer examination of the maximum spins obtained, listed in Table I-9, revealed that quantitative conclusions on possible induced effects of the radiation environment could not be obtained because of the limited sensitivity of the spectrometer. The microwave power saturation level of the spectrometer used would mask any evidence of a small increase in the number of spin centers induced by radiation. Furthermore, the number of such spin centers would be reduced by the decay of free radicals over long periods of time in the air. Consequently, only a gross conclusion could be reached that, within the sensitivity limitations of the instrument, no major degradation was observed.

The EPR spectrometer bridge could be modified to operate in a low power configuration. In this mode, its capability would be extended. However, it was felt that the additional effort required to provide for this improvement of electron paramagnetic resonance measurement was not warranted.

TABLE I-9. ELECTRON PARAMAGNETIC RESONANCE MEASUREMENTS OF ORGANIC MATERIALS

Sample Description		Sample Temperature, °C	Sample Mass, mg	Maximum Possible Spin Density, spins/cm^3
Material	Source			
Teflon TFE	Surveyor III camera	-140 and 25	17	7.8×10^{16}
Teflon TFE	TAT camera	25	68	1.8×10^{16}
Teflon TFE	Surveyor III camera	25	37	3.5×10^{16}
Teflon TFE	Surveyor III camera	25	61	2.1×10^{16}
Nylon	Surveyor III camera	-140 and 25	106	6.2×10^{15}
Nylon	Surveyor III camera	-140 and 25	94	7.1×10^{15}
Nylon	TAT camera	-140	40	1.7×10^{16}
Polyimide	Surveyor III camera	-140 and 25	40	2.1×10^{16}
Polyimide	TAT camera	-140	37	2.3×10^{16}

I.2.6 Differential Thermal Analysis

Differential thermal analysis tests were then conducted on samples of teflon TFE from the Surveyor III and from the spare (TAT) cameras and on nylon from the Surveyor camera to assess any changes in thermal properties resulting from their exposure to the lunar environment. Parameters such as the melting point, glass transition temperature, and decomposition point can be measured by this technique; these, in turn, provide data on any changes in molecular weight or composition of these organic materials.

The differential thermal analysis test was conducted on the organic materials samples and on standard glass bead samples used as reference. It entailed the application of heat inputs at a controlled rate to maintain a constant temperature rise rate of the reference material; the corresponding difference of the resulting temperature rise of the measured sample, heated at the same rate as the reference material, was then plotted as a function of temperature. The DTA thermograms thereby obtained are

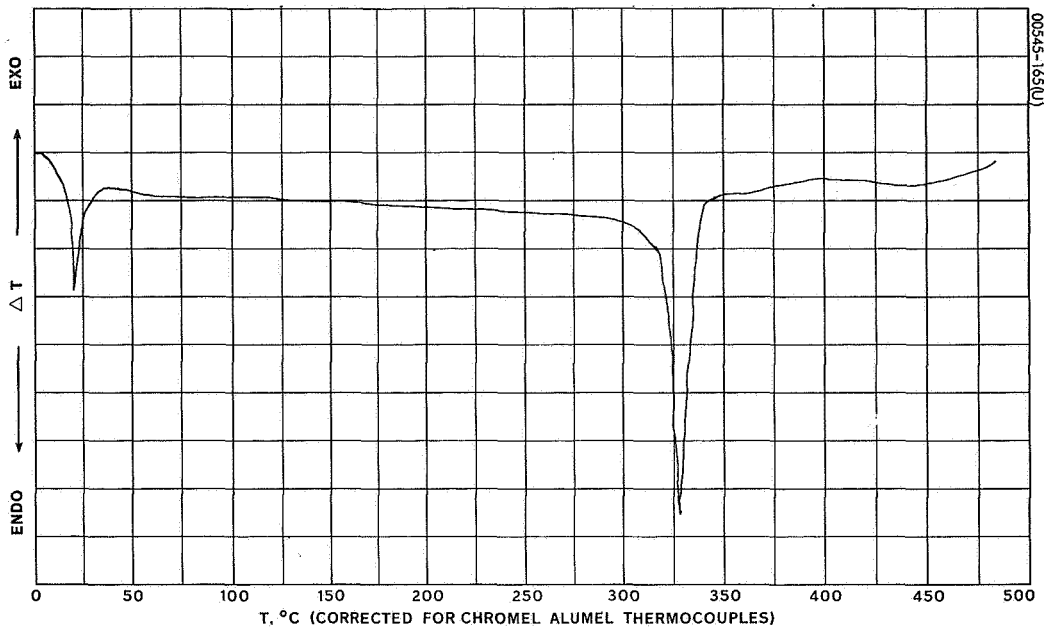

a) Teflon TFE From Surveyor III Camera

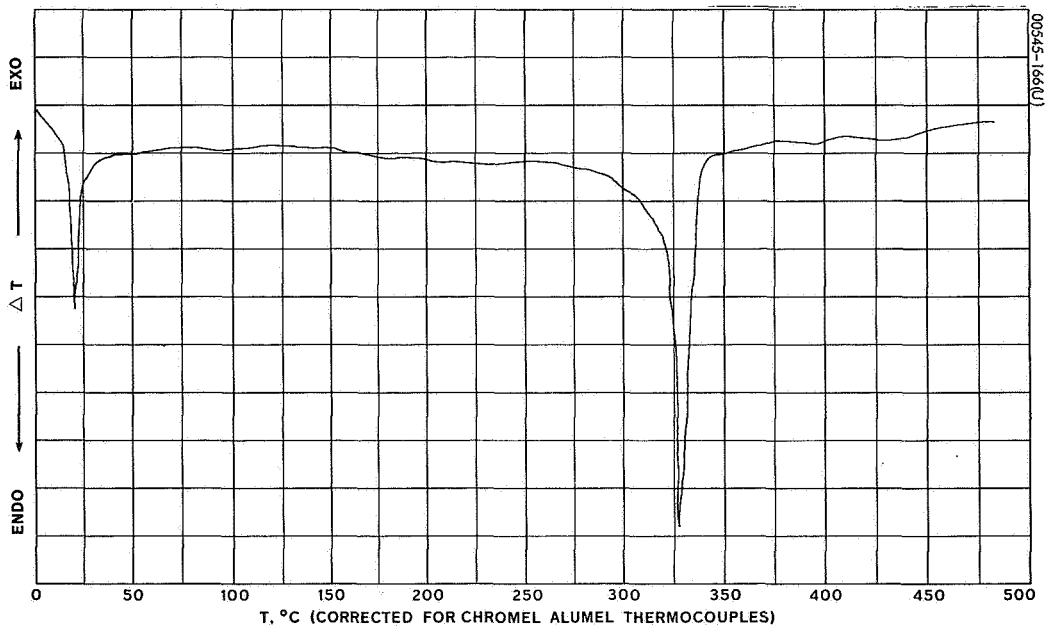

b) Teflon TFE From TAT Camera

Figure I-10. DTA Thermograms

shown in Figure I-10. Figures I-10a and b present data obtained on TFE teflon of the Surveyor III and TAT cameras, respectively. Figure 10c presents data obtained for the Surveyor III nylon sample.

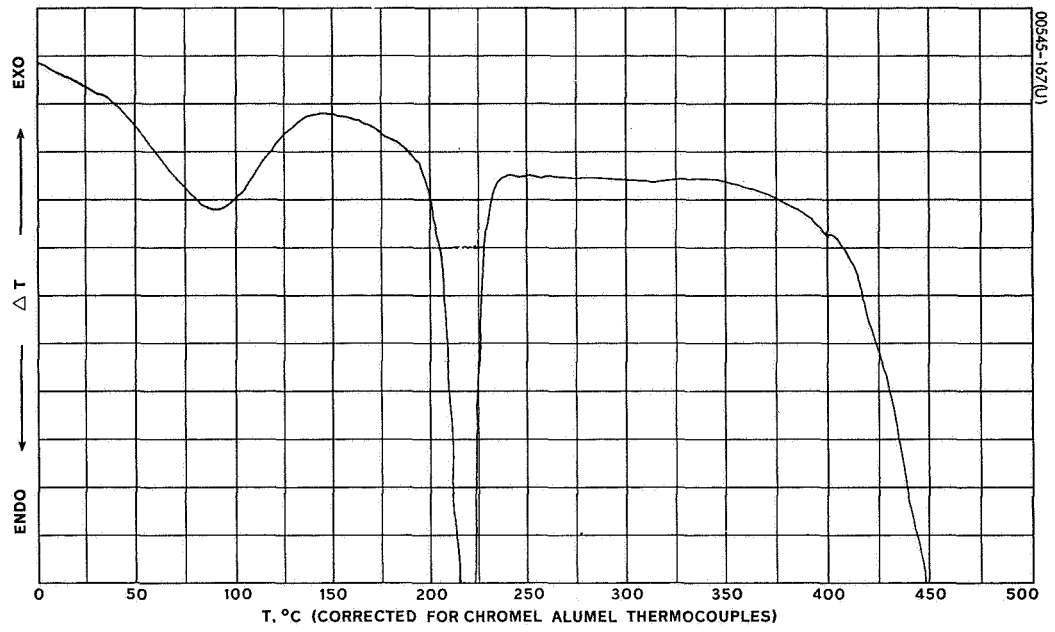

c) Nylon From Surveyor III Camera

Figure I-10 (continued). DTA Thermograms

Results indicated that no significant changes were brought about for the lunar exposure. The thermograms of the two teflon samples are seen to be virtually identical. The thermogram of nylon sample corresponds to that available in literature for standard nylon material and indicates a broad glass transition near 90°C and melting near 245°C.

I.3 DISCUSSION OF FRICTION TEST OF FOCAL LENGTH POTENTIOMETER

The setup and the procedure employed in conducting the friction test, discussed in Section 10.6.3, are described here.

I.3.1 Sample Preparation

A wire section was cut from the helical winding for wear analysis. The first step was to straighten out this wire into a precise taut shape without disturbing its worn surface. This straightening operation was conducted in three steps.

The first step was to unwind the helical shape by hand, using gentle pressure, holding one end of the helical wire firmly against the clean flat surface of the laminar flow bench and unwinding the helix against the bench top. Precautions were taken to ensure that the wear track of the wire or of the adjacent areas of the wear tract tested was never touched during this or any subsequent operation.

The second step was to apply a tensile force to the wire under ambient conditions to achieve the desired degree of tautness. The bend ends of the partially straightened specimen were secured into opposing holes of a laboratory jack, and the jack was opened until the desired tension was validated by microscope examination. The above was also conducted on the laminar flow bench.

The final step entailed annealing of the taut wire to preserve its shape. This was done in a thoroughly clean vacuum oven, preheated to the predetermined temperatures, and triple purged with clean dry nitrogen. The wire was subjected to two cycles in the oven of 16 hours each at oven temperatures of 300° and 230°F, respectively. This was followed by a third cycle in the laminar flow bench at room temperature, lasting 312 hours. The entire stretched assembly was wrapped in aluminum foil, cleaned with a solvent.

Upon completion of the last 312 hour cycle, the taut shape of the wire was then validated by freeing one of its elements from the laboratory jack and observing the unsupported straight wire with a microscope at 40X magnification.

During the above operations, particular care was exercised to ensure extreme cleanliness. The potentiometer and all of its components were handled with tools cleaned with Freon PCA. Double-walled lint-free cotton gloves were used in all manual handling. All assembly steps and ambient operations were performed on the laminar flow bench.

The wire specimen was then cut into sections forming three specimens for test.

I.3.2 Test Setup

A schematic of the friction and wear test setup is shown in Figure I-11. Figure I-12 shows the detailed plan and elevation view of the location of the test specimen and of the position and travel of the test wiper contacts.

Two brand new Paliney 7 contacts used as controls were mounted in the upper specimen holder. As shown in Figure I-12, the rear wiper rubbed over the top horizontal area of the rear wire specimen while the forward contact rubbed with its bevelled surfaces over the two forward specimen elements. The angle of the bevelled surfaces of the forward contact was 26 degrees. The wear areas of the forward wire specimen engaged were accordingly rotated at 26 degrees. The three wire specimen were bonded in the grooves so that corresponding wear areas of the wire elements were engaged by the wipers.

Two friction tests were conducted. For the first test, the areas previously worn on the lunar surface were engaged on all three specimens. Thus, the rear specimen was bonded so that the worn area was on top.

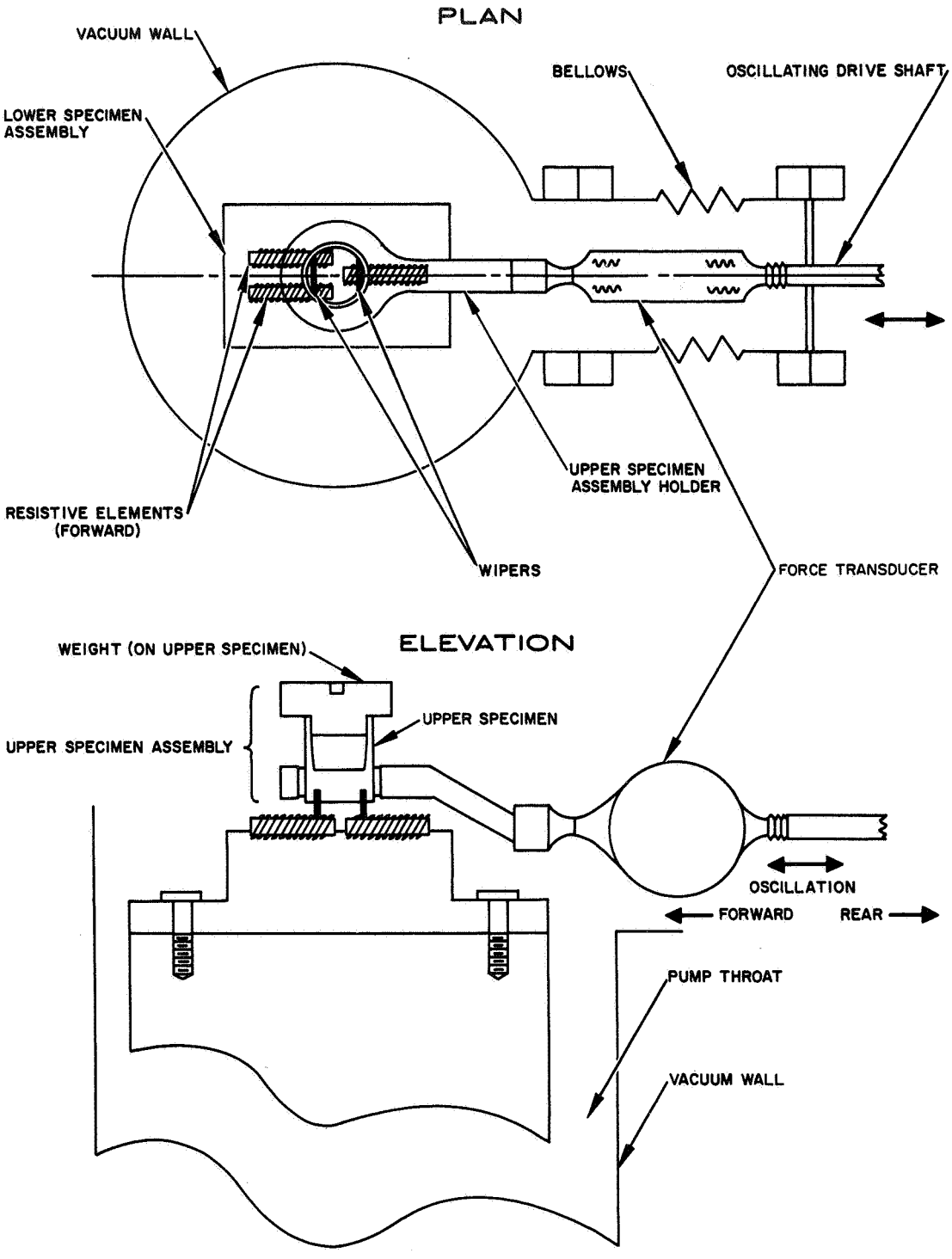

Figure 1-11. Schematic of Friction and Wear Test Assembly

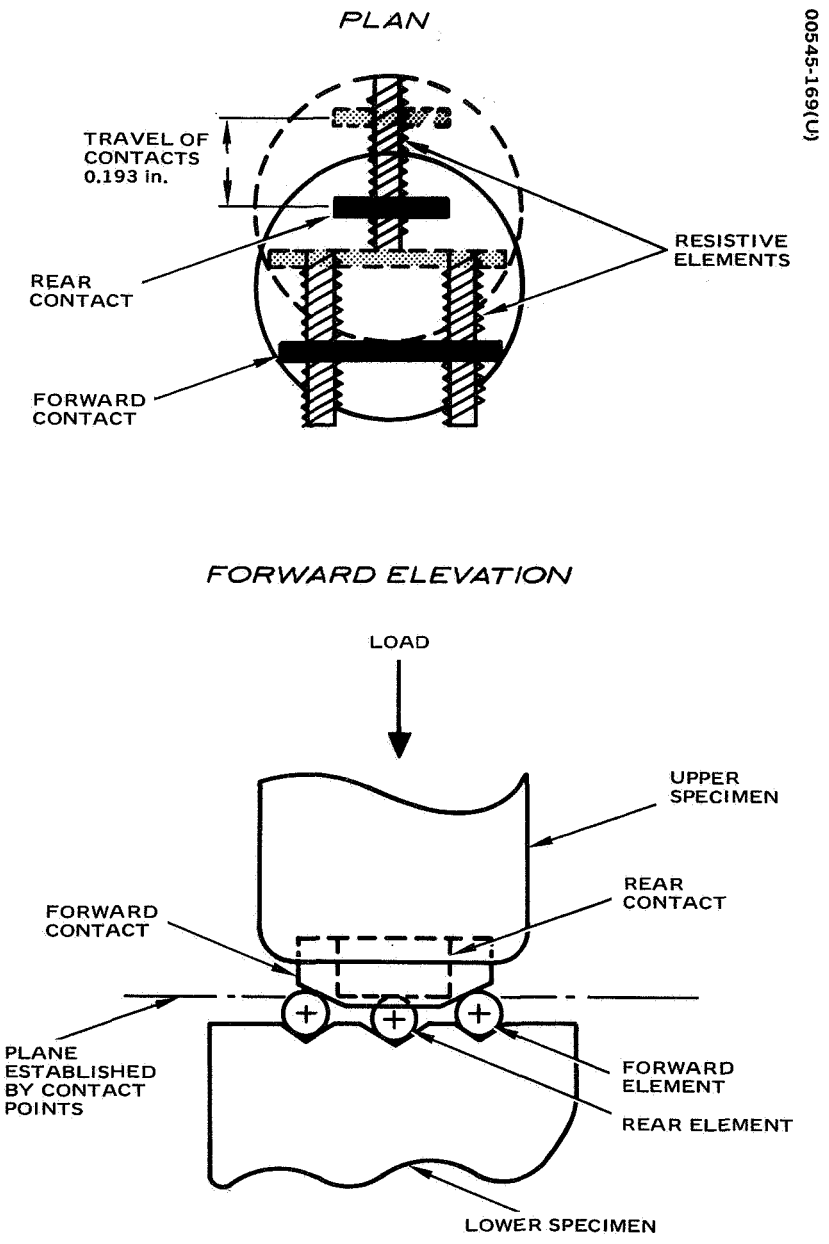

Figure 1-12. Detailed Schematic of Location and Relative Motion of Wire Specimen and Wipers in Friction Test

The forward specimens were bonded in a radially rotated position 26 degrees clockwise and counterclockwise, respectively, so that the bevelled surfaces of the forward wiper also engaged their previously worn areas. For the second frictional test, all three specimens were rebonded after rotating them separately so that all three areas in contact were previously unworn. Separate new contacts were used for the second frictional test. Oscillatory motion at various speeds was provided by the drive shaft through the linkage shown in Figure I-11 with a 14 gram load applied on the rubbing surfaces.

The frictional force, measured by the transducers, was recorded on a strip chart recorder. For each test, this force represented the total of all three frictional forces on the three elements. Ignoring the high value of the static frictional force observed at the end of each travel, the average of the kinetic frictional force observed during the actual motion was recorded.

The test setup allowed performance of the test at various oscillation frequencies. The vacuum chamber shown on Figure I-11 was also provided to allow performance of the test in vacuum, or under ambient conditions, as required.

I.3.3 Test Procedure

Just prior to the assembly, the upper specimen containing the contacts was ultrasonically degreased in Freon PCA. The lower specimen was gently blown off with dry filtered nitrogen gas to remove any dirt or lint before and after bonding of the elements. All subsequent operations were conducted with extreme care to preserve cleanliness. All parts were handled with clean white nylon gloves or with clean stainless steel tweezers.

The force transducer was calibrated immediately before and after each test. The procedure followed in each of the two tests, one on the worn element surfaces and the second on the unworn element surfaces, was similar. The drive was turned on briefly at a cycling frequency of about 3.4 cpm under atmospheric conditions in order to make the final mechanical adjustments. The assembly was then operated under atmospheric conditions at 3.5, 20, and 40 cpm for about 10 cycles each to detemine the value of the friction force in air and its variation with speed. (Relative humidity of the laboratory was maintained at 55 to 65 percent for this test.) The chamber was then evacuated to a pressure lower than 10^{-8} Torr. When this vacuum level was reached, cycling was resumed at 40 cpm and the values of the frictional force recorded until completion of the test.

The duration of each of the two vacuum tests was on the order of 2600 cycles. Onset of cold welding, as evidenced by a violent chatter of the upper specimen, occurred after 800 cycles in the first test and after 400 cycles in the second test. The vacuum test was continued in both tests until 2500 cycles, when it became evident that no further changes were taking place. The final step in the test procedure for each of the two tests was to return the system to ambient pressure and continue the oscillations

for another 100 cycles. This provided the final data for comparison purposes on frictional forces in air.

A microscope, not shown in Figure I-11, was also provided to conduct detailed visual examinations during and upon conclusion of the above tests. The microscope was focused over the surfaces of the specimen, allowing photomicrographs to be taken as the cycling progressed.

Special precautions were followed to prevent contamination of the wire in any way during the disassembly and bonding operations. The elements themselves were not subjected to any cleaning subsequent to disassembly of the potentiometer except for a gentle blast of clean dry nitrogen to remove any dust just prior to disassembly. All glass containers coming into contact with the resistance elements were chemically cleaned in a chromic acid solution. The examining microscope was thoroughly dusted by wiping it with a Freon PCA saturated lint-free cloth, followed by blowing with several strong blasts of dry filtered nitrogen.

The specimen holders and the new contacts were carefully cleaned, and the contact surfaces were abraded with a fine emery cloth until they closely resembled the appearance of the unused portions of the actual potentiometer contact.

The test procedure used was similar to the one used during the original Surveyor lubricant selection tests. The major difference was the addition of tests at the various cycling frequencies.

It should be noted that the cycling of the contacts over the wires in air did not in any way affect the test results in vacuum. A thin film of oxide coating developed and was present during the ambient testing, so that, for a small number of cycles in air, testing in vacuum could be safely presumed to have started with relatively unaltered surfaces.

APPENDIX J. SUPPORTING DATA FOR SURFACE EFFECTS STUDY

J.1 BACKGROUND DATA ON SURVEYOR SURFACE CONDITIONS AND LANDING OPERATIONS

J.1.1 Prelaunch Surface History of Surveyor III

Surveyor III underwent extensive testing prior to launch, during which it was exposed to thermal-vacuum tests in an oil-pumped vacuum chamber (liquid nitrogen trapped). For almost all of the prelaunch testing, the TV camera was not on the spacecraft. The flight camera was placed on Surveyor III in February 1967. The camera also underwent thermal-vacuum testing in a similar vacuum chamber. There were opportunities for contaminants of many types to deposit on the camera prior to launch.

A thermal control surface inspection and rework were held just before launch. Repair of damaged paint surfaces was conducted at this time. These repaired spots were found upon return of the camera. The discoloration of these spots was different than that of the surrounding paint and always appeared lighter in color. The paint used to coat the repaired spots was an organic white (TiO_2 in an acrylic binder), not the inorganic paint used on the rest of the camera.

The clamp which held the camera in place provided a unique spot to observe the apparent effect of the prelaunch contamination. The cleaning procedure for the inorganic white paint was to lightly sand the surface so as to remove the visible contamination. The back side of the clamp had been partially cleaned in this manner and was not repainted. It was uniform in whiteness after cleaning. Upon return of the camera to earth, the cleaned spot was seen to be lighter in color, and where the sanding had stopped the discoloration became deeper. This difference in coloration is attributed to prelaunch contaminants (probably organic) on the surface of the unsanded paint that discolored to a greater degree upon exposure to the lunar environment.*

*This observation is in conflict with other conclusions of the contamination study and should be examined further in possible future studies.

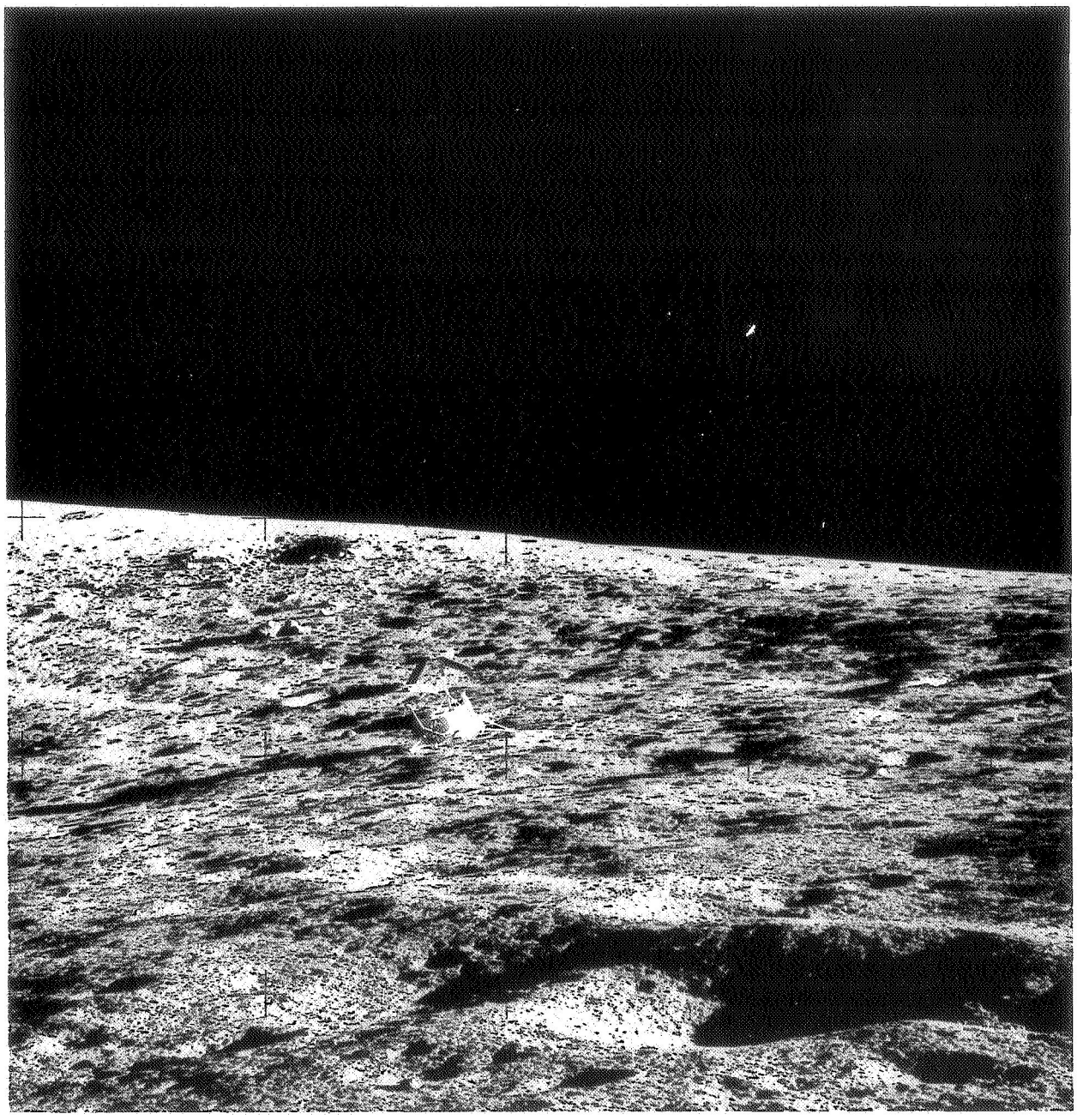

Figure J-1. Surveyor III on Crater Wall (NASA Photo AS12-48-7087)

J.1.2 Lunar Landing and Configuration of Surveyor III

The Surveyor III spacecraft was launched 17 April 1967 and landed on the lunar surface in the Ocean of Storms 20 April 1967. The landing site as determined from Surveyor data was 2.94°S latitude and 23.34°W longitude. The mission details and scientific results, landing site, etc., are described in detail in Reference 105.

The vernier engines remained on through the first two lunar touchdowns of Surveyor III at a thrust level equal to approximately 90 percent of the spacecraft lunar weight. This caused the spacecraft to rebound each time from the lunar surface. The vernier engines were shut down by ground command approximately 1 second before the third touchdown, and the spacecraft came to rest. The spacecraft did not rotate during this maneuver. The uphill leg (2) impacted first on each landing.

There were anomalies in the analog telemetry data after landing which required use of a correction factor to establish the thermal status of the spacecraft and precluded accurate comparison with post-return conditions. Within the limits of the accuracy of the data, Surveyor III appeared to react thermally like Surveyor I except for some differences that could be attributed to landing orientation (Surveyor III was tilted and in a crater). Within the limits possible, there appeared to be a "lack of any thermally significant dust on the compartment faces" (Reference 105). Thus, the presence of dust immediately after landing can neither be ruled out nor verified except as indicated by veiling glare and contrast attenuation observed for the Surveyor III mirror.

Surveyor III came to rest on the sloping wall of a crater about 200 meters in diameter and 15 meters deep. The spacecraft landed on the southeastern wall of the crater almost halfway between the center and the rim crest. The mean elevation of the foot pads was about 7 meters below the mean elevation of the rim crest. The spacecraft was tilted very nearly toward the center of the crater at an angle somewhat steeper than the mean local slope of the crater wall, as seen in Figure J-1 and the cover photograph. Figure J-2 shows the orientation of Surveyor III in the lunar crater.

The spacecraft's camera mirror assembly was rotated through a series of azimuth positions (and the camera mirror rotated through multiple elevation angles) during the TV photography sequence. Thus, the exposure of the mirror assembly to the various elements of the lunar environment during this operation was really a complex summation of its individual exposures during the various azimuth and elevation positions. No effort was made to analyze this portion of the exposure because it constituted such a small part of the total exposure of the camera to the lunar environment during the 2-1/2 years it remained on the moon.

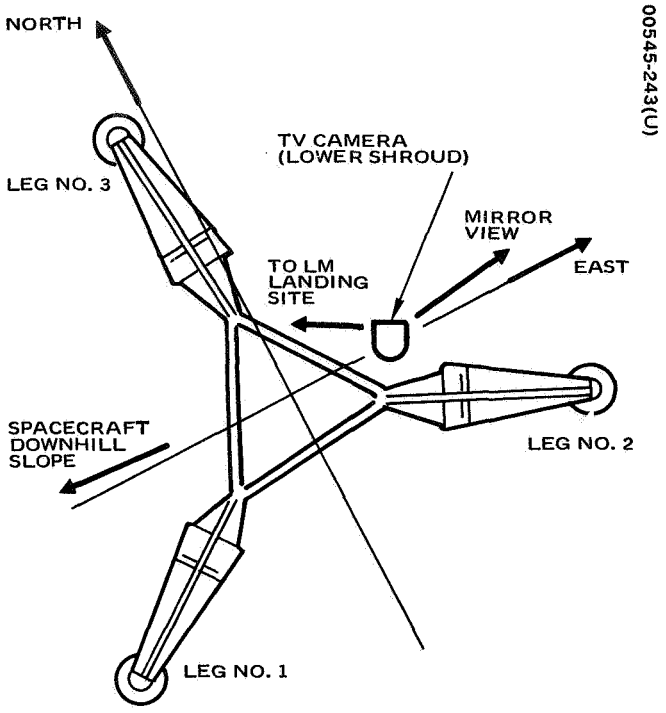

Figure J-2. Orientation of Surveyor III in Crater

The last Surveyor III picture was taken at -39 degrees azimuth of a feature on the eastern horizon illuminated by the setting sun. Following this picture, the camera was stepped 4 or 5 times in elevation to either -28 or -33 degrees elevation position (there is some confusion in the command log). An additional exposure was commanded in this position but, as expected, showed no image of the darkened lunar surface. The Surveyor III spacecraft was apparently in good condition when secured for the lunar night on 4 May 1967, 14 days after touchdown.

No major events occurred in the adjacent area during the 2-1/2 years that Surveyor III was on the moon (Reference 106). Micrometeoroids were not a significant factor. Photographs taken during the recovery of the camera indicate sharp outlines of the imprints of Surveyor III landing pads and the SM/SS trenches, with no erosion noted.

The camera was installed on the spacecraft with its vertical axis skewed with respect to the spacecraft vertical axis and this, combined with the spacecraft tilt (~12 degrees), produced a tilt of the camera vertical axis of 23.5 degrees with respect to local vertical in a direction 43 degrees west of north. The plane of the flat front face of the lower shroud of the camera was nearly vertical and faced approximately 43 degrees east of north. The -39 degree azimuth position of the mirror assembly left it "looking" a few degrees (5 to 15 degrees) north of local east.

A scale model of Surveyor was set up at JPL for a photographic sequence simulating a lunar day. The model was set at a tilt and position duplicating the Surveyor III attitude and orientation on the crater slope.

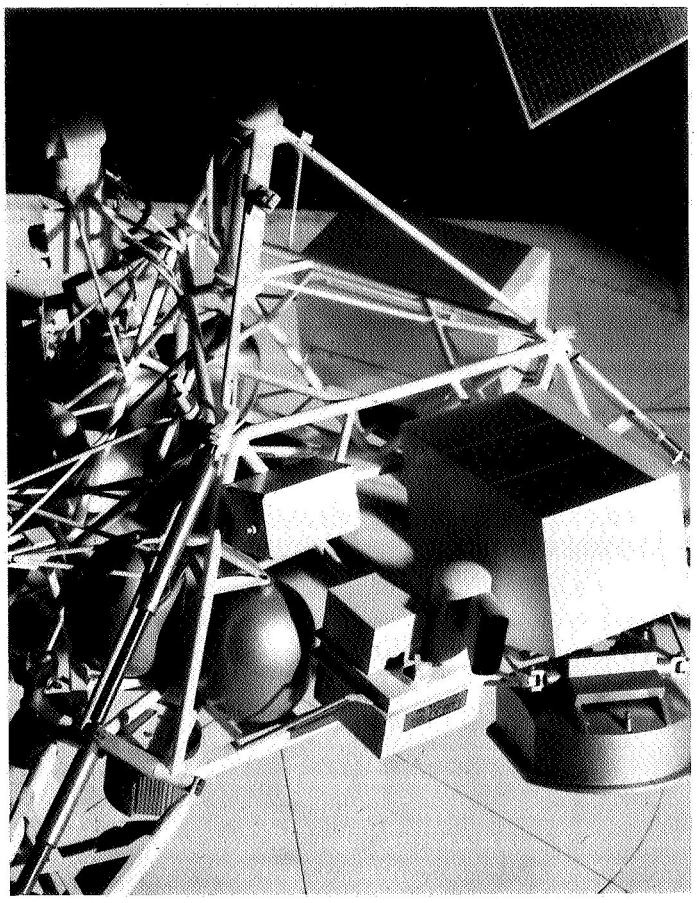

Figure J-3. Shadow Photograph of Surveyor III Model, Simulating Position of Sun at 10 Degrees Before Sunset, Viewed from Lunar Module Position (Photo 211-4068B)

A collimated model sun was oriented such that it traversed the same relative path over the model as the real sun over Surveyor III. Photographs were then taken of the Surveyor model at three different viewing locations. Photographs were made at every 10 degrees of sun elevation and at 2 degrees after sunrise and before sunset. The series of photographs is available from JPL (photographs 211-4042B and 211-4046A through 211-4073B).

Figure J-3* is one photograph from this sequence. Viewing position is from the lunar module landing spot with the sun at 170 degrees (10 degrees before sunset).

J.1.3 Lunar Module Landing

The Apollo XII terminal descent is described in detail in Reference 107 and summarized in Figure J-4. The Apollo landing site was approximately 535 feet northwest of the Surveyor spacecraft.

*Original in color.

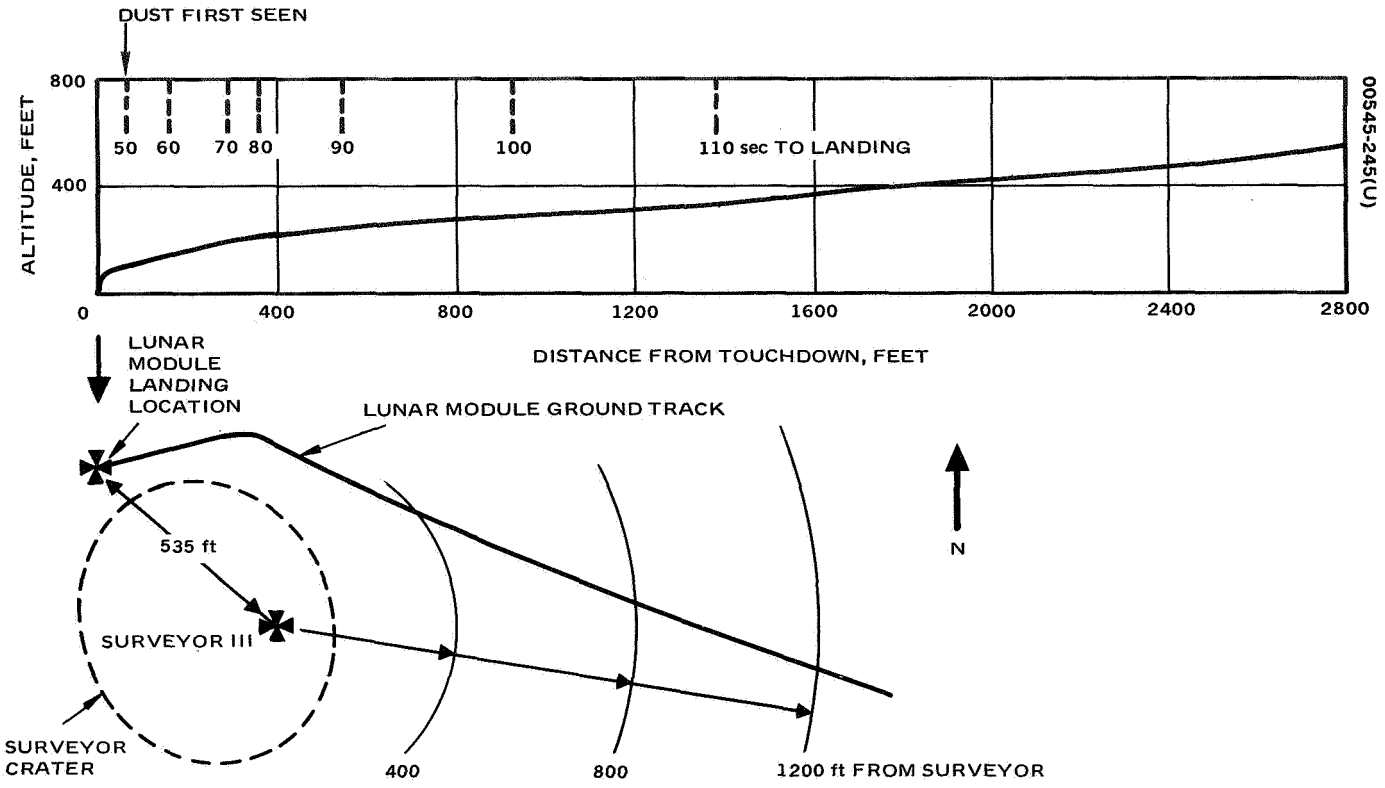

Figure J-4. Approach and Landing Configuration of Lunar Module Relative to Surveyor III

During the terminal descent of the lunar module, the first visible dust was noted approximately 50 seconds before final touchdown and approximately 80 feet east of the final landing site. Subsequent examination of lunar surface photos, discussed in Reference 108, showed clear evidence of surface erosion at least 40 to 50 feet east of the lunar module landing site. If it reached the Surveyor, this dust could have contaminated the front of the lower shroud. It is reasonable to assume that disturbance of the lunar surface and projection of fine particulate material in all directions occurred even earlier, and disturbance early enough to deposit fines on the mirror can not be precluded. In order for the particles disturbed by the lunar module to reach the mirror, they would have to have originated from a location approximately 700 feet east of the lunar module landing site (approximately 300 feet east of Surveyor III) at an altitude of 250 to 275 feet. The relative locations of the lunar module and Surveyor III are illustrated in Figure J-5 and can also be seen on the report cover.

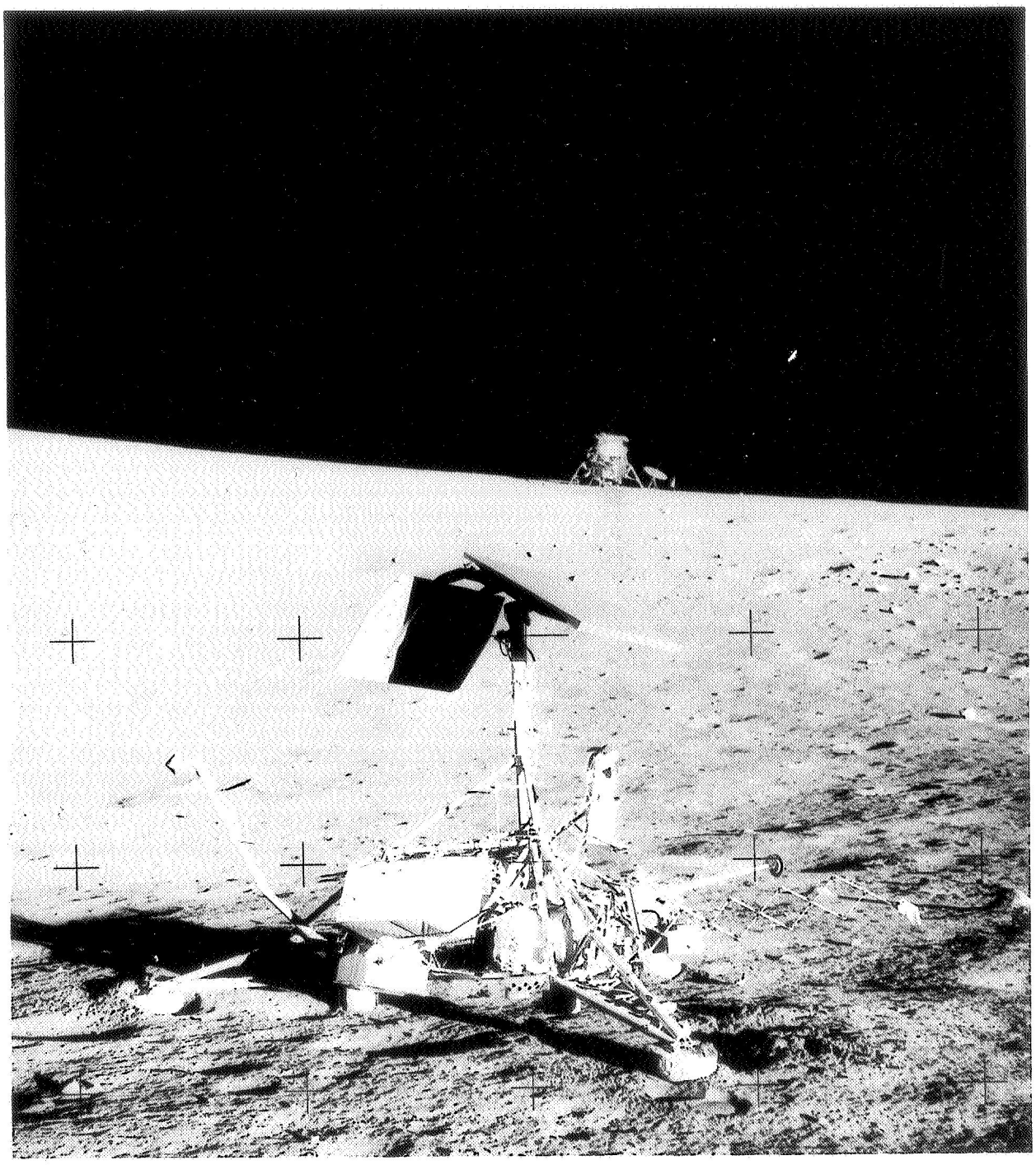

Figure J-5. View of Relative Locations on Lunar Surface of Surveyor III and Lunar Module (NASA Photo AS12-48-7100)

J.2 VISUAL OBSERVATION OF DISCOLORATION

The first indication that severe discoloration had occurred on the surfaces of Surveyor III came during the visit by the Apollo 12 astronauts to the landing site. To them, the once bright white paint and shiny polished aluminum appeared a uniform brown. The spacecraft condition described by the astronauts from the moon did not appear to be any different than anticipated since radiation, discoloration, and some dust coverage were expected in the white paint, as discussed in Section J.3. This aluminum silicate (china clay)/potassium silicate paint did not have superior radiation stability. However, when the parts were returned to earth and viewed for the first time, it was realized that the surfaces were extremely discolored, more so than could be attributed to radiation damage in the paint.

Prior to the Surveyor III parts recovery, it was hoped that two conditions on return of parts could be achieved: 1) to return parts in total darkness and 2) to return parts in vacuum. Except for a piece of painted tube and a cable section, these conditions were not possible because of weight, space, and schedule commitments. Therefore, the parts were returned in November 1969 exposed to air and some light. At the LRL in Houston, the parts were removed from the astronaut's backpack and, after a brief viewing, were double bagged in heat-sealed polyethylene. They were stored until 6 Jaunary 1970, when they were released from quarantine.

At this point in time, there was no great concern over the lack of vacuum environment around the parts since tests conducted by Hughes and others showed that the clay-silicate paint did not demonstrate any oxygen (or air) sensitive bleaching in its optical reflectance. What effect lack of light protection would have was unknown. It could only be hypothesized that there would be some effect. Since the parts were immediately exposed to light upon their return and were photographed at that time and again during survey operation at LRL following release from quarantine, interest in eliminating light exposure to the surface was reduced. As a backup, the white painted tube section was still in the vacuum-tight, light-tight container.

The TV camera was coated over most of its surface with the inorganic white paint. When the camera was removed from its double bag, the extent of discoloration became apparent. In addition, it was observed that significant variations in discoloration occurred over the entire surface. The side of the camera on which the mirror was located was a uniform tan or deep yellow-brown. The top and sides of the mirror hood were gray. The other portions of the camera varied in coloration between these two extremes. As mentioned earlier, the expected patterns of radiation damage were absent. The mirror surface was quite hazy, or diffuse, leading to the conclusion at this early stage of the investigation that the entire camera was covered with a contaminant (probably dust).

The camera was photographed after being placed in a laminar flow bench. Visual examination of the camera was made at this time prior to dismantling for microbiological examination. During this examination,

the first shadow patterns were observed. These patterns are unique in that areas protected to some degree from direct exposure to the outside environment, such as below a wire which was very close to the surface, were darker in coloration than the surrounding area. As the visual examination continued, numerous examples of the shadow patterns were found. All of the shadows were found on the north (lunar) side of the camera.

Partial dismantling occurred next with the removal of the lower shroud to allow microbiological work on the interior of camera. As part of this dismantling, the support collar and the mounting bracket on the lower shroud (through which the three connectors passed) were removed, wrapped in teflon film, and placed in a carrying case. These parts were not exposed to any significant light until May, 4 months after removal from the camera. On the north side of the bracket at the interface between the bracket and the lower shroud, a large amount of dark gray debris was noted.

On the front half of the support collar, located on the north side of the camera, was a hole approximately 1 inch in diameter. The surface of the camera beneath the support collar was unpainted aluminum. When the collar was removed, an image of the hole was noted on the aluminum surface. The image was offset and appeared to be formed by something passing through the hole in the collar off normal. This is shown in Figure J-6.

The image itself was fairly bright, with the area surrounding the image brownish and diffuse. When the support collar was removed, several milligrams of dark gray to black debris were found on the aluminum surface. Some of this debris was brushed into a bottle for arc emission spectrographic analysis, and the majority was picked up on clear pressure-sensitive tape. Analysis indicated that the debris was lunar dust.

When the support collar was removed, a new set of shadow patterns was found, again on the north (lunar) side of the camera, as shown in Figure 11-2 (Section 11). These patterns were associated with the struts which attach the camera to the spacecraft. Again, very sharp images of the struts appear on the painted surface of the camera and are much darker than the surrounding area.

Portions of the TV cabling were still attached to the camera lower shroud. When these were removed, shadow patterns were found on the north side of the camera below this cable which was located quite close to

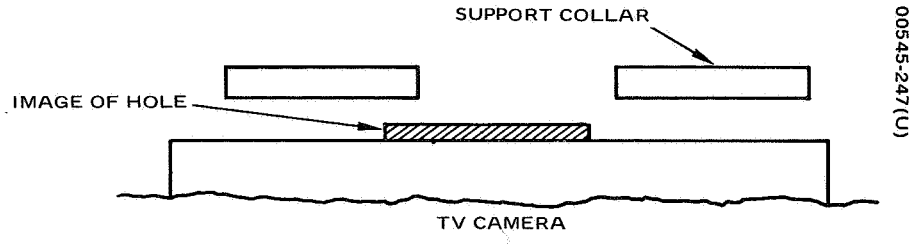

Figure J-6. Illustration of Shadow Through Hole in Camera Clamp

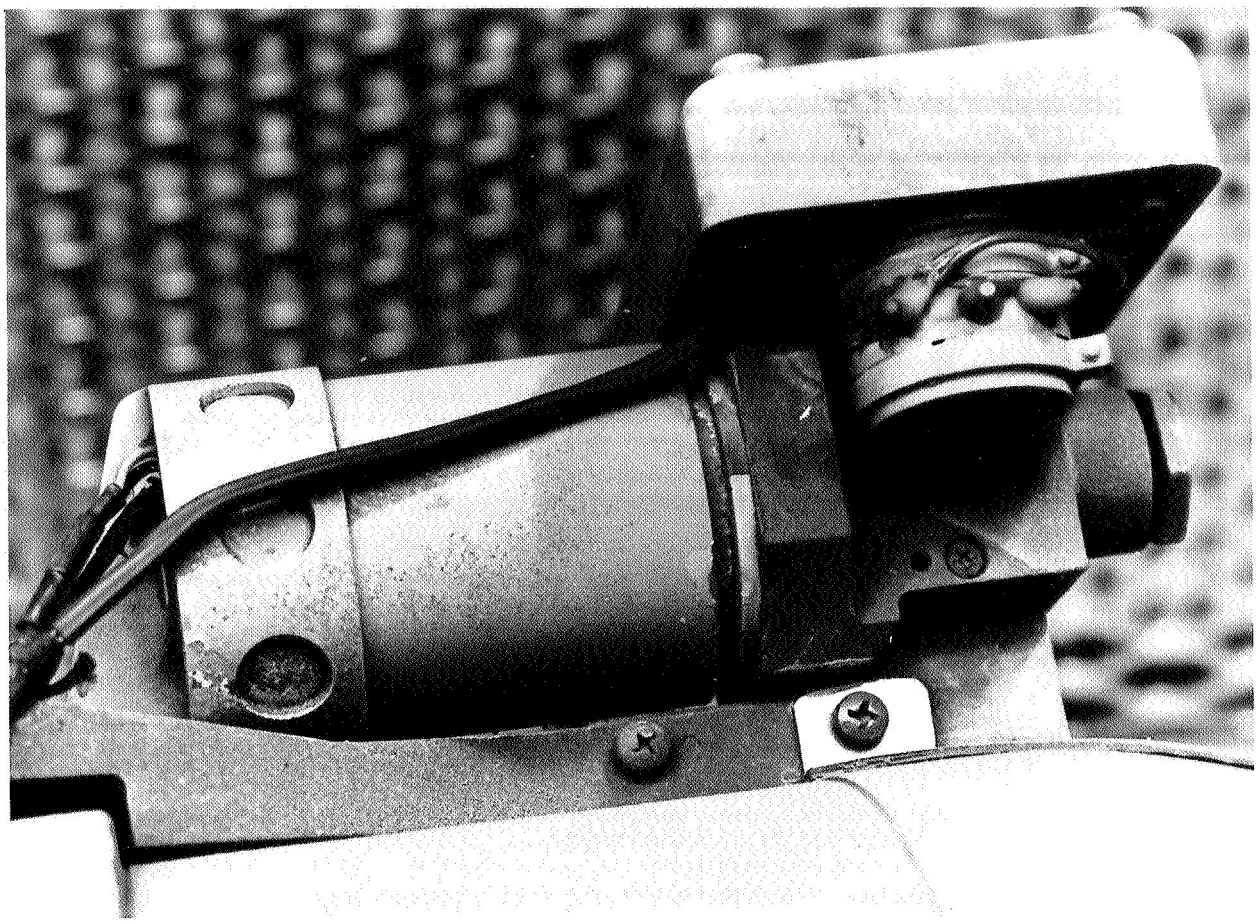

Figure J-7. Shadow Patterns on Elevation Drive Motor Housing (NASA Photo S-70-21149)

the surface. Portions of this cable had been cut free during recovery, but the image of the cable remained on the surface where the cable had been during the camera's lunar stay.

Another set of clear shadow patterns was found to be associated with the elevation motor housing located on the mirror assembly on the north (lunar) side of the camera as shown in Figure J-7.* A clear pattern, much darker, is seen just below the wire running alongside the motor.

Investigation of these shadow patterns dominated the early stages of visual examination of the camera. Heads of the various screws were found imaged on the north side of the camera in the darkened painted surface. These patterns provided the first evidence that all of the shadows had a unique directional characteristic. By visual sighting, it was possible to take a position such that all the darkened patterns disappeared behind the object which they imaged. It was independently discovered by Hughes and by MSC personnel that the shadow patterns were uniquely associated

*Original in color.

with the lunar module landing position. It was assumed at that time that the landing of the lunar module caused a severe dust storm which impinged upon the Surveyor III and sandblasted the surface, removing either earlier deposited debris (dust) or radiation damaged paint and/or contaminants. Subsequent measurements by L. D. Jaffe (JPL) at Hughes identified the coordinates of the origin of the shadows as approximately 90 degrees azimuth and 29 degrees elevation (camera lower shroud coordinates).

J.3 OPTICAL DAMAGE OF SURVEYOR INORGANIC WHITE PAINT

Laboratory tests were conducted before Surveyor launch to determine the ultraviolet radiation stability of the Surveyor inorganic white paint. Ultraviolet tests were conducted at Hughes up to 1000 hours duration, as discussed in Reference 109 using a type BH6 mercury arc lamp. The spectral reflectance measurements were made in air. In 1966, an ultraviolet test was conducted at Hughes with spectral reflectance measurements made in vacuum (Reference 110). This test was also conducted using a mercury arc lamp.

These test data indicate an increase in solar absorptance of the paint of ~ 0.05 in 1000 hours. More important, the test showed that this paint did not exhibit any air bleaching as a result of ultraviolet irradiation.

In 1967, a test was conducted at the Illinois Institute of Technology Research Institute for 2800 hours, using a mercury arc lamp. This test, discussed in Reference 111, was performed with all spectral reflectance measurements made in vacuum. Confirmation was obtained that upon admitting air to the chamber the coating did not show any bleaching or ultraviolet damage.

The spectral character of the damage in the Surveyor inorganic white paint is illustrated in Figure J-8.

The influence of low energy protons, a significant lunar environment factor, on the Surveyor inorganic white paint had not been determined prior to flight. With the return of the Surveyor parts, the question arose concerning the effect of solar wind protons. A test was conducted at Hughes (1970) on a sample painted in 1965 and stored in the dark, free of airborne contaminants. The sample was irradiated at a flux of 1.3×10^{11} protons/cm^2/sec to a total fluence of 2.2×10^{16} protons/cm^2. The optical properties were measured in air to simulate return of the Surveyor parts. It was found that there was no optical damage over the spectral region of interest, 0.3 to 2.6 microns.

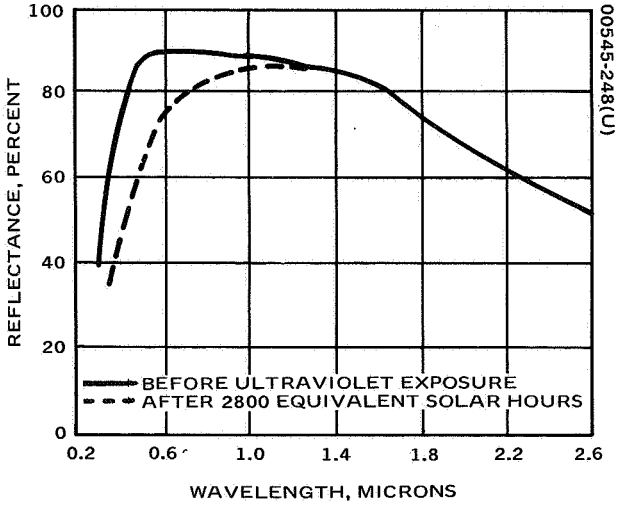

Figure J-8. Spectral Reflectance of White Inorganic Paint Before and After Laboratory Ultraviolet Exposure

J.4 DISCUSSION OF TEST RESULTS

A number of tests were conducted in support of the contamination study. These tests are described in this appendix, and detailed data obtained from each test are presented. The tests are presented in order of actual accomplishment.

J.4.1 Reflectance Measurements of Lower Shroud*

The first series of spectral reflectance measurements on the camera was made on the lower shroud on 28 April 1970. From January 1970 until that time, the shroud was exposed to the fluorescent lighting of a laminar flow bench. It was, however, shielded from the blowing air by a shield of teflon film.

*Conducted by TRW, Inc. on a Hughes subcontract.

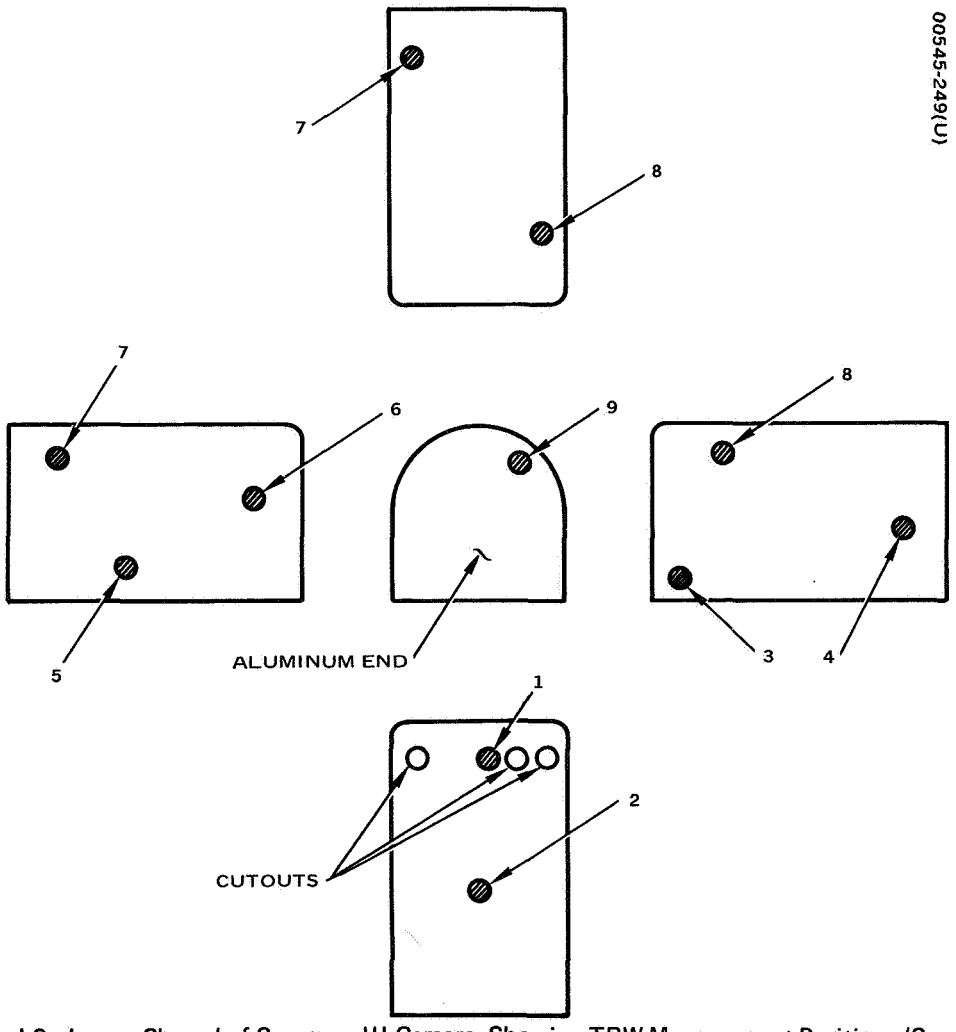

Figure J-9. Lower Shroud of Surveyor III Camera, Showing TRW Measurement Positions (See Text)

This set of measurements was made by TRW at a number of positions on the lower shroud, using a wall-mount integrating sphere. The positions of each measurement are sketched on Figure J-9. Figure J-10 presents spectral plots of these measurements. Table J-1 shows the emittance of each position as measured using a Gier-Dunkle emittance inspection device, model DB-100.

J.4.2 White Painted Tube Section Returned in Vacuum

A 4 inch section from a TV camera support strut was removed by the astronauts and placed in a sample environmental sealed container (SESC). Also included in this container was a section of the teflon wrapped cable from the camera. It was the intent of this experiment to remove both the white painted (inorganic) tube and the teflon FEP cable wrap from the sealed container for a series of optical measurements. The parts were to be maintained under vacuum with no exposure to light. The original test plan called for removal of both test parts from the SESC in a vacuum environment (glove box) and subsequent transfer to vacuum containers for optical measurements (spectral reflectance from 0.25 to 2.5 microns). The transfer was to be accomplished under low level red light illumination, thereby minimizing any photo-induced bleaching.

TABLE J-1. NORMAL EMITTANCE MEASURED ON LOWER SHROUD SURFACE

TRW Position (see Figure J-9)	Normal Emittance
1	0.92_0*
2	0.92_8
3	0.92_0
4	0.92_9
5	0.92_6
6	0.92_0
7	0.92_5
8	0.92_7
9**	0.09_3
Reference paint sample	0.92_0

*Although the accuracy of the measuring instruments does not justify three significant figures, the third figure is retained depressed to indicate trends.

**Note that this was polished aluminum surface.

Lack of equipment availability precluded the transfer of parts in vacuum; thus, the transfer was to be done under inert atmosphere (argon). The facilities, leak checking, and opening of the SESC were provided by and done at JPL. The sectioning of the tube and teflon and the placement of samples in the new test chambers were performed by Hughes and TRW. All facilities and techniques employed including leak checking are described in Reference 112 and are only summarized in this report.

Prior to opening, the SESC was leak checked in May 1970. The returned container from the neon was placed into a vacuum-tight container which was evacuated. This container was then backfilled with SF_6 at 100 mm of mercury over atmospheric pressure and held for 30 hours. The SESC was removed and leak checked; a major leak was found in the SESC in the area of the indium seal. The conclusion was that the leak had existed for some time and had probably been returned from the moon in this condition. Thus, the white paint and teflon both were exposed to air for several months. The vacuum test was lost. However, it was decided to conduct the test sequence per plan; accordingly, the SESC was opened and the samples placed into vacuum chambers.

The interior of the inert atmosphere chamber was sterilized prior to establishment of the inert atmosphere. The O_2, H_2, N_2, H_2O, and hydrocarbon content of the inert gas was monitored during the opening. Total impurities were less than 20 ppm.

The SESC was opened 29 May 1970. The H_2O level rose to 50 ppm and the O_2 to 11 ppm. It was suspected that higher readings of O_2 were not obtained because of the presence of SF_6 in the container, displacing most of the O_2.

A section of white painted tube about 4 inches long was found in the container. The tube was cut into two sections with a jeweler's saw. The longer section (about 3 inches) was placed in a quartz vacuum chamber (Figure J-11) to which a high vacuum valve was connected. The tube section was firmly mounted in place and sealed shut, enclosing the argon inside. A light-tight envelope was placed around the quartz tube.

A section of the teflon wrap was cut from the cable for mounting in a similar vacuum tube. Two sections of teflon about 1 inch by 1 inch were firmly mounted in the second vacuum-tight quartz tube. The chamber was sealed and made light-tight.

The above operations were conducted under very low red light illumination.

The two sealed chambers containing the test specimens were removed from the inert atmosphere chamber and taken to TRW where the initial optical measurements were to be made.* Shortly after reaching TRW, the chambers were evacuated without allowing any oxygen to reach the samples. The samples were retained in darkness, and grounded screens

*These measurements were made at TRW, Inc. under a Hughes subcontract.

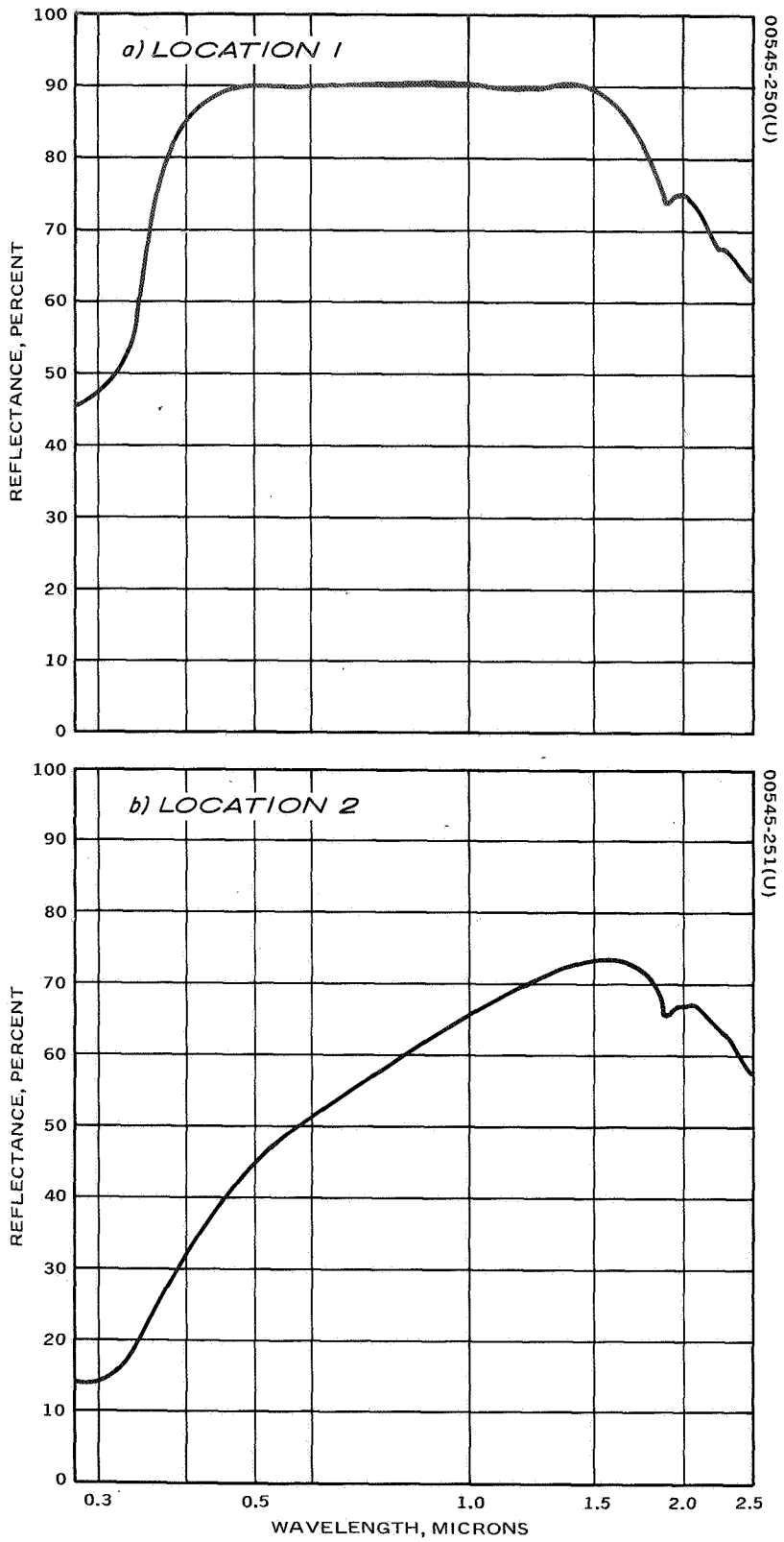

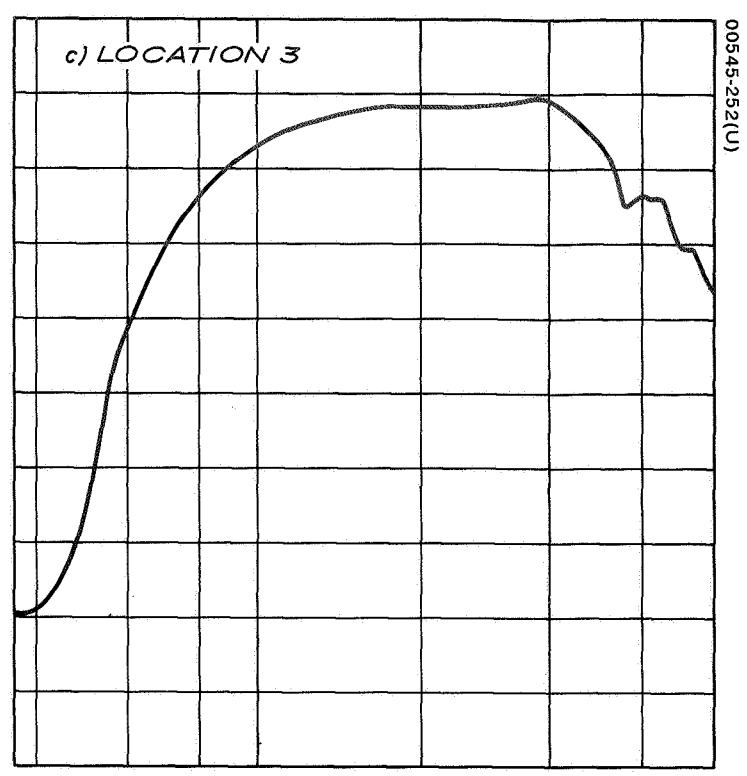

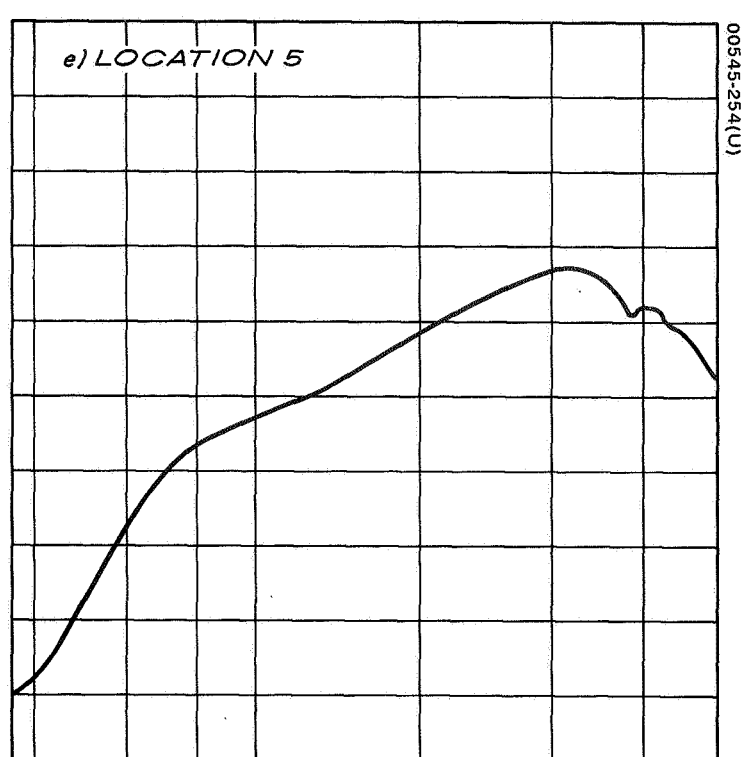

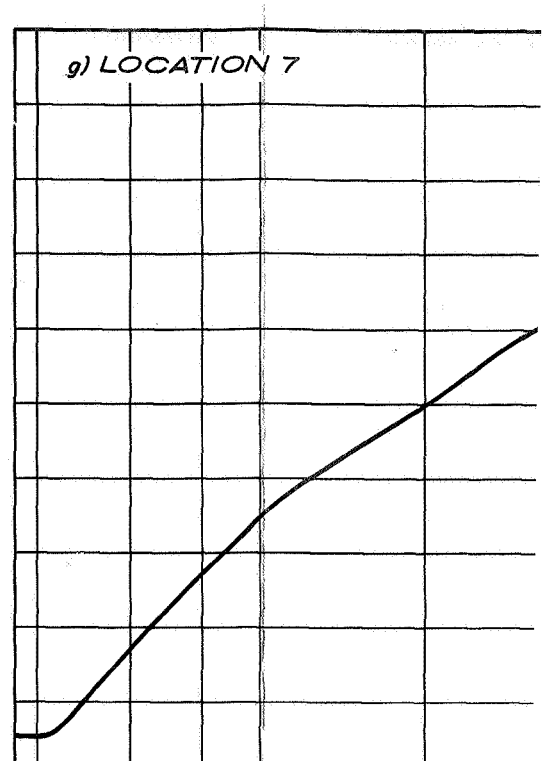

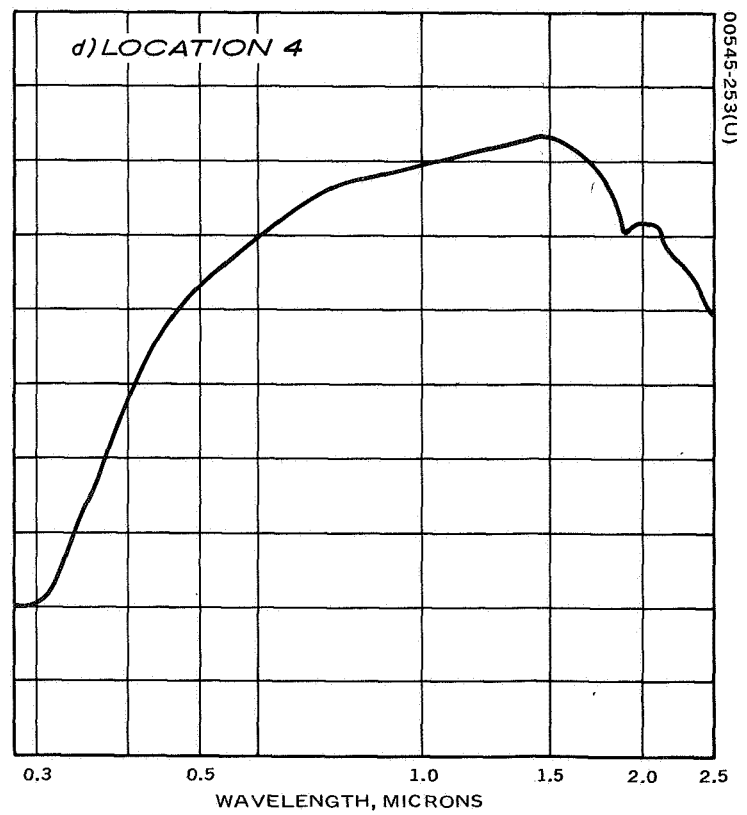

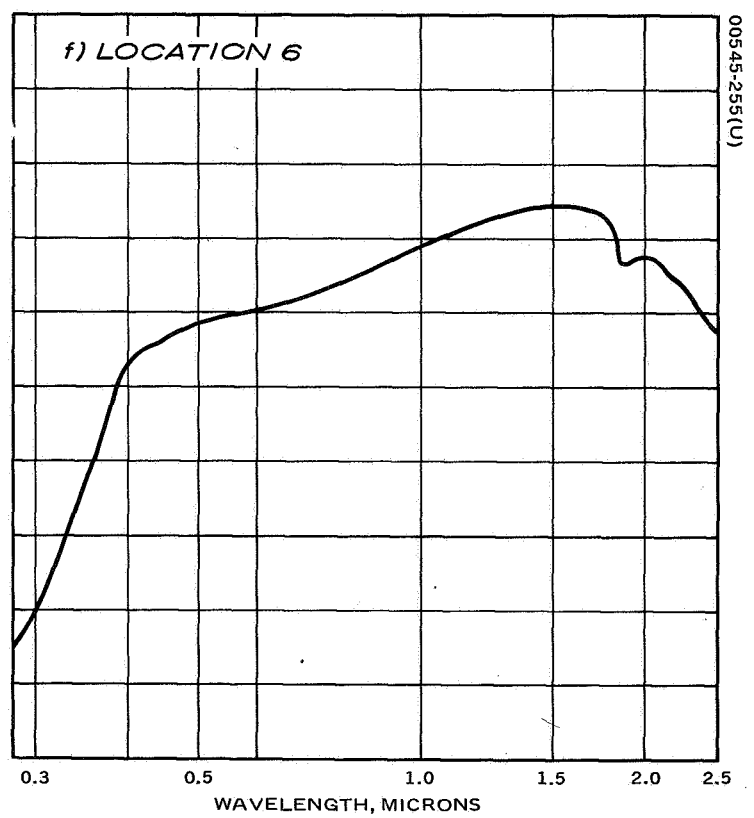

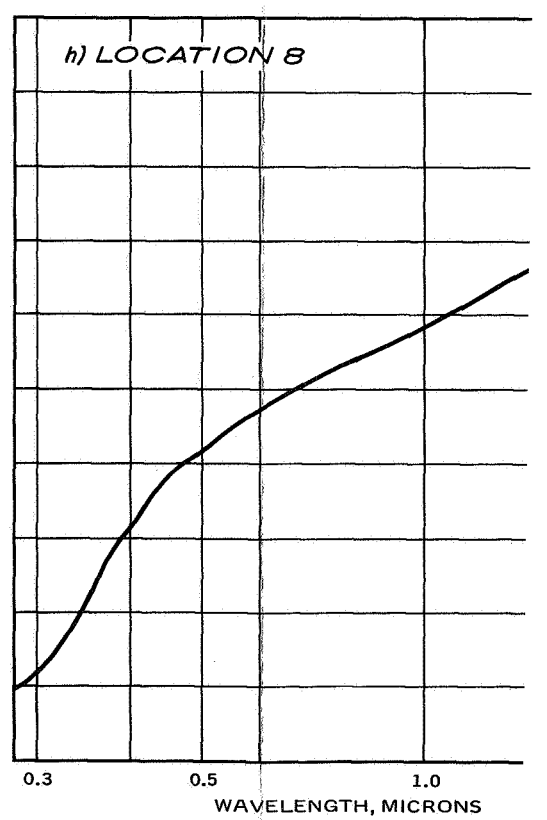

Figure J-10. Reflectance Versus Wavelength of Surveyor III Camera Lower Shroud at Various TRW Locations Shown in Figure J-9

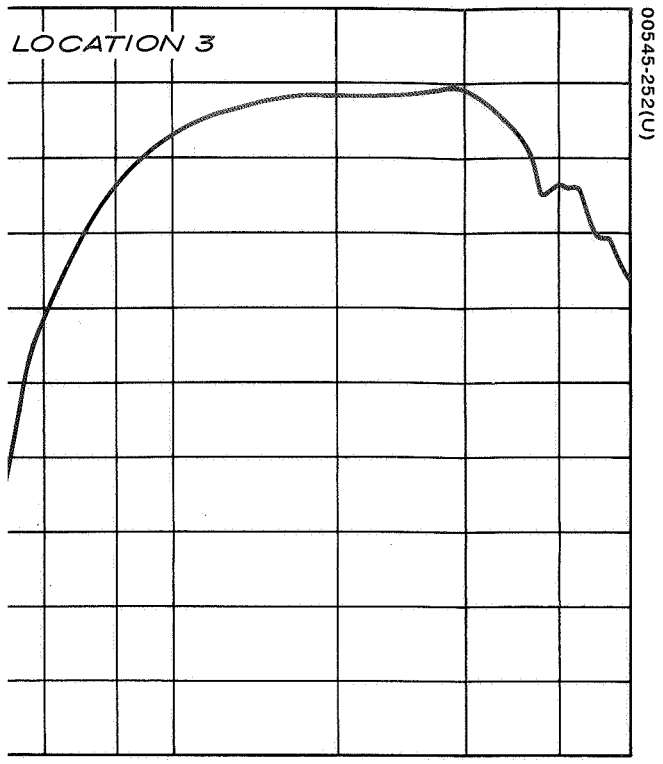

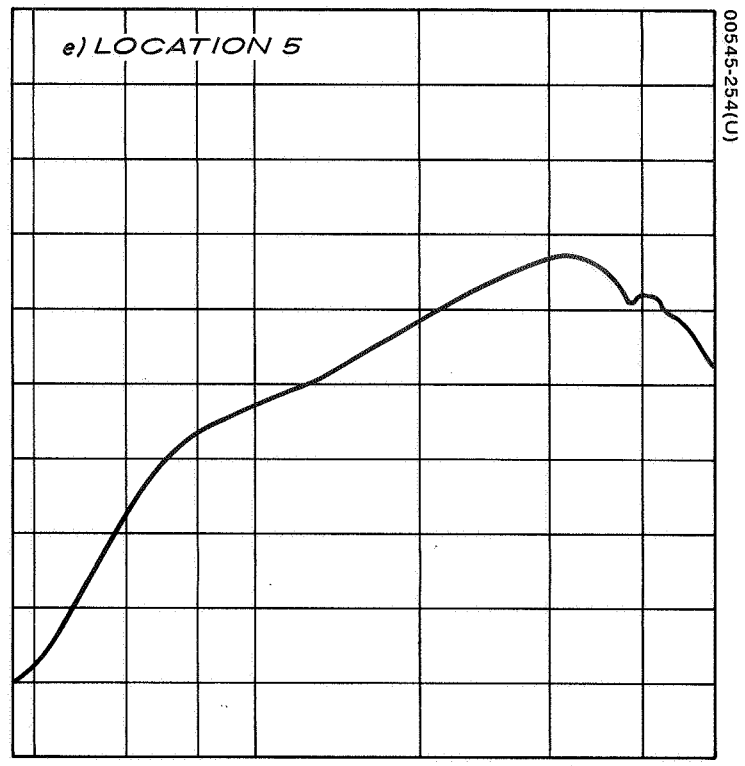

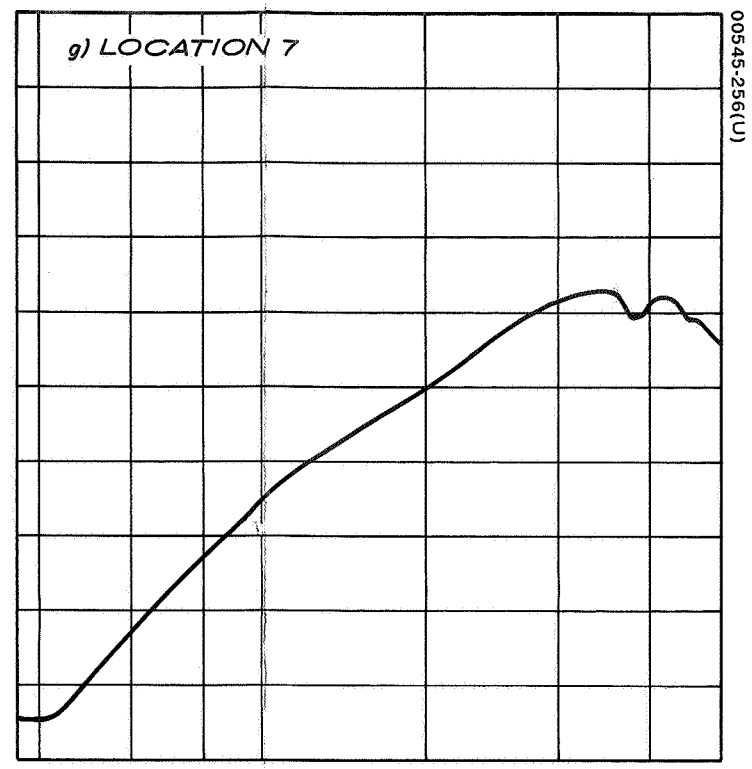

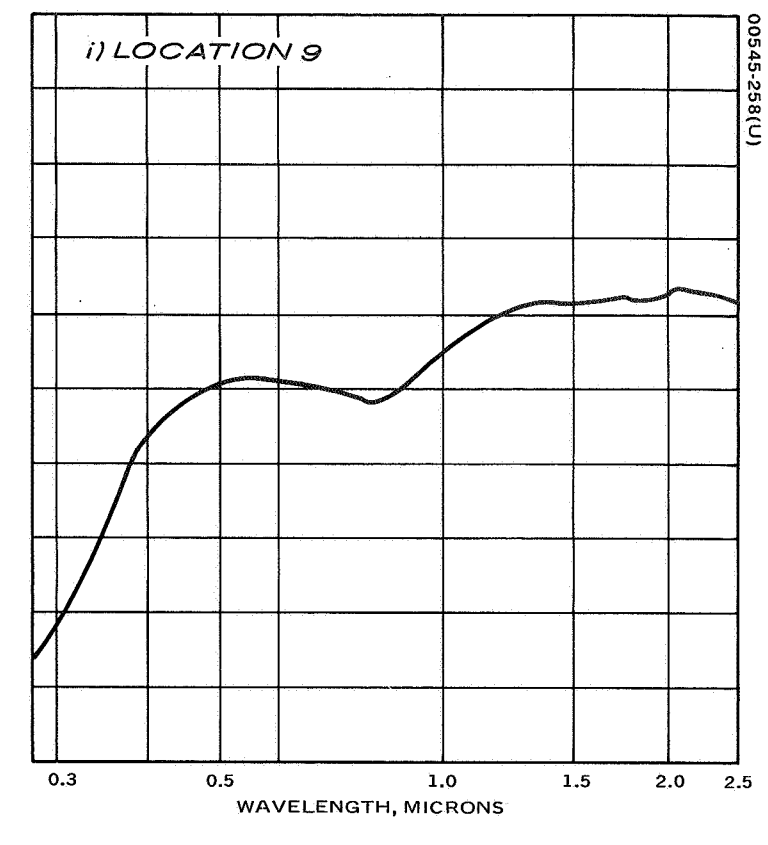

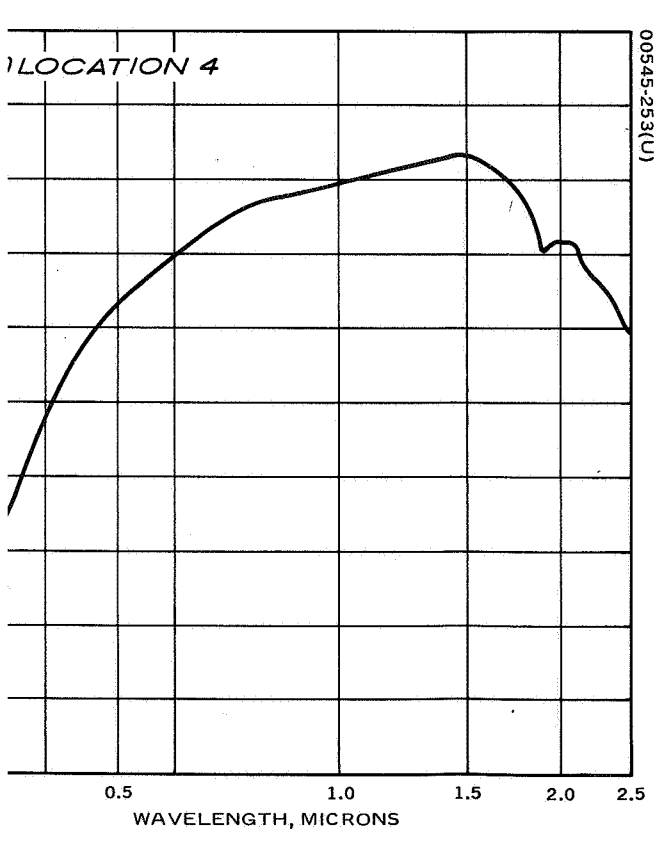

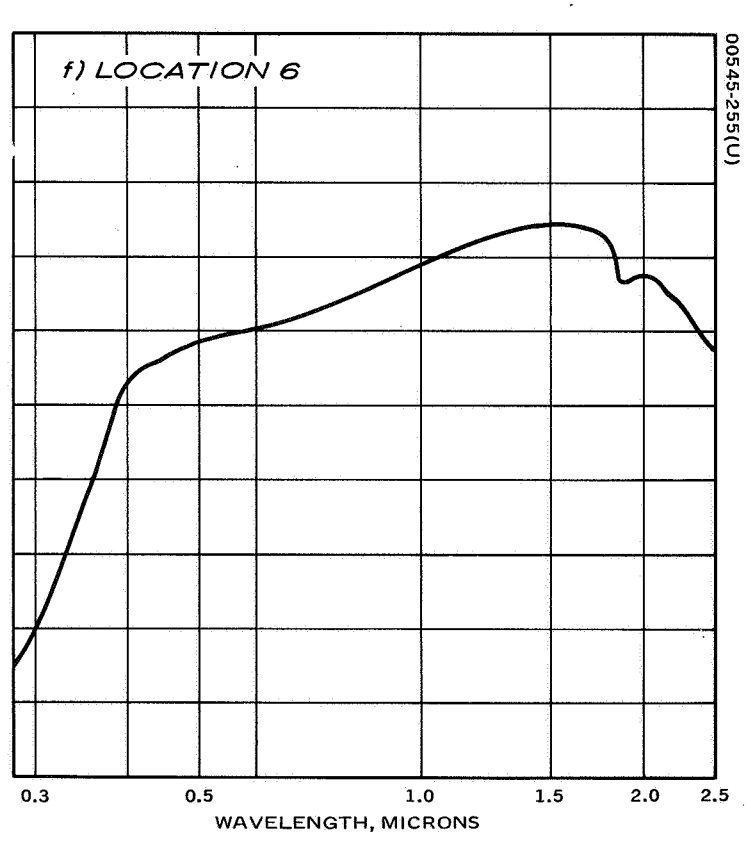

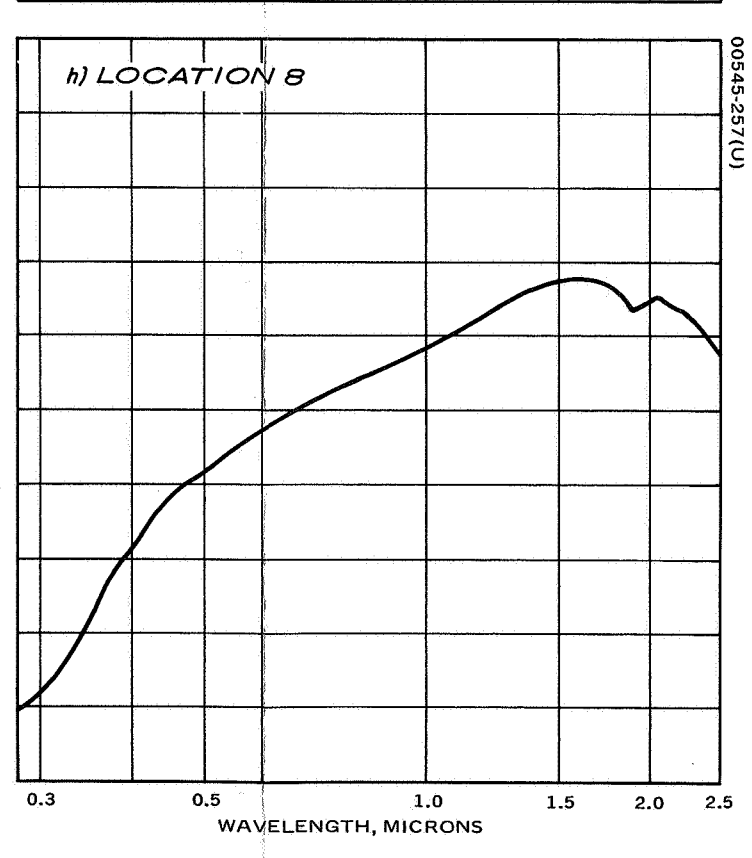

Shroud at Various TRW Locations Shown in Figure J-9

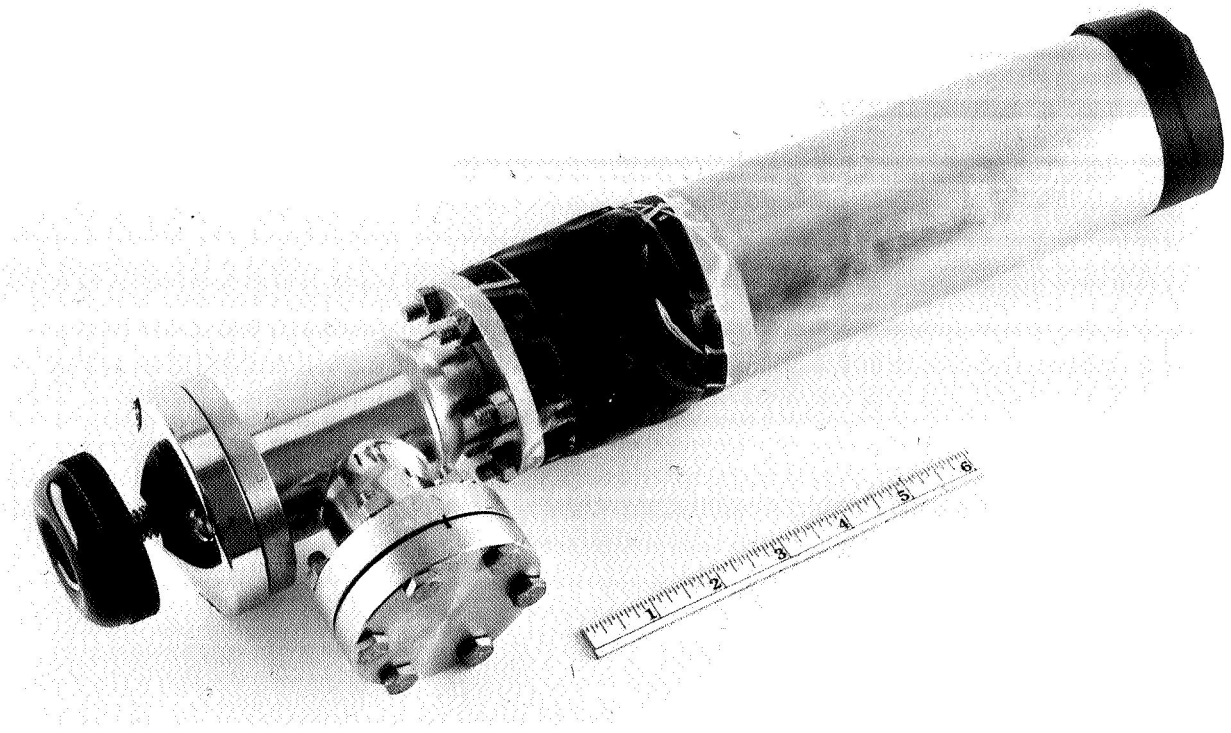

Figure J-11. Quartz Chamber With Light-Tight Shield for Vacuum Tests of White Painted Tube (Photo 4R18635)

were placed in the ion pump throats to ensure that the samples were not exposed to the glow discharge during startup of the ion pump.

The spectral reflectance of the tube was measured around the circumference at 90 degree increments, while the sample was maintained at 5×10^{-7} Torr. The measurements were made by positioning the quartz chamber in an Edwards integrating sphere. Room lights were off during these operations; only dim red light was used to position the sample. It was not possible to rotate the quartz chamber so that each measurement would be made in the same plane. The chamber was raised and lowered so that about 0.63 inch separated the uppermost and lowest measurement. Figure J-12 is a sketch of the tube showing measurement orientation.

At the completion of these vacuum measurements, a leak valve attached to the system was opened and the pressure in the quartz tube was raised to about 10 microns of Hg (10^{-2} Torr). Each sample position was remeasured for optical reflectance. Again, no light was allowed to reach the sample tube except that of the monochromatic spectrophotometer beam. Following this set of measurements, air was admitted to the chamber, bringing the pressure up to 1 atm. The spectral reflectance at four sample positions was measured again. The samples then sat at 1 atm for 6 days in the dark.

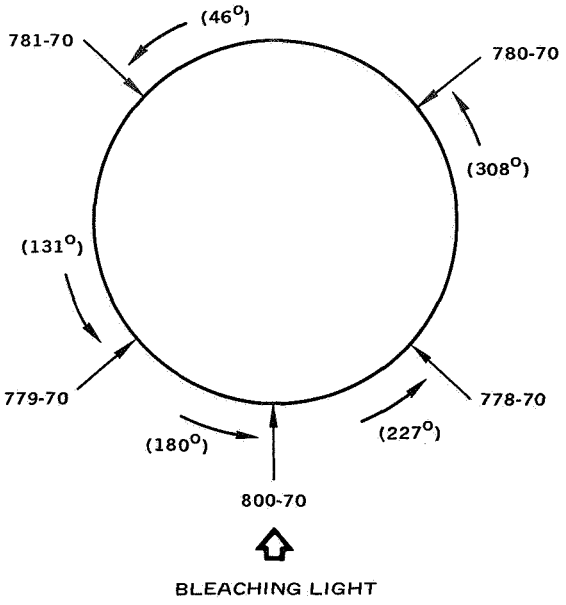

Figure J-12. Sketch of White Painted Section of Tube Returned in SESC Showing Measurement Positions

The spectral reflectance was again measured of the sample position 778-70 shown in Figure J-12. The tube was then exposed to light at position 800-70 from a xenon arc lamp through a Corning CS3-74 yellow filter. This filter removed all illuminating wavelengths less than 0.4 micron. The irradiance for the 48 hour period was 214 $\dot{m}w/cm^2$. The surface of the sample tube closest to the irradiating source (Figure J-12) was halfway between two of the positions which had previously been measured. Following the 48 hour exposure spectral reflectance measurements were again made at the four positions previously measured. A measurement was also made at the surface closest to the irradiating source (sample position 800-70 on Figure J-12).

Results of the measurements of the spectral reflectance of the white painted tube, discussed above, are presented in Figures J-13 through J-18. Figure J-13 shows the reflectance versus wave length of the four samples measured in vacuum prior to exposure. Figure J-14 shows the reflectance after partial pressurization at relatively low pressures. Figure J-15 shows reflectance of the four samples after they were exposed to 1 atm, still prior to any light exposure. Figure J-16 shows the reflectance of one of the samples after 6 days exposure at 1 atm. Figure J-17 shows reflectance of another sample from a different portion of Figure J-12 taken after an exposure to light for 48 hours at 1 atm. Figure J-18 shows reflectance of the original four samples at 1 atm after they had been exposed to 48 hours of light.

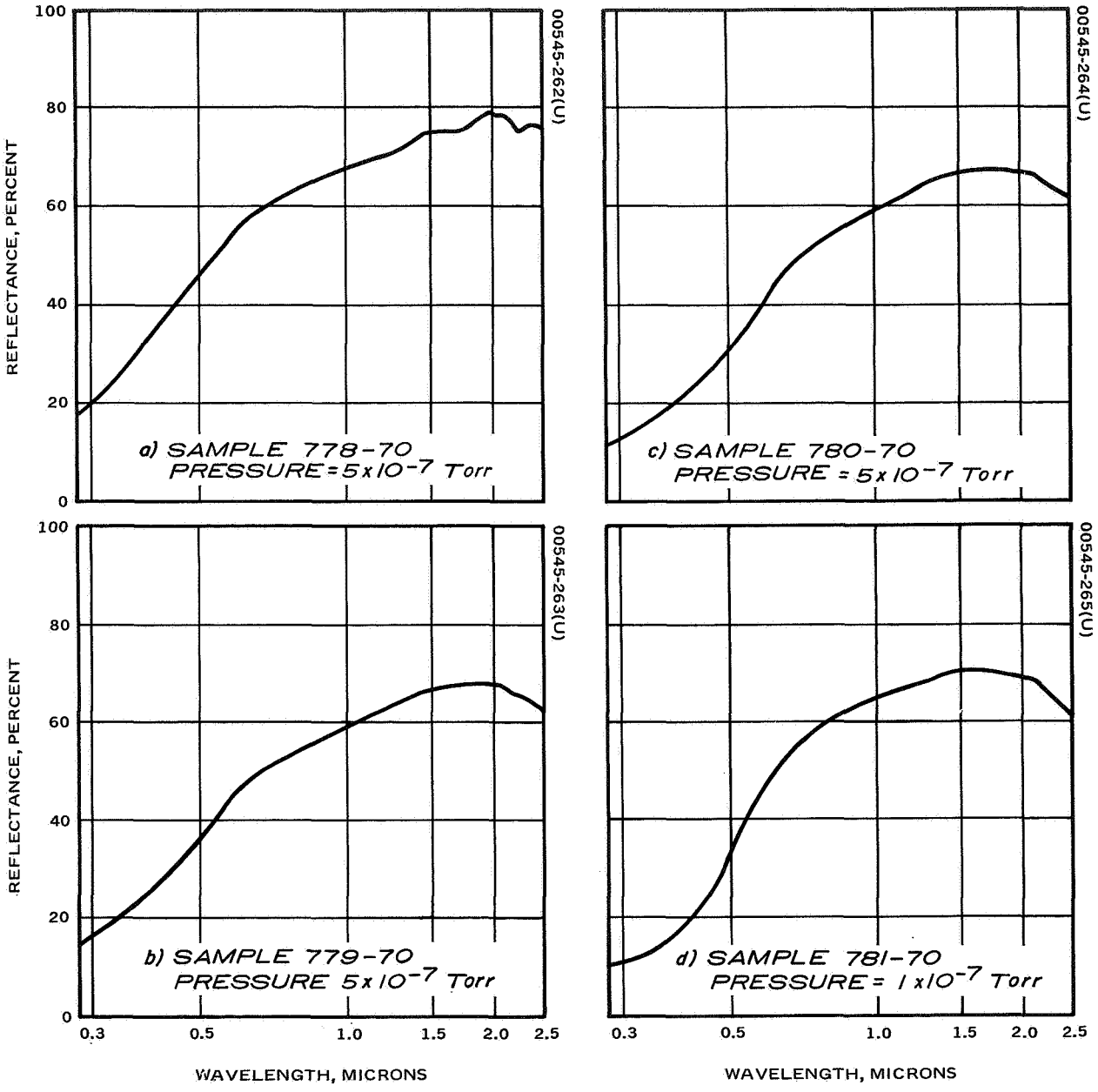

Figure J-13. Spectral Reflectance Versus Wavelength of Four Samples of White Painted Tube – High Vacuum, Prior to Light Exposure

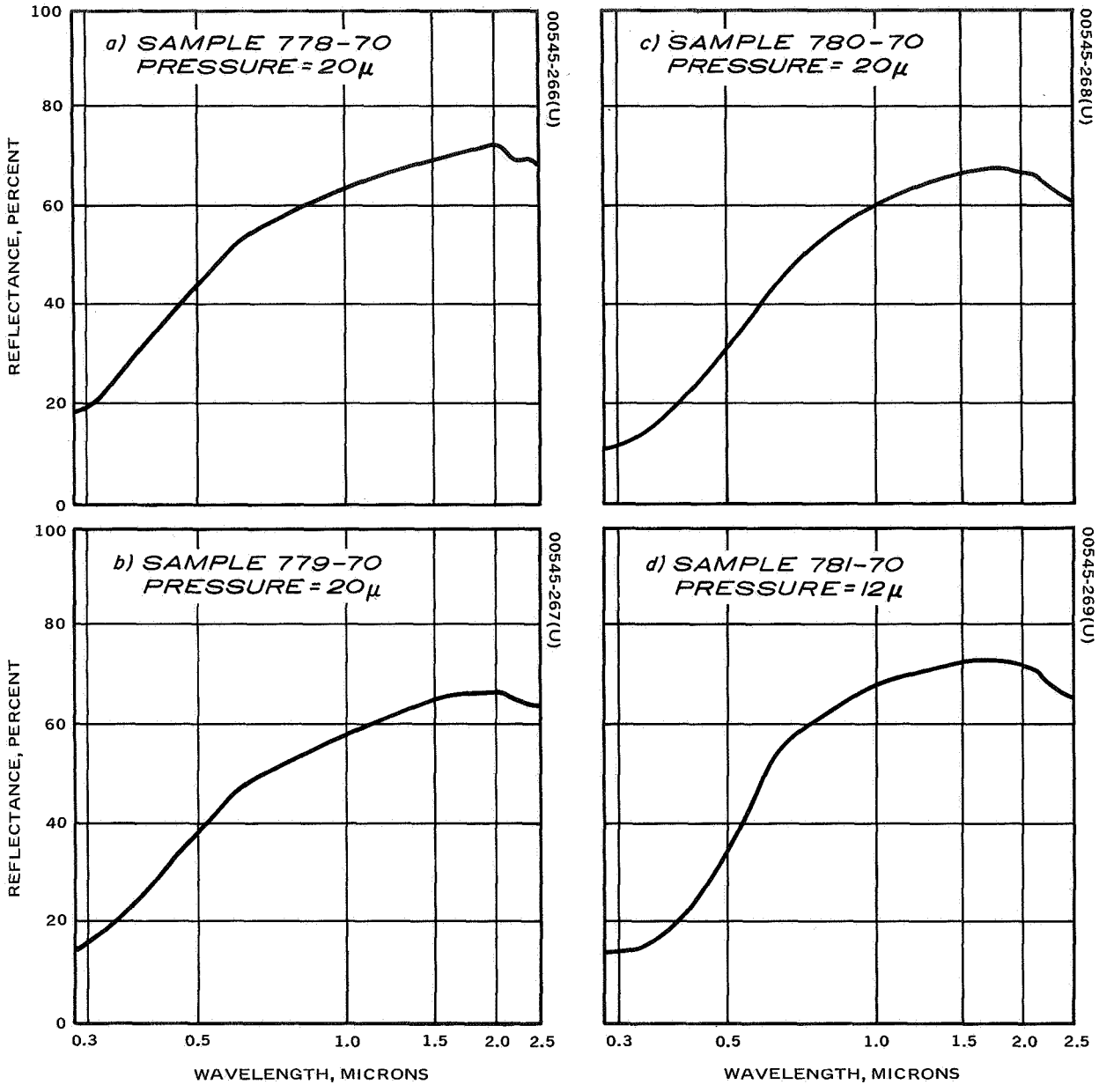

Figure J-14. Spectral Reflectance Versus Wavelength of Four Samples of White Painted Tube – Medium Vacuum, Prior to Light Exposure

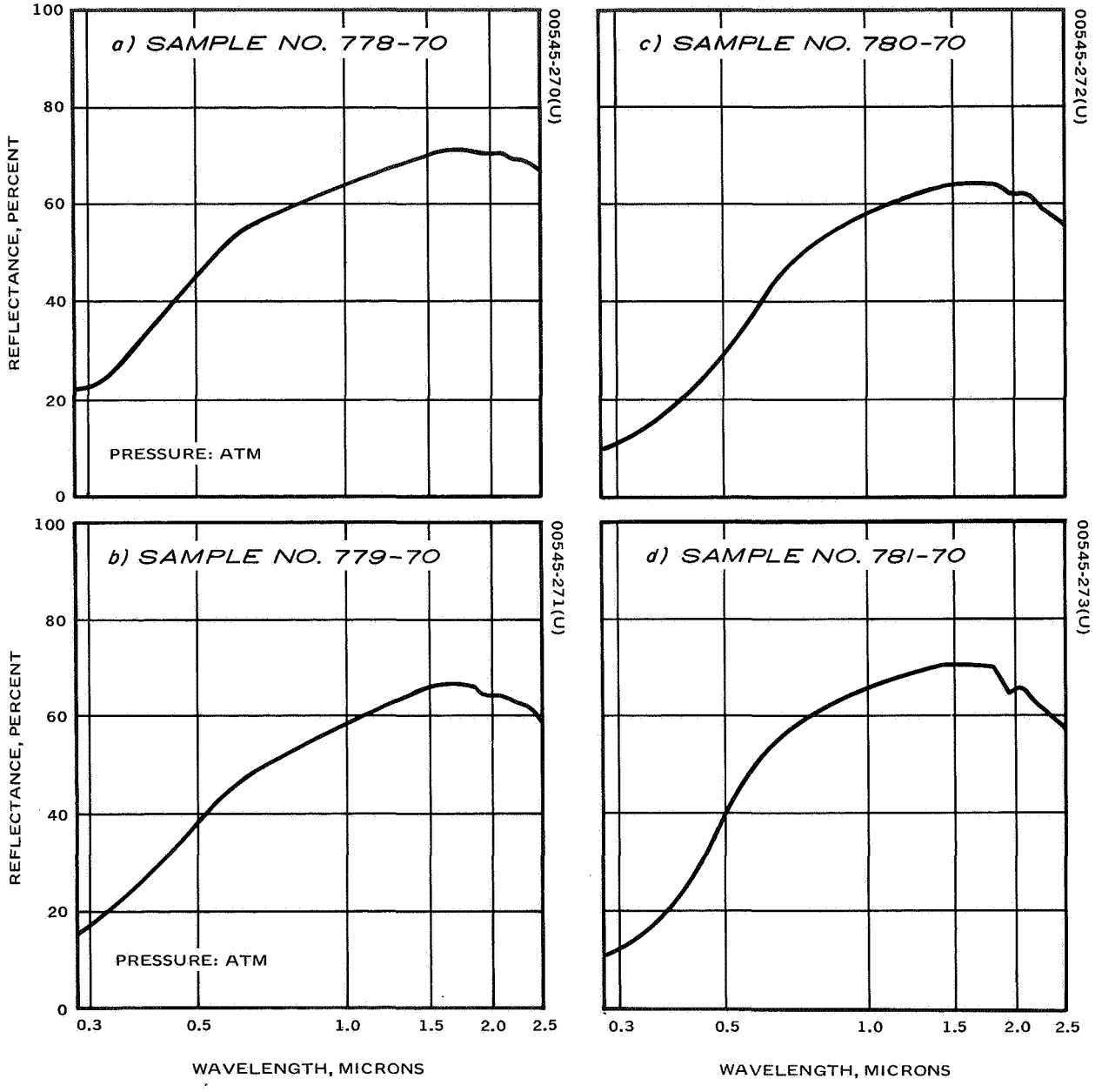

Figure J-15. Spectral Reflectance Versus Wavelength of Four Samples of White Painted Tube – 1 Atmosphere, Prior to Light Exposure

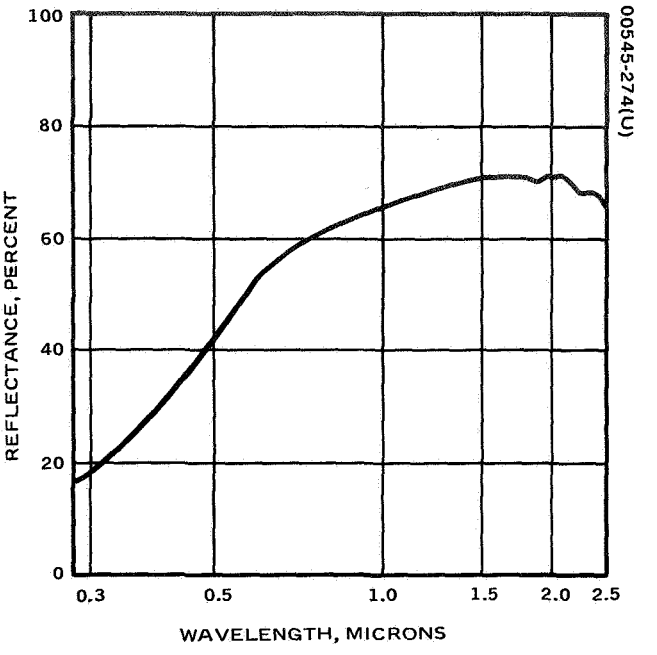

Figure J-16. Spectral Reflectance Versus Wavelength of One Sample of White Painted Tube: Sample 778-70 After 6 Days at 1 Atmosphere. Prior to Light Exposure

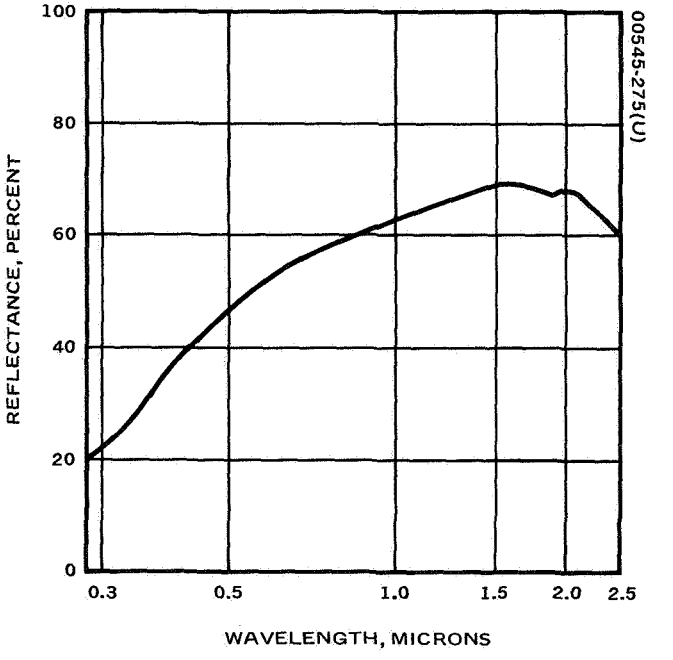

Figure J-17. Spectral Reflectance Versus Wavelength of a Different Sample of White Painted Tube: Sample 800-70 in Figure J-12 After 48 Hours Exposure to Light at 1 Atmosphere

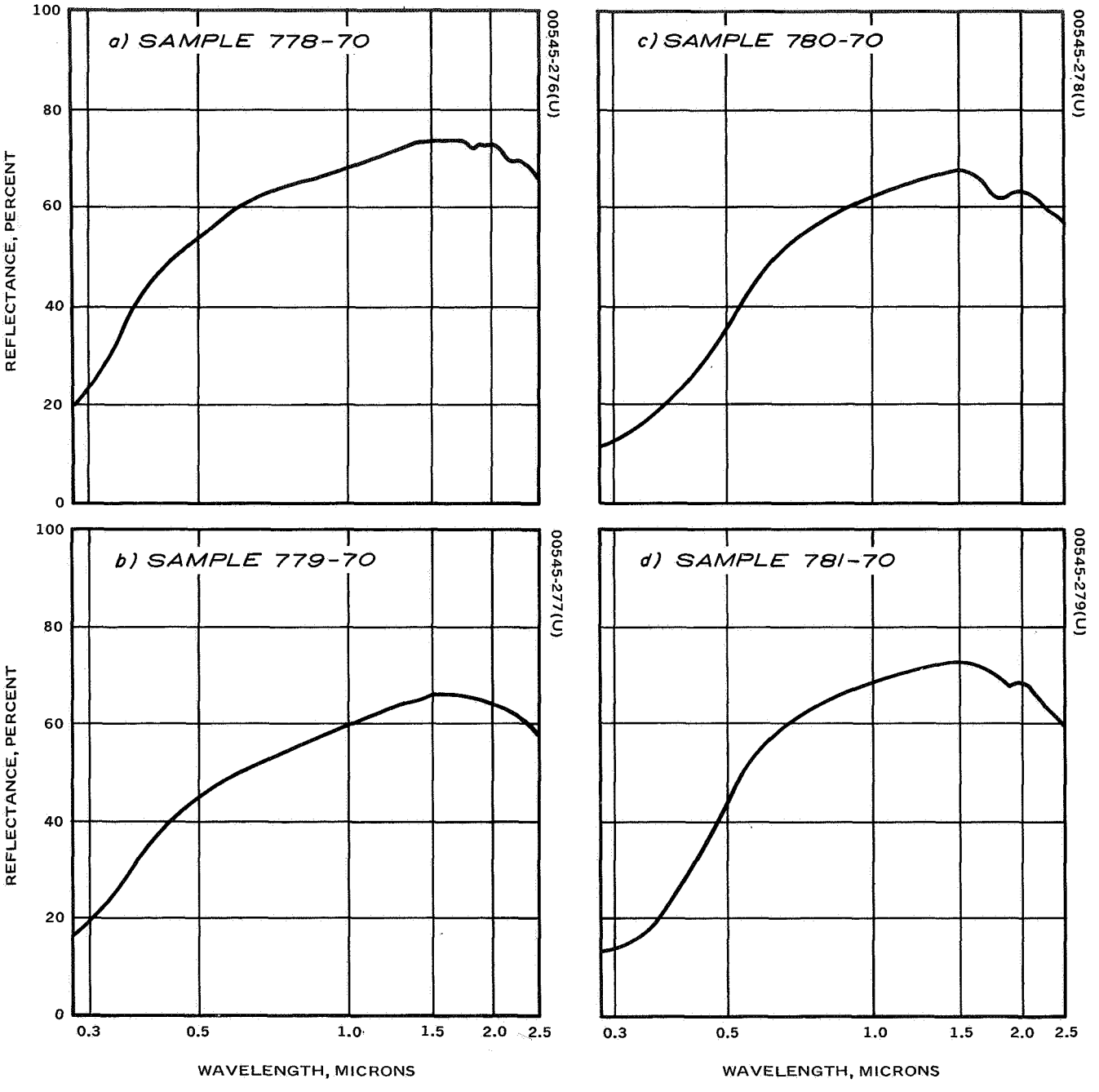

Figure J-18. Spectral Reflectance Versus Wavelength of Four Samples of White Painted Tube After 48 Hours Exposure to Light at 1 Atmosphere

J.4.3 Reflectance of Cable Bracket From Lower Shroud

The bracket shown in Figure J-19* used to attach the TV camera cables to the lower shroud was removed from the camera at the LRL on 6 January 1970. It was wrapped in teflon FEP film and stored in the dark. In May 1970, the bracket was removed from the dark for examination. A large disparity was found in the color of the bracket and that of the lower shroud of the camera. When the bracket was removed initially, the surface of the camera and bracket were a similar brown tone. In May, the shroud was found to be much lighter, with the bracket appearing to be the same color as it was upon the first viewing of the Surveyor III hardware in January 1970. This difference in color is shown in Figure J-20.*

The four test coupons were cut from the bracket, as shown in Figure J-21. Each sample was 1 by 2 cm. The spectral reflectance of these four coupons was measured. One sample, 518 in Figure J-21, was examined with a scanning electron microscope for the presence of lunar soil. Lunar material could not be distinguished from the paint. This was due to the charge buildup in the paint and lunar soil. All samples were then stored in the dark for 3-1/2 months, after which the spectral reflectance was remeasured. The original measurements of spectral reflectance versus wavelength conducted in May 1970 on one of the above samples, 518 mentioned above, are plotted in Figure J-22. Results obtained 3-1/2 months later in August 1970 showed no appreciable change. Results of spectral

*Original in color.

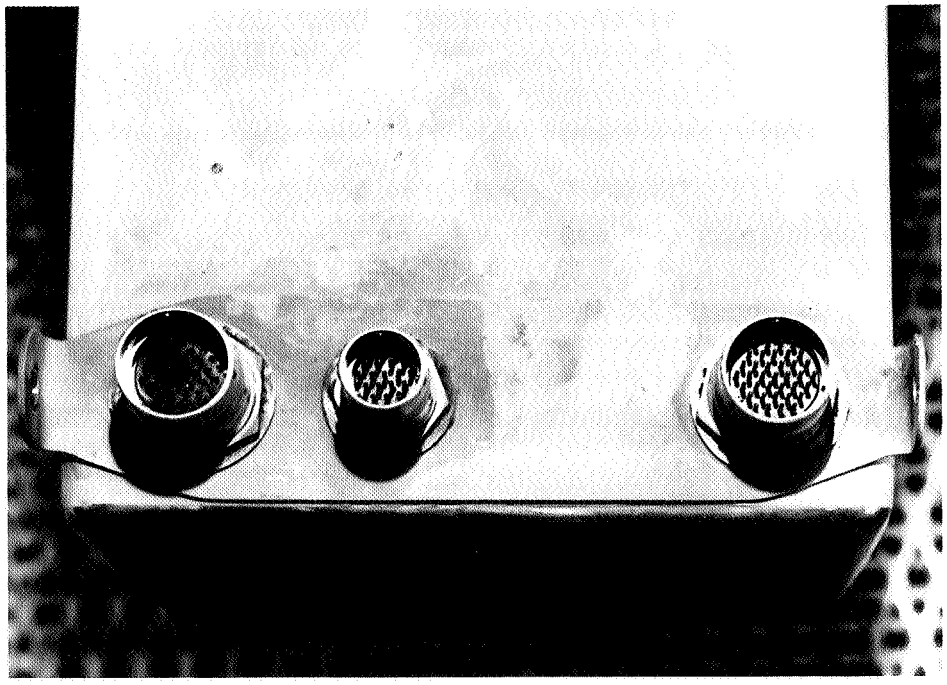

Figure J-19. Lower Shroud of Surveyor III Camera With Attached Cable Bracket Upon Return From Moon (NASA Photo S-70-21142)

reflectance on the other three samples both in May and in August 1970 were similar to those of Figure J-22.

In November 1970, samples 519 and 521 were selected for controlled exposure to fluorescent lights. The samples were remeasured (they were still in dark storage) for spectral reflectance and then exposed to fluorescent light of a laminar flow bench for 72 hours. One sample (521) was double-bagged in polyethylene, with a total thickness of 0.012 inch of clear polyethylene bag separating the sample from the fluorescent lighting. Both

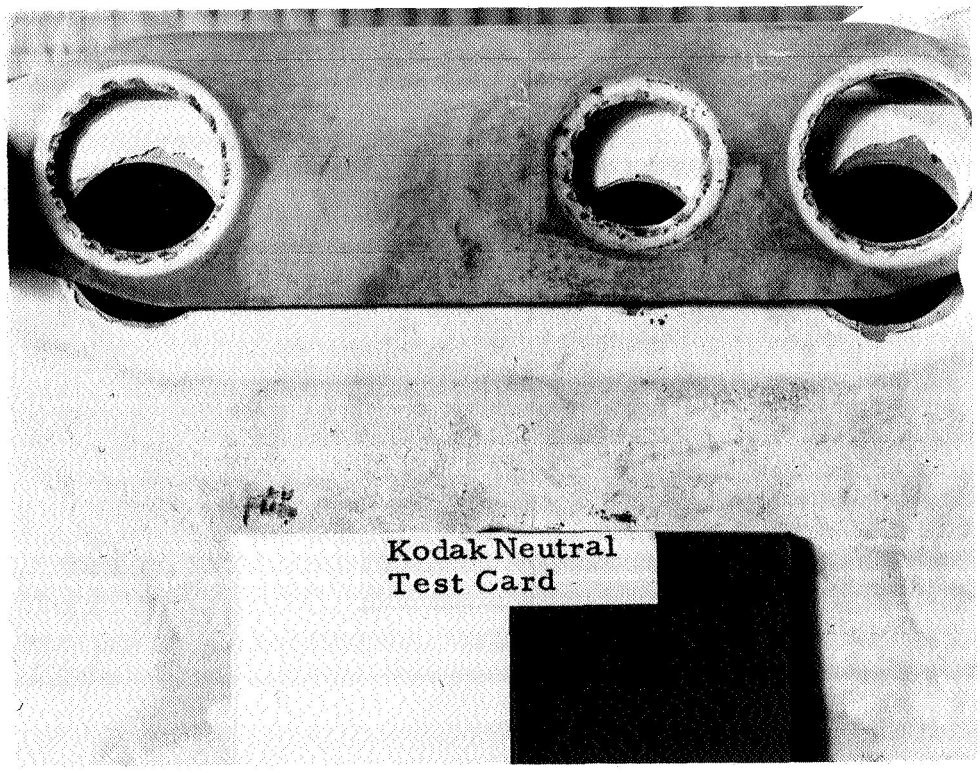

Figure J-20. Cable Bracket Superimposed on Lower Shroud of Surveyor III Television Camera: Shroud Exposed to Light for About 5 Months, Cable Bracket Unexposed (Photo 70-5364)

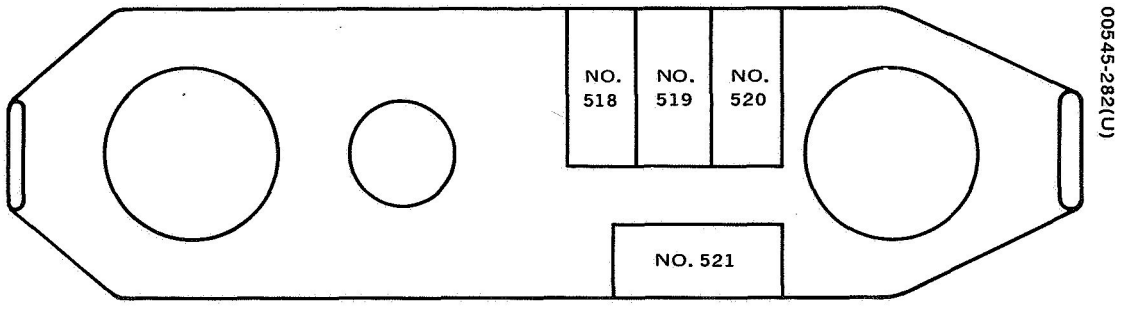

Figure J-21. Location of Samples Cut From Cable Bracket

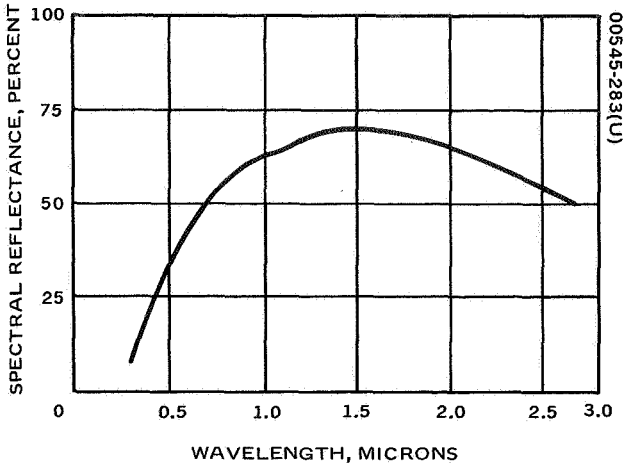

Figure J-22. Spectral Reflectance Versus Wavelength of Sample of Camera Cable Bracket: Sample 518 of Figure J-21: Measurements Taken in May 1970 Prior to Light Exposure

samples were protected with a 0.002 inch thickness of clear teflon FEP film to prevent dust fallout during storage and transit. The irradiance of white light reaching each sample was ~170 mw/cm^2. Following this exposure, the spectral reflectance of each sample was remeasured. The samples were returned to the laminar flow bench for an additional 14 days of exposure (17 days total) and then remeasured. Results of these measurements are shown in Table J-2.

J.4.4 Measurements of Samples of Camera Bipod Bracket Support Tube

In January 1970 when the TV camera was first disassembled, the support collar (Figure J-23)* which was used to attach the camera to the spaceframe was removed, wrapped in teflon FEP film, and stored in the dark. In July 1970, the long tube from the bipod bracket side of the clamp on the left side of Figure J-23 was cut off the assembly for a series of tests.

The bipod side of this assembly was located on the southern side of the spacecraft on the moon, and can be seen in Figure J-24 taken by the astronauts during Surveyor III hardware recovery.

The spectral reflectance of the tube was measured by mounting the tube vertically in a Gier-Dunkle integrating sphere. The tube had three different colors. The general overall color of the tube was light yellow. A dark gray region was noted on the westerly side of the tube, and a very dark yellow region was found on the easterly side. The reflectance was measured in each of these regions.

*Original in color.

TABLE J-2. PERCENT OF SPECTRAL REFLECTANCE VERSUS WAVELENGTH OF SAMPLES FROM SURVEYOR III CAMERA CONNECTOR BRACKET AFTER EXPOSURE TO WHITE LIGHT PHOTO BLEACHING

Wavelength, microns	Spectral Reflectance, percent					
	Before Exposure to Light		After 72 Hours Exposure to Light		After 17 Days Exposure to Light	
	Sample 519*	Sample 521**	Sample 519	Sample 521	Sample 519	Sample 521
0.295	9.0	10.0	12.0	10.0	17.0	14.0
0.355	20.0	18.0	18.0	16.5	28.0	28.0
0.400	25.0	22.0	26.0	23.0	39.0	36.0
0.430	28.5	27.0	28.0	29.5	46.0	45.0
0.458	33.0	33.5	35.0	35.5	47.0	47.5
0.484	35.5	37.0	39.0	38.5	49.0	47.0
0.511	40.5	40.0	42.0	42.0	56.0	50.0
0.540	44.0	45.0	46.0	46.0	56.0	53.0
0.569	47.0	49.0	49.0	49.5	56.0	55.5
0.598	49.0	52.0	51.5	51.0	62.0	58.0
0.630	52.0	53.5	54.5	55.0	63.0	60.0
0.664	55.0	58.0	58.0	58.0	64.0	60.0
0.700	60.0	58.0	59.0	58.0	67.0	61.0
0.738	60.0	59.0	60.0	60.0	67.0	62.0
0.781	67.0	62.0	62.0	62.0	70.0	63.0
0.828	66.0	66.0	65.0	64.0	70.0	63.0
0.880	67.0	65.5	67.0	65.0	72.0	64.0
0.940	70.0	67.0	69.0	68.5	73.9	66.0
1.011	71.0	68.0	70.0	70.0	74.0	67.0
1.096	71.0	72.0	72.0	72.0	75.0	71.0
1.200	74.0	75.0	75.0	73.0	75.0	74.0
1.341	75.0	75.0	74.0	73.0	75.0	74.0
1.536	74.0	72.5	73.5	74.0	75.0	70.0
1.854	68.5	65.5	67.0	68.0	71.0	68.0
2.600	55.0	55.0	57.0	56.5	51.0	56.0

*Sample 519 (Figure J-21) wrapped in polyethylene film.
**Sample 521 (Figure J-21) unwrapped.

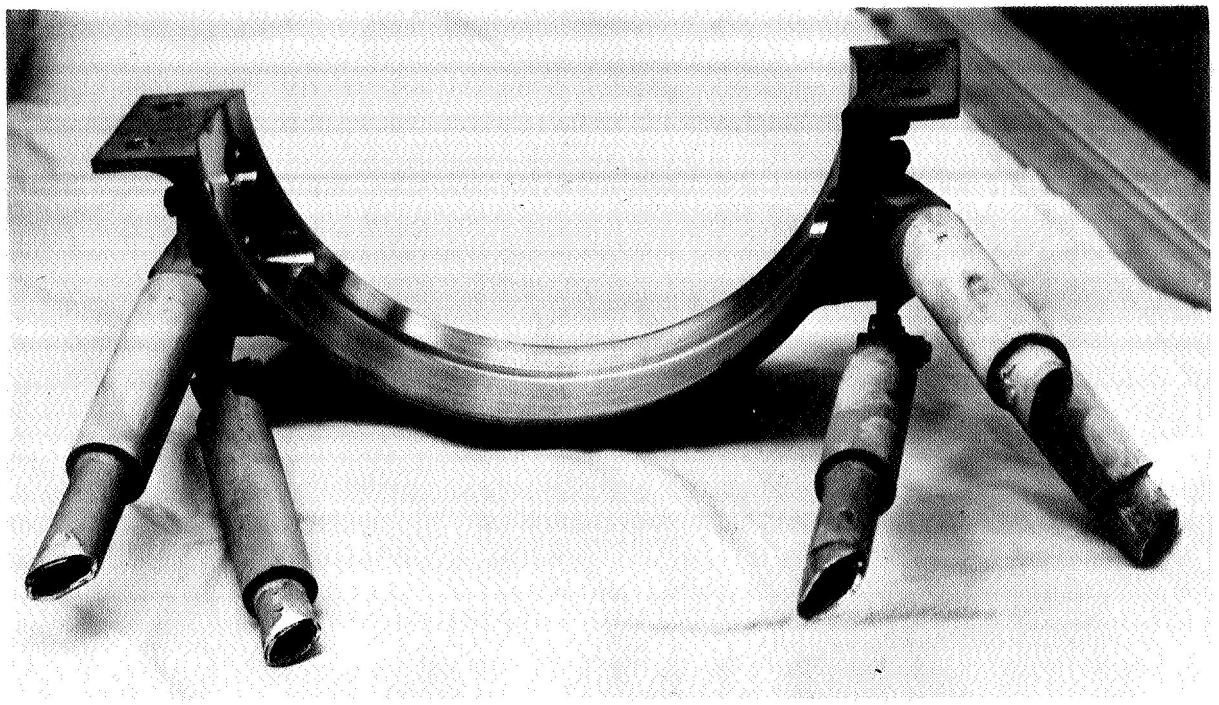

Figure J-23. Support Collar of Surveyor III Television Camera (NASA Photo S-70-21157)

The tube was then suspended in a beaker containing $CC\ell_4$ and soaked for 1 hour. To minimize the washing away of any lunar material on the surface, the tube was not agitated. The tube was gently removed from the beaker, air dried, and soaked again in fresh $CC\ell_4$, this time for 1-1/2 hours. During these experiments, the tube was maintained in the dark.

The $CC\ell_4$ was boiled down and evaporated on an NaCl window for infrared analysis. After the second soak in fresh CCl_4, no organic contaminant was found in the residue. Evidence of silicone was found in the residue from the first wash, but it is believed that faulty technique caused this contamination.

The spectral reflectance of the tube was remeasured at the same three positions on the tube following the $CC\ell_4$ soak. Following the solvent soak experiment, the sample was returned to dark storage.

In September 1970, the tube section was used in another experiment. The sample was suspended in air and heated overnight. The tube section was mounted in a glass test tube that was packed at the open end with glass

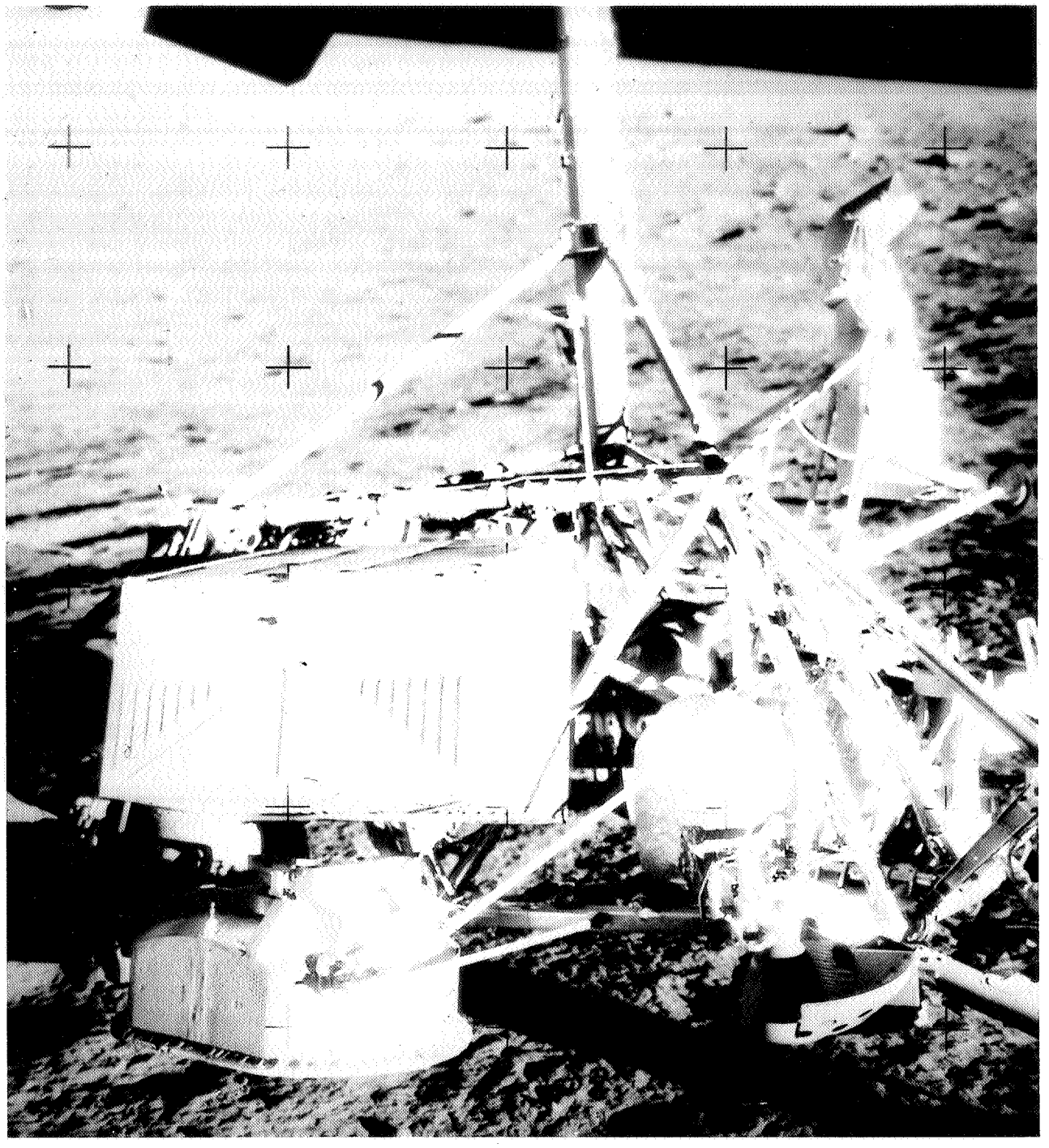

Figure J-24. Photograph of Surveyor III on the Moon, Showing TV Support Tubing (NASA Photo AS12-48-7115)

wool to minimize air currents. A thermocouple was mechanically attached to the tube. The tube temperature was raised to 450°F. Fifteen hours later the temperature had fallen to 420°F due to room cooling. The average temperature for the 15 hours was about 425°F. The tube was maintained in the dark during this experiment. The sample was removed from the tube and the reflectance remeasured at the same three positions.

The data from all three reflectance versus wavelength measurements are shown in Figure J-25.

J.4.5 Thermal Annealing of Unexposed Surveyor White Paint

A thermal annealing test was conducted on a Surveyor inorganic white paint sample that had been stored free of airborne contaminant since painting in 1965. The sample was held in air overnight at 435°F, a time of about 18 hours. The spectral reflectance of this sample was measured before and after thermal exposure in a Gier-Dunkle integrating sphere. No significant spectral difference was noted from 0.3 to 1.3 micron. However, beyond 1.3, a significant increase occurred in the reflectance spectrum, with the reflectance at 2.6 microns increasing 14 percent. This increase was due to the release of chemically combined water in the clay-silicate system.

J.4.6 Reflectance of Surveyor III Samples Used in Science Studies

In accordance with the test plan, a number of samples were cut from the shrouds of the TV camera in July 1970 for use in science studies. The sample cutting is documented in proper files. The samples were photographed and then examined under a light microscope to 40X. The spectral reflectance of these samples was then measured in a Gier-Dunkle integrating sphere. The measurements were made during July 1970. Sample size for each experiment was 1 by 2 cm. Some samples were taken from positions on the lower shroud where earlier spectral reflectance measurements had been made (by TRW). Thus, a time comparison could be made of any change in reflectance from April to July 1970. Table J-3 lists the samples cut in July 1970, location on TV camera, and the corresponding TRW measurement position, if any. The spectral reflectance data for these samples are given in Table J-4. All samples but 894 were painted on the exterior with the Surveyor inorganic white paint. Sample 894 was polished aluminum. Samples 906, 907, 908, and 909 were coated on the interior side with an organic optical black paint. The reflectance of both sides of these samples was measured.

Additional samples were selected and removed from the lower shroud for spectral reflectance measurements in October 1970. Position selection was as close as possible to the TRW positions shown in Figure J-9. Sample size was again 1 by 2 cm. Reflectance measurements were made in

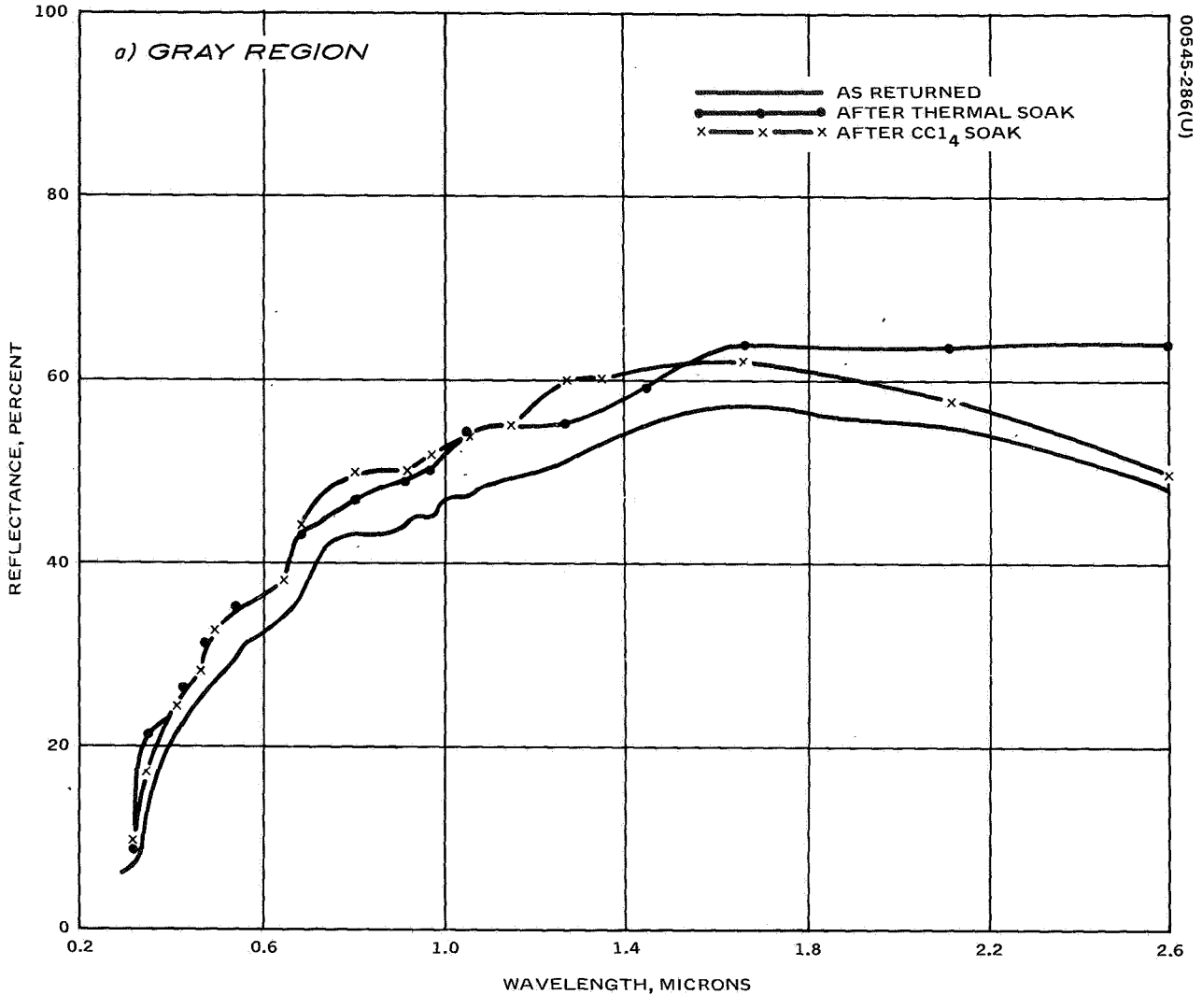

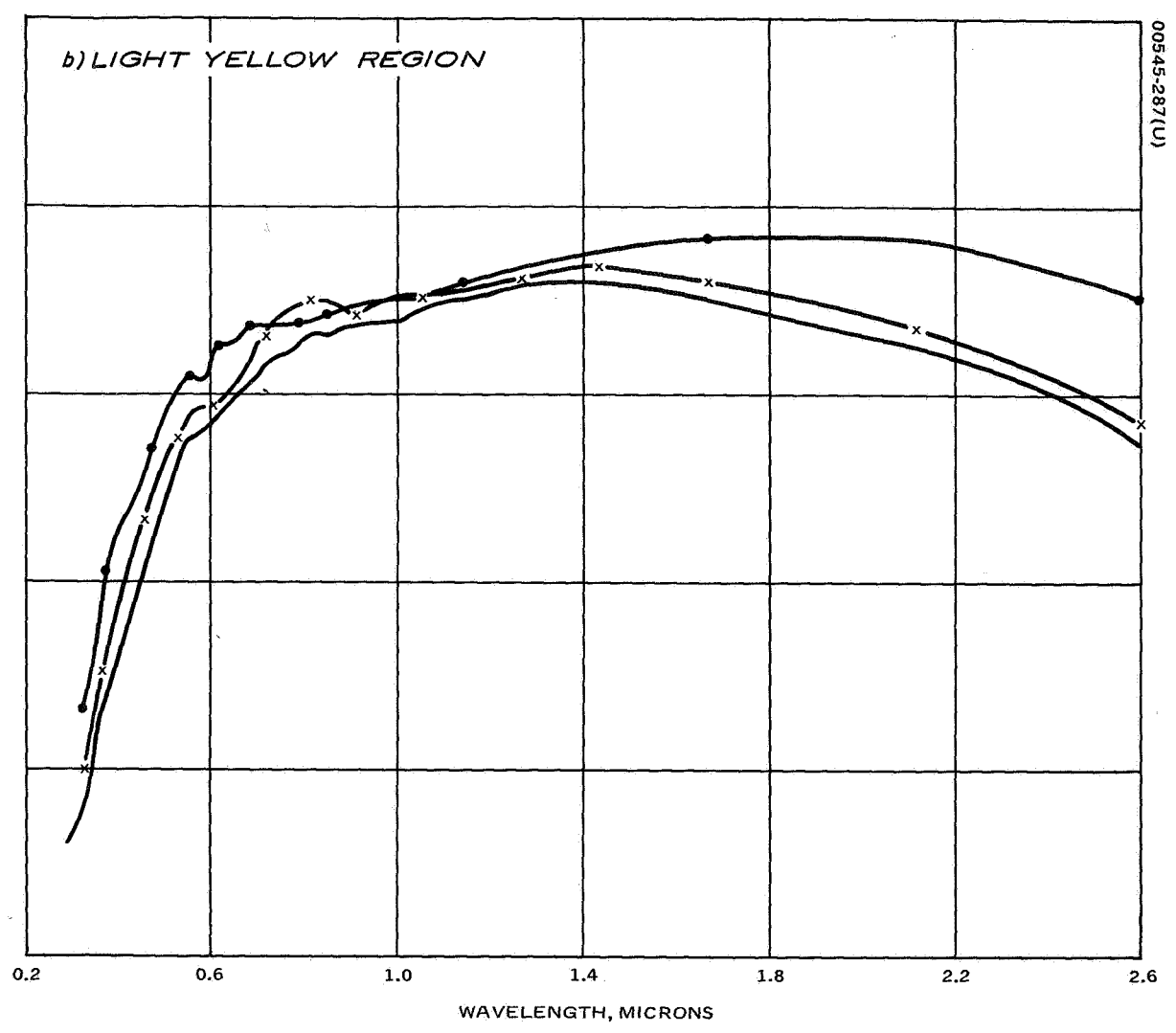

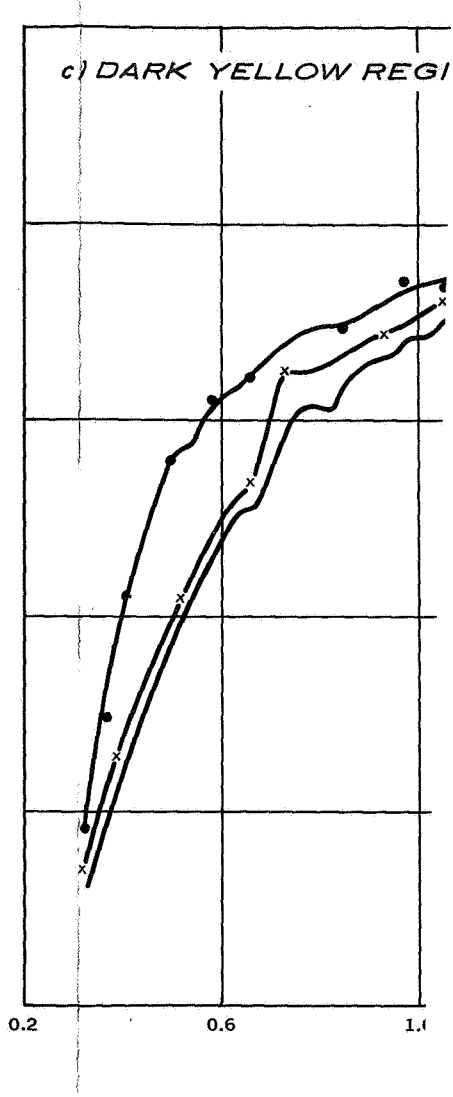

Figure J-25. Reflectance of Bipod Bracket Tube

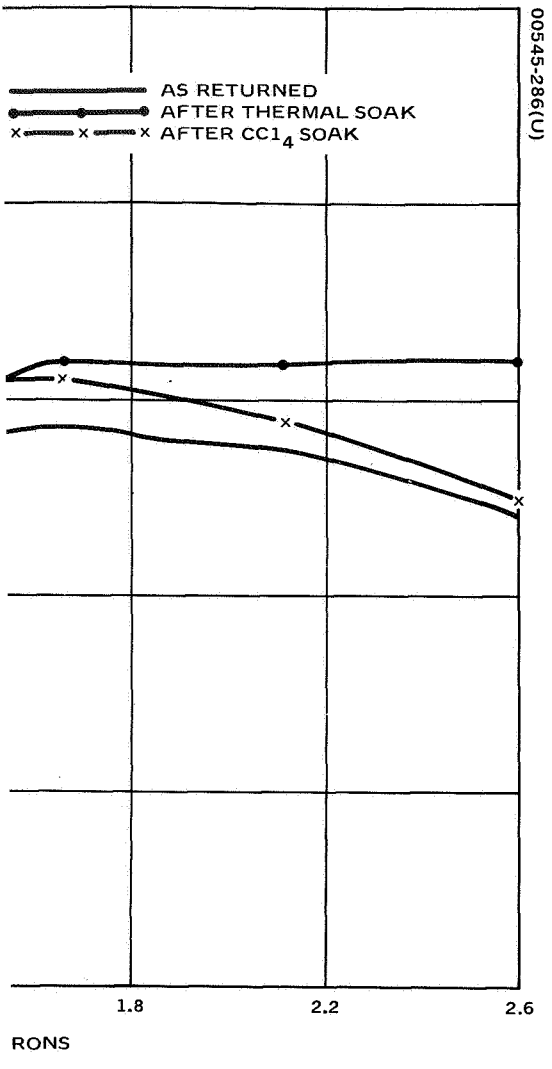

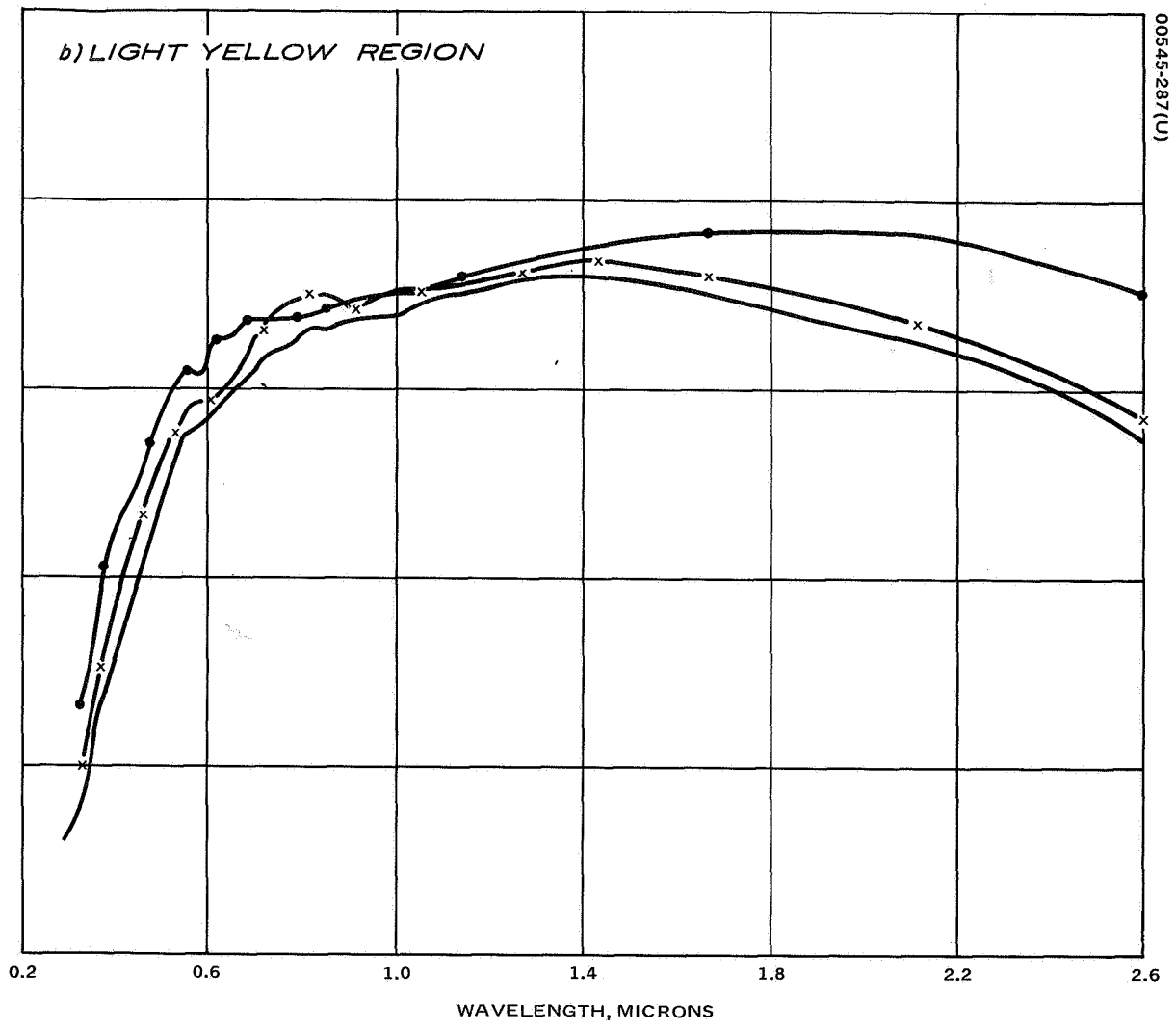

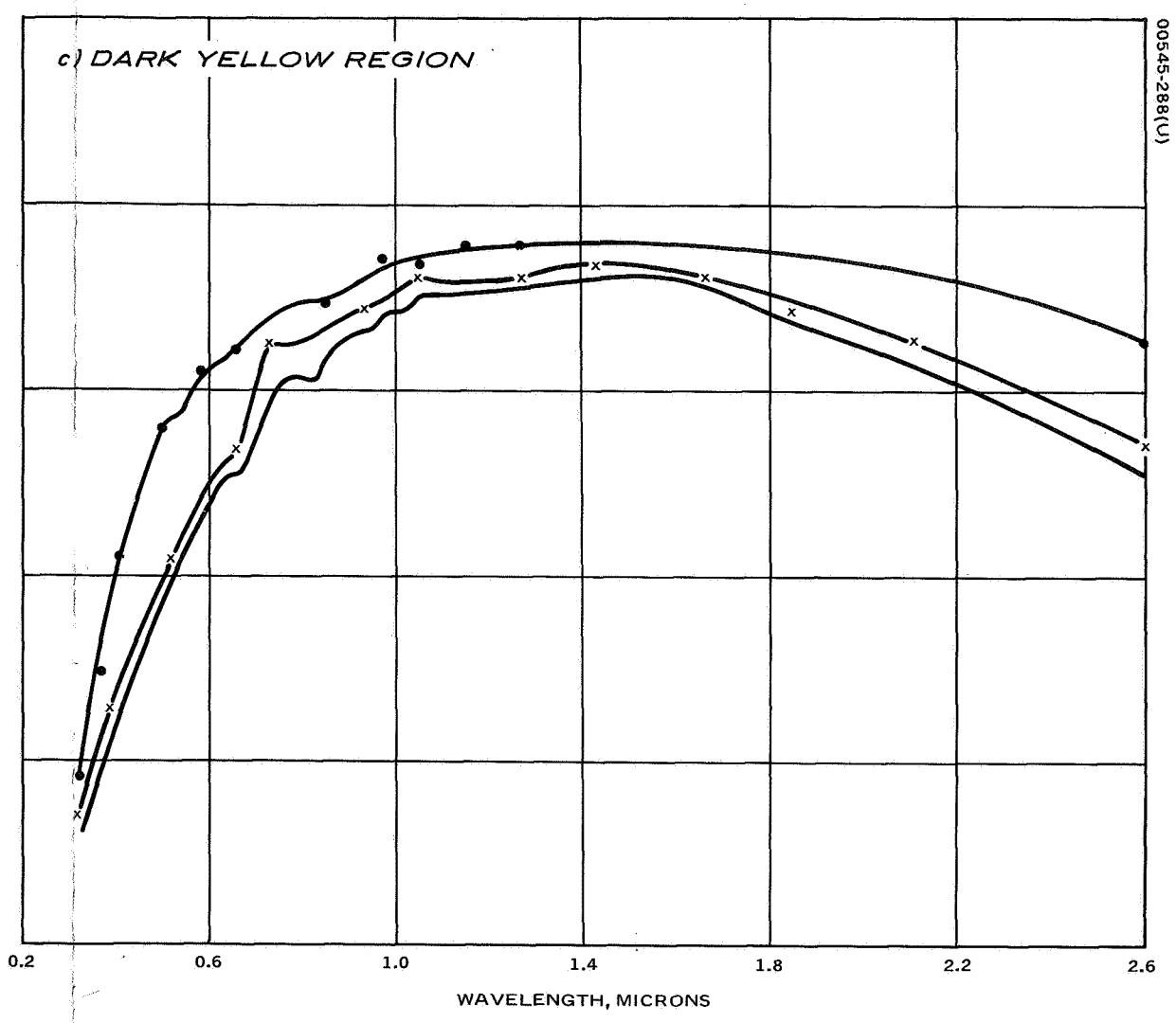

ipod Bracket Tube

TABLE J-3. SAMPLES OF SURVEYOR III CAMERA SHROUD CUT IN JULY 1970 FOR SCIENCE STUDIES

Sample Designation		Sample Location on the Surveyor III Camera Shroud
Log Number (Program Test Files)	TRW Measurement Position (see Figure J-9)	
893	2	Lower shroud, front (flat side) facing northeast (lunar), near center
894	9	Lower shroud, bottom, facing lunar surface, polished aluminum, near back or curved side
898	5	Lower shroud, northwest (lunar) side facing lunar module landing site
900	4	Lower shroud, southeast (lunar) side facing away from lunar module landing site
906	None	Sun visor, top, facing up, centered (opposite side painted with organic optical black)
907	None	Mirror assembly hood, south (lunar) side, facing away from lunar module landing site (opposite side painted with organic optical black)
908	None	Mirror assembly hood, north (lunar) side, facing lunar module landing site (opposite side painted with organic optical black)
909	None	Mirror assembly hood, east (lunar) side, highest solar irradiance (opposite side painted with organic optical black)

TABLE J-4. PERCENT REFLECTANCE OF SAMPLES FROM SURVEYOR III CAMERA SHROUD CUT FOR SCIENCE STUDIES IN JULY 1970

Wavelengths, microns	Sample Designation (see Table J-3)											
					906		907		908		909	
	893	894	898	900	White Paint Side	Black Paint Side	White Paint Side	Black Paint Side	White Paint Side	Black Paint Side	White Paint Side	Black Paint Side
0.295	20.0	-	18.0	20.0	20.0	4.0	16.0	5.0	16.0	4.0	12.0	4.0
0.355	28.0	30.0	26.0	39.0	22.0	4.0	31.0	4.0	25.0	4.0	22.0	4.0
0.400	36.5	40.0	33.0	50.0	24.0	4.0	42.0	4.0	30.0	3.0	33.0	3.5
0.430	38.5	44.0	34.5	54.0	28.0	5.0	44.0	4.0	32.5	4.0	38.0	4.0
0.458	40.0	45.0	40.0	57.5	30.0	4.0	48.0	4.5	34.5	4.0	42.0	4.0
0.484	42.0	46.0	40.0	60.0	32.0	4.5	49.5	4.5	35.5	4.0	46.0	4.0
0.511	43.5	47.5	40.0	61.0	33.5	3.5	50.0	4.5	37.0	4.0	48.0	4.0
0.540	46.0	50.0	42.0	63.0	35.0	3.5	54.0	4.5	38.0	4.0	50.0	4.0
0.569	47.5	50.0	43.0	65.0	36.0	4.0	55.0	4.5	39.0	4.0	52.0	4.0
0.598	48.5	52.0	44.0	65.0	37.0	4.0	55.0	4.0	39.0	4.0	54.0	4.0
0.630	50.5	52.0	46.0	66.0	39.0	4.0	56.5	4.5	40.0	4.5	56.0	4.5
0.664	52.0	52.0	47.5	67.0	40.0	4.0	57.0	5.0	41.0	4.5	56.0	5.0
0.700	54.0	52.0	48.0	67.0	40.0	5.0	57.0	6.0	41.5	5.0	59.0	6.0
0.738	54.0	52.0	50.0	70.0	40.0	5.0	58.0	6.0	43.0	5.0	61.0	6.0
0.781	56.0	52.0	52.0	72.0	46.0	5.0	60.0	6.0	45.0	5.0	65.0	6.0
0.823	56.0	52.0	54.0	74.0	48.0	5.0	63.0	5.0	45.0	5.0	66.0	5.0
0.880	60.0	54.0	54.0	74.0	50.0	5.0	64.0	5.0	47.0	4.0	67.0	4.0
0.940	60.0	60.0	57.0	74.0	50.0	5.0	64.0	5.0	48.0	4.0	68.0	4.0
1.011	63.0	62.0	58.0	75.0	50.0	4.0	66.0	5.0	50.0	4.0	69.0	4.0
1.096	65.0	64.0	59.0	76.0	52.0	4.0	69.0	5.0	51.0	4.0	70.0	4.0
1.200	67.0	65.0	61.0	76.0	56.0	3.0	69.0	5.0	52.0	4.0	70.0	4.0
1.341	68.0	67.0	64.0	77.0	58.0	2.5	69.0	4.0	54.0	3.5	72.0	3.5
1.536	68.0	67.0	64.0	77.0	59.0	3.0	70.5	4.0	55.5	3.5	71.0	3.5
1.854	64.0	74.0	61.0	68.0	58.0	3.0	63.0	4.0	54.0	4.0	66.0	4.0
2.600	50.0	76.0	49.0	53.0	54.0	7.0	56.0	7.0	46.0	5.0	50.0	5.0

a Gier-Dunkle integrating sphere. The shroud had been continuously exposed to fluorescent lighting since the earlier TRW measurements (April 1970) and, in fact, since 6 January 1970, when the television camera was released from quarantine at the LRL. Table J-5 lists samples, corresponding TRW positions, and reflectance data.

J.4.7 Thermal Annealing of Surveyor III Samples

Thermal annealing of several Surveyor III samples was conducted both in air and in vacuum. This section describes the tests conducted on these samples and presents the reflectance data obtained before and after these tests.

In November 1970, three samples that were cut and measured in October 1970 were thermally annealed in air. The samples were thermally exposed in the same manner as the bipod bracket support tube, discussed in Section J.4.4. Temperature of the samples was raised to 450°F and maintained for 18 hours. The reflectance was measured after the thermal exposure. The samples tested were Surveyor III samples 1030 (TRW measurement position 2*), 1031 (TRW position 3), and 1035 (TRW position 7). As described earlier, these samples cut from the lower shroud were continuously exposed to light until their removal from the shroud in October 1970. Until this test, they were stored in the dark. Spectral reflectance values before and after exposure are given in Table J-6.

Vacuum-thermal annealing tests were conducted on a Surveyor III part, designated as sample 909 in Table J-3, and on an inorganic white painted sample previously tested in the Surveyor laboratories at Hughes. The laboratory-tested sample had been exposed to ultraviolet radiation.

Surveyor part 909 was cut from the front of the mirror housing. This part faced east (lunar) while in the Surveyor crater. The exterior surface was coated with inorganic white paint, and the back (inward facing) surface was coated with an organic optical black paint (3M black velvet).

The sample previously exposed to ultraviolet in the Hughes laboratory was painted in January 1965. The ultraviolet source was a BH6 high pressure mercury arc. The sample had been exposed at five times the solar ultraviolet flux for 65 hours at a temperature of 250°F while in vacuum. Following this ultraviolet exposure in 1965, the sample was stored in the dark until November 1970.

The spectral reflectance of both the Surveyor III and the laboratory samples was measured just before test and immediately after test. The two samples were placed in individual glass tubes that were evacuated to 10^{-6} Torr. The samples were then heated to 450°F and held for approximately 18 hours. The samples were then removed from the vacuum chambers and their spectral reflectance was remeasured. Results of these measurements are presented in Table J-7.

*See Figure J-9.

TABLE J-5. PERCENT REFLECTANCE OF SAMPLES FROM SURVEYOR III CAMERA SHROUD CUT FOR SCIENCE STUDIES IN OCTOBER 1970

Wavelength, microns	Sample Designation — Upper Row: Program Log Number							
	1029	1030	1031	1032	1033	1034	1035	1036
	Lower Row: TRW Position Number (see Figure J-9)							
	1	2	3	4	5	6	7	8
0.295	26.0	17.0	23.0	24.0	13.0	17.0	10.0	14.0
0.355	58.0	29.5	44.0	48.0	26.5	32.0	16.0	24.0
0.400	73.0	37.0	60.0	62.0	36.5	38.0	24.5	35.5
0.430	78.0	41.5	66.5	68.0	39.5	44.0	27.5	37.0
0.458	80.0	45.0	70.0	70.5	42.5	48.0	30.5	40.0
0.484	80.0	45.0	70.5	72.0	44.0	48.0	32.5	42.0
0.511	82.5	48.0	74.0	73.0	46.5	48.0	34.0	43.0
0.540	82.5	49.0	75.0	75.0	47.0	50.0	35.0	44.0
0.569	83.0	49.0	76.5	76.0	49.0	51.0	37.0	47.0
0.598	84.0	51.0	78.0	77.0	55.0	53.0	37.5	47.0
0.630	84.0	53.0	78.0	78.0	55.0	53.0	38.5	47.5
0.664	86.0	54.0	78.0	78.0	55.0	54.0	39.0	48.0
0.700	86.0	56.0	79.0	79.0	58.0	57.0	40.0	49.0
0.738	88.0	57.0	79.0	80.5	60.0	59.0	43.0	50.0
0.781	88.0	59.0	80.0	83.0	60.5	59.0	45.0	51.0
0.828	87.0	60.0	80.0	83.0	62.0	60.0	46.0	53.0
0.880	87.0	62.0	82.0	83.0	62.0	60.0	47.0	55.0
0.940	86.0	62.0	81.5	82.5	62.0	61.5	50.0	57.0
1.011	86.0	64.5	81.5	83.0	62.0	65.0	53.0	58.0
1.096	85.5	65.0	82.0	82.5	67.0	66.0	53.0	61.0
1.200	84.5	66.5	81.5	83.5	68.0	69.0	56.0	63.0
1.341	84.0	68.0	82.5	82.5	67.0	69.0	59.0	65.0
1.536	81.0	70.0	81.0	81.5	64.0	68.0	60.5	64.0
1.854	73.0	63.0	73.0	71.5	60.0	65.0	57.0	61.0
2.600	55.0	55.0	56.0	55.0	50.0	56.0	51.0	57.0

TABLE J-6. EFFECT OF THERMAL ANNEALING IN AIR ON SPECTRAL REFLECTANCE OF SAMPLES CUT FROM LOWER SHROUD OF SURVEYOR III CAMERA IN OCTOBER 1970

Wavelength, microns	Spectral Reflectance, percent					
	Program Log 1030, TRW Position 2*		Program Log 1031, TRW Position 3		Program Log 1032 TRW Position 7	
	Before Annealing	After Annealing	Before Annealing	After Annealing	Before Annealing	After Annealing
0.295	17.0	16.0	23.0	25.0	10.0	13.0
0.355	29.5	29.0	44.0	45.0	16.0	20.0
0.400	37.0	38.0	60.0	57.0	24.5	25.0
0.430	41.5	42.0	66.5	65.0	27.5	28.0
0.458	45.0	44.5	70.0	68.0	30.5	31.0
0.484	45.0	46.5	70.5	71.0	32.5	32.0
0.511	48.0	46.5	74.0	73.0	34.0	33.5
0.540	49.0	49.0	75.0	73.0	35.0	35.5
0.569	49.0	49.5	76.5	75.0	37.0	37.5
0.598	51.0	52.0	78.0	77.0	37.5	40.0
0.630	53.0	53.0	78.0	77.0	38.5	41.0
0.664	54.0	53.0	78.0	79.0	39.0	42.0
0.700	56.0	55.0	79.0	80.0	40.0	44.0
0.738	57.0	58.0	79.0	80.0	43.0	47.5
0.781	59.0	60.0	80.0	80.0	45.0	50.0
0.828	60.0	62.0	80.0	80.0	46.0	53.0
0.880	62.0	63.0	82.0	80.0	47.0	55.0
0.940	62.0	65.0	81.5	80.0	50.0	55.0
1.011	64.5	66.0	81.5	81.0	53.0	56.0
1.096	65.0	68.0	82.0	81.0	53.0	57.0
1.200	66.5	70.0	81.5	80.0	56.0	58.0
1.341	68.0	72.0	82.5	85.0	59.0	63.0
1.536	70.0	71.0	81.0	81.0	60.5	64.0
1.854	63.0	70.0	73.0	78.0	57.0	64.0
2.600	55.0	62.0	56.0	65.0	51.0	57.5

*See Figure J-9.

TABLE J-7. EFFECT OF THERMAL ANNEALING IN VACUUM ON SPECTRAL REFLECTANCE OF SURVEYOR III CAMERA AND LABORATORY SAMPLES OF WHITE INORGANIC PAINTED SURFACES

All Thermal Exposures in Air: 18 Hours at 450°F

Wavelength, microns	Spectral Reflectance, percent						
	Surveyor III Camera Sample A*		Laboratory Sample B**			Laboratory Sample C***	
	Before Thermal-Vacuum Exposure	After Thermal-Vacuum Exposure	Before Thermal-Vacuum Exposure	After Thermal-Vacuum Exposure	After Thermal Exposure in Air	Before Thermal-Vacuum Exposure	After Thermal Exposure in Air
0.295	12.0	9.0	20.0	20.0	28.0	22.0	30.0
0.355	22.0	14.5	37.0	34.0	56.0	44.0	56.0
0.400	33.0	18.0	50.0	43.5	71.5	52.0	71.0
0.430	38.0	22.0	55.0	47.0	75.0	58.0	76.0
0.458	41.0	25.0	56.0	49.5	77.0	62.5	77.0
0.484	45.5	26.0	56.0	53.0	78.0	64.0	76.5
0.511	47.0	28.0	63.0	56.0	78.0	66.0	77.0
0.540	51.0	31.0	65.0	58.0	80.0	69.0	78.0
0.569	53.0	32.0	66.0	60.0	80.0	70.0	77.5
0.598	55.0	35.0	68.0	62.5	80.5	70.0	79.0
0.630	56.0	36.0	70.0	65.0	81.0	75.0	79.5
0.664	58.0	40.0	74.0	65.0	81.0	75.0	79.0
0.700	62.0	40.0	77.0	67.0	82.0	78.0	80.0
0.738	62.0	42.0	78.5	70.0	82.0	78.0	81.5
0.781	62.0	43.0	80.0	70.0	82.0	78.0	82.0
0.828	65.0	47.0	80.0	73.0	82.0	78.0	82.0
0.880	66.0	50.0	80.0	75.0	81.0	79.0	82.0
0.940	67.0	53.5	82.0	75.0	81.0	80.0	82.0
1.011	69.0	56.5	81.5	78.0	81.0	80.0	81.0
1.096	70.0	59.5	83.0	81.0	81.5	80.0	80.5
1.200	70.0	60.0	82.5	80.0	81.0	79.5	80.0
1.341	70.0	66.0	83.0	80.0	81.0	77.5	78.0
1.536	73.0	67.5	80.0	78.0	80.0	76.5	78.0
1.854	67.0	63.0	72.0	76.0	77.5	70.0	76.0
2.600	55.0	55.5	52.5	72.0	70.0	56.0	66.0

*Surveyor sample 909 - tests in vacuum (5×10^{-5} Torr)
**Sample of Surveyor white inorganic paint exposed to ultraviolet at 5X for 65 hours in 1965 - tests in vacuum (5×10^{-5} Torr) and air.
**Samples of Surveyor white inorganic paint exposed to ultraviolet at 1X for 96 hours in 1965 - tests in air.

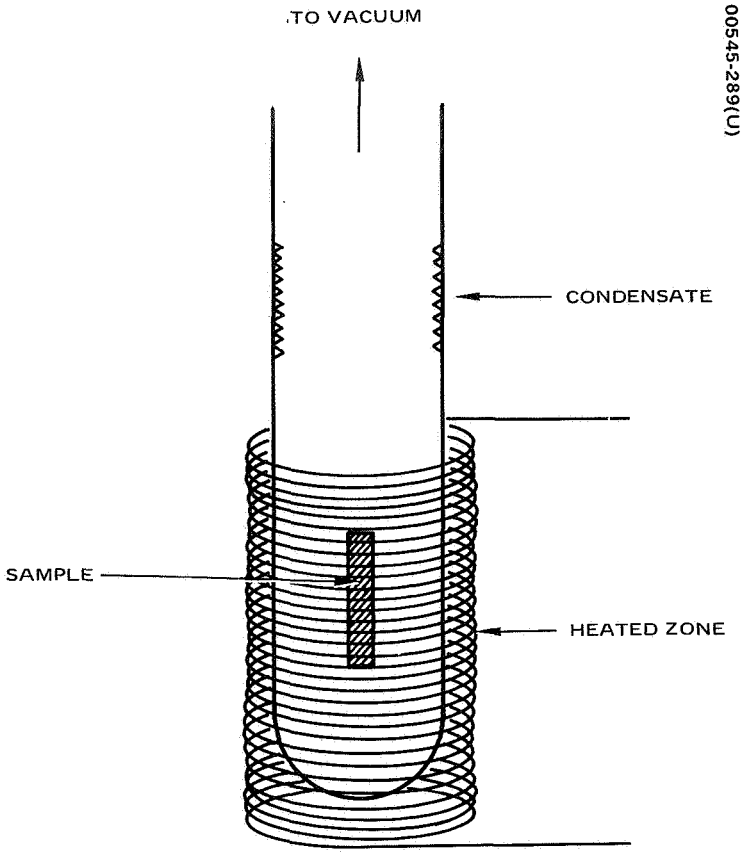

Figure J-26. Experimental Configuration for Thermal-Vacuum Exposure of Surveyor III Sample 909

The Surveyor III sample 909 outgassed a heavy but clear condensate during its thermal-vacuum exposure. This condensate appeared on the glass tube above the heated zone where the glass was at room temperature. The experimental configuration is shown in Figure J-26. No condensate was found on the glass tube where it had been heated. No condensate was found on the tube used to vacuum-thermal anneal the non-flight Surveyor inorganic white paint. The outgassing of sample 909 was due to the black organic paint. This paint has a history of high outgassing and is not used on current designs where outgassing limits are imposed.

A second, laboratory-tested sample of the Surveyor inorganic white paint was selected for similar testing. The sample was exposed for 18 hours at 450°F in air, not vacuum. Results of the spectral reflectance measurements before and after exposure are also shown in Table J-7. This sample was from the same paint lot as the vacuum-tested sample above. The only difference between the two was that this second sample had been exposed to ultraviolet at 1X for 96 hours. Temperature during exposure and storage conditions since 1965 are the same.

An additional test was then conducted on the sample of white paint previously exposed to ultraviolet in the laboratory and then thermally annealed in vacuum. The sample was placed in the air-thermal anneal test chamber and was exposed for 18 hours at 450°F. The spectral reflectance was remeasured, and results are shown in Table J-7.

J.5 MATHEMATICAL ANALYSIS OF LUNAR DUST CONTRIBUTION TO REFLECTANCE

Early in the evaluation, it was clearly established that physical separation of the lunar material from the paint surface without removal of at least a small amount of the degraded coating was impossible. Thus, it became necessary to achieve such separation analytically using measured spectral reflectance values and a knowledge of the Surveyor III orientation.

Energy reflected from the camera surfaces is affected by discoloration of the paint, possibly by discolored contaminants on the surface and by the amount of lunar dust present. In the first order of analysis (direct comparison of reflectance data), it is impossible to separate the effects of contaminants other than dust, degradation of the paint, and the effect of lunar dust. However, separation of dust effects can be accomplished with some degree of success by analyzing the near-infrared spectra. The reduction of the reflectance of the paint at 1.5 microns is due entirely to the lunar dust. The reflectance of the painted surfaces is affected in the visible portion of the spectrum by all the possible discoloration mechanisms: radiation damage to the paint, contaminants, and lunar dust.

This section summarizes results of the effort to derive an equation that could be used to separate the effect of the lunar dust on the reflectance spectrum of the paint. The resultant radiation damage reflectance spectrum could then be compared to the well-established characteristics of the ultraviolet damage in the paint. Any deviation from this curve may then be attributed to radiation damage in contaminants found on the paint surface.

There were several possible effects of a dust layer on the reflectance spectrum of the paint. Dust deposited during the Surveyor III landing would reduce the effect of solar ultraviolet radiation, partially shielding the paint. The dust would also interact with the actual measurement of reflectance in the following manner:

1) Partially absorb incident energy

2) Partially absorb energy reflected from paint surface

3) Back scatter incident energy

4) Forward scatter incident energy

5) Reduce by absorption incident energy transmitted through dust particles

Measured reflectance of bulk lunar fine samples from Apollo XI, reported in Reference 113, as well as examination of the Surveyor surfaces, indicated a non-gray behavior of the lunar dust (i.e., the effect was not the same at all wavelengths). The dust behaved as a broadband selective filter either by absorption or by scattering, with the greatest effect at the short wavelengths.

The following expression could be derived by considering the energy balance of monochromatic illumination on the contaminated, degraded surface, and the mechanism of light interaction with the surface, discussed above:

$$I_m = I_o \rho_d K_i A_d + I_o \rho_p \left[(1-K_2 A_d)(1-K_3 A_d) \right]$$

or

$$\rho_m = \rho_d K_i A_d + \rho_p (1-K_2 A_d)\,(1-K_3 A_d) \qquad (1)$$

I_m = measured radiant flux (reflected from surface)

I_o = radiant flux incident on surface

ρ_m = (reflectance) = $\frac{I_m}{I_o}$

ρ_d = reflectance of lunar dust

ρ_p = reflectance of paint surface

A_d = fraction of surface area covered by dust

K_i, K_2, K_3 = constants

Note that ρ_p is the reflectance of the paint, including degradation due to radiation and possible contaminants. K_2 and K_3 are unknown spectral constants associated with transmission, forward scattering, and geometry of the dust for the incident and leaving beam. (K_1 is discussed below.) It was not practical within the scope of this program to determine the various parameters which are part of K_2 and K_3. It was similarly impossible to directly measure the dust area on the painted surface. Since K_2 and K_3 are related and approximately equal, it is possible to rewrite Equation 1 as follows:

$$\rho_m = \rho_d K_1 A_d + \rho_p (1-K_4 A_d)^2 \qquad (2)$$

where K_4 is an effective average for the incident and reflected beam and K_4A_d can be determined experimentally.

Further defining a term D as the ratio of the reflectance of the degraded paint (ρ_p) to the initial reflectance of the paint (ρ_o), Equation 2 becomes:

$$\rho_m = \rho_d K_1 A_d + \rho_o D(1-K_4A_d)^2 \qquad (3)$$

The quantity D includes both the radiation damage and the effects of contaminants other than lunar dust. The term $\rho_d K_1 A_d$ in Equations 1 through 3, the back reflection from the first surface of the dust, is the product of three factors: reflectance of the dust, a proportionality constant, and an effective area of the dust. The reflectance of the dust ranged between 0.04 and 0.10. The proportionality constant for the back reflection is related to the particle shape and was less than 1.0. The effective area of the dust, expressed as a fraction of surface coverage, was on the order of 0.05 to 0.30 for the returned Surveyor surfaces. The first term $\rho_d K_1 A_d$ above was small compared to the other quantities. In view of the uncertainties associated with the analysis, the errors introduced by disregarding it were negligible. Although inclusion of this term would be possible, it was neglected in the analysis. Equation 3 now becomes:

$$\rho_m = \rho_o D(1-K_4A_d)^2 \qquad (4)$$

Laboratory data on the damage to the Surveyor coatings by ultraviolet radiation and solar wind protons indicated a yellow or brown degradation, with the primary effect in the short wavelengths and little or no effect in the near-infrared. Assumption that this condition existed on the surfaces returned from the moon permitted the determination of the effective dust area (K_4A_d) in the longer wavelengths. Using the spectral character of the dust, as derived from the data shown in Figure J-27, the effect of the dust could be determined over the entire wavelength range measured.

The radiation effects on the reflectance of the paint measured in laboratory were primarily seen at the shorter wavelengths, less than 1.0 micron. The paint reflectance in the near-infrared (1.0 to 2.5 microns) was a function of thickness and possibly of surface finish and porosity. It was also a function of the amount of chemically absorbed water, as shown in Section J.4.5. In view of the above discussion, it was necessary to use some judgment in the selection of wavelengths at which the effective area was determined.

Figure J-27 shows the results of measurements by D. Nash (JPL), discussed in Reference 114, using Apollo XI fines on control samples of Surveyor coatings. The curves are plotted as a ratio of reflectance of surfaces covered with lunar dust, ρ_m, to reflectance of clean surfaces, ρ_0. From

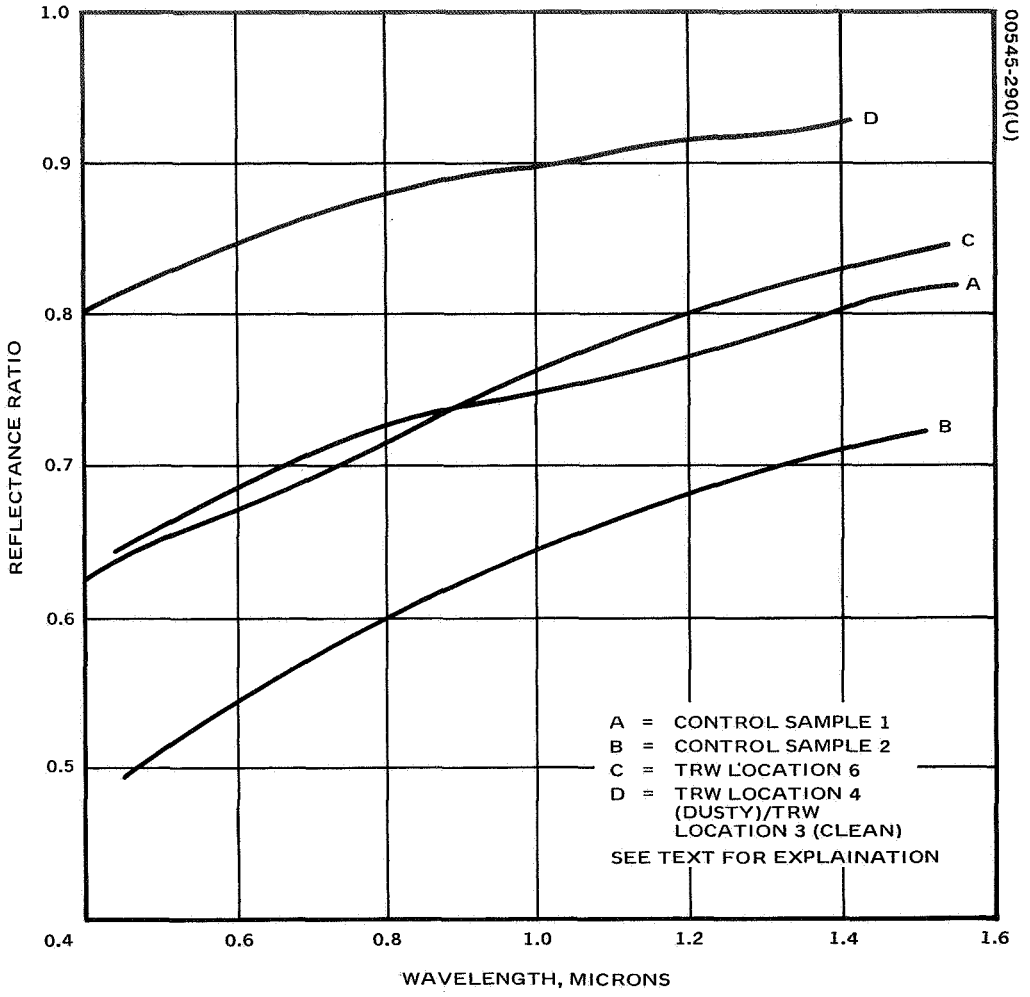

Figure J-27. Ratio of Reflectance of Painted Surfaces Covered With Lunar Dust to the Reflectance of Clean Surfaces (White Inorganic Paint)

this ratio ρ_m/ρ_0, the factor K_4A_d can be computed as a function of wavelength using Equation 4 since there was no degradation (D=1).

Also shown for comparison are results of measurements of samples from Surveyor III surfaces. The ratio ρ_m/ρ_0 is plotted for the sample from TRW position 6,* using the clean undegraded reflectance of TRW position 1 under the connector bracket as ρ_0. Position 6 showed very little or no radiation effect; the discoloration was clearly due to dust. The difference between control sample 1 (curve A in Figure J-27) and TRW sample 6 (curve C) in the near-infrared was probably due to the differences in the reflectance of the paint, discussed above.

In addition $\rho_m/(\rho_0 D)$ for position 4, using $(\rho_0 D)$ from position 3, showed similar agreement on the effects of dust. Positions 3 and 4 were both on the southeast side of the camera and would be expected to have the same degradation; position 3 appeared to be free of dust, as indicated by no decrease in reflectance in the near infrared.

*Shown in Figure J-9.

APPENDIX K. SUPPLEMENTARY DATA ON FAILURE ANALYSES

This appendix contains a supplementary discussion of the analyses conducted on 4 of the 20 anomalies discussed in Section 12: suspected cold welding of a connector, anomalous operation of the filter wheel potentiometer, failure of the shutter drive transistor and damage to the shutter coil, and cracked conformal coatings and glass envelopes of some electrical components. Detailed failure reports on these and other failure analyses conducted are available in program files.

K.1 ANALYSIS OF SUSPECTED COLD WELD OF CONNECTOR J2 SHELL TO SHROUD

K.1.1 Description of Materials

The connector shell was identified as Microdot B43AH10P(017), and was manufactured from 2017-T4 aluminum alloy, per Federal Specification QQ-A-250/11. It was chemically coated per MIL-C-5541 with iridite to a thickness on the order of 0.1 mil. The nominal dimensions were 0.814 inch in diameter and 0.796 inch across the flat area, with no tolerances specified.

The lower shroud was made from 6061-T4 aluminum alloy, 0.031 inch thick, per Federal Specification QQ-A-2255. It was also chemically coated with iridite, and the external surfaces were painted with a white inorganic paint.

The hole for the J2 connector was specified as 0.812 to 0.816 inch in diameter, with a flat area on one side, 0.794 to 0.798 inch, to accommodate the flat of the connector shell.

K.1.2 Microscopic Examination of Connector Shell

In its installed configuration, the connector was wedged against the edge of the hole in the shroud and the nut which was threaded onto the connector shell to hold it rigidly in place was loose. Measurement of the hole in the shroud and the connector shoulder showed a distance of 0.02 inch between the parts.

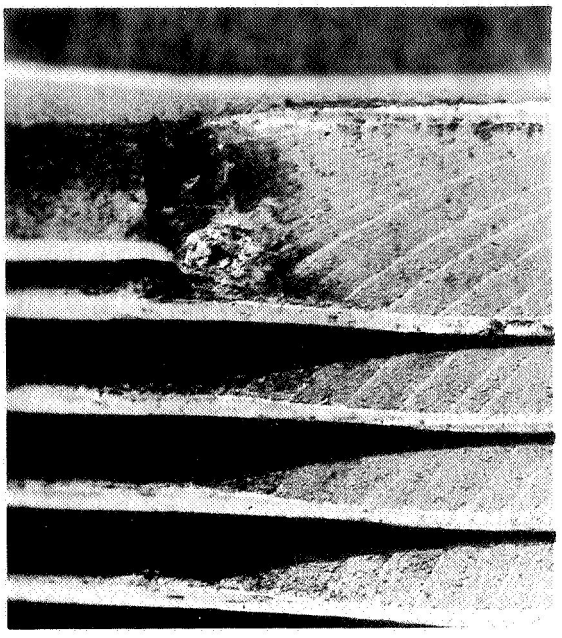

Figure K-1. J2 Connector Thread Area, Showing Metal Blob (13X Magnification) (Photo 00545-217)

Figure K-2. SEM Photograph of Metal Blob of Figure K-1 (230X Magnification) (Photo 00545-218)

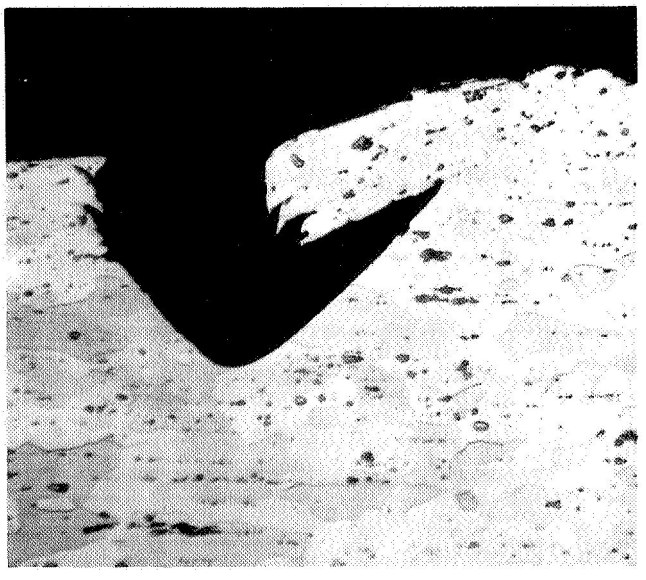

Figure K-3. Transverse Cross Section of Metal Blob Shown in Figure K-2 – Dark Area Corresponds to a Thread (100X Magnification) (Photo 00545-219)

The surface of the connector shell was examined with a binocular microscope at magnifications up to 40X and by a scanning electron microscope (SEM). Corresponding mating surface of the shroud was also examined, as discussed in Section K. 1. 5.

The principal area suspected of cold welding was determined by a visual examination to be in the thread runout area nearest the flange, on the left side of the flat. It was observed that the groove at the end of the thread had been filled with metal (aluminum) in the form of a blob. This is seen in Figure K-1. One of the SEM photographs taken of this area is shown in Figure K-2. A transverse cross section of this metal blob is shown in the SEM photograph of Figure K-3 (see Section K. 1. 4). The deformation of the metal can be clearly seen in these figures.

Figure K-2 also shows a metallic particle about 0. 001 inch thick which had been partially dislodged. This particle is on a plane above the observed scoring marks. It was probably made during disassembly, which suggests that it may have moved from the site of the score marks to its present position. It could not be conclusively stated from the examination of Figure K-2 and other SEM photographs taken whether the appearance of this area was indicative of former cold welding or simply the result of metal abrasion in disassembly.

K. 1. 3 Microprobe Examination

To determine the chemical composition of the metal blob on the connector thread, a microprobe analysis was conducted of the surface of the blob and its adjacent areas. Microprobe photographs (Figure K-4) show the characteristic emission for copper and manganese. Microprobe photographs for chromium were also taken.* The dark areas in Figure K-4 indicate a lesser concentration of the element under analysis.

It should be noted that the aluminum 2017, of which the connector shell was made, and aluminum 6061 used on the shroud differed significantly from each other in the contents of these elements, as indicated in Table K-1. This difference was used in interpreting the microprobe photographs.

Results of this analysis indicated that the material of the blob on the connector shell was, indeed, the aluminum from the connector itself. Little if any transfer of metal from the shroud had occurred. This suggested that the blob was formed in the course of the mechanical motion, either during installation or in subsequent vibration. Such a mechanical motion would rub off the protective iridite coating, setting the stage for possible cold welding of the adjacent areas.

*The sensitivity of chromium microprobe analysis was poor.

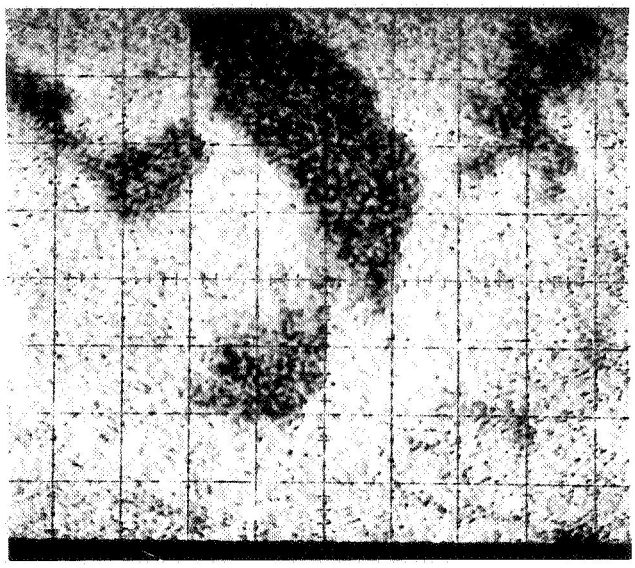

a) Copper Emission (Photo 00545-220)

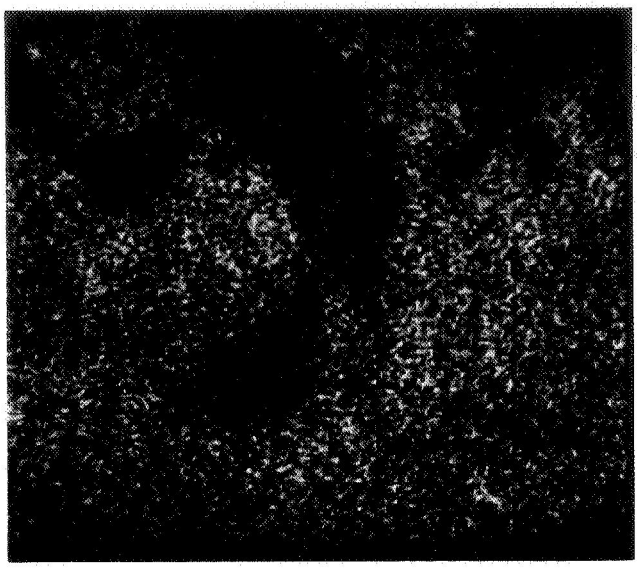

b) Manganese Emission (Photo 00545-221)

Figure K-4. Microprobe Scan of Area Adjacent to Metal Blob of Figure K-2 (200X Magnification)

TABLE K-1. RELATIVE CONTENTS OF COPPER, MANGANESE, AND CHROMIUM IN CONNECTOR AND SHROUD

Element	Percent Content	
	Shroud (6061 Aluminum)	Connector (2017 Aluminum)
Copper	0.15 to 0.40	3.5 to 4.5
Manganese	0.15 maximum	0.4 to 1.0
Chromium	0.15 to 0.35	0.10 maximum

On the other hand, examination of the surfaces adjacent to the blob indicated a definite transfer of metal from the shroud to the connector, as evident in Figure K-4. Microprobe scans of additional areas further away from the suspect region did not indicate any metal transfer.

The absence of metal transfer to the blob on the last thread of the connector also tended to dispel the theory that the shroud was wedged into the connector. Rather, it appeared that the faulty installation and the loose retaining nut had resulted in the shroud bearing on the last thread of the connector shell. The high unit loading in handling, in launch vibration, or in subsequent operations caused a deformation of aluminum from the connector shell itself onto the thread. This may have been aggravated by the burr on the shell, noted in Figure K-2.

K.1.4 Metallographic Examination

Attempts were made to conduct a metallographic examination of the suspect area. The result of the metallographic examination of the cross section of the metal blob taken transverse to the thread is shown in Figure K-3. No evidence of shroud metal adhering to the connector was visible on this one plane, confirming the previously noted results of microprobe analysis. The metal that partially filled the thread appeared to have resulted from the deformation of the shell itself.

The more significant metallographic examination of the surface itself to search for a definitive evidence of cold welding was, however, unsuccessful. Such an examination would show the grain structure of the surface and might have indicated the typical metal transfer/diffusion pattern characteristic of cold welded surfaces. The process of attempting to obtain such a cross section entails successive polishing of the surface. Unfortunately, in this process of polishing, the area of interest was polished through and thus inadvertently destroyed before this examination could be made.

K.1.5 Microscopic Examination of Shroud Contact Area

A visual and a microscopic examination were then conducted of a section of the shroud which had been in contact with the connector. This section was cut from the shroud for this purpose. It became immediately apparent that the edge of the shroud, as shown in Figure K-5, was unduly rough. This evidence corroborated the postulate of excessive wear caused by handling or by vibration of the loose connector.

Additional SEM photographs of this region, not included here, revealed many score marks running both longitudinally and transverse to the axis of the connector. The scoring appeared to have taken place in several steps. A ridge was observed in the center, suggesting that the scoring was caused by the flexing of the connector shell in the shroud.

SEM photographs were then taken of the edge surface of the hole in the shroud, directly above the suspected cold welded spot on the connector shell and of the adjacent areas. Three of the SEM photographs taken are presented in Figure K-6. Figure K-6a shows the appearance of the suspected cold welded area; the appearance is typical of such a cold welded region after the materials have been torn apart. The picture is indicative of strong forces which held the surfaces in question together before they were separated in disassembly. This is clearly seen by comparing Figure K-6a with Figure K-7, which shows the appearance of a typical cold welded surface of an aluminum specimen in the laboratory after cold welding and subsequent forced separation.

Figures K-6b and c are SEM photographs of areas on the inner edge of the shroud adjacent to the suspected cold welded spot. The typical pattern generated by the tearing apart of a cold welded region is absent in both of these photographs. Figure K-6b, however, which is closer to the cold weld

Figure K-5. Edge of Shroud in Contact With J2 Connector Wheel (22X Magnification) (Photo 00545-222)

spot, shows some evidence of rupture without abrasion. Figure K-6c of the area further away exhibits a definite indication of abrasion such as would result from twisting and pulling of the shell from the shroud, with score marks running in many directions.

K. 2 DISCUSSION OF TESTS OF FILTER WHEEL POTENTIOMETER

Some of the tests conducted as part of the failure analysis of the filter wheel potentiometer are discussed here in support of the failure analysis summary presented in Section 12. 4.

K. 2. 1 Measurement of Forces Required to Break Off Guide

A control test was performed to break the guide off the block of the Surveyor III focal length potentiometer to obtain comparison data for the assessment of the forces entailed in the breaking off of the filter wheel guide. The block was placed in a vise, and a 2. 5 inch diameter piston was used to shear load the guide with the application of a strain rate of 0. 05 in/min.

The focal length potentiometer guide failed at a load of 8. 0 pounds, with the failure occurring over approximately 80 percent of the load surface. The calculated shear strength was 2700 psi. The specified flexural strength of the FS-80 DAP material was 16, 000 psi. The 2700 psi which caused the failure of the focal length potentiometer thus suggested that the DAP material was basically defective.

Calculations of the forces present during the operation of the filter wheel potentiometer indicated that the maximum force was 5 pounds. This corresponds to 0. 25 in-lb of torque applied at the outside edge 0. 005 inch

a) Suspect Cold Weld Area (570X Magnification) (Photo 00545-223)

b) Area Adjacent to Suspect Cold Weld (560X Magnification) (Photo 00545-224)

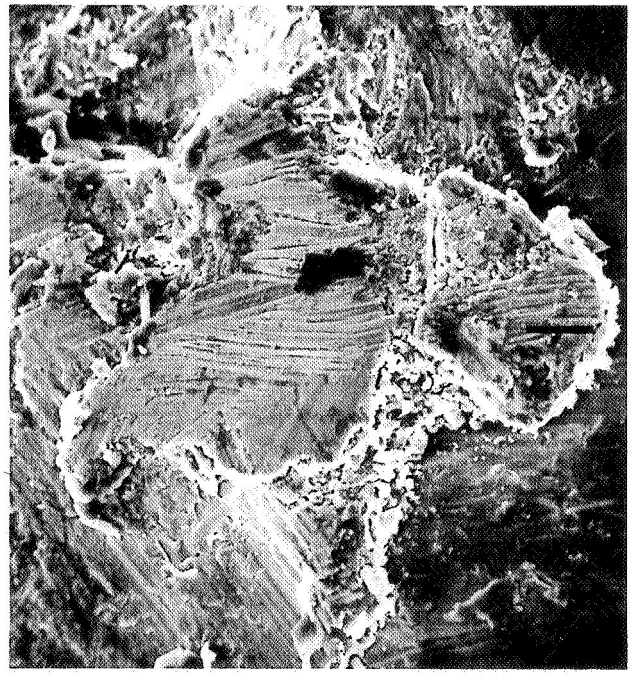

c) Another Area Adjacent to Suspect Cold Weld (314X Magnification) (Photo 00545-225)

Figure K-6. SEM Photographs of Edge Surface of Hole in Shroud

Figure K-7. Typical Cold Welded Area of 2014 Aluminum Specimen After Separation (1400X Magnification) (Photo 00545-226)

away from the block. Thus, the experienced force was still about 50 percent lower than the above measured force of 8 pounds, which resulted in the failure of the focal length block. Even with its defective DAP material, the guide of the filter wheel potentiometer should have been able to withstand the operational loads unless other factors were present (e. g., cracks, extraneous forces, or cold welding).

K. 2. 2 SEM Examination of Surfaces

An SEM examination was then conducted of the surfaces of the two guide blocks in areas directly under the severed guides of the filter wheel and focal length potentiometers, as well as of other areas of the blocks and guides. This examination was performed to help evaluate the suspected defective DAP materials used and to assess the filter wheel block for the presence of irregularities. Samples of a good FS-80 DAP material were also examined.

Results of the examination of the two blocks in the areas directly under the broken off guides are shown in Figures K-8a through d. The filter wheel potentiometer block area under the broken off guide is shown in Figure K-8a. An enlarged view of a portion of this surface is shown in Figure K-8b. Figures K-8c and d are the corresponding SEM pictures of the focal length block.

The difference in the texture of the two surfaces was apparent by a comparison of Figure K-8a with Figure K-8c and especially by a comparison of the enlarged SEM photographs, Figure K-8b versus K-8d. The surface of the filter wheel block revealed many incipient cracks and had a generally defective appearance. It is seen that the failure observed on both blocks is noncrystalline. The fibers failed in an adhesive mode, indicating the absence of a bond between the fibers and the matrix. However, the photograph of the focal length block (Figure K-8d) does not show the evidence of microcracking of the surface, which is noticeable on the surface of the filter wheel block on Figure K-8b. It appeared that a fault may have existed in these areas of extensive microcracking. When subjected to a slightly abnormal load, such a fault would propagate to other areas, resulting in a failure of the guide.

SEM photographs of other portions of the filter wheel DAP block which appeared nominal were then compared with photographs taken of a sample of the FS-80 DAP material from the manufacturer. Figure K-9 compares the results obtained. The significant observation was that the fiber concentration was much greater in the FS-80 sample in Figure K-9b than in the filter wheel sample in Figure K-9a. Furthermore, the fibers of the FS-80 sample were considerably longer. The glass fibers in the filter wheel sample appeared to be poorly bonded in the diallyl phthalate.

SEM analysis thus revealed that the material used on the Surveyor III potentiometers was not a properly manufactured FS-80 DAP. The analysis further revealed a distinct degradation of the microstructure in the cracked areas of the filter wheel block compared with that of the focal length block after its guide was intentionally severed.

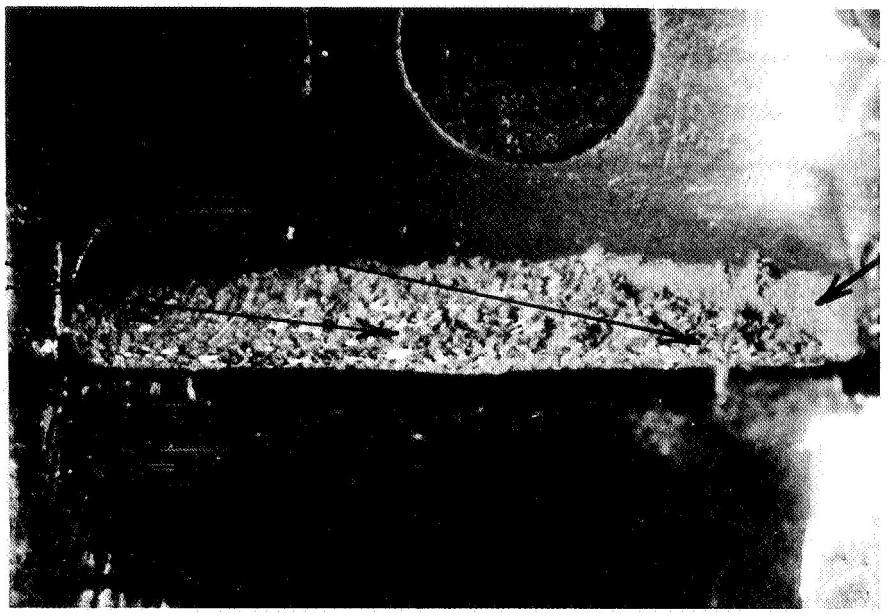

a) Surface of Failed Filter Wheel Block (Photo 00545-227)

b) Portion of Surface Shown in Figure K-8a (10,000X Magnification) (Photo 00545-228)

Figure K-8. Surfaces of Potentiometer Blocks Under Broken Off Guides

c) Surface of Control Focal Length Potentiometer Block (Photo 00545-229)

d) Portion of Surface Shown in Figure K-8c (10,000X Magnification) (Photo 00545-230)

Figure K-8 (continued). Surfaces of Potentiometer Blocks Under Broken Off Guides

a) Surface of Filter Wheel Potentiometer Block (1000X Magnification of Defective Glass Fiber Structure) (Photo 00545-231)

b) Sample of FS-80 DAP From Manufacturer (1000X Magnification of Filled Glass Fiber Structure) (Photo 00545-232)

Figure K-9. SEM Comparison of DAP Materials

K.3 SUPPLEMENTARY DISCUSSION OF FAILURE ANALYSIS OF SHUTTER COIL AND TRANSISTOR

This section of the appendix contains supplementary data in support of the discussion in Section 12.5 on the tests conducted on the failed parts and on the failure mode investigation performed.

K.3.1 Tests of Shutter Drive Transistor, Q-5

A detailed failure analysis was conducted of shutter drive transistor Q-5, similar to Fairchild type 2N3891. This analysis included visual examination, electrical tests, X-ray analysis, seal test, internal microscopic examination, and metallurgical sectioning.

Following the visual inspection, preliminary electrical tests revealed a short between the collector and the base and an open condition between the collector and the emitter, confirming previous findings on the

chassis. Results of the seal test were nominal. The package leak rate was 4×10^{-8} atm cc/sec, compared to the specified maximum of 5.0×10^{-7} atm cc/sec.

Internal microscopic examination revealed that the emitter had melted open, and that the metallization around the emitter had melted (Figure K-10).

Further analysis of the failed region was conducted to determine whether the failure was associated with an overcurrent condition caused by a voltage breakdown mechanism. As part of this analysis, it was also of interest to determine, if possible, whether a postulated prior stress, coupled with exposure to lunar thermal cycling, could have lowered the breakdown voltage to the point where a voltage puncture would occur upon the application of a normal voltage of the device.

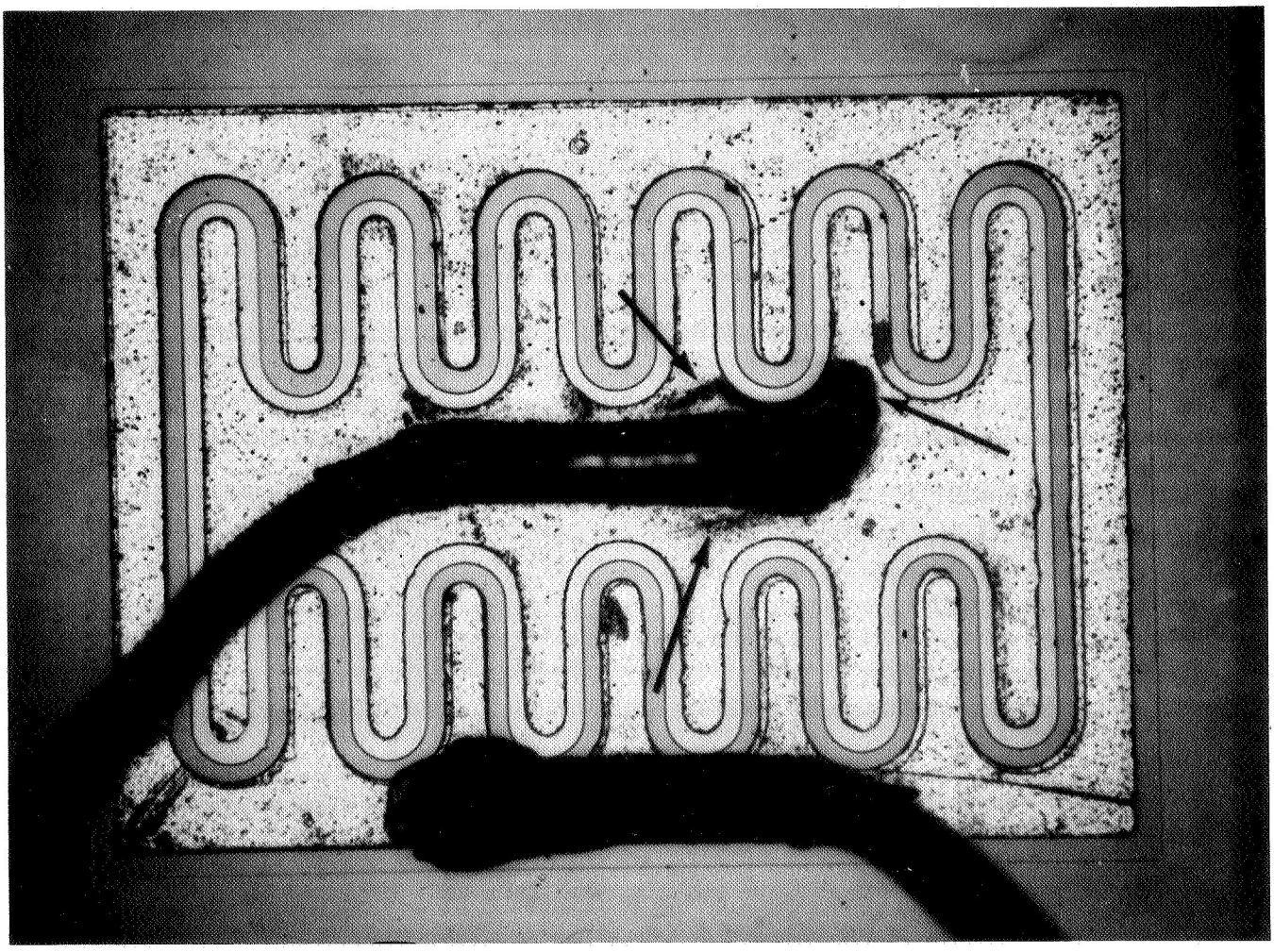

Figure K-10. Chip of Shutter Coil Drive Transistor Q5 Showing Melted Metallization Under Emitter Bond (44X Magnification) (Photo 00545-233)

The transistor was microsectioned, and the junction was examined microscopically. Results of this analysis are shown in Figure K-11. The numerals in Figure K-11b indicate the following significant areas: 1) emitter lead, 2) emitter metallization, 3) emitter diffusion, 4) base diffusion, 5) collector region, 6) "punched through" eutectic, and 7) die bonding eutectic. The appearance of the metallization on the chip was not consistent with that caused by an overcurrent condition. Such a condition would cause a more uniform melting rather than the localized observed evidence of a voltage punch-through. No evidence of rediffusion was seen which would indicate excessive junction current prior to breakdown. The analysis definitely established the voltage punch-through as the initial mechanism of failure.

No evidence was uncovered to conclude that lunar thermal cycling had in any way contributed to the failure. Additional tests considered, which might have shed further light on the condition of the transistor, included sectioning past the failure and etching the exposed silicon. These tests might have determined the breakdown voltage of the remainder of the device. However, it was decided not to conduct these tests within the scope of the program, primarily because of the likelihood that these sectioning processes would destroy the evidence: the edge lattice structure of the crystal would probably be disturbed and exposed surfaces contaminated.

K.3.2 Tests of Burned Shutter Solenoid Coil

Reported here are the results of the visual, electrical, and diagnostic examination of the failed solenoid coil, previously shown in Figure 12-9 in Section 12.5.4. Visual examination indicated extensive burning of the insulation, such as would result from excessive heat. This is apparent in Figure K-12.

Electrical tests consisted of the measurement of coil resistances, voltage breakdown, proper sequencing of the motion of the blades, and detent breakaway voltage and current.

Measurement of coil resistances, summarized in Section 5.5 on Table 5-3, indicated nominal values for the windings of solenoid B but degraded readings for the two windings of solenoid A: 24 ohms for coil A1 and 0.2 ohm for coil A2, versus 33 ohms nominal. Results of the voltage breakdown test with 500 volts dc applied between each terminal and the base plate were nominal.

With coil A2 obviously shorted, the sequence of shutter operation for the remaining coils was examined by applying 20 volts dc to each of the three remaining windings. Normal operation of the shutters was observed. Manual movement of blade A had to be made in the performance of this test in lieu of electrical actuation by the A2 winding.

Detent breakaway voltage and current were measured on the three windings other than A2. The solenoid coil A with the shorted winding was then physically replaced by coil B. Test results are summarized in Table K-2.

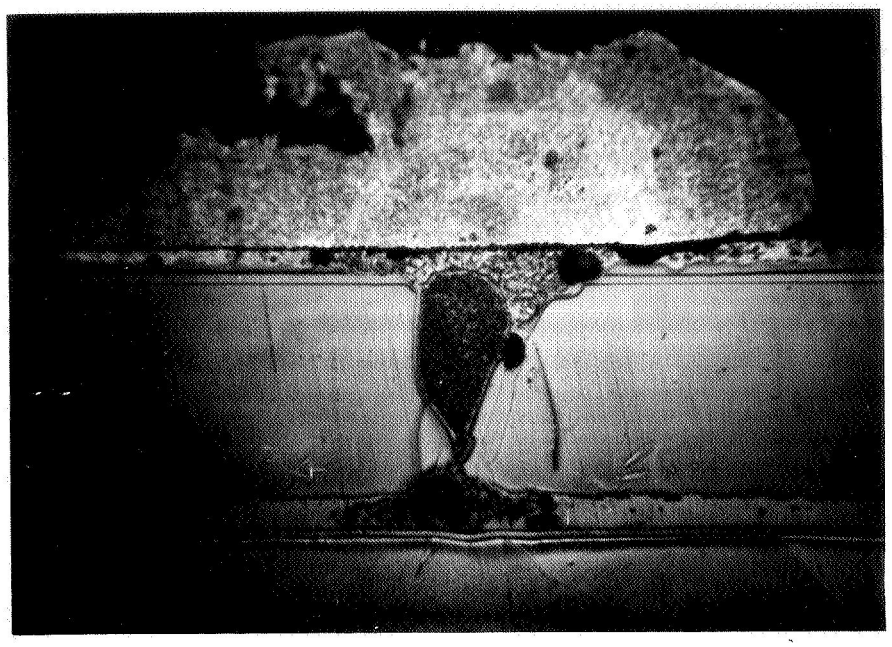

a) 250X Magnification (Photo 00545-234)

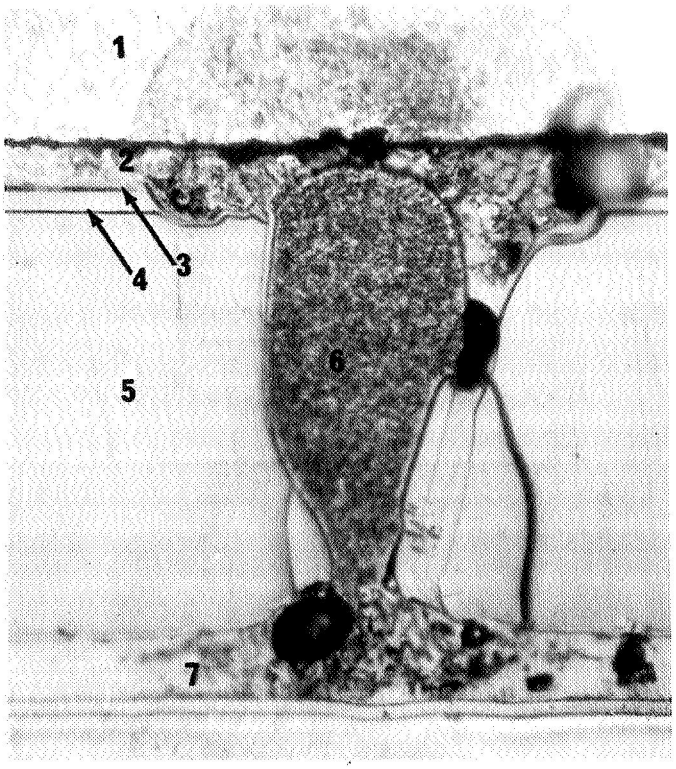

b) Section Through Center (600X Magnification)
(Photo 00545-235)

Figure K-11. "Punch Through" Region of Shutter Drive Transistor Q5

The results of this test indicated that the mechanical operation of the shutter was still acceptable if proper electromagnetic excitation was provided. However, the current readings indicated that a somewhat higher force was now required than that corresponding to the original current specification of from 190 to 230 ma. This result confirmed previous findings reported in Section 5.5. This separate anomaly (item 17 in Table 12-1) is discussed in Section 12.9.

TABLE K-2. RESULTS OF DETENT BREAKAWAY VOLTAGE AND CURRENT MEASUREMENTS OF SHUTTER ASSEMBLY

Configuration	Coil	Detent Breakaway Voltage, volts	Current, ma
Original	B1	10.77	2.86
	B2	11.50	3.06
	A1	7.70	2.39
Solenoid B in place of solenoid A	B1	8.58	2.48
	B2	7.82	2.24

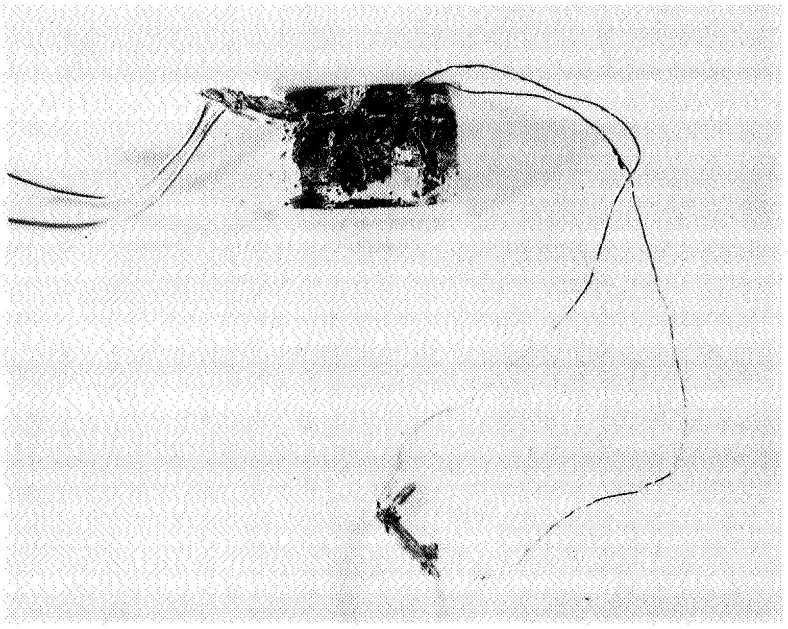

Figure K-12. Solenoid Coil Showing Effects of Excessive Heat (Photo 00545-236)

Figure K-13. Shorted Wires of Figure K-12 (50X Magnification) (Photo 00545-237)

X-ray analysis did not disclose any significant data. The device was then dissected. Diagnostic examination confirmed the melting of the insulation caused by overheating and revealed the presence of several shorts. These shorts were observed in the vicinity of turns 2, 75, and 167. A magnified view of the short on turn 75 is shown in Figure K-13, where the melted insulation and base wires are clearly visible.

The power ratings of the solenoid coils were not shown. It was estimated that the coils would certainly not be able to sustain more than 200 ma for an appreciable length of time. In normal operation, the current through the coil was in the order of 0.7 ampere for a time period not exceeding 200 ms, corresponding to the maximum duration of the activation signals. If the damage to the insulation resulted from a prolonged duration of this current in the order of 0.7 ampere, it was estimated that the length of time required to produce the observed damage would be in the order of 10 or more seconds.

K.3.3 Assessment of Drive Circuit of Failed Transistor Q5

The following discussion summarizes the results of the analysis conducted in support of the discussion presented in Section 12.5.5 to determine whether an inadvertent prolonged activation of transistor Q5 may have taken place. Such an anomaly may have been caused either by the application of a prolonged triggering signal (not confirmed by operational records) or by a fault in the drive circuit coupled with other hypothetical signals and failures in the Surveyor spacecraft.

Fortunately, the whole spectrum of possibilities did not have to be analyzed in detail. Regardless of the cause of such an activation of transistor Q5, its drive circuit would have had to remain conductive for a length of time corresponding to that required to damage the solenoid coil, i.e., on the order of a second. Since the chassis containing the circuit was retrieved, the examination of the components on the chassis would conclusively determine whether or not such conditions had prevailed.

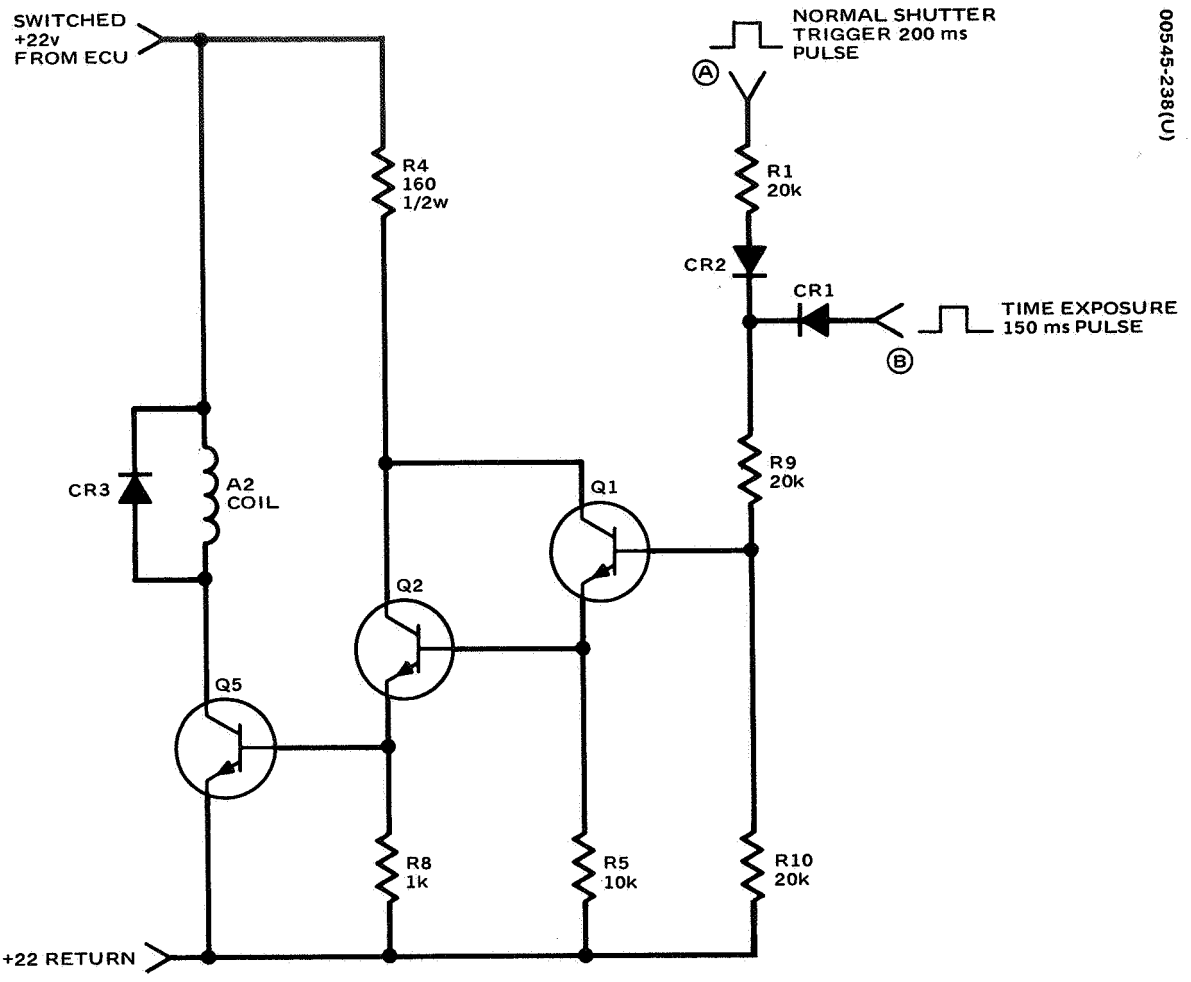

Figure K-14. Drive Circuit of Shutter Solenoid A2

Figure K-14 shows the schematic of the drive circuit on coil A2 and of transistor Q5 shown on Figure 12-6. Under normal circuit operation, there are two paths for energizing the shutter drive transistor Q5. The first is to send a START FRAME command which causes a 200 ms pulse to appear at point A. This causes the cascade drive circuit of Q1, Q2, and Q5 to conduct for the 200 ms period, which drives the shutter A2 blade to the open position. The second is to send a SHUTTER OPEN command which causes a 150 ms pulse to appear at point B. This causes the cascade drive circuit Q1, Q2, and Q5 to conduct for the 150 ms period, which drives the shutter A2 blade to the open position. In both cases, turnon of transistor Q5 completes the ground path for the A2 solenoid coil connected to the +22 volt source.

A detailed analysis was conducted of the two pulse circuits and of the cascaded drive circuit shown. The circuits were tested both under ambient conditions and at elevated temperatures. A complete analysis of possible suspect components was also conducted in the Hughes Components and Materials Laboratories.

No evidence of failure, other than that of the Q5 transistor, was found in either of the two pulse circuits. Excessive duration currents would have overstressed the 160 ohm, 0.5 watt resistor R4 in the collector circuit of the Q2 transistor. In normal operation, this resistor dissipates somewhere between 1-1/2 and 4 watts peak (depending on the line voltage) during the period of circuit activation. The 0.042 duty cycle of this dissipation is well within design margins. However, resistor R4 could not dissipate such a power for any significant length of time without evidencing degradation, overstress, or most likely, total failure. No degradation or even discoloration of resistor R4 was noted, and its resistance measured 159 ohms. Similarly, no other components showed any sign of overstress or degradation. This analysis proved conclusively that the failure of transistor Q5 was not caused by any anomaly that might have been attributable to its drive circuits.

K.3.4 Assessment of ECU Circuits

Two of the possible modes of inadvertent appearance of voltage across the solenoid coil entailed failure of one or more components of the electronic conversion unit (ECU) of the TV camera. These two modes, A and D in Figure 12-10, were discussed in Section 12.5.5. Results of the study of the ECU circuits, conducted in support of the discussion presented in that section, are summarized below.

The circuit diagram of the command and power control circuits of the ECU is shown in Figure K-15. The OTC ON signal applies +29 volts to TB1-11 of the ECU. A dc-to-dc converter in the ECU converts this +29 volt input into a 5 kHz square wave which is applied to the primary of transformer T1. The heart of the converter is a transformer coupled transistor oscillator consisting of transistor Q2 and Q3. The transistor oscillator will not go into oscillation unless it is triggered. The trigger is a 20 ms positive POWER ON command which is applied to TB1-2 of the ECU, where it is coupled through a 7 volt zener diode, CR23, and is applied to the base of transistor switch Q9. The applied pulse closes the transistor switch, allowing +29 volts to be applied to the bases of Q2 and Q3 through R17, the transistor switch, and the secondary winding of transformer T1, which triggers the circuit into oscillation. Once this occurs, a voltage is induced in the secondary windings of transformer T1.

The voltage induced in the secondary winding between terminals 22 and 24 is converted into a negative dc voltage by a full-wave rectifier consisting of CR11 and CR12. The voltage is applied to the base of transistor switch Q4, turning the switch on. When Q4 is turned on, it completes the ground path for base current flow for oscillator transistors Q2 and Q3. The oscillator continues to oscillate until the path through switch Q4 is opened.

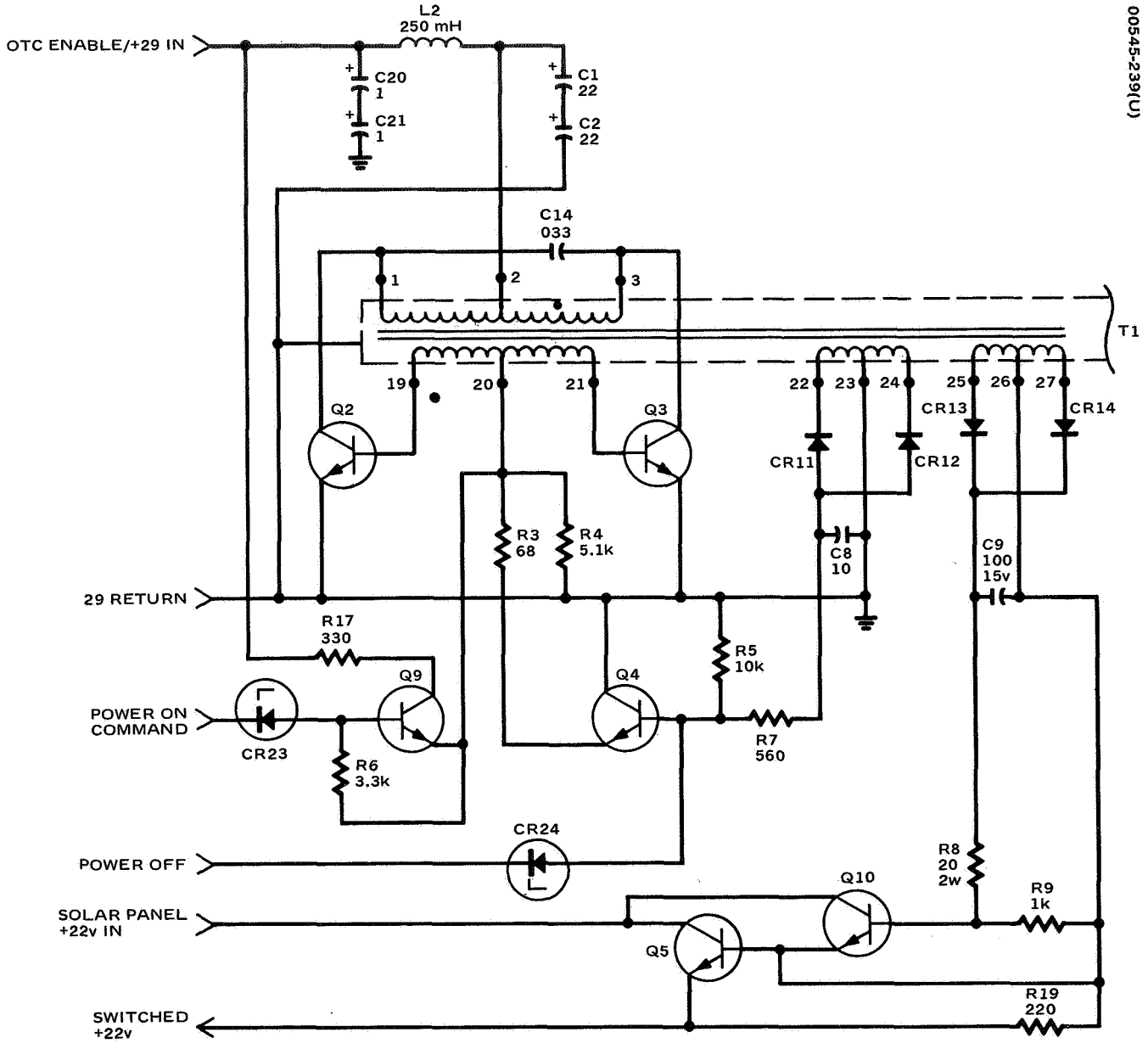

Figure K-15. Command and Power Control Circuit of ECU

This is accomplished when a POWER OFF command is applied at pin 1 of the ECU, which is then routed through a 7 volt zener CR-24 to the base of Q4. The positive pulse at the base of Q4 causes the switch to turn off, thereby interrupting the base current flow through Q2 and Q3, causing the oscillator circuit to turn off. When a POWER ON command is received, the converter circuit in the ECU produces a 3.2 volt output that is utilized to forward bias the 22 volt switching transistor Q5, causing the Q5 transistor to turn on.

A complete examination was conducted on the components of the ECU, which might be associated with the two postulated modes of failure. In particular, the ECU transistor Q5 was tested in detail since its degradation would be a necessary consequence of such a failure. No component anomalies were uncovered which could explain such postulated failure modes. The collector-to-base breakdown voltage of ECU transistor Q5 was nominal at 80 volts dc. Its leakage current was 75 microamperes.

It was concluded that the only way in which a voltage could be applied to the shutter coil was by a command to turn the ECU on or by other nondestructive techniques if applicable. The only other such nondestructive possibility (path A in Figure 12-10) had been determined to be incompatible with the capability of the solar panel, as discussed in Section 12.5.5.

K.4 SUMMARY OF FAILURE ANALYSIS OF TWO FAULTY DIODES

The results of the failure analysis conducted on the two diodes which exhibited electrical anomalies are presented here in support of the discussion in Section 12.7.

K.4.1 Open Diode

One Fairchild type IN3070 high speed switching diode on chassis A3 was found electrically open in the returned camera; its DO-7 glass case envelope was found cracked. A failure analysis was conducted to determine the nature of this anomaly. The tests conducted included a visual and microscopic examination, electrical tests, and dissection and internal microscopic examination.

Visual examination revealed, in addition to the cracked glass case, numerous cracks in the conformal coating applied over the case. Manipulation of the diode leads caused movement of the diode body around the crack in the glass.

Initial electrical tests confirmed that the diode was open. However, it was found that manipulation of the leads could readily restore the internal contact. In this restored condition, electrical tests could then be performed. Results indicated that all functional parameters were nominal, as summarized in Table K-3.

Internal microscopic examination revealed that the intermittance found was associated with the contact between the whisker spring and the gold ball on the die. This is shown in Figure K-16. Moving the unsoldered lead caused the gold ball contact to shift relative to the chip. This movement was made possible by the crack in the glass envelope.

K.4.2 High Leakage Diode

One Raytheon type IN3730 high conductance switching diode on chassis A5 was found to exhibit a very high reverse leakage current during the initial functional chassis tests of the returned camera. A failure

TABLE K-3. MEASURED ELECTRICAL CHARACTERISTICS OF OPEN DIODE WITH CONTACT RESTORED BY LEAD MANIPULATION

Test Parameter	Measured Voltage, volts	Specified Value, volts	Test Condition
Forward voltage drop	0.95	1.0 maximum	$I_F = 100_{ma}$
Breakdown voltage	340	200 minimum	I_R = 10 microamperes

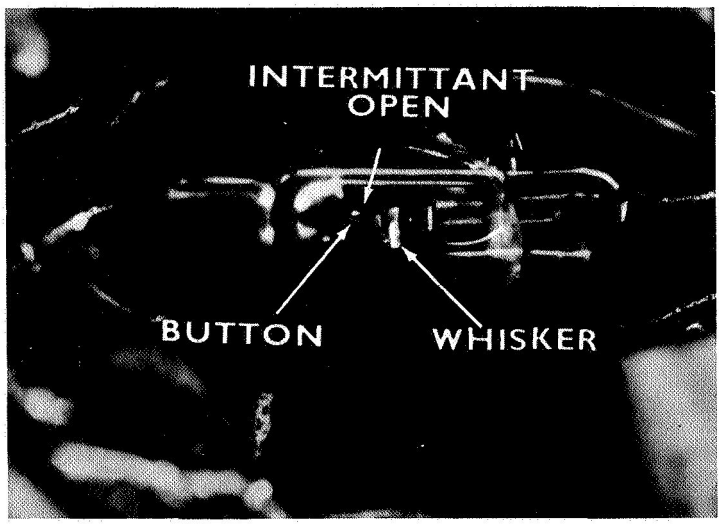

Figure K-16. Internal View of Open Diode Showing Intermittent Contact (12X Magnification) (Photo 00545-240)

analysis was concluded to determine the nature of this anomaly. This analysis included a visual and a microscopic examination, electrical tests, dissection and an internal microscopic examination, and microprobe tests.

Visual examination revealed that the DO-7 glass envelope of this device was cracked. Numerous cracks were also noted on the conformal coating applied over the case.

Electrical tests confirmed the high reverse leakage current. The measured value was 6.6 microamperes, compared to a maximum of 0.1 microampere specified. The measured value was, in fact, at least two or three orders of magnitude higher than expected in practice. Other parameters measured indicated further discrepancies, as summarized in Table K-4.

TABLE K-4. VOLTAGE CHARACTERISTICS OF HIGH LEAKAGE DIODE

Parameter	Measured Voltage, volts		Specified Value	Test Condition
	On Chassis Prior to Removal	After Removal		
Forward voltage V_{F1}	0.89	1.12	1 maximum	$I_F = 750_{ma}$
Forward voltage V_{F2}	Not measured	0.79	0.65 - 0.8	$I_F = 100_{ma}$
Breakdown voltage	Not measured	50	200 minimum	I_R = 100 micro-amperes

Attempts to remove the paint and the conformal coating from the exterior to allow for the examination and photographing of the interior portions of the diode through the glass were not successful since the envelope was too badly shattered. The cracked glass was then removed from around the stud on which the die was mounted.

The stud with the die attached was removed for a microscopic examination. This examination disclosed a hairline fracture in the diode chip, extending from the edge of the die to the metallization above the junction. This fracture can be seen in Figure K-17.

Further examination did not disclose any anomaly in the construction, such as a void in the preform, that might have caused this fracture. The chip was well supported and bonded to its post, indicating that forces applied to it by the contact were not likely to have been a factor in the fracture. It was concluded that the fracture undoubtedly occurred during the mounting or sealing operations in the original manufacture.

The diode was then microprobed, and previous measurements were repeated. No significant changes were noted either in microscopic examination or in electrical performance. Repeated subsequent probings did not change these values. The diode was also subjected to a heating cycle, but no significant changes in performance were observed.

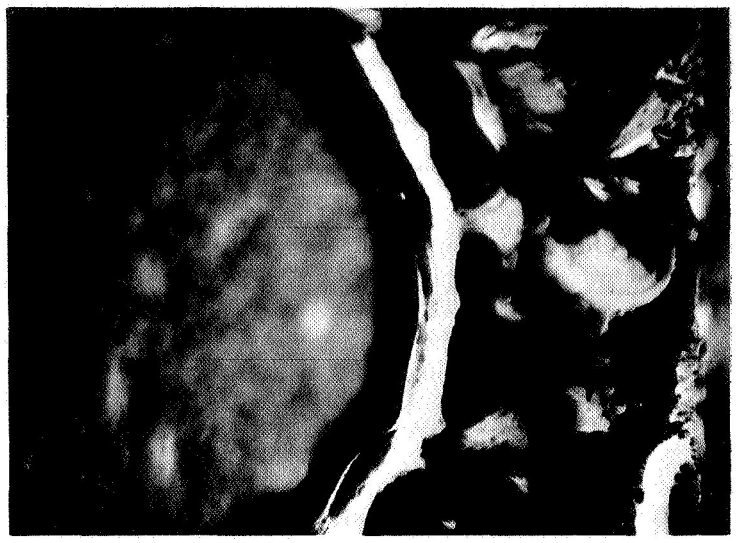

Figure K-17. Die of High Leakage Diode Showing Fracture in Chip (110X Magnification) (Photo 00545-241)

It was concluded from these observations and measurements that the malfunction was definitely caused by the above-mentioned, original manufacturing defect. Exposure to the lunar environment undoubtedly contributed to produce the anomalous electrical characteristics. Cracking of the glass and associated stress forces, and the effects of repeated thermal cycling of the cracked chip, may have resulted in a vertical displacement of half of the cracked chip. Because the two parts of the chip were each well bonded to their posts, the amount of relative motion between them was limited; however, even this limited motion could aggravate the condition of the junction and decrease the depletion region, thus reducing the breakdown voltage.

It appeared likely that the diode had performed satisfactorily on the lunar surface in spite of its crack. It is conjectured that subsequent handling during the return of the camera and its exposure to air may have aggravated this electrical anomaly. The extremely high leakage could thus be associated, in part, with the higher breakdown voltage, but may also be largely attributable to the exposure of the diode to moisture and other contaminants entering through its cracked glass envelope and affecting its previously cracked chip.

REFERENCES

1. Surveyor III Parts and Materials: Evaluation of Lunar Effects, Hughes Aircraft Company Report P70-504, December 1970.

2. Plan for Postflight Test and Analysis of Parts and Materials of Surveyor III Retrieved From Lunar Surface by Apollo 12, Volume I, Technical Plan, Hughes Aircraft Company Report SSD 90397, November 1969.

3. Memorandum 2292/163 from L. E. Blanchard to R. K. Cheng, 11 January 1967, "Surveyor Spacecraft Components of Scientific and Engineering Value Worthy of Recovery During Apollo Missions."

4. Memorandum from E. I. Hawthorne to R. E. Sears, 1 August 1969, "Surveyor III Recovery Operations Plan."

5. Letter from E. I. Hawthorne to James Peacock, NASA-MSC, 8 August 1969.

6. Hughes Aircraft Company letter 69(22)6679/C0116, 22 August 1969, "Apollo 12 Recovery Operations of Parts of Surveyor III."

7. Apollo 12 Preliminary Science Report, NASA SP-235, Section 13, "Preliminary Results from Surveyor III Analysis."

8. D. R. Montgomery and F. J. Wolf, "The Surveyor Lunar Landing Television System," IEEE Spectrum, Volume 3, August 1966, pp. 54-61.

9. Surveyor Final Engineering Report, Hughes Aircraft Company, June 1968.

10. Surveyor III Mission Report, JPL Technical Report 32-1177, 1967.

11. NASA Headquarters letter to Surveyor Parts Steering Group, 18 June 1970, "Approval of Expanded Surveyor III Parts Analysis Plan."

12. Memorandum from Stephen Jacobs, ES8, NASA-MSC, with eight enclosures, 2 February 1970, "Summary of Activity From Release of Surveyor III Returned Materials to Shipment to Hughes January 7, 1970."

13. Memorandum from Richard E. Benson, NASA-MSC, 22 January 1970, "Gamma Spectrometric Analysis of the Surveyor III Television Camera."

14. S. Dushman, Scientific Foundation of Vacuum Technique, John Wiley and Sons, first edition, 1949.

15. A. Fafarman and D. K. Matherly, "Gas Ratio Measurement by Ion Growth," IEEE Transactions, Ed-17, February 1970.

16. S. C. Brown, Basic Data of Plasma Physics, John Wiley and Sons, 1959.

17. J. T. Tate and P. T. Smith, Physical Review, 1932.

18. A. Fafarman and R. S. Burritz, "Beam Transmission in Electron Guns Having a Single-Apertured Control Grid," IEEE Transactions, Ed-15, October 1968.

19. W. A. Hagemeyer, "Surveyor Camera Vidicon Face Plate Temperatures," JPL interoffice memorandum, 1 June 1970.

20. C. T. Leondes and R. W. Vance, editors, Lunar Missions and Explorations, John Wiley and Sons, Inc., 1964.

21. Surveyor V: A Preliminary Report, NASA SP-163, 1967.

22. Surveyor Program Results, NASA SP-184, 1969.

23. J. W. Haffner, Radiation and Shielding in Space, Academic Press, 1967.

24. W. R. Webber, An Evaluation of Solar Cosmic-Ray Events During Solar Minimum, Boeing Company Report DZ-84274, June 1966.

25. W. R. Webber, "An Evaluation of the Radiation Hazard Due to Solar Particle Events," Boeing Company Report DZ-90469, 1963.

26. W. R. Webber, An Evaluation of the Radiation Hazard Due to Solar-Particle Events, Boeing Company Report DZ-90469, December 1963.

27. R. Boring, "Lunar Surface Solar Array Characteristics," Intersociety Energy Conversion Engineering Converence, 1968.

28. R. E. Smith et al., Space Environment Criteria Guidelines for Use in Space Vehicle Development, NASA TM-X-53521, 1967.

29. M. Knoll and B. Kazan, Storage Tubes and Their Basic Principles, John Wiley and Sons, New York, 1952.

30. P. K. Weimer, S. V. Forgue, and R. Goodrich, Electronics, Volume 23, May 1950.

31. H. B. Law, Review of Scientific Instruments, Volume 19, 1948.

REFERENCES FOR SURFACE DISCOLORATION AND CONTAMINATION STUDIES*

101. Surveyor III Parts and Materials: Evaluation of Lunar Effects, Hughes Aircraft Company Report P70-504, December 1970.

102. B. Cour-Palais (NASA MSC), private communication.

103. O. Schaeffer (SUNY), private communication.

104. F. G. Satkiewicz (GCA), private communication.

105. Surveyor III Mission Report, JPL TR 32-1177.

106. L. D. Jaffee (JPL), private communication.

107. Apollo 12 Mission Report, MSC 01855, NASA MSC, Houston, Texas, March 1970.

108. R. F. Scott et al., Apollo 12 Preliminary Science Report, NASA SP-235.

109. P. M. Blair and G. R. Blair, "Summary Report on White Paint Development for Surveyor Spacecraft," Hughes Aircraft Company, TM 800, Culver City, California, December 1964.

110. P. M. Blair et al., Development of a Low Solar Absorptance Thermal Control Coating, Hughes Aircraft Company, P69-147, Culver City, California, April 1969.

111. G. A. Zerlaut and J. E. Gilligan, "Study of In-situ Degradation of Thermal Control Surfaces," IITRI-U6061, 17 March 1969.

112. Mark Adams (JPL), private communication.

113. J. B. Adams et al., "Spectral Reflectivity of Lunar Samples," Science, Volume 167, No. 3918, January 1970.

114. D. Nash (JPL), private communication.

*Included in both Hughes reports on returned Surveyor III parts (SSD 00545R and P70-504).